UNIVERSITA' DELLA CALABRIA

Dipartimento di Ingegneria Informatica, Modellistica, Elettronica e Sistemistica

Scuola di Dottorato

"Life Sciences"

Indirizzo

Ambiente, Salute e Processi Ecosostenibili

Con il contributo di (Ente finanziatore) FSE

CICLO XXVIII

A RHEOLOGICAL APPROACH TO THE NEW ORGANOGELATION PROCESS FOR STRUCTURING VEGETABLE OILS

Settore Scientifico Disciplinare ING-IND/24
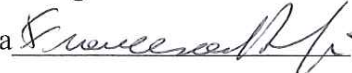
Direttore: Ch.mo Prof. Marcello Canonaco

Firma _____

Supervisore: Ch.mo Prof. Bruno de Cindio

Firma _____

Tutor: Dott.ssa Ing. Francesca Romana Lupi

Firma _____

Dottoranda: Dott.ssa Valeria Greco

Firma _____

Relazione del Collegio dei Docenti della Scuola di Dottorato "Life Sciences"
Università della Calabria
XXVIII Ciclo

Nell'ambito dell'indirizzo "Ambiente, Salute e Processi Ecosostenibili" afferente alla scuola di dottorato "Life Sciences", l'ing.**Valeria Greco**, sotto la direzione del prof. Bruno de Cindio, ha svolto una ricerca dal titolo "**A Rheological Approach To The New Organogelation Process For Structuring Vegetable Oils**", riguardante lo studio reologico e microstrutturale di gel a base organica, nonché di emulsioni prodotte con i suddetti gel.

La ricerca è stata realizzata presso il Laboratorio di Reologia ed Ingegneria Alimentare (LaRIA) del Dipartimento DIMES (UNICAL) e, per un periodo di sei mesi, presso l'Institute of Food, Nutrition and Health, "Laboratory of Food Process Engineering" dell' ETH di Zurigo (Svizzera).

Il lavoro svolto dall'ing.Greco si è distinto per originalità e completezza, ed ha affrontato una tematica attuale per la quale le competenze tipiche dell'ingegneria chimica sono state dirette al product design di alimenti. Il lavoro si è incentrato sull'analisi reologica e microstrutturale di organogel a base di oli vegetali, strutturati tramite l'aggiunta di organogelatori a basso peso molecolare capaci di auto-aggregarsi in un network di unità interagenti.

In questo contesto, è da rimarcare come lo studio sperimentale sia stato condotto con diverse metodiche al fine di individuare il legame texture-struttura dei materiali, e di predirne il comportamento mediante modelli reologici. Le misure reologiche, microscopiche e di FT-IR effettuate presso il LaRIA, sono, quindi, state affiancate a misure di DSC e di NMR (solid fat content) realizzate presso presso l'ETH di Zurigo, in cui l'ing.Greco ha trascorso sei mesi di soggiorno-studio sotto la supervisione del prof. Peter Fischer. L'intera campagna sperimentale ha consentito di caratterizzare completamente gli organogel. È stato ottenuto un modello reologico, basato sul modello frattale, capace di predire la temperatura di inizio cristallizzazione dei gel, e il loro modulo dinamico in funzione della quantità di organogelatore aggiunto al sistema. Lo sviluppo della struttura è stato studiato mediante l'analisi della cinetica di evoluzione del network. Infine, l'indagine FT-IR ha consentito di misurare l'effetto della concentrazione degli organogelatori sulla comparsa dei legami idrogeno o di interazioni deboli nei gel. La caratterizzazione dei gel è stata propedeutica alla produzione e allo studio di emulsioni strutturate di tipo W/O ad uso alimentare.

Il lavoro è risultato esaustivo dell'argomento ed eseguito con estrema competenza; i risultati sono stati ampiamente usati in realtà produttive (Spin-off universitari) anche in collaborazione con aziende operanti nel settore, suscitandone l'interesse.
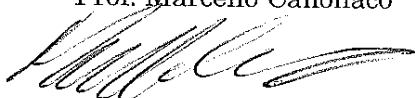
L'ing.Valeria Greco ha mostrato spiccata autonomia, professionalità e capacità di apprendere, ed ha, oltretutto, partecipato alle attività del laboratorio acquisendo dimestichezza anche in altri settori, mettendo in evidenza buone doti e capacità scientifiche, oltre che ammirevoli qualità relazionali. Il Collegio dei Docenti, visto l'impegno profuso e la qualità della sua attività, esprime un giudizio pienamente favorevole ai fini dell'ammissione dell'ing.Valeria Greco all'esame finale per il

conseguimento del titolo di Dottore di Ricerca in "Life Sciences", indirizzo "Ambiente, Salute e Processi Ecosostenibili".
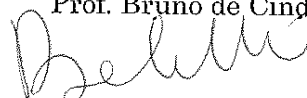

Addì, 19 novembre 2015

il Direttore della Scuola di Dottorato

Prof. Marcello Canonaco

il Supervisore della Tesi di Dottorato

Prof. Bruno de Cindio

Table of contents

I would like to express my deeply-felt thanks to my academic supervisor, Prof. Bruno de Cindio, who always believed in me and encouraged my research. Working in your laboratory allowed me to grow as a research scientist and as a person.

Profound gratitude goes to Dr. Francesca Romana Lupi, who has been a truly dedicated research advisor. Your enthusiasm for research was motivational for me. Your advice on research and your human support have been very precious.

I also have to thank Dr. Domenico Gabriele, who always provided insightful discussions about the research, and Dr. Noemi Baldino, for her cooperation and support.

I would also like to thank Prof. Peter Fischer and all the members of the "Laboratory of Food Process Engineering" (ETH Zürich) for their cooperation and willingness and for their contribution to my personal and professional time at Zürich.

Finally, I want to thank present and past members of the "Laboratory of Rheology and Food Engineering" (UNICAL) for providing me a beautiful working environment. I am particularly grateful to Dr. Lucia Seta, for her willingness and support, and to Maria Luisa, Valentina, Olga, Federica, Stefania, Ilaria, Stefania, Francesca and Gessica for sharing time and hopes.

Introduction

In the present PhD thesis, the rheological and microstructural study of vegetable oil-based organogels and of "organogelled" W/O emulsions, is reported. Organogels are solid-like systems based on gelation of organic solvents by means of either low molecular weight components or oil soluble polymers able to self-assemble into aggregates which interact with each other to build a three-dimensional network. From a research perspective, organogelation is an interesting topic as it deals with different area of research such as crystallization, chemistry, physics and materials science. Nevertheless, the gelation of organic solvents has, potentially, a wide range of industrial uses.

The aim of the present work is the rheological and structural characterisation of organogels (alone or emulsified with water), produced with low molecular weight organogelators and edible oils, and their applications for the product design of healthy potential alternatives to commercial fats. The potential use of organogels in foods, which has provided a persistent interest in recent years, is the development of alternative structuring methods for edible oils, principally because of the increasing demand to reduce saturated and/or trans-fats from the consumers' diet.

One of the most interesting characteristics of organogels is that most of them are formed from low-molecular weight compounds, while historically, the majority of gels (mainly water-based) have always been polymeric in nature. Organogels produced with low-molecular weight organogelators have potentially many uses, because one of their most promising characteristics is the possibility of tailoring their physical properties by changing the amount and/or the chemical nature of the molecule used as organogelators or by modifying process parameters. Since organogelation is a recent field of research and organogels have potentially various uses, research has mainly focused on the screening of potential new structurants until now. Thus, nowadays, the comprehension of the organogelation mechanism is still not at a level that allows *a priori* the design of structures. For this purpose, it is important to relate the rheological properties of the organogel network, which determines its potential for use in applications, to its microstructure.

Within this framework, the main aim of the present work is the rheological and structural investigation of organogels for their potential use in food. In particular, the structuring capability of two low-molecular weight organogelators in edible oils were studied: a

commercial mixture of monoglycerides of fatty acids (Myverol 18-04K) and a mixture of primary fatty alcohols, well known for its nutraceutical properties (policosanol).

The characterisation of all raw materials, both solvents and organogelators, used in the present work will be shown and discussed in Chapter 2, whereas Chapter 3 and 4 deal with the rheological and microstructural analysis of monoglycerides and policosanol organogels, respectively. In order to study the role of both organogelators, the investigation was carried out preparing gels within a broad range of organogelator concentrations. Some semi-empirical equations, based on the fractal nature of these systems, were proposed to relate the temperature of crystallisation onset to the organogelator content, with the aim of helping the design of organogels with controlled properties. Furthermore, the role of the botanical source of vegetable oil used as the solvent, and the effect of the addition of hard fats were studied. Finally, complex systems produced with mixtures of organogelators (policosanol and glyceryl stearate) for both potential food and cosmetic uses have been studied in this work. The obtained results will be discussed in Chapter 4.

Following the results reported in Chapter 3, Chapter 5 presents the formulation and the stability study of structured W/O emulsions. These systems represent potential healthy replacers of commercial shortenings. As mentioned above, the importance of designing healthy foods can be understood looking in the recent literature at the growing interest of research in this topic.

Chapter 1: state of the art

Introduction

In the present work, the study of vegetable oil organogelation was initially carried out with a complete characterisation of raw materials (as reported in Chapter 2). In the following Chapters, in particular in Chapter 3 and 4, the rheological and structural study of vegetable oil-based organogels will be presented: organogels were produced using two different low molecular weight organogelators, monoglycerides of fatty acids (MAGs), commonly used in food industry as emulsifiers, and policosanol, a mixture of long chain fatty alcohols. Policosanol is well known for its nutraceutical properties and it was used in this work for the first time as a potential organogelator. Moreover, the ability of mixtures of both organogelators to allow the gelation of olive oil was investigated and W/O structured emulsions were formulated as potential alternatives to commercial fats.

In the present chapter, a general overview of gels and gelators is presented, showing the main differences between hydro- and organo-gels and between polymeric and low-molecular weight gelators. Moreover, a discussion of all current methods of organogel analysis will be reported. Finally, models for properties and structuring of organogels and the proposed applications of these systems will be discussed in Paragraph 1.6 and 1.7, respectively.

1.1 Soft materials: definition of the gel

The term *soft matter* originates from the macroscopic properties of some categories of materials, such as colloids, surfactants, liquid crystals and gels, which can be induced to flow under certain conditions. Indeed, soft materials are characterised by a weak ordering resulting from the lack of three-dimensional atomic long-range order found in a crystalline solid. From the viewpoint of kinetic energy, the molecular kinetic energy for *soft materials* is approximately close to k_BT, whereas for the so-called *hard materials* molecular kinetic energy is much less than k_BT when near ambient temperature [1].

From a structural point of view, the ordering of *soft material* is generally intermediate between a crystalline solid and a liquid. This lack of crystalline order leads to the "soft" mechanical response of the materials. The periodicity of the structures formed in soft

materials is typically in the range 1-1000 nm which corresponds to nanoscale ordering. The length-scale of the structures is also often referred to as *mesoscopic* because it is intermediate between the microscopic (atomic) and the macroscopic scales.

Many soft materials form a disordered phase at high temperatures but adopt ordered structures, with different degrees of translational and orientational order, at low temperatures. The transition from the isotropic phase to ordered phase is a symmetry breaking transition, because the symmetry of the isotropic phase, with full rotational and translational symmetry, is broken at low temperatures. Examples of symmetry breaking transitions include the isotropic-nematic phase transition in liquid crystals and the isotropic-lamellar phase transition observed for amphiphiles or block co-polymers [1].

Molecular gels, one kind of soft material, have generated enormous interest recently for both scientific and technological reasons [2]. Being unique materials, gels combine rigidity with elasticity[3], and they are well known in daily life and have a wide range of uses in food, medicine, biomaterial and cosmetic technologies.

For the past few decades, gels have been referred to as materials "easier to recognize than define" [4]. A comprehensive definition of a gel was made by Flory [5] who proposed a gel as a material which "has a continuous structure with macroscopic dimensions that is permanent on the time scale of an analytical experiment and is solid-like in its rheological properties". According to Ferry "a gel is a substantially diluted system which exhibits no steady state flow" [6]. Almdal et al. [7], refining Ferry's definition, identified two key aspects of a gel, namely the presence of substantial amounts of liquid and the solid-like rheological properties. Nowadays it is generally accepted that a gel is a semi-solid material composed of low concentrations (typically less than 15%) of gelator molecules that, in the presence of an appropriate solvent, self-assemble *via* physical or chemical interactions into an extensive mesh network, preventing solvent flow as a result of surface tension [10, 11]. A gel can also be defined as a colloidal system of solid character in which the dispersed substance forms a coherent framework that is interpenetrated by a system, usually a liquid solvent, consisting of units smaller than colloidal entities [10].

The structural definition of a gel is based on the connectivity of the system: gels are systems consisting of molecules, particles and chains, which are partially connected to each other in a fluid medium and the loss of fluidity is the result of connectivity [12]. The stability of the gel is determined by the balance between gelator aggregating forces and solvent/aggregate interactions. The overall thermodynamic and kinetic stability results

from the interplay of the opposing forces related to the gelator partial solubility in the continuous phase [10].

Gels are semi-solid formulations and, as a consequence, they demonstrate certain solid-like properties but also liquid-like ones. From a rheological viewpoint, a gel is a system that does not flow and shows a plateau region of the storage modulus and low values of the loss tangent at an angular frequency from 10^{-3} to 10^2 rad/s [12]. In more detail, the rheological behaviour of gels is according to the strength of the network: the storage modulus of *strong* gels exhibits values at least one order of magnitude higher than values of loss modulus and it is independent or nearly independent of frequency. On the contrary, the values of the storage modulus for *weak* gels show frequency dependence for the whole region of frequencies applied during small amplitude oscillation tests (SAOTs). Values of the storage modulus, for *weak* gels, are still higher than values of the loss modulus and the material still shows solid-like behaviour. However, at higher frequencies the crossover between G' and G'' can occur and that means that the network is broken and the gel will become liquid-like material (Figure 1.1) [13]. It is worth noticing that from a theoretical point of view a gel is defined as a system that does not flow; indeed at the gel point steady shear viscosity tends to go to infinity [13]. Nevertheless, it is common practice to perform experimental measurements of gel viscosity in order to investigate the structure and the potential rate of destructuring of the gel system [13].
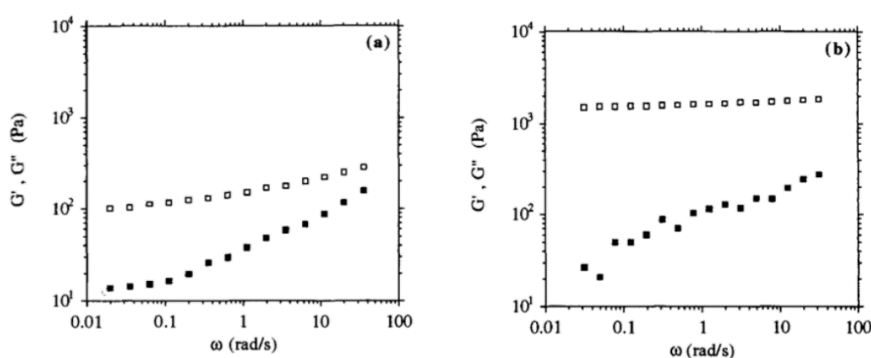
Figure 1.1 Examples of *weak* and *strong* high-methoxyl pectin gels: (a) weak gel behaviour, (b) strong gel behaviour [13].

Gels can be classified according to different criteria. Generally speaking, gels can be separated into two different classes according to the nature of the continuous phase: according to the polarity of the liquid immobilized within the network structure, gels can be regarded as hydrogels (polar solvent) or organogels (organic solvent) [14, 15, 16]. A

general overview on the state of the art in hydrogels and organogels will be reported below.

Nevertheless, it should be highlighted that in recent studies additional kinds of gel have been reported [17], such as niosomal and proniosomal gels (formed by liposomes consisting of a non-ionic surfactants, which can be of a hydrogel or organogel nature) [17, 18, 19], emulgels (consisting of a combination of an hydrogel or an organogel and an o/w or w/o emulsion) [17, 20, 21], bigels (prepared as stable mixtures of organogels and hydrogels) [22,17], aerogels (consisting of a flexible material with customizable pore size and surface area, made of inorganic silica gels dried under supercritical conditions) and xerogels (consisting of a dense material with a relatively small pore size formed of inorganic silica dried at normal pressure) [23, 17].

1.2   Hydrogels

Hydrogels can be subdivided into two main categories on the basis of the nature of gelling molecules, that is, low molecular weight (LMW) or polymeric hydrogelators. Historically, most hydrogels have been polymeric in nature. Indeed, hydrogels are usually referred to as three-dimensional, hydrophilic networks of polymer chains capable of retaining and immobilising large amounts of aqueous phase [24, 25, 26, 27].

However, recently more and more examples of LMW gelators for water have appeared in the literature in a move towards new materials especially suitable for drug delivery and tissue engineering processes [28, 29, 30, 31].

1.2.1 Hydrogels from polymeric gelators

Hydrogels containing polymeric gelators can be described as three-dimensional cross-linked hydrophilic polymer networks capable of swelling or de-swelling reversibly in water and retaining a large volume of liquid in a swollen state [24]. Smart hydrogels have been formulated in order to change their volume and/or shape significantly in response to small alterations of certain parameters of the environment [25]. Indeed, hydrogels can be designed with controllable responses (in terms of volume variation) to various physical and chemical stimuli, where the physical stimuli include temperature, electric or magnetic field, light, pressure, and sound, whereas the chemical stimuli include pH, solvent composition, ionic strength, and molecular species (Figure 1.2) [24, 32].
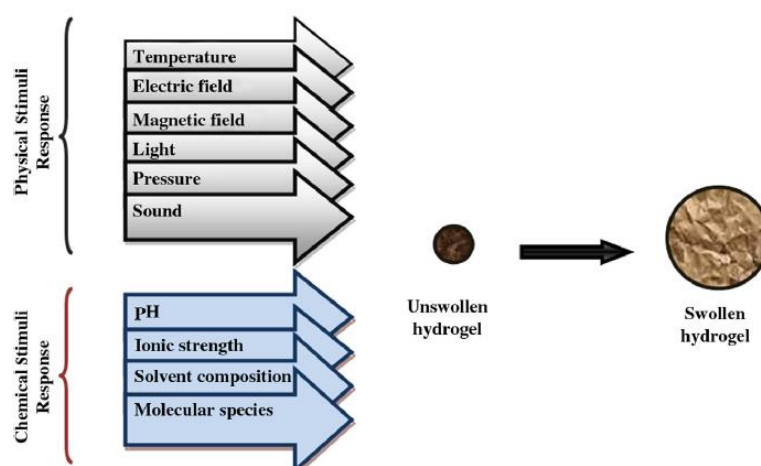
Figure 1.2 Schematic representation of stimuli affecting hydrogel swelling [24].

The character of water in a hydrogel is also related to the swelling process. When a dry hydrogel begins to absorb water, the first water molecules entering the matrix will hydrate the most polar hydrophilic groups giving *primary bound water*. As a consequence of polar groups hydration, the network swells, then the exposed hydrophobic groups interact with the water molecules, leading to *secondary bound water* or hydrophobically bound water. After the hydrophilic and hydrophobic sites have bound water molecules, the network will absorb additional water, owing to the osmotic driving force of polymer chains towards infinite dilution. This additional swelling is opposed by the network crosslinks, leading to an elastic network retraction force. Hence, the hydrogel will achieve an equilibrium swelling level. The additional swelling water, known as *free water* or *bulk water*, is assumed to fill the space between the network chains and/or the centre of macropores and voids [33].

Ahmed [24] reported all proposed classifications of polymeric hydrogels. According to the origin of gelling polymers, hydrogels can be classified into natural or synthetic gels [24, 34]. Examples of natural polymeric gelators are anionic polymers (such as hyaluronic acid, alginic acid, pectin, carrageenan, chondroitin and dextran sulphate), cationic polymers (such as chitosan and polylysine), amphipathic polymers (as collagen, gelatin, carboxymethyl chitin, fibrin) and neutral polymers (such as dextran, agarose and pullulan) [33]. Alginate, chitosan, methylcellulose, gellan and guar gum have also been used as natural polymeric gelling molecules for pharmaceutical and biomedical applications [35, 36, 37, 38, 39]. With regard to synthetic polymers, a wide range of polyesters have been used to prepare hydrogels, including polyhydroxybutyrate, PEG-PLA-PEG (polyethylene

glycol-polylactic acid-polyethylene glycol), PEG-PLGA-PEG (polyethylene glycol-polylactic-co-glycolic acid-polyethylene glycol), PEG-PCL-PEG (polyethylene glycol-polycaprolactone- polyethylene glycol-), PLA-PEG-PLA (polylactic acid-polyethylene glycol- polylactic acid), P(PEG/PBO terephthalate) [33]. Other examples of synthetic polymeric hydrogelators are PEG-bis-(PLA-acrylate), PEG-g-P(AAm-co-Vamine), PAAm, P(NIPAAm-co-AAc), P(NIPAAm-co-EMA), PVAc/PVA, PNVP, P(MMA-co-HEMA), P(AN-co-allyl sulfonate), P(biscarboxy-phenoxy-phosphazene), P(GEMA-sulfate), PEO, poly(N-isopropylacrylamide), poly(vinyl alcohol) [35, 40, 41].

As far as polymeric composition is concerned, hydrogels can be classified into homopolymeric, co-polymeric and multi-polymer interpenetrating polymeric (IPN) hydrogels [24]. Homopolymeric hydrogels are polymeric networks derived from a single species of monomer and their cross-linked skeletal structure can be determined by the nature of the monomer and polymerization technique [24, 42]. Co-polymeric hydrogels are referred to as polymeric networks resulting from two or more different monomer species with at least one hydrophilic component, arranged in a random, block or alternating configuration along the chain of the polymer network [24, 43]. Multipolymer interpenetrating polymeric hydrogels have been classified as "alloys" of cross-linked synthetic and/or natural polymers; at least one of them being synthesized and/or cross-linked within the immediate presence of the other, without any covalent bonds between them, which cannot be separated unless chemical bonds are broken [25, 24, 44]. IPNs have been described as an important class of hydrogels, because of their enhanced mechanical strength and swelling/de-swelling response [25]. IPN hydrogels can be further subdivided into two groups: *simultaneous IPN*, prepared mixing the precursors of both networks and synthesizing the two networks at the same time by independent routes, and *sequential IPN*, usually prepared by swelling of a single-network hydrogel into a solution containing the mixture of monomer, initiator and activator, eventually in the presence of a cross-linker (Figure 1.3) [25, 44, 45, 46].
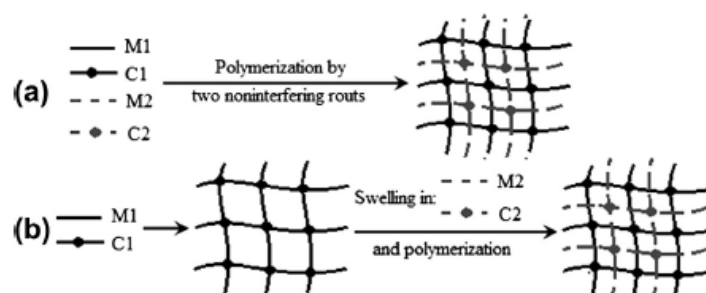
Figure 1.3 Schematic representation of IPN formation by simultaneous (a) or sequential (b) strategy [25].

Moreover, hydrogels can be classified on the basis of their configuration and physical structure as *amorphous* or *non-crystalline*, *crystalline* and *semi-crystalline*, the last being a complex mixture of both amorphous and crystalline phases.

In the literature, polymeric hydrogels are also often divided into two categories based on the chemical or physical nature of the cross-link junctions [24, 33, 47, 48, 49]. In *physical* or *reversible* hydrogels, polymeric networks are held together by molecular entanglements and/or secondary forces, including ionic, H-bonding or hydrophobic forces [33, 48, 49]. Since there are no chemical reactions involved, *physical* hydrogels are often thermoreversible gels, as they show gel-to-sol transition with increased temperature and sol-to-gel transition when temperature is decreased [26]. *Physical* hydrogels quite often show pseudoplastic flow behaviour and their stability is sensitive to various environmental conditions, such as pH, salt concentration in the formulation and temperature [26]. Methods for synthesizing *physical* polymeric hydrogels include warming of a polymer solution (e.g. PEO-PPO-PEO block co-polymers in water), cooling a polymer solution (e.g. agarose or gelatin in water), cross-linking of a polymer in aqueous solution using freeze-thaw cycles (e.g. freeze–thaw PVA in aqueous solution) and lowering pH to form an H-bonded gel between two different polymers in the same aqueous solution (e.g. PEO and PAAc), mixing solutions of a polyanion and a polycation to form a complex co-acervate gel (e.g. sodium alginate plus polylysine), gelling a polyelectrolyte solution with a multivalent ion of opposite charge (e.g. $Na^+alginate^-+Ca^{2+}+2Cl^-$) [33]. The combination of a polyelectrolyte with a multivalent ion of the opposite charge can lead to the formation of a physical polymeric hydrogel known as *ionotropic* hydrogel [33].

On the contrary, *chemical* or *permanent* hydrogels are polymeric networks formed by permanent covalently cross-linked junctions [24, 33]. Chemical hydrogels are produced by cross-linking polymers in the solid state or in solution with radiation (e.g. irradiate PEO in

water) or with chemical crosslinkers (e.g. treat collagen with glutaraldehyde or a bis-epoxide) or with multi-functional reactive compounds (e.g. PEG+diisocyanate), co-polymerizing a monomer with a crosslinker in solution (e.g. HEMA+EGDMA), co-polymerizing a monomer with a multifunctional macromer (e.g. bis-methacrylate terminated PLA-PEO-PLA+photosensitizer+visible light radiation), polymerizing a monomer within a different solid polymer to form an IPN gel (e.g. AN+starch) [33]. Both *physical* and *chemical* polymeric hydrogels may be generated using chemically modified hydrophobic polymers, as shown in Figure 1.4 [33].
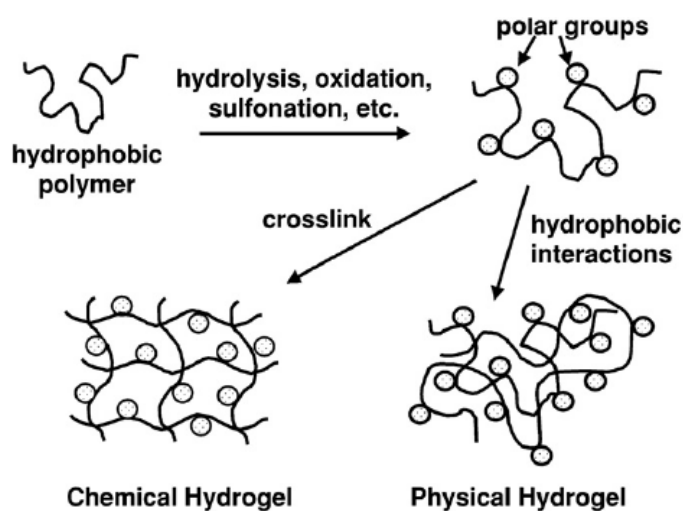
Figure 1.4 Methods for hydrogels production by chemical modification of hydrophobic polymers [33].

Finally, polymeric hydrogels may be categorized on the basis of the presence or the absence of electrical charge located on the cross-linked chains as *non-ionic* or *neutral* gels, *ionic* gels (both anionic or cationic), *amphoteric electrolyte* or *ampholytic* gels (with both acidic and basic groups), *zwitterionic* gels (containing both anionic and cationic groups in each structural repeating unit) [24].

1.2.2 Hydrogels from LMW gelators

An alternative strategy to produce hydrogels is via the self-assembly of small molecules: low molecular weight hydrogelators are organic molecules able to self-assemble into extended three-dimensional, often fibrous networks in which water molecules become trapped leading to gel formation (Figure 1.5) [28, 50, 51]. The design of LMW hydrogelators is an expanding area of research because they are often derived from biocompatible compounds [51, 52].
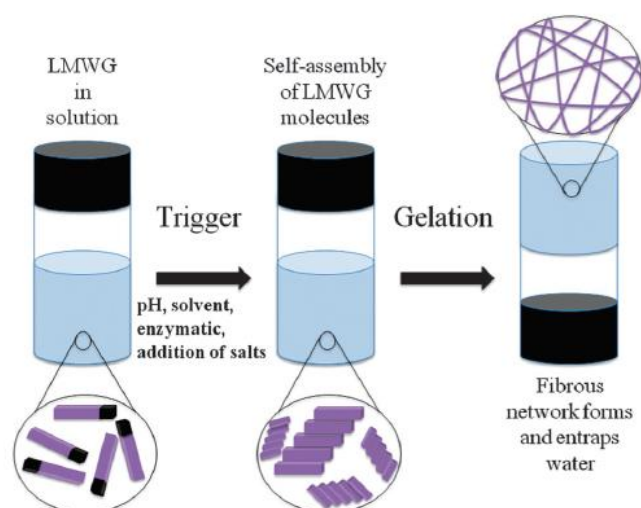
Figure 1.5 Schematic representation of the self-assembly of a LMW hydrogelator leading to the formation of a fibrous network [50].

To achieve gelation of small organic molecules in aqueous solvents, there must be a balance between the tendency of the molecules to dissolve into water and the tendency to aggregate [51]. The formation of a fibrous network occurs via multiple hierarchical assembly from molecule to network [50]. First, molecular interactions must drive self-assembly in order to favour the formation of one-dimensional fibres over other possible structures [50]. Assembly is driven by one-dimensional non-covalent interactions between gelator molecules, such as hydrogen-bonding, π-π stacking, electrostatic and van der Waals interactions [28, 50, 51].

Hydrogen bonds, a common driving force for aggregation in organic solvents, are of course weak in water unless many of them are protected from solvent [51, 53]. Therefore, hydrophobic forces become most important in aqueous environments [51, 54] and the control of hydrophobic interactions is the critical parameter to the design of organic hydrogelators. Other kinds of molecular interactions can also play a role in gelation, including salt bridges and transition metal coordination [51, 55].

Furthermore, hydrogelation requires the formation of a continuous network by means of cross-links between fibres. These cross-links can either arise from entanglement or branching of fibres. Since both assembling of LMW hydrogel strands and cross-links between fibres are non-covalent in nature, LMW hydrogels are reversible [50, 51]. Thermoreversiblility (i.e. melting and re-forming of gels on warming and cooling respectively) makes LMW hydrogels particularly interesting and attractive for use in thermo-sensing [28, 50].

Hydrogels formed from LMW gelators typically show very different mechanical properties in comparison to those of polymeric or biopolymer gels [50]. For instance, LMW hydrogels tend to break at relatively low strains [50, 56]. The macroscopic mechanical properties of LMW hydrogels are strongly affected by the average thickness and mechanical properties of the network fibres, the degree of branching (i.e. the distance between cross-linking points), the type of crosslink and the microstructure (i.e. how the fibres are distributed at a larger length scale) [50, 51].

Hydrogels containing LMW gelators can be often prepared using a heat–cool cycle: heating solubilises gelator molecules, after cooling gelators are no longer soluble so they begin to self-assemble [50]. Self-assembly occurs because of the relatively high hydrophobicity of LMW hydrogelators. Other factors affecting self-assembly include changes in pH, a change in solvent polarity (LMW hydrogelators often have high solubility in a water-miscible organic solvent, but low solubility in water) and the use of an enzyme to cut a functional group from a pro-gelator, significantly reducing the solubility of the molecule in water [50, 57, 58].

Examples of LMW hydrogelators include molecules from classes such as bile salts, functionalised sugars, oligopeptides, surfactant-like molecules and dendrimers. Chirality is a common feature of all classes of hydrogelators [50].

Conventional amphiphilic molecules are known to have gelling properties in aqueous solvents (Figure 1.6) [51, 55, 59]. Gelation is a balance between crystallization and solubilisation. Hence, to gel a given solvent, a molecule should have functionality that will provide both. In this sense, amphiphilic molecules are promising hydrogelators since they are characterised by the presence of both hydrophobic groups to promote aggregation and hydrophilic groups to provide solubility. Furthermore, charged groups can also provide triggers for gelation via a change in solution pH or ionic strength [51]. Kunitake et al. [60] studied the relationships between the structure of gelling amphiphilic molecules and the morphology of aggregates formed in water. They divided the amphiphilic structure into four parts: the flexible tail, a rigid segment, a spacer group and the hydrophilic headgroup. By varying the length of the tail, flexible linker or both, the structure of the aggregate (globules, vesicles, lamellae, rods, tubes or disks) could be changed [60].

Lipids have been extensively studied as amphiphilic LMW hydrogelators [61, 62, 51]. In addition, Fuhrhop et al. [63, 64] showed that both *N*-alkylaldonamides and *N*-dodecanoyl-(D- and L-)-serine have gelling properties in water and exhibit chiral bilayer effect. Imae et al. [65] have also studied amphiphilic amino acid surfactants. Some of the

lowest molecular weight organic hydrogelators (MW below 250 Da) are serine-based amphiphiles [51, 66].
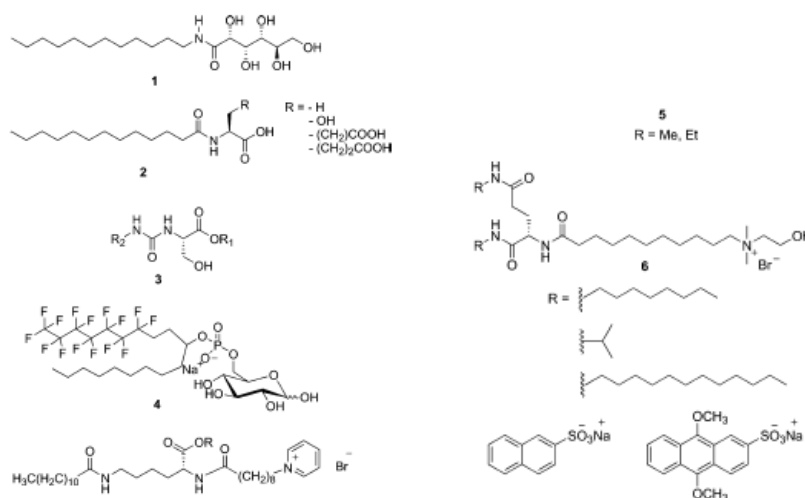
Figure 1.6 Examples of amphiphilic hydrogelators [51].

The two-headed amphiphiles or so-called *bolaamphiphiles*, including those with nucleotides, amino acids and sugars as headgroups, have also been investigated as LMW hydrogelators [51, 67].

Moreover, Menger at al. [68] found several families of *gemini surfactants* that form hydrogels: these molecules possess, in sequence, a long hydrocarbon chain, an ionic group, a rigid spacer, a second ionic group and another hydrocarbon tail.

Carbohydrates have also been used successfully in the design of LMW hydrogelators [51]. As an example, Bhattacharya and Acharya have examined the hydrogelation abilities of a series of disaccharide amphiphiles with both one and two alkyl tails in the presence of alcohol co-solvents [69]. The biocompatibility of sugars makes them attractive candidates for hydrogels with biological applications [51].

Additionally, the family of bis(urea) dicarboxylic acids was found to self-assemble to form hydrogels, at very low concentrations ($0.3\%_{wt/wt}$), according to both pH and ionic strength [51].

A further interesting example of an LWM hydrogelator is Fmoc-tyrosine (FmocY), a commercially available N-protected amino acid. Hydrogels from Fmoc-tyrosine can be either produced via dephosphorylation of FmocY-phosphate or adjusting the pH of a solution of FmocY from high pH to a lower pH [50]. A related LMW hydrogelator is Fmoc-diphenilalanine [50].

LMW hydrogels, prepared with *N,N'*-dibenzoyl-L-cystine (DBC) as gelling molecule, have also been investigated by Friggeri et al. [28] as controlled release systems for small drug molecules.

1.3   Organogels

Organogels (or oleogels in the case of food systems) are usually defined as non-glassy, thermoreversible, semi-solid systems composed of an organic liquid entrapped within a 3-D network [70]. The 3-D organogel structure is affected by several factors, such as the method of gel preparation, the nature of the solvent, gelator and co-gelator, and the interactions between the components involved [70]. Organogels can be distinguished from hydrogels by the presence of an organic continuous phase and can be further subdivided on the basis of the nature of gelling molecules, polymeric or low molecular weight organogelators (LMOGs) (Figure 1.7) [8].

Polymeric organogelators entrap the organic solvent by forming a network of either cross-linked or entangled macromolecular chains for chemical and physical gels, respectively. The formation of polymeric chemical organogels progresses from gelling molecules that are initially held together topologically in at least one-dimension by co-valent bonds [2]. In regard to physical organogels, networks can be further stabilized by weak inter-chain interactions such as hydrogen bonding, van der Waals forces, and π-stacking [8].

In contrast to hydrogels, the majority of organogels are formed from non-polymeric compounds [71]. LMOGs typically assemble into supra-molecular structures via non-covalent interactions [71]: the self-assembly of LMW organogelators is driven by physical interactions leading to the formation of aggregates sufficiently long to interact with each other and induce solvent gelation [8]. LMW organogels are self-standing, thermo-reversible, anhydrous, viscoelastic materials structured by a three-dimensional supra-molecular network composed of self-assembled small molecules at concentrations usually lower than 2%$_{wt/wt}$ [72].

The properties of LMW organogels are highly sensitive to temperature, because they behave as soft materials and the dominant molecular interactions are usually in the order $\approx RT$ (2.48 kJ/mol for T=298 K) [71]. LMW organogelators typically self-assemble into liquid crystals, reverse worm-like or reverse spherical micelles, nanotubes, aggregates due to organometallic bonding or electron transfer, gel strands in lamellar form, crystal

networks and self-assembled fibrillar networks (SAFiNs) [73, 74, 15, 75, 76, 77]. Three-dimensional SAFINs comprise fibrillar objects: LMW gelators are topologically zero-dimensional objects as viewed on the micrometer scale, but they must possess anisotropy on the molecular scale, which permits the formation of fibres [2]. One-dimensional growth is promoted by self-assembly in stochastic nucleation events with highly specific interactions [73, 74]. Instead, when the growth of LMOG aggregates is restricted to two dimensions, platelet-like structures are obtained [71]. The formation of a network consisting of these supra-molecular entities, either 1-D or 2-D structures, results in gelation [71].
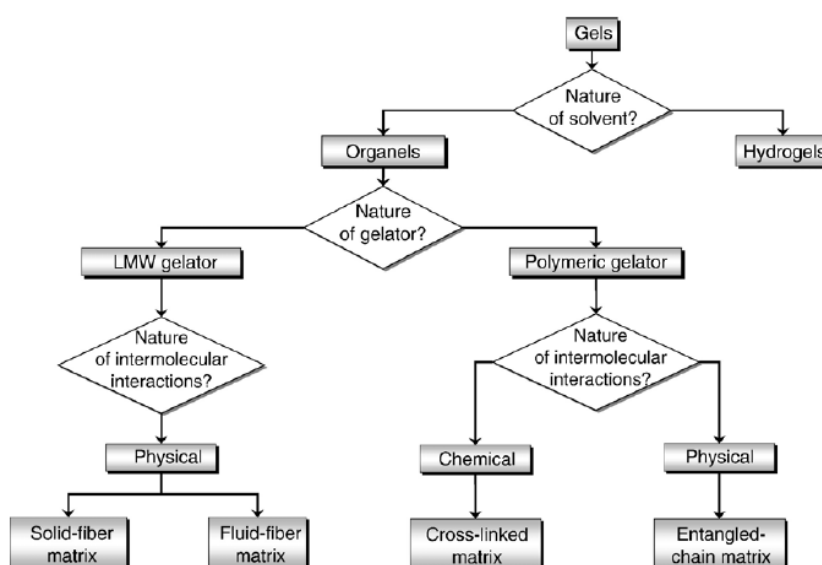
Figure 1.7 Classification of organogels [8].

Since the main aim of the present thesis is the study of the rheological and microstructural properties of organogels and their applications, the state of the art of organogelator molecules will be discussed in further detail in Paragraph 1.4.

General mechanism of organogel formation will be now described. These mechanism include the creation of fluid fibre matrix or solid fibre matrix organogels from LMOGs and cross-linked or entangled-chain polymeric networks [70, 8].

Among LMW organogels, an important distinction depending on the kinetic properties of aggregates is made between networks composed of solid or fluid fibres [8, 9]. The main distinction between the two systems is the kinetic stability of the networks constituting the gel (Figure 1.8): strong gels are formed of permanent, often crystalline networks, in which junction points are composed of quite large pseudo-crystalline micro-domains, whereas

weak gels are formed of transient networks, characterized by the continuous breaking and recombination of the constituent units [8, 9, 78]. In other words, solid matrix organogels exhibit a permanent gel network over the gel lifetime, while fluid matrix organogels form a dynamic gel structure which undergoes constant remodelling [9, 70, 8].
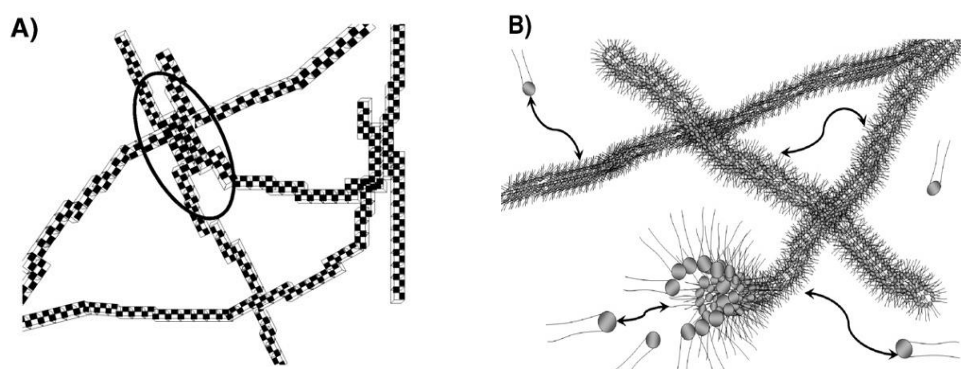
Figure 1.8 Schematic representation of: A) solid-matrix organogel (strong gel), B) fluid-matrix organogel (weak gel) [8].

The majority of LMOGs discovered typically self-assemble into solid networks when added to appropriate organic solvents [8]. The mechanism of solid matrix formation involves the creation of networks resulting from the interactions among gelator solid fibres during organogel formation [70]. Solid matrix organogels are produced dissolving the gelator in the heated solvent, at concentrations usually less than 15% by weight (organogels containing super-gelators require only less than 0.1%), following a drop in temperature below the organogelator solubility limit [8, 70, 79, 80]. The solution cooling causes a decrease in solvent/organogelator affinity, then gelator molecules partially precipitate and undergo self-alignment to form fibres [70, 8]. Physical interactions between fibres result in the formation of solid aggregates in the networked structure (Figure 1.9) [70]. The remaining solvent–aggregate affinity stabilizes the system by preventing phase separation [8].
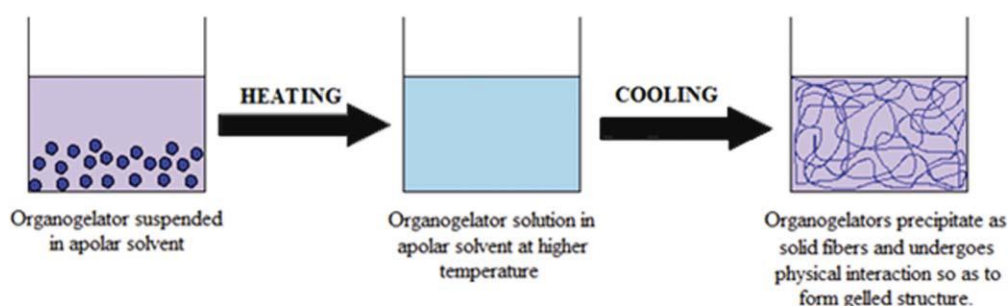
Figure 1.9 Mechanism of solid matrix organogel formation [70].

16

Aggregates more often grow as solid 1D fibres with high aspect ratios, whereas 2D growth results in platelet formation [70, 8]. Upon cooling, super-saturation is the dynamic driving force for gelation kinetics and it can also determine the type of networked structure [82]. At the equilibration temperature, the degree of super-saturation is defined as follows:

$$\sigma_T = \Delta C \big/ C_{sol}^T \qquad (1.3.1)$$

and

$$\Delta C = C_0 - C_{sol}^T \qquad (1.3.2)$$

where C_{sol}^T is the gelator solubility at temperature T, C_0 is the initial gelator concentration, hence ΔC is the driving force for fibres formation [70]. Under a low degree of super-saturation usually a fibrillar network is formed, con the contrary high degree of super-saturation leads to the formation of spherulitic networks (Figure 1.10) [82].
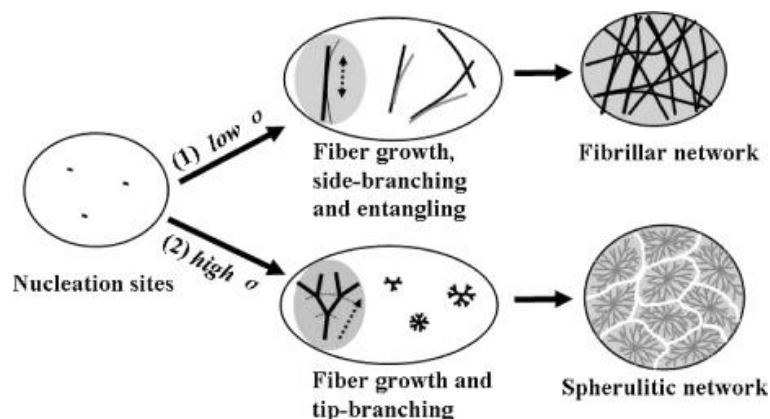
Figure 1.10 Growth models for network formation based on the degree of supersaturation [82].

Although chirality may enhance organogelator function, it is not compulsory [8, 70, 79]. Chirality of an organogelator can play an important role in solid fibre matrix organogel formation and stability, since solid fibres have marked rigidity [8, 70, 9].

Macroscopically, solid matrix organogels range from white opaque to translucent systems, according to aggregate size and the consequent gel ability to scatter incoming light [8]. From a rheological viewpoint, solid matrix organogels exhibit solid-like, viscoelastic, mechanical behaviour, since they are made of permanent networks often obtained through a sharp solution or sol-to-gel phase transition at a specific temperature [9].

In fluid matrix organogels, aggregate size increases and the eventual entanglement of these structures immobilizes the solvent [8]. Owing to aggregate fluidity and transience of

junction points, fluid matrix organogels are also referred to as *worm-like* or *polymer-like* networks [8, 9]. Fluid matrix organogels are formed with or without the presence of an aqueous phase and show various structures [70]. Anhydrous gels are prepared by heating the mixture of organogelator and organic solvent above the melting point of the gelling molecule followed by cooling to form inverse micellar bilayers resulting in organogel formation according the solubility profile of the gelators [70, 8, 83, 84, 85]. In the case of water containing organogels, gelling molecules (often surfactants) are first dissolved in the organic solvent. Then, aqueous phase is added to the apolar solution resulting in the formation of reverse micellar structures. Hydrogen bonds form between the polar solvent and polar head of the surfactants within the reverse micellar structures. Hence, the reverse micellar structures immobilize the organic solvents. The further addition of water produces tubular structure elongation and entanglement, as a consequence a 3-D network is formed (Figure 1.11) [70].
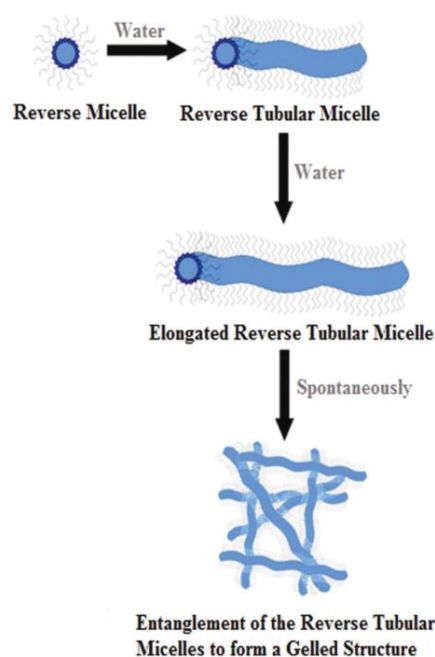
Figure 1.11 Mechanism of fluid matrix organogel formation [70].

As described before, fluid matrix organogels are made of transient networks, so they typically exhibit a liquid-like viscoelastic behaviour and enhanced elasticity on short time scales [9].

The third mechanism of organogels formation explains *in situ* cross-linking of solvated polymeric organogelators via covalent bonds and/or ionic interactions which results in solvent immobilization within the cross-linked polymeric network (Figure 1.12). The

presence of the solvent within the polymeric structure increases gel stability and prevents the structure from collapsing [70].
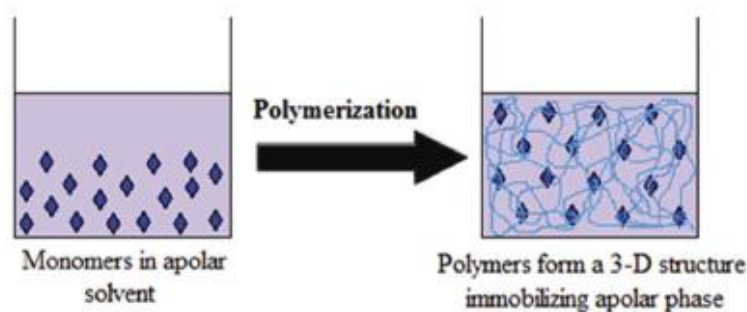
Figure 1.12 Mechanism of polymeric organogel formation [70].

The method of cross-linking may be either chemical or physical [70, 8]. In the case of physical entangled chain networks, polymeric gelators behave similarly to their LMW counterparts, solidifying organic solvents based on physical intermolecular interactions [8].

1.4 Organogelator molecules

Nowadays, the discovery of molecules able to gel organic solvents is still achieved by serendipity or via trial and error procedures [8, 71]. Prediction of the gelation potential of a given molecule could be possible by investigation of its propensity towards chemical or physical intermolecular interactions, even if generalizations are up to now not possible.

Many factors such as steric effects, rigidity, and polarity can affect the molecule tendency to aggregate [8]. The ability of a given organogelator to gel a solvent is believed to be a balance between the solubility and insolubility of the organogelator within the solvent: on the one hand, a gelator molecule should be relatively insoluble in order to crystallize or self-assemble to form mesoscale structures, on the other hand, the gelator must be relatively soluble in order to interact with solvent molecules [71]. In other words, if the gelator is too soluble in a given solvent, a solution instead of a gel will be formed, if the gelator is too insoluble, it will not interact with the solvent and will form a precipitate instead of a gel [71].

Organogel formation by means of a given gelling molecule is also strongly determined by the process of preparation, indeed a given precursor can have different process-dependent pathways of assembly (Figure 1.13) [50]. For instance, the formation of fibres can be described as a consequence of inhibited precipitation and, as such, could not represent the thermodynamic minimum, but rather a kinetically trapped structure [50, 86].
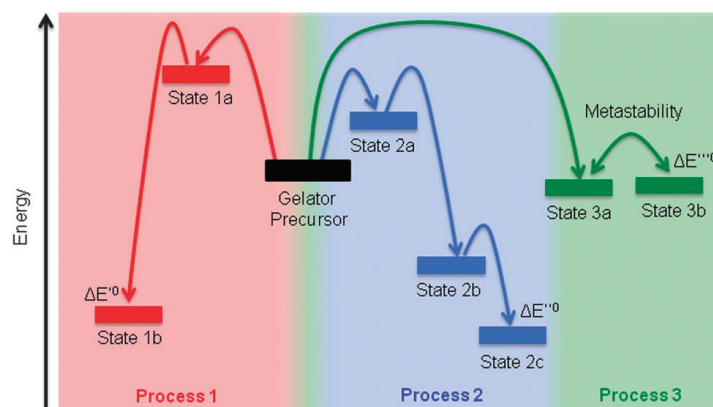
Figure 1.13 Schematically shown of process-dependent pathways of gelator assembly [50].

A wide array of discovered organogelators will be listed and described below.

1.4.1. LMOGs

Figure 1.14 shows some classes of LMW molecules able to gel organic solvents.
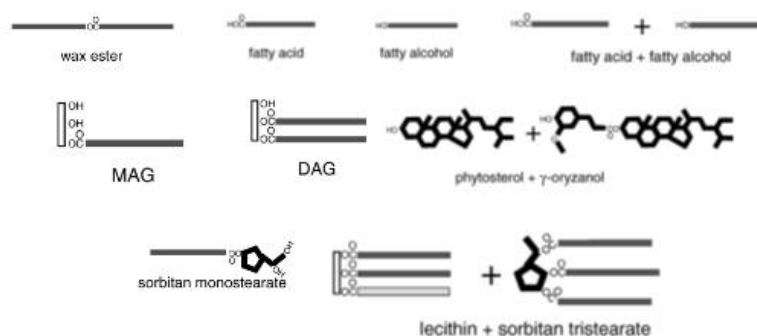
Figure 1.14 Schematic representation of some classes of LMOGs [87].

n-Alkanes have been defined as the simplest organogelators in existence [71]. It is well-known from petrochemical literature that the crystallization of paraffin can cause the undesirable thickening and gelation of crude oil [71, 88]. Abdallah and Weiss [15] investigated the gelling properties of long-chain *n*-alkanes, such as *n*-tetracosane (C-24), *n*-

octacosane (C-28), *n*-dotriacontane (C-32) and *n*-hexatriacontane (C-36). The authors found that the minimum concentration necessary for gelation decreased with an increase in the chain length of the *n*-alkane, whereas the gel stability increased with an increase in the chain length. Long *n*-alkanes, with chain length varying from 24 to 36 carbon atoms, are able to gel short-chain *n*-alkanes and several other organic solvents by means of only weak physical interactions. As far as this class of organogelator is concerned, only van der Waals forces play a role in organogelation, while hydrogen bonding is not relevant as organogelation mechanism [8, 15]. *n*-hexatriacontane form micro-platelet crystals during crystallization, following two-dimensional growth patterns of aggregates, as schematically shown in Figure 1.14 [8, 71, 15].
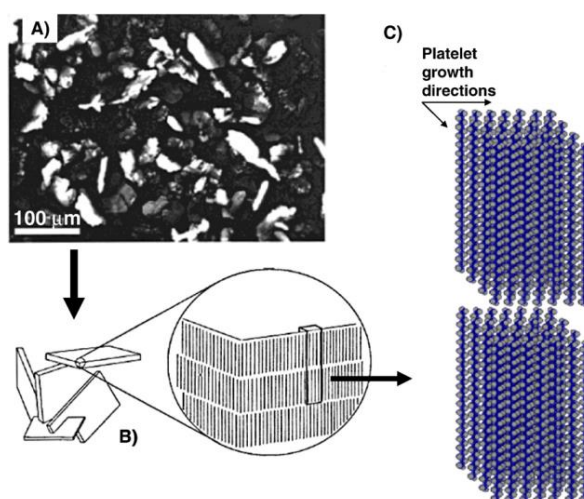
Figure 1.14 A) optical micrograph of a *n*-hexatriacontane organogel in octanol, B) schematic representation of micro-platelets, C) depiction of the lamellar orthorhombic molecular packing inside the platelets [8].

Waxes are fatty substances containing long hydrocarbon chains with or without a functional group (alcohol, ester, ketone or aldehyde). Wax esters derived from plants, insects, marine animals and petroleum are used nowadays in various industrial applications such as cosmetics, lubricants, inks and food products [89]. Toro-Vazquez et al. demonstrated that candelilla wax is able to structure vegetable oils such as safflower oil at concentrations as low as 2%$_{wt/wt}$ [90, 71]. Candelilla wax is a complex mixture of high-melting alkanes (C$_{29}$ to C$_{33}$), sterols, fatty alcohols, fatty acids and waxy esters, with predominantly odd-numbered hydrocarbons. It has been shown that at least one component of candelilla wax, the *n*-alkane hentriacontane, possess organogelling ability [71]. Candelilla wax organogels are characterised by the presence of micro-platelets formed by

n-alkanes and all impurities act as crystal habit modifiers [71, 91]. Candelilla wax/safflower oil gels are thermoreversible: it has been shown that identical thermal parameters can be obtained over several melting/crystallization cycles [71, 90]. Both thermal and rheological parameters are sensitive to the applied cooling rate, with crystallization enthalpy and temperature of gelation decreasing at higher cooling rate [71, 91]. It was also shown that the application of shear had an effect on the microstructural morphology and rheological properties but not on the thermal properties of the organogels [71]. Recently, it has been suggested that waxes can act as triacylglycerol crystals modifiers. The development of such crystallized mixed systems ought to have implications in the microstructural organization and therefore in the thermo-mechanical properties of organogels [89]. Toro-Vazquez et al. [92] investigated the effect of tripalmitin crystallization on the thermo-mechanical properties of candelilla wax/safflower oil organogels.

Rice bran wax is a natural plant wax derived from rice bran, which is a by-product of rice milling [89]. Rice bran wax contains long saturated fatty acids esterified to fatty alcohols. Fatty acids of rice bran wax are even-numbered molecules with carbon chain length from C_{16} to C_{32} and fatty alcohols range from C_{24} to C_{38}. Both provide strong hydrophobic character while the ester functionality in the centre of the molecules provides the hydrophilic character [89]. This molecular structure with very long hydrocarbon chains develops strong intermolecular interactions resulting in the formation of organogels with unique crystal morphology and physical properties [89, 93]. Dassanayake et al. [94] reported that at ambient temperatures an amount as low as 0.5 %$_{wt/wt}$ of rice bran wax is sufficient to form organogels. According to the same authors, both the hardness assessed by penetration depth measurements and the rate of formation of organogels from rice bran wax are higher than the ones obtained using other typical plant waxes [94].

Carnauba wax is obtained from the leaves of the Brazilian palm *Copernicia prunifera* and contains approximately 1%$_{wt/wt}$ hydrocarbons, with approximately 40% aliphatic esters. Carnauba contains also a high proportion of unesterified alcohols (12%), ω-hydroxy esters (14%) and esters of hydroxylated cinnamic acid (30%). Carnauba wax form gels at the relatively high minimum concentration of 4.0 %$_{wt/wt}$ [71].

Daniel and Rajasekaran [95] investigated the structuring potential of saturated wax esters, such as behenic acid esterified with 14–22 chain length alcohols, in edible oils, essential oils and hydrocarbons. Organogelling capabilities of saturated wax esters are similar to those of their fatty acids counterparts.

Fatty acids and fatty acid salts have been described as the prototype for structuring oil phases [87]. Gandolfo et al. [96] investigated palmitic, stearic, arachidic and behenic acid and found that the minimum concentration for gelation of sunflower oil at 5°C is 2%wt/wt. Daniel and Rajasekharan [95] studied a wider range of fatty acids and showed that an increase in the chain length of the fatty acid reduced the minimum concentration required to structure oil, even though this concentration does not decrease much further with chain lengths up from 31. The authors also elucidated the role of several functional groups in structuring: dicarboxylic acids such as adipic, suberic and sebacic acids were more efficient at gelling vegetable oils than monocarboxylic acids of the same chain length, but these dicarboxylic acids were not able to gel hydrocarbons [95, 71]. Moreover, the substitution of a hydroxyl group at position 12 of stearic acid to give 12-hydroxystearic acid (12-HSA) resulted in a 100% increase in the structuring efficiency of a given oil, whereas the addition of a methyl group at position 12 resulted in a decrease in the gelation efficiency [95, 71].

Hydroxylated fatty acids, such as 12-HSA and ricinelaidic acid, are promising potential oil structuring agents. 12-HSA is particularly suitable for gelling waste engine and vegetable oils as it can produce firm gels at concentrations as low as 1%wt/wt [71]. This behaviour is mainly due the morphology of 12-HSA crystals, since they show a preference for growing along a single dimension. Kuwahara et al. [97] showed that the 12-HSA molecule bends around the region where the 12-OH group is located, hence the molecule adopts a shallow V-shaped conformation and the bending induces 12-HSA molecule to fill up the free space within the crystal [97, 71]. 12-HSA crystals are fibre-like in appearance and have high aspect ratios. Crystallization in this configuration is energetically favourable because of the formation of hydrogen bonds [71]. Then, fibrillar crystals interact and form a self-assembled fibrillar network. In regard to rheological properties, 12-HSA/canola oil gels prepared with less than 0.5%wt/wt of gelator exhibit frequency-dependent behaviour, while gels prepared with higher 12-HSA concentration showed a strong gel behaviour [71].

Kirilov et al. [98] prepared a stable dispersion of organogel nanoparticles in water, using 12-HSA as organogelator. Moniruzzaman et al. [99] reported a carbon nanotube/organogel composition, prepared using 12-HSA as the gelator molecule, multi-wall carbon nanotubes as the nanofillers and 1,2-dichlorobenzene as the organic solvent. Toro-Vazquez et al. [100] investigated the organogelling properties of amides derived from (*R*)-12-HSA in safflower oil showing that the attractive interactions, such as hydrogen bonding and dipolar interactions, between amide groups and between hydroxyl groups

present in the amides resulted in the formation of organogels with high melting temperature, heat of melting and crystallization parameters.

Ricinoleic acid is also a hydroxylated fatty acid which can be thought of as the C_{18} oleic acid with an attached hydroxyl group at C_{12} [71]. The trans-isomer of ricinoleic acid, ricinelaidic acid, has also been shown to exhibit organogelling ability [71]. Like 12-HSA, upon crystallization, ricinelaidic acid forms dimers that stack to form crystalline fibres [71]. Organogel formation of ricinelaidic acid occurred with as little as 0.5%wt/wt of gelator depending on concentration, temperature and the presence of hydrogen bonding moieties in the solvent [89].

Wright and Marangoni [101] showed that as little as 2.5%wt/wt ricinelaidic acid was sufficient to form gels in canola oil at ambient temperatures. The same authors also demonstrated that at a given temperature, the G' of the gels scaled with the concentration of ricinelaidic acid in a power-law fashion [102]. The exponents of these power-law scaling relationships give an indication of the structure of the gel [71].

Fatty alcohols have also been investigated as potential LMOGs. Daniel and Rajasekaran [95] studied the gelation of sunflower oil by means of long fatty alcohols, with chain lengths in the range of 22–30. Saturated fatty alcohols showed lower gelling efficiencies compared to saturated fatty acids of the same lengths in various oils.

Gandolfo et al. [96] found that the fatty palmityl, stearyl, arachyl and behenyl alcohols provide firmness to sunflower oil at concentrations above 2%wt/wt at 5 °C. In oils rich in saturated fatty acids, such as soybean oil or olive oil a synergistic effect between the oil and the fatty alcohol used as gelator was observed: fatty alcohols gave harder products than fatty acids at the same concentration, with the exception of palmitic acid [96]. Schaink et al. [103] demonstrated that stearyl alcohol structures the oil by means of thick crystals with an orthorhombic packing and orthogonal chain stacking.

Long-chain fatty acids and fatty alcohols can not only structure edible oils by themselves but also in combination [87, 89, 71]. Gandolfo et al. [96] studied the organogelation of vegetable oils using mixtures of fatty acids and fatty alcohols with the same chain length. They showed that mixing fatty alcohols and fatty acids of the same chain length induced a synergistic effect which led to a more elastic gel in comparison to gels formed by pure components. This was most evident in mixtures of stearyl alcohol and stearic acid at ratios of 7:3 [96, 71, 95]. Examination of the microstructure of these gels showed the presence of platelet crystals of about 200μm along the longest dimension

(Figure 1.15) [96, 71]. X-ray diffraction measurements of fatty acid/fatty alcohol organogels showed that both compounds formed mixed crystals [103]. Gels containing only stearic acid formed lamella composed of a double layer of stearic acid molecules, while stearyl alcohol formed lamella composed of both double and triple layers of stearyl alcohol molecules [71, 103]. On the contrary, in a mixture of stearyl alcohol and stearic acid, molecules were packed in a double layer arrangement with very minimal tilting. The sub-cell packing of the mixed crystals was found to be triclinic, hence mixed crystals were more thermodynamically stable than crystals formed from pure compounds [103].
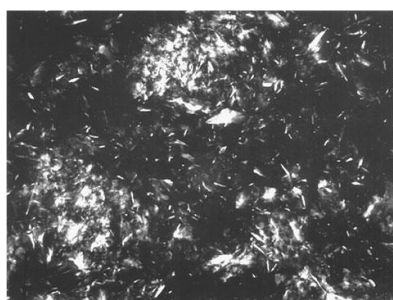
Figure 1.15 Polarized light micrograph of crystals of 7:3 stearyl alcohol:stearic acid mixture in sunflower oil [96].

Monoacylglycerols (MAGs) are polar lipid emulsifiers widely used in food products [89, 104]. MAGs are among the rare components that can structure both organic and aqueous phases [87, 106, 105]. MAGs are able to self-assemble into numerous structures (including lamellar, micellar, cubic and hexagonal mesophases) due to their amphiphilic character [73]. Crystallization of MAGs in water involves polymorphic transformation from lamellar liquid-crystalline state (L_α) to α-gel to the so-called coagel, in which MAG molecules form plate-like β-gel crystals [89, 107]. MAGs are thought to form reversed bilayers in vegetable oils (Figure 1.16) [87, 108]. It was proposed that the gelation mechanism involved two steps described as follows: first, a rapid crystallization in lateral direction occurs after formation of a nucleus of MAGs crystals, forming the first space filling network, then stacks of crystalline bilayers resulting in the reinforcement of the network [89, 107].

Ojijo et al. [108] demonstrated that mixtures of monopalmitin and monostearin are able to form networks in olive oil under quiescent cooling at low concentrations [87]. The authors also proposed a staged crystallization mechanism to explain the increased firmness observed in gels subjected to faster cooling: at low cooling rates, the first crystallising

MAGs form a "backbone" network, on which the remaining MAGs deposit subsequently; at high cooling rates numerous fine crystals are formed in a single crystallisation step [108, 87]. Crystallisation in stages leads to more weak spots, increasing firmness failure, while increasing gel resistance to small deformations [87].

The formation of organogels from MAGs is a process influenced by thermal, mechanical or chemical treatments [89]. For proper gel formation, the amounts of non-ionic and anionic surfactant and of salt and pH have to be matched carefully. As an example, electrostatic interactions between added proteins and the bilayer in the lamellar phase strongly stabilize the α-gel state [89]. In addition, the application of shear at or above the gel point for quiescent crystallisation leads to finer homogeneous gels at lower temperatures. This suggests that shear disturbs the initial stage of crystallisation for example by modifying the mesophases present above the melting temperatures of the crystallites [87]. During weeks of storage with temperature cycling, the firmness of these networks increases, while the melting onset decreases and no increase in crystallinity is observed, thereby a reorganisation of the network building blocks occurs [108].
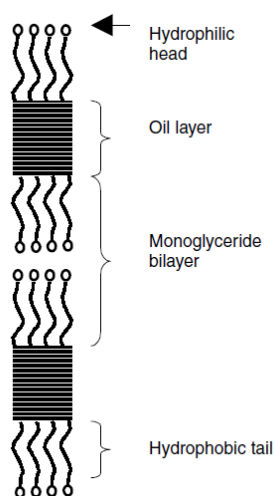
Figure 1.16 Schematic representation of MAG reverse lamellar bilayers in vegetable oil [107].

Diacylglycerols (DAGs) have also been investigated as potential organogelators. Dipalmitin and distearin form crystal networks in a relatively similar way as triacylglycerols (TAGs), even though DAG gels are slightly soft compared to TAG crystal networks of similar concentration [87].

Sterol derivatives are often reported in the literature as common low molecular mass organogelators [71]. Recently, phytosterols have been extensively studied as lowering

agents of LDL serum level, a risk marker for cardiovascular diseases [71, 109]. Organogels can be produced using mixtures of the sterol ester γ-oryzanol and a phytosterol such as dihydrocholesterol, cholesterol, β-sitosterol, cholestanol and stigmasterol. Organogelling properties of the mixture are affected by the type of sterol used, for instance ergosterol and 5α-cholestane are not able to form gels [71, 110].

Organogels formed by an equimolar mixture of β-sitosterol and γ-oryzanol have optimal properties, such as rapid gelation and nucleation/crystallization, high firmness and high melting point [71]. According to a molecular energy minimisation calculation (Figure 1.17), γ-oryzanol and β-sitosterol molecules dock their sitosterol units on top of each other, with the ferulic acid moiety of the γ-oryzanol sticking out. The stacking on a molecular scale does not predict how many of these molecules assemble, but the slight wedge shape of the stacked molecules suggest the formation of a curved supramolecular structure [87]. Microstructural studies showed that sterols and sterol esters self-assemble into nano-scale hollow tubules (diameter ranging from 6.7 to 8.0 nm and wall thickness of the tubule between 0.8 and 1.2 nm) in vegetable oils. The most likely growth mechanism for these tubules would be via a helical ribbon, with the wall spirals along the central axis [89]. Tubules, only formed when both sterol and sterol ester are present, create a space-filling network which entraps the solvent. In the absence of either component, sterol or sterol ester crystals are formed but these crystals do not form a gel network [71].
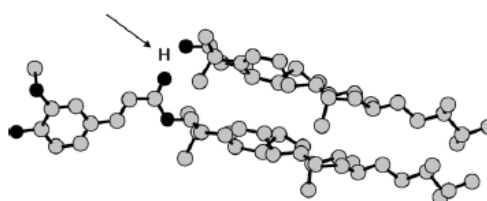
Figure 1.17 Stacking of sitosterol and oryzanol mixture based on an energy minimisation calculation [87].

Ceramides belong to a subclass of lipids called sphingolipids. Sphingolipids are similar to acylglycerols except that they contain the amino alcohol sphingosine instead of the polyhydroxy alcohol glycerol. Ceramides are formed via the amidation of a fatty acid into the amine group of sphingosine [71]. Rogers et al. [72] have reported the organogelation of vegetable oils using chemically synthetized and enzymatically converted egg ceramide sphingolipids. The chain length of the fatty acid moiety of ceramides was found to affect the gelation capability of these molecules. Unlike the majority of organogelators, shorter

fatty acid chain lengths in ceramides were found to result in more efficient organogelation [71, 72]. Rogers et al. [72] showed that translucent ceramide/canola oil gels were formed at concentrations as low as 2.0%$_{wt/wt}$ using synthetically pure ceramide, whereas opaque gels were produced using an enzymatically converted egg sphingomyelin in canola oil at 5.0%$_{wt/wt}$. From a structural point of view, morphology of ceramide organogels is typically fibrillar or needle-like [71, 72].

Peptides are very promising structuring agents, since a large diversity of structures seems capable of gelling oil, including dipeptides of phenylalanine and dendrimers of L-aspartic acid and succinic acid [73, 111, 112]. The dipeptides of phenylalanine self-assemble into long fibres stabilized by π–π interactions of the aromatic groups. Similarly to ceramides organogels, fibres are then capable of forming a continuous network (SAFIN) [73].

Enzymatically derived sugars with long fatty acids chains esterified onto trehalose are able to structure olive oil at very low concentrations [73]. In order to immobilize vegetable oil, the trehalose must be esterified to a long hydrocarbon chain with a minimum of 10 carbons. According to John et al. [113], trehalose disaccharide was capable of immobilizing vegetable oil at less than 1% gelator.

Lecithin organogels are very interesting systems for drug delivery and cosmetic applications, owing to the biocompatibility of the gelling molecule. Owing to its amphiphilic structure, lecithin is able to assume many different forms such as mono- and bi-molecular films, vesicles or liquid crystals. When mixed with organic solvents, lecithin forms isotropic reverse-micelle solutions. When small amounts of polar solvents are added to the solution, cylindrical reverse micelles start to grow until they entangle into a gelling network (Figure 1.18) [8]. This mechanism of network formation was proven by infrared spectroscopy studies showing a low-frequency shift of the $P = O$ vibration band for lecithin molecules upon gel formation, indicating the involvement of the phosphate group in H-bonding with the added polar solvent. In terms of organic solvents compatible with gel formation, Scartazzini et al. [114] found that the more apolar solvents such as alkanes, followed by cycloalkanes, allow a higher state of structural organization of the lecithin molecules, leading to the formation of more stable gels. Although slight variations occurred for certain other organic solvents, the evolution of the lecithin systems structure upon addition of a polar solvent is a constant [8].
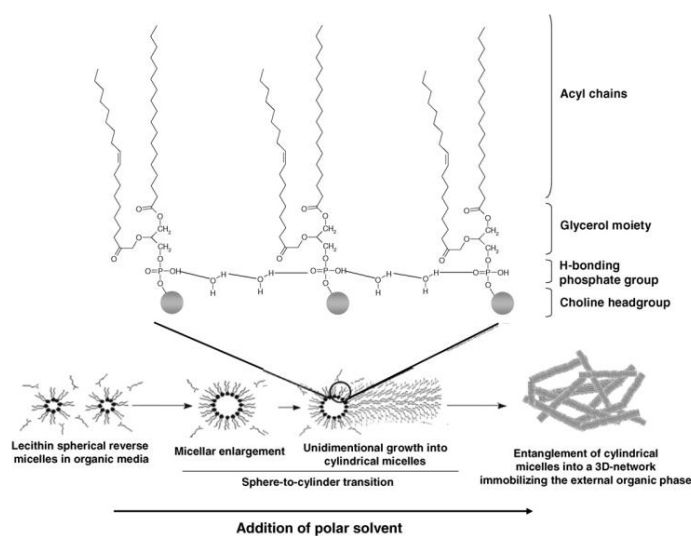
Figure 1.18 Formation of 3D network of reverse cylindrical micelles in lecithin organogels [8].

Sorbitan monostearate (SMS) is a hydrophobic non-ionic surfactant that forms organogels in several organic solvents and vegetable oils [89]. Murdan et al. [115] demonstrated that SMS molecules self-assemble into toroidal inverse vesicles at the gelation temperature. Upon further cooling, conversion of the toroids into rod-shaped tubules occurs. Tubules then associate with others and a three-dimensional network is formed immobilizing the solvent. SMS organogels are opaque, thermoreversible semi-solids, stable at room temperature for weeks [89].

Sorbitan monopalmitate (SMP), often referred to as Span 40, belongs to the same surfactant family. SMP forms opaque, thermoreversible, semi-solid organogels with organic solvents and the microstructure is composed of an interconnected network of rod like tubules. SMS and SMP organogels and SMS/SMP organogels containing niosomes have been described as promising systems as potential delivery vehicles for drugs and antigens [89, 116, 117].

Pernetti et al. [118] studied the structuring of vegetable oils using a mixture of unpurified lecithins and sorbitan triesters. Structuring of vegetable oil was achieved with a mixture of sorbitan tristearate (STS) at a minimum structurant concentration of $4\%_{wt/wt}$. Micrographs of the lecithin-STS gels showed that the gel was structured by a dispersion of needle-like crystals with an average length of approximately $10\mu m$ [118]. It was concluded that lecithin acted as a crystal morphology modifier and possible co-crystallization of the lecithin with STS led to the needle-like STS crystals morphology. A synergistic effect was

observed with mixtures at specific ratios of lecithin/STS, between 40:60 and 60:40, when firm organogels in edible oil were obtained [89, 118].

Romoscanu and Mezzenga reported the formation of an oleogel by drying a cross-linked protein-stabilized oil-in-water emulsion [119]. The authors produced a space-filling emulsion of very mono-disperse protein-stabilised droplets and subsequent cross-linked the proteins at the droplet interface. After the addition of 0.5%$_{wt/wt}$ glycerol, the emulsions were allowed to dry, leading to the formation of a high internal phase emulsion that created a foam of protein lamella in a continuous oil phase. The final gel is transparent and exhibits a weak frequency dependence of the elastic properties, in agreement with strong gel behaviour. Droplets can be re-dispersed on rehydration, as they dissociate again. The reversibility of the process is better for very pure oils, and less in edible oil [118, 87].

Among protein based organogelator, a simple amphiphilic LMOG based on N^{α}-acetyl-N^{ε}-lauroyl-*L*-lysine and its alkali metal salts was synthetized by Suzuki et al. [120]. All molecules containing two *L*-Lysine derivatives linked to alkene chains through amide bonds are referred to as gemini organogelators.

Aromatic-linker-steroid (ALS) organogelators are a novel but wide family of cholesterol-based systems. The organogelators in this class have an aromatic moiety, which is bound to a steroidal group through a linker group (Figure 1.19) [70, 2]. According to the nature of these three groups, ALS organogelators can immobilize a wide range of solvents including polar and apolar solvents. The chemical nature of the aromatic group, as well as the length and flexibility of the linker group, has a large impact on solubility and, in turn, on the gelation ability of the molecule [70]. During self-aggregation of these gelators, the aromatic-aromatic and steroidal-steroidal groups stack among themselves and extend unidirectionally resulting in the formation of a helical array of unit fibres. As an example, cholesteryl 4-(2-anthryloxy) butanoate (CAB) and its analogues and derivatives readily form SAFINs in organic solvents [70, 121].
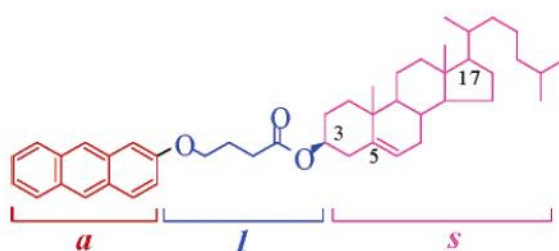
Figure 1.19 Schematic representation of an ALS molecule [2].

Dimeric cholesterol-based derivatives A(LS)$_2$, with the aromatic moiety located two linker and steroid groups, have also been reported as potential organogelators [70, 122].

Novel organometallic cholesterol derivatives have been synthesized to be used as organogelators. The organometallic moiety can consist of derivatives of ferrocene, titanocene, copper, zinc, rhodium, iridium and palladium [70].

Bile acids, such as cholic acid and chenodeoxycholic acid, are vital biosurfactants produced by the liver that help in digestion of food by emulsifying fats. Conjugation of bile acids with aminoacids produces bile salts. These structural components with the addition of some functional groups impart organogelator capabilities. Gelation of organic solvents can be achieved by derivatives of bile acids bearing an aromatic group at the C3 position and simple esters of cholic acid and allyl cholate [70].

Sugar-based organogelators can be identified by the presence of α-glucose and an aromatic moiety in their structure. Their capacity to aid in the formation of fibrillar structures is associated with the intermolecular hydrogen bonding amongst the sugar moieties and subsequent exposure of aromatic moieties to the apolar solvent. Such organogelators are derived from monosacharides such as D-sorbitol, D-glucose, D-galactose, D-mannose, D-allose, D-altrose and β-cyclodextrin. Organogelators in this category include derivatives of methyl glycosides of 4,6-O-benzylidine and 4''-butoxy-4-hydroxy-*p*-terphenyl-β-d-glucoside (BHTG) [70, 123].

1.4.2 Polymeric organogelators

Polymeric organogelators can either undergo chemical reaction or physical interactions to form a network structure. Conventionally polymeric organogelators form irreversible gels by entanglement of covalently-bonded chains in their 3-D network. Development of organogels using polymeric gelators is more difficult than using LMOGs because the density of cross-linking points is significantly less for polymeric gelators. Nevertheless, some examples of polymeric organogelators have been reported in the literature, such as supra-molecular polymers formed from L-lysine derivatives, polyethylene, polycarbonate, polyesters, polyethylene glycol, ethyl methacrylate and methacrylic acid co-polymers [70].

Since the majority of food biopolymers are hydrophilic molecules, to date the only polymer reported as suitable for the gelation of vegetable oils is ethyl cellulose. Ethyl cellulose has also been found to form gels in other hydrophobic solvents [71]. Dey et al.

[124] studied a system composed of ethyl cellulose as organogelator and a food surfactant as plasticizer. The surfactant enhanced the dissolution of the polymer in the oil but it was found that it was not necessary for gelation. As far as the type of ethyl cellulose is concerned, the authors showed that the use of a higher molecular weight ethyl cellulose as organogelator resulted in a gel with a higher elastic modulus and yield stress. With regards to the type of surfactant used, the gel containing sorbitan mono-stearate had the highest storage modulus [124]. Laredo et al. [125] found that ethyl cellulose organogels prepared with highly unsaturated vegetable oils were stronger than gels produced using vegetable oils relatively rich in saturated fats, because the low molar volume of unsaturated oils allowed for the formation of more hydrogen bonds between the ethyl cellulose molecules [125, 71].

1.5   Methods for characterisation of organogels

Characterization of organogels involves the investigation of properties such as gelator assemblies, the eventual gelator-co-gelator interactions, the gelator-polar/apolar solvent interactions, polar-apolar solvent interactions. Temperature dependence on the gelation mechanism, thermoreversibility, viscoelastic properties, flow behavior and thermodynamic parameters of the gels may be evaluated using thermal and rheological studies [70]. Most efforts in the field of organogelation research now aim at gaining understanding of the connection between molecular structure, nano- and meso-scale self-assembled morphology and macroscopic materials properties. In the following sections, various techniques for gels analysis across the full range of length scales will be discussed.

1.5.1 Microstructural analysis

Several techniques for microstructural analysis including scanning and transmission electron microscopies (SEM, TEM), small-angle neutron scattering (SANS) and small angle X-ray scattering (SAXS) measurements and atomic force microscopy (AFM) allow many features of organogels to be deciphered at the 1-1000nm scale [123]. Sometimes combinatorial techniques are necessary, even if they are often less widely available [87].

The least complex method to analyse the microstructural features of organogels is microscopy analysis. As an example, polarized light microscopy has been used to analyse the crystalline structure of the ricinelaidic acid/canola oil organogels [102] and 12-HSA/edible oil organogels [129], the effect of storage conditions and rate of cooling on the

candelilla wax/tripalmitin/safflower oil organogels [90], and birefringence of the crystalline platelets formed by the hexatriacontane organogels [128, 70]. Light microscopy has also been used to reveal that sorbitan ester organogels consist of aggregated rod-like tubules [70].

Recently, SAXS has become an important method in determining absolute quantities such as diameters, lengths or topologies in gels. SAXS is a powerful technique to explore directly the supra-molecular structure: since the packing of fibrils and fibres within the network structure is usually irregular, solvated molecular gels generally scatter X-rays, which can be fitted to a computer model at low angles of scattering [123, 126]. Therefore, X-ray scattering analysis provides a way of understanding and visualizing the molecular-scale fibrils present in the gel. X-ray methods can also be used on the dried gels (xerogels), in which case diffraction peaks are generally observed. This can lead to a more precise understanding of the molecular packing within fibrils, although it must be taken into account that drying can lead to morphological change [126]. SAXS and SANS are often used to investigate the structural features of aggregates, their junction zones in the network, presence of hydrogen bonds and shape of fibres (circular or slightly rectangular) [70]. For example, the diameter of hexagonally-arranged cholesteryl derivative (ALS organogelator) bundles was calculated using SAXS and SANS [70, 9]. Terech et al. [127] investigated several organogelators with SAXS and found that most of the scattering data could be fitted by a randomly orientated long cylinder model.

With regards to crystal networks, standard X-ray powder diffraction is the most suitable method to identify crystal structure or polymorph. The molecular structure of crystalline particles can be investigated using X-ray diffraction (XRD) but it should be taken into account that crystal structure determination requires single crystals that are much larger than the typical crystals of lipids [87]. The second option is X-ray powder diffraction (XRPD), even if it requires high-resolution data, preferably from a synchrotron source [87, 123]. In the event that a mixture of structurants is used, XRD can reveal whether mixed crystals provide synergy or if each component forms its own particles [87, 103]. Abdallah et al. [128] used X-ray diffraction for the investigation of gel containing hexatriacontane as organogelator and hexadecane, 1-octanol glycidyl methacrylate and silicone oil as solvent. They concluded that the conformation and packing of the gelator can be known if the single-crystal diffraction or other structural analysis are available for the matching morph.

Cryo-TEM and -SEM are not quantitative techniques of analysis, but they allow the determination of the structure of the building blocks in organogels. They also allow direct investigation of the bridging elements of the network structure, provided that appropriate sample preparation methods are used [87]. Usually, the sample is first dried on a substrate under ambient conditions or *in vacuo* and then coated under vacuum with a thin metallic layer. The gel structure collapses on itself during drying, leading to the formation of a xerogel. Changes in the nanostructure could occur during drying, however it is often assumed that such effects are negligible [126]. A wide array of morphologies have been observed using SEM, in particular nanofibres, tapes, ribbons and tubules (Figure 1.20) [126, 71].

TEM can also be applied to gel imaging, although it is often necessary to apply a heavy metal staining agent to improve image contrast [126]. In any case, it should be noted that the technique used could influence the morphology, crystallisation and polymorphism, especially when small amounts of sample are put between glass or polyethylene layers or when the solvent has to be removed [87].
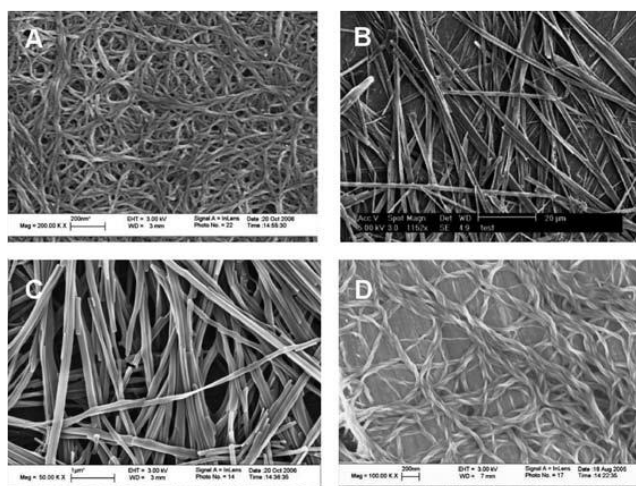
Figure 1.20 SEM images of organogels showing (A) fibrillar, (B) tape-like, (C) rod-like and (D) helical ribbon gelator morphologies [126].

Palui et al. [130] investigated the properties of organogels developed from different dendritic self-assembling peptides, using field emission scanning electron microscopy (FE-SEM) and atomic force microscopy (AFM). They proved that the network structure was composed of dendrimers with a size range of 30–200 nm, according to the type of dendrimer used [130, 70]. Duffy et al. [131] hypothesized that the triacylglycerols of edible oils were incorporated in tubules formed by γ-oryzanol and β-sitosterol phytosterols, based

on results obtained from bright field and phase contrast microscopy, confocal laser scanning microsopy, TEM and cryo-SEM.

Spectroscopic techniques, such as NMR and FTIR, provide information on the various chemical interactions that occur in organogels and can be helpful in studying the morphology, molecular structure and component dynamics of organogel networks. Shchipunov and Shumilina [132] demonstrated the crystalline and non-birefringent nature of lecithin organogels using NMR spectroscopy, while FTIR spectroscopy has been used to determine the intermolecular interactions amongst individual components present within the gel. Generally speaking, infrared spectroscopy is very useful for proving hydrogen bond interactions between the molecular building blocks. In particular, O-H, N-H and C=O stretches all show distinctive responses to hydrogen bonding. Van der Waals interactions can also be detected by investigating changes in C-H stretching interactions. Typically, it is necessary to compare IR spectra of the organogelator in both the sol and the gel state in order to determine the key non-covalent interactions. Variable temperature IR measurements can be useful to probe the response of these interactions to temperature changes [126, 133].

Fluorescence spectroscopy could also be used in the event that organogelators include fluorochromes, since these molecules can exhibit changes in their spectra on aggregation. For instance, many fluorochromes emit as excimers when in close proximity, such as in a gel fiber, but emit as monomers when present in dilute solution. In pyrene-containing oligo(glutamic acid)s organogels, excimers were present in the sol, but not in the gel [126, 134]. Fluorescence can also detect smaller changes associated with differences in polarity between the organogelator in aggregated and non-aggregated states. Therefore, fluorescence can be a useful technique to determine which spectral features are responsive to the aggregation process [126].

NMR spectra provide information on the chemical nature and on the molecular or collective mobility of an observed component. In most cases, attention is paid to the analysis of the variation of chemical shifts, spin relaxation times, or intensity of the NMR signals along with concentration, solvent composition, or temperature. Those data can be used to gather information on the nature of the intermolecular interactions, the critical organogelator concentration values, the change in the motion of the molecules or thermodynamic parameters associated with the gel formation [10]. In order to facilitate the study of molecular gels, NMR experiments are often performed on soft solids/partial gels

or on samples at temperatures just above gelation point. Under these conditions of concentration and/or temperature, the hierarchical assembly is at the initial stage (rather than fully formed network) and NMR is therefore very suitable for monitoring the way in which one molecule interacts with another to form an assembled structure [126].

In NMR titration experiments, NMR spectra are recorded at increasing concentration of organogelator. As the concentration increases, the NMR spectra should broaden due to gel formation and decreased gelator mobility. However, the NMR peaks should also shift, especially when non-covalent interactions between molecules occur. For example, N-H protons are often observed to shift downfield as gelator concentration increases, indicating that these peaks become increasingly involved in hydrogen bond interactions [126].

In variable temperature NMR experiments, NMR peaks shift at increasing temperature, due to the increased gel mobility. Therefore, molecule interactions tend to weaken and peak shift is associated with the breakage of hydrogen bonding and π-π interactions [126].

Nuclear Overhauser Enhancement (NOE) experiments can provide information on the way in which one molecule interacts with another through space and this can help to describe the interactions present within a gel. Finally, relaxation time experiments performed on the broadened peaks at known concentrations can be used to estimate the molecular mobility of the aggregated species [126].

More sophisticated experiments, such as magic angle spinning (MAS), multiple-quantum (MQ) spectroscopy, as well as pulse field gradient (PFG) technique and magnetic resonance imaging (MRI) can provide detailed information about molecular organization, specific interactions and internal mobility of gel constituents [10].

1.5.2 Macroscopic behaviour: rheological and thermal analysis

The least complex method to confirm organogel formation is to carry out the inverted test-tube method. After homogenizing the solvent and the organogelator at high temperature, the gel is allowed to form into the test-tube and then the test-tube is inverted. If the contents of the test-tube flow, the system is regarded as sol (or maybe a weak organogel), whereas if the contents of the test-tube do not flow the system is regarded as a true organogel [70].

According to the dropping ball method, a small metal ball is placed on the gel and the dropping of the ball through the gel is observed. Ideally the ball should be immobile in the gel but drop rapidly in the sol, therefore the temperature of gelation at any given concentration of gelator can be determined. Since the yield stress is determined by the

density of the ball and its radius, the ball must be kept constant across the experiment in order to ensure that data can be comparable. The sample tube should also be significantly larger than the ball, otherwise the presence of the nearby walls can affect the motion of the ball. Schrader's relationship can be used to generate plots of logarithm of gelator concentration against the reciprocal of gelation temperature, in which the gradient is equal to $-\Delta H/R$, where ΔH can be approximated to the enthalpy associated with the gel–sol transition [126].

Rheological characterization is useful in unfolding the physical properties of organogels, such as viscosity, viscoelasticity, and mechanical strength [70]. In typical small amplitude oscillation tests, the magnitudes and ratios of the elastic (G') and loss (G'') moduli are determined [126]. Generally speaking, the investigation of rheological or dynamic parameters allow the rheological properties of organogels to be explained. Dynamic moduli are related to the storage of elastic energy and dissipation of viscous energy, respectively. By using these parameters, the curves of complex modulus G* and complex viscosity η* can be evaluated [70]. In addition, consistency parameters, including the yield value, loss angle, and viscosity, can be estimated from rheological studies. The flow properties can be generally investigated with the viscosity functionality with imposed stress or strain. As an example, the complex modulus and the consistency parameters affect the "rubbing" or the "picking-up" parameters of the semi-solid formulations for drug delivery and biomedical applications which can influence the resident period on the application region and medication absorption when applied topically or transdermally [70].

Molecular organogels can be classified rheologically as cellular solids, fractal or colloidal systems or soft glassy materials, according to their behaviour [126].

Small oscillation rheological tests are well suited for investigating the viscoelastic characteristics of organogels and also to study the gelation and melting of organogels. Three types of dynamic tests can be performed in the linear viscoelastic regime in order to measure useful properties of organogels and to evaluate gelation and melting points: in frequency sweep tests G', G'' and the loss tangent are obtained as a function of frequency at fixed temperatures, in temperature sweep tests dynamic moduli and the loss tangent are determined as a function of temperature at fixed frequency, whereas time sweep tests allow the measurement of G', G'' and loss tangent as a function of time at fixed frequency and temperature [135]. Many authors have reported the above-mentioned tests to describe the rheological characteristics of various organogels, for example, 12-HSA/canola oil organogels [136], ricinelaidic acid/canola oil based organogels [102], mixture of γ-

Oryzanol and β-sitosterol/sunflower oil based organogels [110], monoglycerides/safflower oil based organogels [137].

Temperature is a significant parameter affecting organogel rheology. On the whole, with the rise in temperature, there is a resultant decrease in viscosity and in dynamic moduli values. This pattern can be ascribed to an increase in the kinetic energy among the fibres in the network structure thus weakening their interactions. If the temperature is increased further beyond a critical temperature, complete disruption of the network happens, causing the organogel to flow. Physical organogels are thermoreversible and have the capacity to recapture their highly viscous state once cooled below the critical temperature [70]. As an example, Pernetti et al. [118] investigated mixture of 50:50 STS:lecithin/edible oil based organogels. The authors used temperature-dependent rheological measurements in combination with polarised light microscopy to prove that the lecithin helps to create a weak interaction between the crystals, whereas STS crystals themselves have no tendency to aggregate (Figure 1.21) [87].
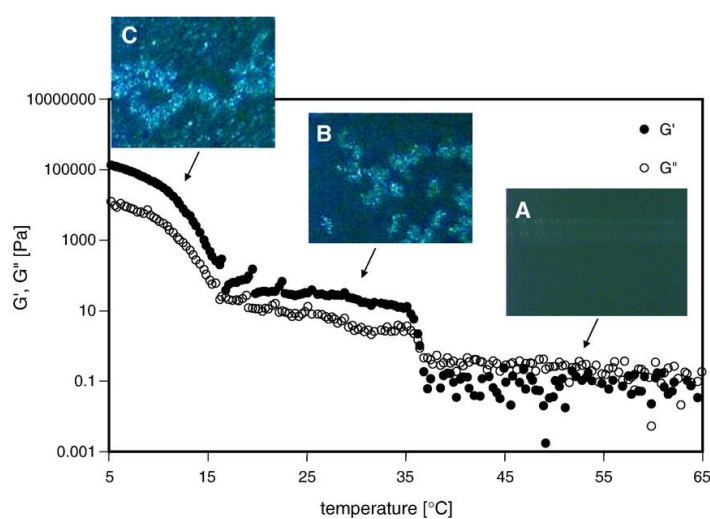
Figure 1.21 Rheological profile over temperature and polarised light micrographs of 50:50 STS:lecithin based organogel [87].

Evidently, rheological studies of organogels may provide a deeper knowledge of the relationship between organogelator structures on the molecular scale and the macroscopic mechanical properties of the self-assembled material.

With regards to thermal characterisation of organogels, differential scanning calorimetry (DSC) and differential thermal analysis (DTA) investigation report organogel thermal transitions in terms of exo- and endo-thermic peaks, respectively [70]. In more

detail, in DSC the difference in the amount of heat required to increase the temperature of the sample and a reference is measured as a function of temperature. When the sample undergoes a physical transformation, such as a gel–sol phase transition, more heat is needed in comparison to the reference in order to maintain both at the same temperature. The difference in heat flow associated with this endothermic phase transition allows the measurement of the amount of heat absorbed or released by integration of the DSC trace. In this way, a direct measurement of the phase-change enthalpy ($\Delta H_{gel-sol}$) is obtained and can provide an insight into the thermodynamics of the gelator–gelator interactions.

DSC should be performed in both heating and cooling modes in order to evaluate both endothermic and exothermic transitions and assess the thermo-reversibility of the gel–sol phase transition [126]. DSC data are also used as an indicator for the amount of solids in the gelled system and to identify if polymorphic transitions in crystalline networks occur [87].

Thermal analysis has been utilized in the investigation of organogels comprising γ-oryzanol and β-sitosterol [110], rice bran wax, carnauba wax and candelilla wax [94], candelilla wax and tripalmitin [138].

1.6   Modelling properties and structuring of organogels

1.6.1 Fractal model for fat crystal networks [139]

For most soft fat materials, textural properties are determined by the solid component of the system, which exists as a three-dimensional colloidal fat crystal network. Upon crystallization, fat crystals aggregate and grow into clusters, then flocs finally resulting into a network structure formation.

The shear elastic modulus G' obtained from small oscillation rheological measurements has been found to be a suitable indicator of the hardness of the material, as well as being sensitive to the microstructure of the system. The rheological properties of fat crystal networks result from both the volume fraction of solids and the micro-structural features of the network, including shape, size and spatial distribution pattern of crystals. In order to fully understand and eventually predict the macroscopic properties of soft materials, it is necessary to define and investigate all levels of structure (Figure 1.21) and their relationship to macroscopic mechanical properties.
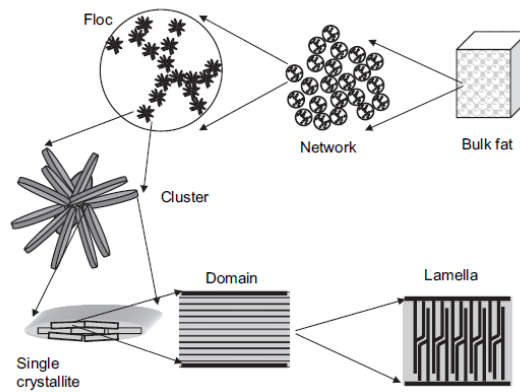
Figure 1.21 Structural hierarchy in fat crystal networks [138].

The first model used in the study of colloidal fat crystal networks was the linear chain model, proposed by Van den Tempel [140]. According to this model, fat structure can be described as flocculated solid particles of colloidal dimensions embedded in a liquid phase. The three-dimensional network is formed via aggregation of the dispersed particles, held together by irreversible primary bonds and reversible secondary bonds. These particles form linear chains, which eventually form the fat crystal network. In the linear chain model, the shear modulus, G, is predicted to be directly proportional to the volume fraction of solids, Φ:

$$G = \frac{5A\Phi a^{0.5}}{24\pi H_0^{3.5}} \tag{1.6.1}$$

where A is Hamaker's constant, H_0 the interparticle distance and a the particle size, in the hypothesis where the geometry of particles is between that of spheres and cubes.

Nevertheless, experimental results showed that modulus G increases in a power law fashion as function of Φ, hence several later studies attempted to modify the model by introducing an intermediate level of structure between the primary fat crystals and the infinite network. Van den Tempel [141] himself proposed an "extended" linear chain model, describing the linear chain as composed of crystal aggregates instead of primary crystals. Hence, the shear modulus G was calculated as follows:

$$G = G_{th} \frac{nD_a}{Na} \tag{1.6.2}$$

where G_{th} is the modulus calculated according to the linear chain model, n is the number of connecting chains between two neighbouring aggregates, N is the average number of primary particles in an aggregate, D_a is the average diameter of an aggregate, and a is the average primary particle diameter. This model has not been broadly adopted since it could

not explain successfully the scaling behaviour between the elastic shear modulus and the solid fat content.

The fractal nature of fat crystal network was first demonstrated by Vreeker at al. [142]. The distinctive feature of fractal objects is their self-similar or self-affine character. Indeed, the geometric pattern of a fractal object is repeated at different length scales. In 1975 Benoît Mandelbrot used the term "fractal" (from the Latin "fractus", i.e. broken) for the first time to indicate a geometric object with fractional dimension, the so-called "fractal dimension" [143]. According to the rigorous Hausdorff-Besicovitch definition of the fractal dimension D of a set of points, a measure M_d of the set of points is expressed as:

$$M_d = \sum r(d)\delta^d = r(d)N(\delta)\delta^d \xrightarrow[\delta \to 0]{} \begin{cases} 0, d > D \\ \infty, d < D \end{cases} \qquad (1.6.12)$$

where d is the dimension of the measurement, $r(d)$ is the geometrical factor (1 for line, square and cubes, $\pi/4$ for disks, and $\pi/6$ for spheres), δ is the measurement interval, and $N(\delta)$ is the number of measurement intervals required to cover the object. The critical value of d, where M_d jumps from zero to infinity or vice versa, is the Hausdorff-Besicovitch dimension, used as the fractal dimension of the object. Therefore, the fractal dimension represent an extended Euclidean dimension. For instance, an object with Euclidean dimension 2 has finite measurement M_d only at fractal dimension $D=2$, because M_d is infinity at $d < 2$ and is zero at $d > 2$ for a two-dimensional object. Similarly, the fractal dimension of a self-similar or self-affine fractal object is the critical dimension of a specific measurement where it jumps from zero to infinity or vice versa [139].

As far as natural systems are concerned, it should be considered that they do not exhibit exact self-similarity, owing to the inherent complexity of both natural raw materials and the processes responsible for structure formation [144]. Furthermore, it must be taken into account that statistical self-similarity may not be recognized over countless decades in order of length scale. In colloidal gels, for example, fractality is usually encountered between the size of a primary colloidal particle and a floc of these primary particles [144].

Shih et al. [145] described the three-dimensional colloidal network as composed of interconnected flocs. Based on the relative value of the elastic constant of the interfloc links to that of the flocs, the authors identified two rheological regimes: the strong-link regime, where the elastic constant of the interfloc links is higher than that of the flocs, and weak-link regime, where the elastic constant of the interfloc links is lower than that of the flocs [139, 145]. From a rheological point of view, the elastic constant has been found to increase more slowly in the weak-link regime than in the strong-link regime, whereas the

limit of linearity increases with increasing particle concentration in the weak-link regime but decreases with increasing particle concentration in the strong-link regime [145]. The equations for the strong-link (applicable at low volume fractions, usually $\Phi<0.1$) and the weak-link regimes (applicable at high volume fractions, usually $\Phi>0.1$) are, respectively:

$$G_{SLR} \sim \Phi^{\frac{d+x}{d-D}} \qquad (1.6.3)$$

$$G_{WLR} \sim \Phi^{\frac{1}{d-D}} \qquad (1.6.4)$$

where d is the Euclidean dimension, D the fractal dimension and x is the chemical length exponent, also called backbone fractal dimension, which represent the tortuosity of the effective chain of stress transduction within a cluster of particles yielding under an external applied stress. Parameter x is very difficult to estimate and usually is assumed to be in the range $1<x<1.3$ [144, 145].

Vreeker et al. [142] demonstrated the fractal nature of fat crystal networks and related the power law relationship between the dynamic shear modulus G' and the solid fat content to the strong-link regime behaviour hypothesized by Shih et al.

According to Narine and Marangoni [146], fat crystal networks at high solid fat contents behave rheologically as if they were in the weak-link regime. It was found that the interfloc links of the network carry most of the stress loaded on the material and both the elastic constant and the limit of linearity increase with increasing particle concentration, thus networks behave as materials belonging to the weak-link regime.

By combining the weak-link regime theory and fractal geometry, a fractal model of fat crystal networks has been proposed by Tang and Marangoni [139]. Based on this model, the macroscopic elastic constant K can be expressed as a function of the force constant of the links between fat crystal flocs as follows:

$$K = k_1 \left[\frac{L}{\xi}\right]^{d-2} \qquad (1.6.5)$$

where ξ is the diameter of a floc, L is the macroscopic size of the system, and d is the Euclidean dimension of the sample (Figure 1.22). If an external force F act upon the network, the links between flocs tend to yield and both the original length of the system in the direction of the applied force (ΔL) and the interfloc separation distance l will change. Assuming that all fat crystal clusters are the same, for a close packed fat crystal network the volume fraction of solids within the cluster, Φ_ξ, is the same as the volume fraction of solids of the entire network, Φ. Since the structure within the particle floc exhibit a fractal

nature, the mass of a fat crystal cluster M_c can be related to its fractal dimension D as follows:

$$M_c \sim \xi^D \tag{1.6.6}$$

The total mass of oil, both solid and liquid, M_v, within the volume where the fat cluster is embedded is related to the cluster size as follows:

$$M_v \sim \xi^3 \tag{1.6.7}$$

Thus, the relationship between the volume fraction of solids in the network and the cluster size is:

$$\Phi = \frac{M_c}{M_v} \sim \xi^{D-3} \tag{1.6.8}$$

or, in the same way:

$$\xi \sim \Phi^{1/(D-3)} \tag{1.6.9}$$

By substituting this expression in Equation (1.6.5) and assuming that the links between flocs are statistically identical, yields:

$$K \sim \Phi^{1/(3-D)} \tag{1.6.10}$$

Since the shear elastic modulus of the network G' is related in a proportional manner to the elastic constant K, G' can be expressed as a function of the particle volume fraction as follows:

$$G' = \lambda \Phi^{1/(3-D)} \tag{1.6.11}$$

where the λ is a constant depending on the links between fat crystal flocs, the relationship between ξ, Φ, D and the nature of the proportionality between the SFC of the system, Φ, and the SFC within a cluster, Φ_c.
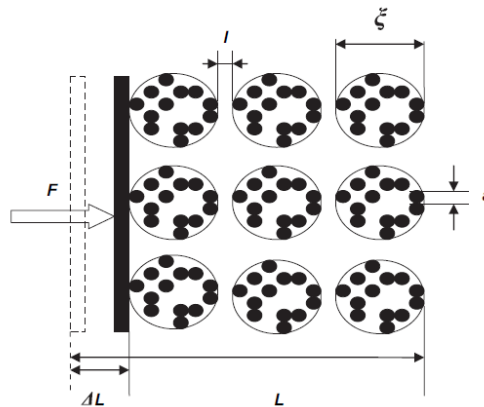

Figure 1.22 Schematic representation of fat crystal network under small deformation [138].

The fractal dimension D is an intensive property of a fractal object and is used to quantify the microstructure of the network. Namely, the fractal dimension define the spatial distribution of mass within the network. Furthermore, this parameter describes the combined effects of morphology and spatial distribution patterns of the fat crystal clusters in the fat crystal networks [139]. The beauty of the fractal dimension is that this parameter can capture the complexity of a structure's geometry in a single number. On the other hand, the trial is to give physical meaning to the number obtained [144].

The fractal dimension of fat crystal networks can be determined by several methods including rheology, microscopy, oil migration and light scattering methods. The determination of fractal dimension by means of light scattering is accurate only at very low volume fractions of solids [144].

Microscopy, and especially polarized light microscopy, is often used to determine the fractal dimension of fat crystal networks. Based on the particle-counting procedure, D can be evaluated counting the number of crystal reflections or particles within boxes of increasing size placed over a micrograph given a proper threshold and inverted. The slope of the log–log plot of the number of particles as function of the box size corresponds to the fractal dimension of the network (Figure 1.23) [144].
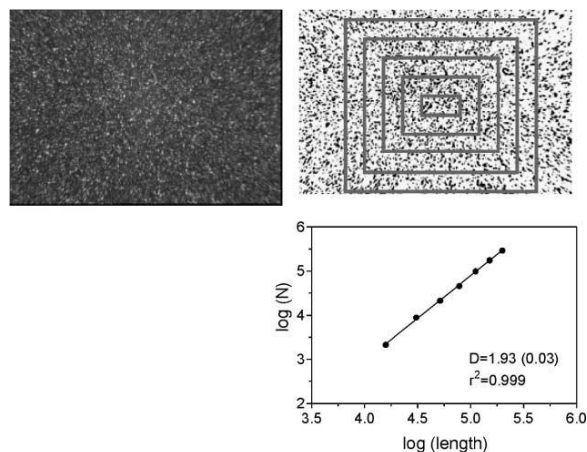
Figure 1.23 Fractal dimension D calculation using the particle-counting method [142].

In this procedure, the number of particles within an ROI (region of interest) must be counted, including as well as excluding particles that touch the edge of the boxes. The final value of the fractal dimension of a network is obtained by averaging the fractal dimensions obtained from counts including and excluding particles touching the edge of the boxes [144].

The fractal dimension of a fat crystal network can be also evaluated using small deformation rheological tests. In practice, it is common to assume that the volume fraction of solids Φ is equal to the measured SFC/100. Hence, by measuring the shear modulus G' within the linear viscoelastic region at different values of SFC and plotting G' against SFC/100 in a log-log plot, the fractal dimension can be determined from the slope of the curve (see Eq. 1.6.11). However, it should be noted that the SFC usually determined through spectroscopic techniques represents the mass fraction of solids within the investigated system, therefore the volume fraction of solids Φ is not exactly equal to SFC/100. Nevertheless, the volume fraction Φ can be calculated from the experimental values of SFC, as will be further discussed in the following Chapters.

The fractal model as described up to now (Eq. 1.6.11) has often been referred to as "original fractal model". The model has been further modified by Tang and Marangoni [139] to take into account an apparent change in fractal dimension over a large range of solid fat content. This apparent variation was associated with a heterogeneous distribution of stresses within the network. When a colloidal network is stressed, a small part of the material carries most of the stress, while the other part of the material contributes very little to the elastic properties of the material.

A colloidal network can be depicted as a mesh composed of interconnected structural clusters with hollow spaces in between. The hollow space of the largest size in a region is a sort of flaw which acts as a stress concentrator in that area. Then, the elastic properties of the whole network are dominated by the elastic strength of these stress concentrators. Even for some apparent perfect networks, the stress distribution is heterogeneous because of the differences between the structural clusters. In addition, it should be considered that, in a fat crystal network, crystal flocs are also not uniform, thus the weakest floc will become a flaw and acts as a stress concentrator. As a result, the stress distribution between fat crystal flocs in a fat crystal network is also heterogeneous.

The connectivity also plays an important role in the heterogeneous stress distribution within colloidal networks. It has been demonstrated that colloidal networks show some "dangling ends", that is mass not included in the 3-D network. Owing to the existence of these "dangling ends", some clusters do not have a connection with neighbouring clusters or are only connected to one of the neighbouring clusters, and thus they are not included in the network and do not contribute to the elastic properties of the material. An increased connectivity results in a higher value of the elastic modulus of the material. Taking into account that real networks are not fully connected and that connectivity of networks

increases with the volume fraction of solids, it was concluded that the effective load-bearing volume fraction of solids increases in an exponential fashion with the apparent volume fraction of solids.

The increase in the load-bearing volume fraction with the apparent volume fraction of solids is similar to the process of increase in SFC with time during crystallization. Indeed, SFC increases with time in an exponential fashion at the beginning and the middle stage of the crystallization process and gradually approaches the maximum SFC at the end of the crystallization process. Since only load-bearing solids contribute to the elastic properties of the network, an effective volume fraction of solids, Φ_e, can be estimated as follows:

$$\Phi_e = 1 - e^{-k\Phi^b} \tag{1.6.13}$$

where Φ is the apparent fraction of solids, while k and b are constants.

By assuming a spherical geometry for the particles and using the "original fractal model", Narine and Marangoni [145] derived an expression for the elastic modulus of the fat crystal networks:

$$G' = \frac{mA}{6c\pi a\xi l_0^3} \Phi^{1/(d-D)} \tag{1.6.14}$$

where m is the number of interacting particles at the interface between two flocs, A is Hamaker's constant, c is the constant of the expression $N=c\xi^D$ (N is the number of primary particles in a floc, ξ is the diameter of a floc, and D is the mass fractal dimension of a floc), a is the average diameter of the particles present in each floc, and l_0 is the average equilibrium distance between particles.

By substituting Eq. 1.6.13 into this expression, the final "modified fractal model" is obtained:

$$G' \sim \frac{mA}{6c\pi a\xi l_0^3} \left(1 - e^{-k\Phi^b}\right)^{1/(3-D)} \tag{1.6.15}$$

Awad et al. [146] found that *ln(G')* of various fat systems increased with *ln(SFC/100)* faster in the low SFC region, more slowly in the intermediate SFC region and almost remained unchanged at high SFC values (Figure 1.24). The authors applied the "original fractal model" to different SFC regions separately and obtained different values of the fractal dimension of the network, implying that the microstructure of the system was different at different SFC values. According to the "modified fractal model", the microstructure of the networks does not change much at different SFC values, but when the network undergoes an external stress, the volume fraction of the stress-carrying solids increases with SFC dramatically in the low SFC region, and does not change much at

higher SFC values. The "modified fractal model" is able to describe well the increase of *G'* with SFC (Figure 1.24).
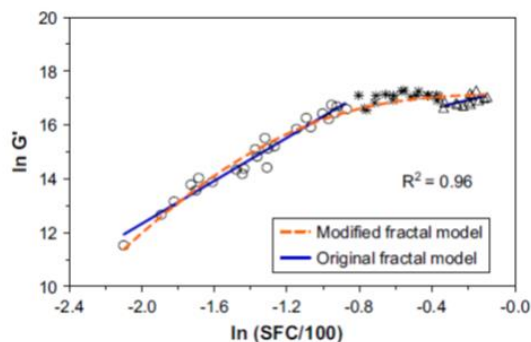
Figure 1.24 Fit of the original and the modified fractal model for *G'-SFC* data to mixture of cocoa butter with canola oil [138].

1.6.2 Studies on gelation kinetics

The process of fat crystallization may be studied through several models. One of the most extensively used is the Avrami model [148]:

$$1 - F = e^{-zt^n}$$

(1.6.16)

where *F* denotes the reduction of crystallinity (since it associates the crystallinity of the system at a given time (*t*) with the total crystallinity), the exponent *n* is associated with the mechanisms of crystal growth and *z* represents a composite rate constant involving nucleation and crystal growth rate. Avrami model is often used in the literature for the estimation of parameter *n*: in homogeneous nucleation, a crystallization process with $n = 4$ follows a 3-D crystal growth mechanism, a value of $n = 3$ a 2-D mechanism and $n = 2$ a 1-D crystal growth. Non-integer values of *n* are associated with heterogeneous and secondary nucleation. The *F* value is usually calculated with a property proportional to the change in solid phase or crystallinity developed in the system as a function of time. The values of *n* and *z* are calculated from the linear form of the Avrami equation as the slope and intercept at *ln(t) = 0*, respectively, assuming that a single slope, associated with the value of *n*, is obtained from a plot of *ln [−ln(1 − F)]* vs. *ln(t)* [148].

However, the application of this procedure to crystallization data from vegetable oils has given inconsistent results, because two regions with different slopes have often been obtained. Toro-Vazquez et al. [148] studied the behaviour of oil blends of palm stearin (26 and 80%$_{wt/wt}$) in sesame oil using DSC and rheological measurements, at different crystallization temperatures obtained under several cooling rate conditions (1, 10, and

30°C/min). The authors proposed that *n* calculated from the second region of the Avrami plot is a parameter mainly associated with crystal growth, whereas *n* from the first region is associated more with nucleation process [148].

Lopes da Silva et al. [149] investigated the gelation kinetics of high-methoxyl pectins/sucrose hydrogels. They proposed a definition of the average SDR (structure development rate) based on the variation in the elastic modulus *G'* during the gelation process, which could be also extended to other gelled systems. Gradual development of the network structure is reflected by a progressive increase in the elastic modulus *G'* over time. Thus, the SDR can be easily defined as follows:

$$SDR = \frac{dG'}{dt} \qquad (1.6.17)$$

Lopes da Silva et al. [149] evaluated the SDR at each time during small amplitude oscillation tests using either a simple forward-difference numerical method or after a polynomial fit or cubic spline interpolation to smooth the data points. SDR calculated from *G'* time data without previous fit and using the simple forward-difference numerical method showed much more scatter, hence a subsequent smoothing of the *dG'/dt* data using a moving average procedure was performed.

Plotting the SDR against the time of ageing, the authors observed an initial increase in SDR, followed by a decrease in the SDR, which continued to decrease steadily until the end of the ageing period. The initial increase in SDR was attributed to the rapid formation of junction zones between pectin chains which results in an initial rapid increase in the storage modulus during the ageing of the pectin gel. After this stage, the SDR decreases until it reaches a value that is always higher than zero but is almost independent of the ageing time. This stage corresponds to a slow reorganization of the network involving the creation of new junction zones or an increase in the extension of the junctions between molecular chains.

In order to compare results obtained under different experimental conditions, Lopes da Silva et al. [148] defined the average SDR in the time interval between t_1 and t_2 as follows:

$$SDR_{av} = \frac{1}{t_1 - t_2} \int_{t_1}^{t_2} SDR \, dt \qquad (1.6.18)$$

As an example, Lopes da Silva et al. [149] investigated the effect of ageing temperature on SDR_{av} values and showed that results followed the same bell-shaped temperature dependence already found for the elastic modulus *G'* of pectin gels.

1.6.3 Determination of gel point

Gelation is a critical phenomenon where the transition variable will be the connectivity of the physical or chemical bonds linking the basic structural units of the network. Before the gel point, the connectivity is small and the material typically relaxes rapidly. Near the gel point, the relaxation time increases sharply and exactly at the gel point it diverges to infinity. In addition, the relaxation spectrum does not contain a characteristic time anymore. After the gel point, when the network has reached a high degree of development, the maximum relaxation time of the final network is again very short [150].

The determination of gel point from experimental results could be difficult. According to the classical theory, the gel point occurs when steady shear viscosity tends to go to infinity and equilibrium modulus is equal to zero. The classical theory has been broadly employed to determine the gel point of chemical gels (Figure 1.25). However, it must be considered that continuous shearing could affect gel formation, hence accurate information from viscosity measurements is not possible near the gel point and extrapolation is needed [150].
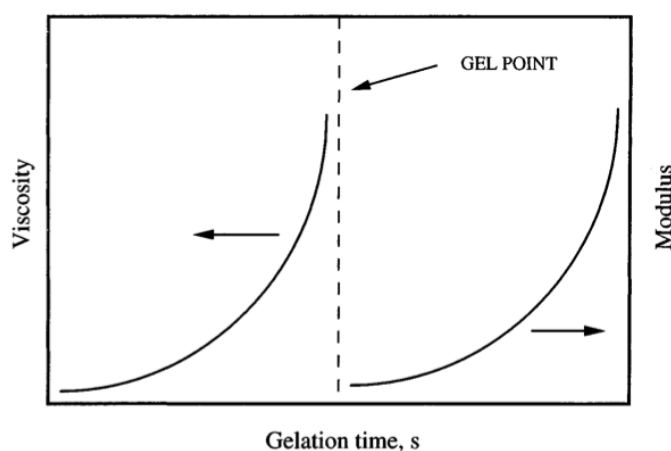
Figure 1.25 Classical theory for the determination of gel point [148].

On the contrary, small amplitude oscillation shear measurements allow the progressive evolution of the viscoelastic properties to be followed throughout the gelation process and the modification of molecular structure caused by shear is minimized, since the applied stress is very small. As a consequence, the majority of techniques used to detect the gel point involves the evaluation of dynamic rheological properties [150].

Studies on thermosetting resins suggested that the gel point could occur at the time at which G' and G'' cross each other at a given frequency. In addition, when a constant

cooling rate is applied to hydrocolloid gelling solution, it was found that at high temperatures the gelation process is dominated by the viscous behaviour of the system, then *G'* is lower than *G''*. By decreasing the temperature, junction zones are formed among the macro-molecules resulting in the increase of both moduli, until the elastic behaviour becomes predominant (i.e. *G'* becomes higher than *G''*) and the point at which *G'-G''* crossover occurs might be considered as the gel point [151, 152]. This criterion was then often applied to obtain a rapid estimation of the gel point [150, 151, 152, 153]. Even though the time and/or temperature of the *G'-G''* crossover is a function of the frequency, it is likely that the *G'-G''* crossover time might be close to the sol/gel transition point [150, 153].

   A more rigorous approach is provided by Winter theory. Winter studied the viscoelasticity of cross-linking polymer at the gel point for both stoichiometry-balanced and imbalanced systems [154, 155, 156]. It was found that the relaxation modulus at the gel point followed the power-law:

$$G(t) = At^{-n} \qquad (1.6.19)$$

valid for the values of $0<n<1$. For stoichiometry-balanced systems, it was demonstrated that $n=1/2$. Since the oscillation test at fixed frequency, ω, is qualitatively equivalent to a transient experiment at time $t=1/\omega$, if the linear viscoelasticity holds, the previous equation transforms into:

$$G(t) = A\omega^{n} \qquad (1.6.20)$$

for $0<\omega<1/\lambda_0$, where λ_0 represents the characteristic shortest time for the crossover to small scale dynamics. A more general method for gel point determination is based on the observation of the loss tangent, *tgδ*:

$$tg\delta = \frac{G''(\omega)}{G'(\omega)} = tg\left(\frac{n\pi}{2}\right) \qquad (1.6.21)$$

where $0<n<1$ and is independent of frequency. Hence, the gel point can be evaluated as the point at which *tgδ* is independent of the applied frequency and the value of the exponent *n* can be directly deduced from the amplitude of *tgδ* at that point [154, 155, 156]. Even though equation 1.6.21 represents the most generally valid gel point criterion and the Winter theory is the rigorous method to determine the gel point, sometimes it can be difficult to adopt it in practical experiments. Then, as stated before, the easier criterion based on *G'-G''* crossover at a frequency of 1Hz is often used for practical applications.

1.7 Potential applications of organogels

Organogels have already been used for industrial applications due to the great diversity of the structures that they display on microscopic and mesoscopic scales [9, 157]. Recovery of spilled crude oil or disposal of used cooking oil frequently involves gels or complex micro-emulsions [9]. Since the 1970s, the lubrication industry has used metal salts of 12-hydroxystearic acid to gel oil and grease-based lubricants in order to restrict their mobility once they are applied to metallic surfaces [157, 9]. Other current applications of organogels include the phase-selective recovery of crude oil spills, the gelation of flammable solvents [3, 157], structuring of dermal pharmaceuticals [157] as well as the gelation of solvents used to clean oil paintings, in order to prevent them from penetrating into the original paint layers and damaging the artwork [158]. Presently, the cosmetics industry uses organogelation technology to impart structure to the apolar components of personal care products such as lipsticks, moisturizers, and sunscreens [158].

From an applied research perspective, organogels have a wide range of futuristic applications such as tissue engineering, templated synthesis of inorganic nanostructures, biosensors and nanowires. It has been proposed that some organometallic organogelators can form aerogels. Actually, membranes with aerogel networks, providing small and large diameter holes, should become useful as purification/separation tools [9]. Gels composed of anisotropic networks and mixed with low molecular mass liquid crystals have been used as active or passive optical components. Anisotropic organogels, obtained from organogelators forming rods, are of interest for electronic conduction or semi-conduction [9]. The ordered micro-structure of some organogels can be of interest in templating for materials synthesis. Luminescent gels can find applications for linear, anisotropic energy transfer while some chiral organogels can be used for molecular and chiral recognition. For instance, molecular transducers formed by cholesterol-based organogelators are promising examples of host-guest signal-responsive chemistry, because of their capability to translate some chiral recognition interactions into readable outputs [9].

Another important area of research deals with potential uses of organogels for controlled drug delivery. Despite the large abundance and variety of organogel systems, relatively few have current applications in drug delivery, mainly because of the lack of information on the biocompatibility and toxicity of organogelator molecules and their degradation products [8].

Generally speaking, organogelation is an interesting topic for basic research as it raises important questions in several fields of study such as crystallization, surface chemistry/physics and materials science. Nevertheless, it seems clear that gelation of organic solvents has a broad range of potential industrial applications.

Since the main aim of the present work is the investigation of organogels for potential use in food, all current potential proposed applications of edible oil organogels will be discussed in more detail below. Furthermore, mixtures of organogelators for both potential food and cosmetic applications have also been studied in this work, thus a review on current and potential cosmetic applications of organogels will be reported in Paragraph 1.7.2.

1.7.1 Potential food applications of organogels: structuring edible oils

Structuring vegetable oils has become an active area of research in recent years, mainly owing to pressures to reduce saturated fats and eliminate trans-fats from our diets. Indeed, the potential use of organogelation in foods providing the strongest impetus is the development of an alternative triacylglyceride-structuring method for edible oils. Organogelators, especially LMOGs, can be employed as an interesting alternative, promoting the formation of a crystalline network able to give the proper rheological properties to foodstuffs and to stabilise them in the meantime, even at a very low concentration [71].

In comparison to other organic solvents, the structuring of edible oils introduces some restrictions. Edible oils are more polar than many organic chemical solvents, such as mineral oils or alkanes, influencing the solubility of potential structuring agents. Potential food organogelators should provide structure to edible oils at chilled and/or ambient temperatures to make them relevant for food applications. Fundamentally, a potential organogelators should impart structure to the oil phase as well as prevent the exudation of the structured oil phase from the material. According to Co and Marangoni [71], an ideal fat structurant should have the following requirements with regards to food applications:

- Food-grade: obviously, all tested ingredients must be food-grade, which means that a potential organogelator must meet strict regulatory requirements for use in foods. This is also true for cosmetics and pharmaceuticals. The majority of organogelators are toxic and unsuitable for use in such applications. Luckily, a wide range of organogelators is still available for use in food, pharmaceutical

and cosmetic applications although some of these structuring agents still require regulatory approval.

- Economical: an ideal organogelator should be affordable and readily available. Some of the organic structurants are very expensive due to the cost required to isolate or synthesize them. For instance, phytosterols and ceramides are both high-cost structurants. Lecithin, plant waxes and monoglycerides are relatively cheaper and more economical because only a minor purification or concentration step is necessary to convert these compounds into functional structurants.

- Efficient: an ideal organogelator should be able to structure edible oils at relatively low concentrations. The efficiency of organogelator is related to economics, since the structurant is typically more expensive than the structured phase. The unknown consequences of ingesting too much of the structurant must also be taken into account.

- Matching physical properties: an ideal organogelator should exhibit similar physical properties (hardness/plasticity at a given temperature, melting point, melting profile) as the fat material it is expected to replace.

- Versatility: fats are among the most versatile ingredients available in food industry. Physical properties of fats can be easily tailored: for instance, the melting temperature and profile of fats can be modified by blending different fats and oils, inter-esterification, fractionation, hydrogenation as well as by changing the crystallization conditions. As a result, the same fat can be employed in several applications.

Despite the restrictions related to the nature of the solvents and the specific characteristics required for fat structurants, a quite large number of systems capable of structuring edible oils have already been identified, including mono- and di-acylglycerols, fatty acids, fatty alcohols and their mixtures, wax esters, sorbitan monostearate, lecithin, mixtures of lecithin and sorbitan tristearate and mixtures of phytosterol and γ-oryzanol [87]. The properties of organogels containing this molecules have already been discussed in Paragraph 1.4.1.

Edible organogels have several potential different functionalities in food products including the restriction of oil mobility and migration, the stabilization of emulsions and

the ability to control the rate of nutraceutical delivery and the above-mentioned replacement of saturated and trans fats [157].

It has been proposed that the oil binding capacity of LMOGs might be useful for the prevention of oil migration in composite food products. Rogers et al. [158] investigated the mobility of canola oil gelled with varying concentrations of 12-HSA, showing that the mobility and the migration rate of canola oil triacylglycerols through a filter paper was highly dependent on the set isothermal crystallisation temperature. The migration of oil is a particular problem in filled chocolate foodstuffs, where unsaturated triacylglycerols from the soft filling tend to diffuse into the cocoa butter and migrate towards the external surface of the product [157]. In addition, oil migration is responsible for the process of "fat blooming" in chocolate: oil acts as a solvent for high melting cocoa butter triacylglycerols which usually recrystallize in the β_{VI} polymorphic form yielding to the formation of a dull white or grey film on the product. Lipid scientists and confectionary technologists are currently searching for new strategies to control and/or prevent oil migration. It has been proposed that the organogelation of the liquid oil fraction could delay or inhibit oil migration.

Elliger et al. [160] aimed at avoiding destabilisation phenomena by thickening/gelling the peanut oil with 12-HSA. The authors found that the addition of 12-HSA to peanut butter significantly reduced the rate of oil syneresis due to the increased viscosity of the system.

Marty et al. [160] investigated the effect of 12-HSA on the oil migration of a fat based model filling containing 60:40 canola oil: IHPO (Inter-esterified Hydrogenated Palm Oil). They showed that the incorporation of 12-HSA into the filling of the model chocolate confection significantly increased the rate of oil migration through non-tempered cocoa butter. In addition to this unexpected result, the addition of 12-HSA does not yield to a higher SFC of the mixture, suggesting that its addition delays or slows the normal crystallisation. In order to eliminate the influence of the co-crystallization of IHPO and 12-HSA, the experiment was repeated using three different formulations: liquid canola oil, canola oil gelled with 12-HSA (2%wt/wt) and canola oil structured with IHPO (40%wt/wt). The oil binding capacity of the conventional fat crystal network formed by IHPO was significantly higher in comparison to that of the self-assembled fibrillar organogel network formed by 12-HSA. Interestingly, there were no significant differences in the migration rate of liquid canola oil and canola oil gelled with 12-HSA. This result was ascribed to the low SFC value measured for gels containing 12-HSA, suggesting that the SFC of the

filling, which is very similar for canola oil organogels and control samples, plays an important role in determining the oil mobility and migration. Although the results from these experiments suggested that organogelation did not inhibit oil migration in confectionary products, more work needs to be done in order to consider the effects of other organogelators in different types of food products [157].

According to Rogers et al. [136], from the perspective of structuring liquid oils using self-assembled fibrillar networks, the yield strain and hardness can be manipulated in a predictable way, in order to allow for the creation of new novel foods without the need for saturated or trans fatty acids.

The rate of release of nutrients from food products and their bio-availability are both very important parameters for the development of value-added food products and nutraceuticals, since it is often beneficial to control the rate at which the bioactive compound is released into the bloodstream [157]. It has been shown that the characteristic pattern of uncontrolled release involves high plasma concentrations of the bioactive compound immediately following ingestion, followed by sharp decrease, because the active compound is quickly absorbed into the bloodstream and cleared from the system. The eventual presence of a bioactive compound at concentrations either above or below its therapeutic range may lead to negative side effects [157]. On the contrary, if the bioactive compound is released into the bloodstream at controlled rate, its concentration will not deviate significantly above or below the therapeutic range throughout the absorption process.

Nowadays, controlled release technology is broadly used in pharmaceutics, where drugs are encapsulated by materials or incorporated into tablets designed specifically to delay or control the rate of drug release into the bloodstream after ingestion [157]. Hydrogels have been extensively used for this purpose, but it must be considered that many important bioactive compounds are hydrophobic. Thus, organogels may be employed to increase the solubility and control the release of apolar pharmaceuticals and nutraceuticals upon dissolution or deformation of the gel. [136, 157]. Moreover, encapsulation of such lipophilic compounds within a gel should enhance their stability against oxidation.

As an example, carotenoids are hydrophobic plant-derived pigment molecules with anti-oxidant properties. Their limited bioavailability is affected by the presence, amount and type of lipid in the digestive tract at the time of absorption [157]. It has been suggested that the encapsulation of carotenoids into vegetable oil organogels could increase their bio-

availability and control the rate of absorption. Hughes et al. [157] demonstrated that organogelation of β-carotene enriched canola oil using 12-HSA slowed the release of β-carotene in an *in vitro* human stomach model. These results suggest that physiologically responsive organogels with the capability of delivering bioactive compounds at predefined rates or in response to certain conditions is a real possibility [71].

Lecithin organogels are particularly suitable for use in pharmaceuticals and neutraceuticals, due to its safety and amphiphilic qualities that allow it to solubilize both aqueous and hydrophobic drugs [71].

Among the most interesting potential food applications of organogels, a standout is the possibility of structuring edible oils via organogelation as an alternative to the traditional saturated and trans-fats structuring. Indeed, the benchmark for any form of oil structuring is the gelling of a liquid triacylglycerol phase or oil by means of a crystalline triacylglycerol phase or fat [162]. Crystalline triacylglycerol hardstocks usually contain high amounts of saturated fatty acids [87]. Both saturated fatty acids and trans-fatty acids are known to contribute to an elevated blood cholesterol level and are therefore associated with a higher risk on cardiovascular diseases [87, 162]. Unfortunately, owing to their excellent functionality, the removal or replacement of both saturated and trans-fatty acids in complex lipid food products is a very difficult task [157].

According to Pernetti et al. [87], structuring methods for organic solvents, including edible oils, can be divided into two main categories: suspensions and networks. The self-assembled low molecular weight organogelators, able to form a network structure, are currently considered the most interesting option for application in food systems [87, 157, 71]. Since organogels possess solid-like properties, they can exhibit mechanical properties, such as plasticity and elasticity, which allow them to be used in place of hardstock fats with the aim of reducing the amount of saturated and trans-fatty acids consumed [71].

Duffy et al. [131] conducted an *in vitro* study simulating the duodenal digestion of an o/w emulsion containing a dispersed phase gelled by phytosterols. They showed that organogelation affects the digestion of lipids, decreasing triacylglycerols lipolysis. It was hypothesized that organogelation retarded the diffusion of triacylglycerols to the surface of the oil droplet, where lipases are active.

Hughes et al. [157] conducted a clinical trial to study the post-prandial increase in variables considered as risk markers for cardiovascular diseases (triacylglycerols, free fatty acids, glucose and insulin) after ingestion of various structured and unstructured lipid

products. In order to evaluate the health benefits of structuring edible oils with an organogel network, the authors compared the nutritional response to the acute ingestion of an organogel (canola oil gelled with 2%$_{wt/wt}$ 12-HSA) to that of two commercial spreads (butter and margarine) as well as pure canola oil. Hughes et al. [157] carried out a clinical trial involving twelve (six male and six female) young, healthy individuals, approved by the Office of Research Ethics. After ingestion of 48 grams of fat from one of the four sample treatments (organogel, butter, margarine or canola oil), subjects consumed a test meal consisting of 400 kcal, 2 g of fat, 0 g of saturated fat, 82.4 g of carbohydrates and 14.6 g of protein. After the consumption of one of the four treatments with the test meal, venous blood samples were collected every hour for six hours. All cardiovascular disease markers were plotted against time and it was found that the mean post-prandial serum triacylglycerol levels corresponding to the organogel were significantly lower than those of butter and margarine but were not significantly different from canola oil (Figure 1.26). In order to explore the full nutritional potential of organogels, the authors suggested conducting longer-term dietary interventions and monitoring of cardiovascular disease indicators in future works [157].
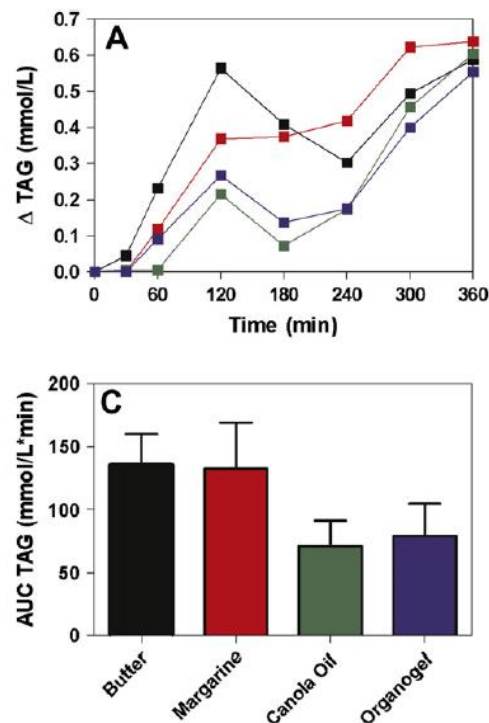
Figure 1.26 Baseline corrected post-prandial serum triacylglycerols response curves (A) and values of the area under the triacylglycerols response curves (C) for butter, margarine, canola oil and 12-HSA/canola oil organogel [156].

The above-reported studies illustrate that organogels, while exhibiting mechanical properties similar to that shown by hardstock fats, do not give the same post-prandial lipid response as hardstock structured fats. In this sense, organogels may be regarded as a valid healthy alternative to traditional triacylglycerols structuring.

1.7.2 Organogels for cosmetics

Cosmetics are substances which can be used to beautify the human body. The US Food and Drug Administration (FDA) which legalizes cosmetics in the United States, proposed a wide definition of cosmetics as substances to be applied to the human body for cleansing, beautifying, promoting attractiveness or altering the appearance without affecting body structure or functions [163]. Organogels have various uses in cosmetics. Many cosmetic preparations such as lipsticks, lip balms, lip liners and lip glosses are organogels although they are not usually referred to as such [71]. Cosmetic organogels are expected to be relatively solid as they must keep their shape inside the packaging. However, cosmetics must yield quickly upon application on the lips or skin. Nevertheless, upon yielding, the cosmetic preparation must retain its ability to entrap oil [71].

LMOGs are commonly used in cosmetology for their required physical organization properties inside the oil phase or their ability to gel organic liquids in smaller quantities (typically 0.1-15%$_{wt/wt}$). Fukasawa et al. [164] developed new organogelators consisting of a long-chain dialkyl phosphate surfactant and aluminium ion or multinuclear aluminum ion with the cosmetic advantage of "good skin feeling". In addition to these distinctive features, these organogelators have the advantage of being safe on the skin.

Martinez et al. [165] reported the gelation of olive oil by using ethylcellulose as an organogelator and Olivem 300, Olivem 700 & Olivem 900 as surfactants. The organogels prepared with Olivem 700 and 900 showed the finest homogeneity and texture. By increasing the concentration of organogelator, the final consistence of the system was more solid-like even if spreadability decreased. As far as the relationship between rheology and temperature is concerned, all the samples showed a more solid-like behaviour at room temperature (25°C) whereas these textures became more liquid-like at higher temperature (37°C). On the basis of their features, various potential applications of these organogels can be predicted not only in cosmetic area but also in pharmaceutics where the use of vegetable oils as carriers for active ingredients is very common. In some sense, cosmetic organogels themselves can be considered as "delivery vehicles" since they deliver certain

functional ingredients such as moisturizers and colouring agents to the surface of the skin [71].

Villalobos-Hernandez & Muller-Goymann [166] characterized organogels composed of carnauba wax and decyl oleate as potential carrier systems for inorganic sunscreens. The organic matrices were both used as capsules for UV radiation attenuators (barium sulphate, strontium carbonate and titanium dioxide) or as associated vehicles for the pigments in aqueous dispersions. As far as rheological analysis is concerned, all preparations behaved as Newtonian fluids. The authors concluded that the use of nanoparticles comprising of matrices based on a mixture between a solid lipid (i.e. carnauba wax) and a liquid lipid (i.e. decyl oleate) as vehicles for inorganic nanocrystals was a promising technology for future sunscreen formulations, since the stability of the composition was enhanced by the use of these lipid matrices.

Kirilov et al. [167] also investigated a stable dispersion of organogel nanoparticles in water. Organogel particles comprised an organic liquid (almond oil and Vaseline oil), a sunscreen molecule (2-ethylhexyl-p-dimethylaminobenzoate, EHMAB) and 12-HSA as organogelator. Acetylated glycol stearate (AGS), sodium hyaluronate (SH) and polyvinyl alcohol (PVA 80) hydrolysed at 80% for dermo-cosmetic use were also added as stabilizing, thickening and emulsifying agents. The lowest value of the minimum gelation concentration for 12-HSA was obtained using Vaseline oil as the solvent, while the limit concentration in EHMAB was found to be much higher. Therefore, Vaseline oil (showing the lower MGC) and almond oil (largely use for its cosmetic and dermo-cosmetic properties) were used as organic solvents. The mixture containing $16.8\%_{wt/wt}$ almond oil and $3.2\%_{wt/wt}$ EHMAB displayed the typical Newtonian rheological behaviour of diluted systems, since no dynamic viscosity growth with the shear rate increase was observed. The presence of 12-HSA led to systems with non-Newtonian shear-thinning behaviour, corresponded to a decrease in the viscosity by increasing of the shear rate. This rheological behaviour describes concentrated systems, where the concentration and the viscosity of the dispersed phase favour particle interactions under shearing. Moreover, the percentage of EHMAB did not affect the gel-sol phase-transition temperature values. In conclusion, the study verified the importance of these gelled nanoparticles and their aqueous dispersion for the production of new formulations for cosmetic and dermo-cosmetic applications.

Morales et al. [168] reported the design of hydrogels and pluronic-lecithin organogels as carriers of cosmetic active ingredients (Aloe vera and Hydrocotyle asiatica). Both formulations were creamy and easily spread and absorbed into the skin. Rheological

characterisation confirmed the good spreadability observed: all samples exhibited a plastic behaviour, they started to flow when the applied shear stress approached the critical value of the yield stress (σ_0) and compression force values were low, in spite of the fact that the organogels offered higher viscosity. All these properties provided them an agreeable texture.

Stortz and Marangoni [169] also reported the production of organogels by using ethyl cellulose as an organogelator with different vegetable oils (sunflower oil, canola oil, soybean oil, flaxseed oil and avocado oil) as the solvent phase for substituting petrolatum. The flow behaviour of the organogels was very well described by a power law model. The authors also studied the effect of addition of large amounts of surfactant (glycerol mono-oleate) on viscosity of the organogels. The highest viscosity was attained for glycerol mono-oleate concentrations between 40-50%. Samples prepared with 40-45% glycerol mono-oleate were therefore considered as the most promising due to their high viscosity and fully thixotropic character. Moreover, petroleum jelly is thixotropic so this property was highly desirable in a replacement product. The samples with 40-45% glycerol mono-oleate had also good texture when spread on the skin which is a key characteristic for a cosmetic product. The effect of ethyl cellulose concentration was also studied. As the concentration of ethyl cellulose increased the consistency of the organogel also increased. The authors reported that organogels which exhibited full texture recovery showed great potential for use in food and cosmetic products exclusively in those products that would introduce shear at temperatures where the gel has already set. Developed organogels have promising textural and water vapour barrier properties for use on the skin and lips.

References

[1] Hamley, Ian W., *Introduction to Soft Matter: Synthetic and Biological Self-Assembling Materials. Revised Edition*. Wiley, Chichester, 2007.

[2] George, M., and R.G., Weiss, *Molecular organogels. Soft matter comprised of low-molecular-mass organic gelators and organic liquids*. Accounts of Chemical Research, 2006. 36: p. 489-497.

[3] Abdallah, D.J., and R.G.,Weiss, *Organogels and low molecular mass organic gelators*. Advanced Materials, 2000. 12: p. 1237-1247.

[4] Lloyd, J., *Colloid Chemistry*. The Chemical Catalog Co., New York, 1926.

[5] Flory, P.J., *Principles of polymer chemistry*. Cornell University Press, Ithaca, 1953.

[6] Ferry, J.D., *Viscoelastic properties of polymers*, 3rd *edn*., Wiley, New York, 1980.

[7] Almdal, K., Dyre, J., Hvidt, S., and O., Kramer, *Towards a phenomenological definition of the term 'gel',* Polymer Gels and Networks, 1992. 1: p. 5–17.

[8] Vintiloiu, A., and J.C., Leroux, *Organogels and their use in drug delivery – A review*. Journal of Controlled Release, 2008. 125: p. 179-192.

[9] Terech, P., and R.G., Weiss., *Low molecular mass gelators of organic liquids and the properties of their gels*. Chemical Reviews, 1997. 97: p. 3133-3159.

[10] Shapiro, Y.E., *Structure and dynamics of hydrogels and organogels: An NMR spectroscopy approach*. Progress in Polymer Science, 2011. 36: p. 1184-1253.

[11] Nishinari, K., "Some thoughts on the definition of a gel," in *Gels: Structures, Properties, and Functions*, Tokita M. and K. Nishinari, Eds., Springer, Berlin, 2009.

[12] Rocha-Amador, O.G., Gallegos-Infante, J.A., Huang, Q., Rocha-Guzman, N.E., Moreno-Jimenez, M.R., and R.F., Gonzalez-Laredo, *Influence of Commercial Saturated Monoglyceride, Mono-/Diglycerides Mixtures, Vegetable Oil, Stirring Speed, and Temperature on the Physical Properties of Organogels*. International Journal of Food Science, 2014. p. 1-8.

[13] Lopes da Silva, J.A., and M.P., Gocalves, *Rheological study into the ageing process of high methoxyl pectin/sucrose aqueous gels*, Carbohydrate Polymers, 1994. 24: p. 235-245.

[14] Murdan, S., *Organogels in drug delivery*, Expert Opinion on Drug Delivery, 2005. 2: p. 489–505.

[15] Abdallah, D.J., and R.G., Weiss, *n-Alkanes gel and many other organic liquids*, Langmuir, 1999. 16: p. 352–355.

[16] Singh, V.K., Banerjee, I., Agarwal, T., Pramanik, K., Bhattacharya, M.K., and K., Pal, *Guar gum and sesame oil based novel bigels for controlled drug delivery*, Colloids and Surfaces B: Biointerfaces, 2014. 123: p. 582-592.

[17] Rehman, K., and M.H., Zulfakar, *Recent advances in gel technologies for topical and transdermal drug delivery*, Drug development and industrial pharmacy, 2014. 40; p. 433–440.

[18] Gonnet, M., Lethuaut, L., and F., Boury, *New trends in encapsulation of liposoluble vitamins*, Journal of Controlled Release, 2010. 146: p. 276–90.

[19] Manosroi, A., Ruksiriwanich, W., Abe, M., Manosroi, W., and J., Manosroi, *Transfollicular enhancement of gel containing cationic niosomes loaded with unsaturated fatty acids in rice (Oryza sativa) bran semi-purified fraction*, European Journal of Pharmaceutics and Biopharmaceutics, 2012. 81: p. 303–13.

[20] Zhang, X.L., Zhao, R., and W., Qian, *Preparation of an emulgel for treatment of aphthous ulcer on basis of carbomers*, Chinese Pharmaceutical Journal, 1995. 30: p. 417–18.

[21] Rahmani-Neishaboor, E., Jallili, R., Hartwell, R., Leung, V., Carr, N., and A., Ghahary, *Topical application of a film-forming emulgel dressing that controls the release of stratifin and acetylsalicylic acid and improves/prevents hypertrophic scarring*, Wound Repair Regeneration, 2013. 21: p. 55–65.

[22] Rhee, G.J., Woo, J.S., Hwang, S.J., Lee, Y.W., and C.H., Lee, *Topical oleo-hydrogel preparation of ketoprofen with enhanced skin permeability*, Drug Development and Industrial Pharmacy, 1999. 25: p. 717–26.

[23] Garcia-Gonzalez, C.A., Uy, J.J., Alnaief, M., and I., Smirnova, *Preparation of tailor made starch based aerogel microsphers by the emulsion-gelation method*, Carbohydrate Polymers, 2012. 88: p. 1378–86.

[24] Ahmed, E.M., *Hydrogel: Preparation, characterization, and applications: A review*, Journal of Advanced Research, 2015. 6: p. 105–121.

[25] Dragan, E.S., *Design and applications of interpenetrating polymer network hydrogels. A review*, Chemical Engineering Journal, 2014. 243: p. 572–590.

[26] Singh, V.K., Ramesh, S., Pal, K., Anis, A., Pradhan, D.K., and K., Pramanik, *Olive oil based novel thermo-reversible emulsion hydrogels for controlled delivery applications*, Journal of Materials Science: Materials in Medicine, 2014. 25: p. 703–721.

[27] Peppas, N.A., Bures, P., Leobandung, W., and H., Ichikawa, *Hydrogels in pharmaceutical formulations*, European Journal of Pharmaceutics and Biopharmaceutics, 2000. 50: 27–46.

[28] Friggeri, A., Feringa, B.L., and J., van Esch, *Entrapment and release of quinoline derivatives using a hydrogel of a low molecular weight gelator*, Journal of Controlled Release, 2004. 97: 241–248.

[29] Heeres, A., van der Pol, C., Stuart, M., Friggeri, A., Feringa, B.L., and J., van Esch, *Orthogonal self-assembly of low molecular weight hydrogelators and surfactants*, Journal of the American Chemical Society, 2003. 125: p. 14252– 14253.

[30] Kobayashi, H., Friggeri, A., Koumoto, K., Amaike, M., Shinkai, S., and D.N., Reinhoudt, *Molecular design of ''super'' hydrogelators: understanding the gelation process of azobenzene-based sugar derivatives in water*, Organic Letters, 2002. 4: p. 1423–1426.

[31] Collier, J.H., Hu, B.-H., Ruberti, J.W., Zhang, J., Shum, P., Thompson, D.H., and P.B., Messersmith, *Thermally and photochemically triggered self-assembly of peptide hydrogels*, Journal of the American Chemical Society, 2001. 123: p. 9463–9464.

[32] Jinsub, S., Braun, P.V., and L., Wonmok, *Fast response photonic crystal pH sensor based on templated photo-polymerized hydrogel inverse photo-polymerized hydrogel inverse opal*, Sensors and Actuators B: Chemical, 2010. 150: p. 183–90.

[33] Hoffman, A.S., *Hydrogels for biomedical applications*, Advanced Drug Delivery Reviews, 2012. 64: p. 18–23.

[34] Zhao, W., Jin, X., Cong, Y., Yuying, L., and J., Fu, *Degradable natural polymer hydrogels for articular cartilage tissue engineering*, Journal of Chemical Technology and Biotechnology, 2013. 88: p. 327-339.

[35] Kim, J.K., Kim, H.J., Chung, J., Lee, J., Young, S.B., and Y.H., Kim, *Natural and synthetic biomaterials for controlled drug delivery*, Archives of Pharmacal Research, 2014. 37: p. 60–68.

[36] Ruel-Gari, E., and J.-C., Leroux, *In situ-forming hydrogels - review of temperature-sensitive systems*. European Journal of Pharmaceutics and Biopharmaceutics, 2004. 58: p. 409–426.

[37] Li, Z., S., Cho, I.C., Kwon, M.M. Janat-Amsbury, and K.M., Huh., *Preparation and characterization of glycol chitin as a new thermogelling polymer for biomedical applications*. Carbohydrate Polymers, 2013. 92: p. 2267–2275.

[38] Sinha, V.R., and R., Kumria. *Polysaccharides in colon-specific drug delivery*. International Journal of Pharmaceutics, 2001. 224: p. 19–38.

[39] Liu, W., Zhang, B., Lu, W.W., Li, X., Zhu, D., De Yao, K., Wang, Q., Zhao, C., and C., Wang, *A rapid temperature-responsive sol–gel reversible poly(N-isopropylacrylamide)-g-methylcellulose copolymer hydrogel,* Biomaterials, 2004. 25: p. 3005–3012.

[40] Andreopoulos, F.M., Deible, C.R., Stauffer, M.T., Weber, S.G., Wagner, W.R., Beckman, E.J., and A.J., Russell, *Photoscissable hydrogel synthesis via rapid photopolymerization of novel PEG-based polymers in the absence of photoinitiators,* Journal of the American Chemical Society, 1996. 118: p. 6235–6240.

[41] Kim, S., and K.E., Healy, Synthesis and characterization of injectable poly(N-isopropylacrylamide-co-acrylic acid) hydrogels with proteolytically degradable cross-links. Biomacromolecules, 2003. 4: p. 1214–1223.

[42] Takashi, L., Hatsumi, T., Makoto, M., Takashi, I., Takehiko, G., and S., Shuji, *Synthesis of porous poly(N-isopropylacrylamide) gel beads by sedimentation polymerization and their morphology,* Journal of Applied Polymer Science, 2007. 104: p. 842-850.

[43] Yang, L., Chu, J.S., and J.A., Fix, *Colon-specific drug delivery: new approaches and in vitro/in vivo evaluation,* International Journal of Pharmaceutics, 2002. 235: p. 1–15.

[44] Myung, D., Waters, D., Wiseman, M., Duhamel, P.E., Noolandi, J., Ta, C.N., and C.W., Frank, *Progress in the development of interpenetrating polymer network hydrogels,* Polymers for Advanced Technologies, 2008. 19: p. 647–657.

[45] Kim, S.J., Yoon, S.G., and S.I., Kim, *Synthesis and characterization of interpenetrating polymer network hydrogels composed of alginate and poly(diallyldimethylammonium chloride)*, Journal of Applied Polymer Science, 2004. 91: p. 3705–3709.

[46] Wang, J.J., and F., Liu, *Enhanced adsorption of heavy metal ions onto simultaneous interpenetrating polymer network hydrogels synthesized by UV irradiation*, Polymer Bulletin, 2013. 70: p. 1415–1430.

[47] Wichterle, O., and D., Lim, *Hydrophilic gels in biologic use*, Nature, 1960. 185: 117-118.

[48] Campoccia, D., Doherty, P., Radice, M., Brun, P., Abatangelo, G., and D.F., Williams, *Semisynthetic resorbable materials from hyaluronan esterification*, Biomaterials, 1998. 19: p. 2101–2127.

[49] Prestwich, G.D., Marecak, D.M., Marecak, J.F., Vercruysse, K.P., and M.R., Ziebell, *Controlled chemical modification of hyaluronic acid*, Journal of Controlled Release, 1998. 53: 93–103.

[50] Raeburn, J., Zamith Cardoso, A., and D.J., Adams, *The importance of the self-assembly process to control mechanical properties of low molecular weight hydrogels*, Chemical Society Reviews, 2013. 42: p. 5143-56.

[51] Estroff, L.A., and A.D., Hamilton, *Water Gelation by Small Organic Molecules*, Chemical Reviews, 2004. 104: p. 1201-1217.

[52] Tiller, J.C., *Increasing the local concentration of drugs by hydrogel formation*, Angewandte Chemie International Edition, 2003. 42: p. 3072-3075.

[53] Fenniri, H., Mathivanan, P., Vidale, K.L., Sherman, D.M., Hallenga, K., Wood, K.V., and J.G., Stowell, *Helical rosette nanotubes: design, self-assembly, and characterization*, Journal of the American Chemical Society, 2001. 123: p. 3854-3855.

[54] Israelachvili, J.N., *Intermolecular and Surface Forces, 2nd ed.*, Academic Press, New York, 1991.

[55] Xing, B., Choi, M.F., and B., Xu, *A stable metal coordination polymer gel based on a calix[4]arene and its 'uptake' of non-ionic organic molecules from the aqueous phase*, Chemical Communications, 2002. 4: p. 362-363.

[56] Menger, F.M., and K.L., Caran, *Anatomy of a Gel. Amino Acid Derivatives That Rigidify Water at Submillimolar Concentrations*, Journal of the American Chemical Society, 2000. 122: p. 11679–11691.

[57] Yang, Z., Liang, G., Ma, M., Gao, Y., and B., Xu, *Conjugates of naphthalene and dipeptides produce molecular hydrogelators with high efficiency of hydrogelation and superhelical nanofibers*, Journal of Materials Chemistry, 2007. 17: p. 850-854.

[58] Mahler, A., Reches, M., Rechter, M., Cohen, S., and E., Rigid, *Self-Assembled Hydrogel Composed of a Modified Aromatic Dipeptide Gazit*, Advanced Materials, 2006. 18: p. 1365–1370.

[59] Fuhrhop, J.H., and W., Helfrich, *Fluid and solid fibers made of lipid molecular bilayers*, Chemical Reviews, 1993. 93: p. 1565-1582.

[60] Kunitake, T., Okahata, Y., Shimomura, M., Yasunami, S., and K., Takarabe, *Formation of stable bilayer assemblies in water from single-chain amphiphiles. Relationship between the amphiphile structure and the aggregate morphology*, Journal of the American Chemical Society, 1981. 103: 5401-5413.

[61] Schnur, J.M., *Lipid Tubules: A Paradigm for Molecularly Engineered Structures*, Science, 1993. 262: p. 1669-1676.

[62] Thomas, B.N., Safinya, C.R., Plano, R.J., and N.A., Clark, *Lipid tubule self-assembly: length dependence on cooling rate through a first-order phase transition*, Science, 1995. 267: p. 1635-1638.

[63] Fuhrhop, J.H., Svenson, S., Boettcher, C., Rossler, E., and H.M., Vieth, *Long-lived micellar N-alkylaldonamide fiber gels. Solid-state NMR and electron microscopic studies*, Journal of the American Chemical Society, 1990. 112: p. 4307-4312.

[64] Boettcher, C., Schade, B., and J.H., Fuhrhop, *Comparative Cryo-Electron Microscopy of Noncovalent N-Dodecanoyl-(D- and L-) serine Assemblies in Vitreous Toluene and Water*, Langmuir, 2001. 17: p. 873-877.

[65] Imae, T., Takahashi, Y., and H., Muramatsu, *Formation of fibrous molecular assemblies by amino acid surfactants in water*, Journal of the American Chemical Society, 1992. 114: p. 3414-3419.

[66] Wang, G., and A.D., Hamilton, *Low molecular weight organogelators for water*, Chemical Communications, 2003. 3: 310-311.

[67] Shimizu, T., Iwaura, R., Masuda, M., Hanada, T., and K., Yase, *Internucleobase-Interaction-Directed Self-Assembly of Nanofibers from Homo- and Heteroditopic 1,ω-Nucleobase Bolaamphiphiles*, Journal of the American Chemical Society, 2001. 123: p. 5947-5955.

[68] Menger, F.M., and C.A., Littau, *Gemini-surfactants: synthesis and properties*, Journal of the American Chemical Society, 1991. 113: p. 1451-1452.

[69] Bhattacharya, S., and S.N.G., Acharya, *Pronounced Hydrogel Formation by the Self-Assembled Aggregates of N-Alkyl Disaccharide Amphiphiles*, Chemistry of Materials, 1999. 11: p. 3504-3511.

[70] Sagiri, S.S., Behera, B., Rafanan, R.R., Bhattacharya, C., Pal, K., Banerjee, I., and D., Rousseau, *Organogels as Matrices for Controlled Drug Delivery: A Review on the Current State*, Soft Materials, 2014. 12: p. 47-72.

[71] Co, E.D., and A.G., Marangoni, *Organogels: An Alternative Edible Oil-Structuring Method*, Journal of the American Chemical Society, 2012. 89: p. 749-780.

[72] Rogers, M.A., Wright, A.J., and A.G., Marangoni, *Oil organogels: the fat of the future?*, Soft Matter, 2009. 5: p. 1594-1596.

[73] Rogers, M.A., *Novel structuring strategies for unsaturated fats – Meeting the zero-trans, zero-saturated fat challenge: A review*, Food Research International, 2009. 42: p. 747-753.

[74] Weiss, R.G., and P., Terech, *Molecular gels materials with self-assembled fibrillar networks*, Weiss, R.G., and P., Terech, Eds., Springer, Dordrecht, 2006.

[75] Hashizaki, K., Taguchi, H. and Y., Saito, *A novel reverse wormlike micelle from a lecithin/sucrose fatty acid ester/oil system*, Colloil & Polymer Science, 2009. 287: p. 1099–1105.

[76] Trickett, K., Brice, H., Myakonkaya, O., Eastoe, J., Rogers, S.E., Heenan, R.K. and I., Grillo, *Microemulsion-based organogels containing inorganic nanoparticles*, Soft Matter, 2010. 6: p. 1291–1296.

[77] Trivedi, D.R., Ballabh, A., Dastidar, P., and B., Ganguly, *Structure-property correlation of a new family of organogelators based on organic salts and their selective gelation of oil from oil/water mixtures*, Chemistry - A European Journal, 2010. 10: p. 5311–5322.

[78] Shchipunov, Y.A., *Self-organising structures of lecithin*, Russian Chemical Reviews, 1997. 66: p. 301–322.

[79] Brizard, A., Oda, R., and I., Huc, *Chirality effects in self-assembled fibrillar networks*, Topics in Current Chemistry, 2005. 256: p. 167–218.

[80] Gronwald, O., and S., Shinkai, *Sugar-integrated gelators of organic solvents*, Chemistry, 2001. 7: p. 4328–4334.

[81] Fuhrhop, J.H., and W., Helfrich, *Fluid and solid fibers made of lipid molecular bilayers*, Chemical Reviews, 1993. 93: p. 1565–1582.

[82] Wang, R., Liu, X.Y., Xiong, J., and J., Li, *Real-Time Observation of Fiber Network Formation in Molecular Organogel: Supersaturation-Dependent Microstructure and Its Related Rheological Property*, The Journal of Physical Chemistry B, 2006. 110: p. 7275-7280.

[83] Kumar, R., and O.P., Katare, *Lecithin organogels as a potential phospholipid-structured system for topical drug delivery: a review*, AAPS PharmSciTech, 2005. 6: p. 298-310.

[84] Jibry, N., Heenan, R.K., and S., Murdan, *Amphiphilogels for drug delivery: Formulation and characterization*, Pharmaceutical Research, 2004. 21: p. 1852–1861.

[85] Willard, D.M., Riter, R.E., and N.E., Levinger, *Dynamics of polar solvation in lecithin/water/cyclohexane reverse micelles*, Journal of American Chemical Society, 1998. 120: p. 4151–4160.

[86] Brizard, A., Stuart, M., van Bommel, K., Friggeri, A., de Jong, M., and J., van Esch, *Preparation of Nanostructures by Orthogonal Self-Assembly of Hydrogelators and Surfactants*, Angewandte Chemie International Edition, 2008. 47: p. 2063–2066.

[87] Pernetti, M., van Malssen, K.F., Flöter, E., and A., Bot, *Structuring of edible oils by alternatives to crystalline fat*, Current Opinion in Colloid & Interface Science, 2007. 12: p. 221–231.

[88] Srivastava, S.P., Saxena, A.K., Tandon, R.S., and V., Shekher, *Measurement and prediction of solubility of petroleum waxes in organic solvents*, Fuel, 1997. 76: p. 625–630.

[89] Dassanayake, L.S.K., Kodali, D.R., and S., Ueno, *Formation of oleogels based on edible lipid materials*, Current Opinion in Colloid & Interface Science, 2011. 16: p. 432–439.

[90] Toro-Vazquez, J.F., Morales-Rueda, J.A., Dibildox-Alvarado, E., Charó-Alonso, M., Alonzo-Macia,s M., and M.M., González-Chávez, *Thermal and textural properties of organogels developed by candelilla wax in safflower oil*, Journal of the American Oil Chemists' Society, 2007. 84: p. 989–1000.

[91] Morales-Rueda, J.A., Dibildox-Alvarado, E., Charó-Alonso, M., Weiss, R.G., and J.F., Toro-Vazquez, *Thermo-mechanical properties of candelilla wax and dotriacontane organogels in safflower oil*, European Journal of Lipid Science and Technology, 2009. 111: p. 207–215.

[92] Toro-Vazquez, J.F., Alonzo-Macias, M., Dibildox-Alvarado, E., and M.A., Charó-Alonso, *The effect of tripalmitin crystallization on the thermomechanical properties of candelilla wax organogels*, Food Biophysics, 2009. 4: p. 199–212.

[93] Kodali, D.R., *The utilization of rice bran wax to stabilize long chain ω-3 polyunsaturated fatty acid esters*, Lipid Technology, 2009. 21: p. 254–256.

[94] Dassanayake, L.S.K., Kodali, D.R., Ueno, S., and K., Sato, *Physical properties of rice bran wax in bulk and organogels*, Journal of the American Oil Chemists' Society, 2009. 86: p. 1163–73.

[95] Daniel, J., and R., Rajasekaran, *Organogelation of plant oils and hydrocarbons by long-chain saturated FA, fatty alcohols, wax esters, and dicarboxylic acids*, Journal of the American Oil Chemists' Society, 2003. 80: p. 417–21.

[96] Gandolfo, F.G., Bot, A, and E., Flöter, *Structuring of edible oils by long-chain FA, fatty alcohols, and their mixtures*, Journal of the American Oil Chemists' Society, 2004. 81: p. 1–6.

[97] Kuwahara, T., Nagase, H., Endo, T., Ueda, H., and M., Nakagaki, *Crystal structure of DL-12-hydroxystearic acid*, Chemistry Letters, 1996. p. 435–436.

[98] Kirilov, P., Lukyanova, L., Franceschi-Messant, S., Perier, V., Pereza, E., and I., Rico-Lattes, *A new type of colloidal dispersions based on nanoparticles of gelled oil*, Colloids and Surfaces A: Physicochemical and Engineering Aspects, 2008. 328: p. 1–7.

[99] Moniruzzaman, M., Sahin, A., and K.I., Winey, *Improved mechanical strength and electrical conductivity of organogels containing carbon nanotubes*, Carbon, 2009. 47: p. 645–650.

[100] Toro-Vazquez, J.F., Morales-Rueda, J., Mallia, V.A., and R.G., Weiss, *Relationship Between Molecular Structure and Thermo-mechanical Properties of Candelilla Wax and Amides Derived from (R)-12-Hydroxystearic Acid as Gelators of Safflower Oil*, Food Biophysics, 2010. 5: p. 193–202.

[101] Wright, A.J., and A.G., Marangoni, *Formation, structure, and rheological properties of ricinelaidic acid-vegetable oil organogels*, Journal of the American Oil Chemists' Society, 2006. 83: p. 497–503.

[102] Wright, A.J., and A.G., Marangoni, *Time, temperature and concentration dependence of ricinelaidic acid–canola oil organogelation*, Journal of the American Oil Chemists' Society, 2007. 84: p. 3–9.

[103] Schaink, H.M., van Malssen, K.F., Morgado-Alves, S., Kalnin, D., and E., van der Linden, *Crystal network for edible oil organogels: possibilities and limitations of the fatty acid and fatty alcohol systems*, Food Research International, 2007. 40: p. 1185–93.

[104] Lupi, F.R., Gabriele, D., Facciolo, D., Baldino, N., Seta, L., de Cindio, B., *Effect of organogelator and fat source on rheological properties of olive oil-based organogels*, Food Research International, 2012. 46: p. 177–184.

[105] Realdon, N., Ragazzi, E., and E., Ragazzi, *Effect of gelling conditions and mechanical treatment on drug availability from a lipogel,* Drug Development and Industrial Pharmacy, 2001. 27: p. 165–70.

[106] Heertje, I., Roijers, E.C., and H.A.C.M., Hendrickx, *Liquid crystalline phases in the structuring of food products*, LWT - Food Science and Technology, 1998. 31: p. 387–96.

[107] Sein, A., Verheij, J.A., and W.G.M., Agterof, *Rheological Characterization, Crystallization, and Gelation Behavior of Monoglyceride Gels*, Journal of Colloid and Interface Science, 2002. 249: p. 412–422.

[108] Ojijo, N.K.O., Neeman, I., Eger, S., and E., Shimoni, *Effects of monoglyceride content, cooling rate and shear on the rheological properties of olive oil/monoglyceride gel networks*, Journal of the Science of Food and Agriculture, 2004. 84: p. 1585–93.

[109] Katan, M.B., Grundy, S.M., Jones, P., Law, M., Miettinen, T., and R., Paoletti, *Efficacy and safety of plant stanols and sterols in the management of blood cholesterol concentrations*, Mayo Clinic Proceedings, 2003. 78:965–978.

[110] Bot, A, and W.G.M., Agterof, *Structuring of edible oils by mixtures of γ-oryzanol with β-sitosterol or related phytosterols*, Journal of the American Oil Chemists' Society, 2006. 83: p. 513–521.

[111] Yan, X., Cui, Y., He, Q., Wang, K., and J., Li, *Organogels based on self-assembly of diphenylalanine peptide and their application to immobilize quantum dots*, Chemical Matter, 2008. 20: p. 1522–1526.

[112] Palui, G., Simon, F. X., Schmutz, M., Mesini, P. J., and A., Banerjee, *Organogelators form self-assembling peptide based dendrimers: Structural and morphological features*, Tetrahedron, 2008. 64: p. 175–185.

[113] John, G., Zhu, G., Li, J., and J.S., Dordick, *Enzymatically derived sugar-containing self-assembled organogels with nanostructured morphologies*, Angewandte Chemie, 2006. 118: p. 4890–4893.

[114] Scartazzini, R., and P.L. Luisi, *Organogels from lecithins*, The Journal of Physical Chemistry, 1988. 92: p. 829–833.

[115] Murdan, S., Gregoriadis, G., and A.T., Florence, *Inverse toroidal vesicles: precursors of tubules in sorbitan monostearte organogels,* International Journal of Pharmaceutics, 1999. 183: p. 47–49.

[116] Jibry, N., Sarwar, T. and S., Murdan, *Amphiphilogels as drug carriers: effects of drug incorporation on the gel and on active drug,* Journal of Pharmacology and Pharmacotherapeutics, 2006. 58: p. 187–94.

[117] Murdan, S., Gregoriadis, G., and A.T., Florence, *Sorbitan monostearate/polysorbate 20 organogels containing niosomes: a delivery vehicle for antigens?*, European Journal of Pharmaceutical Sciences, 1999. 8: p. 177–185.

[118] Pernetti, M., van Malssen, K.F., Kalnin, D., and E., Flöter, *Structuring edible oil with lecithin and sorbitan tri-stearate*, Food Hydrocolloids, 2007. 21: p. 855–861.

[119] Romoscanu, A.I., and R., Mezzenga, *Emulsion-templated fully reversible protein-in-oil gels*, Langmuir, 2006. 22: p. 7812–7818.

[120] Suzuki, M., Tomoko, A., and K., Hanabusa, *Low-molecular-weight gelators based on N^{α}-acetyl-N^{ϵ}-lauroyl-L-lysineand their amphiphilic gelation properties*, Journal of Colloid and Interface Science, 2010. 341: p. 69–74.

[121] Mukkamala, R., and R.G., Weiss, *Physical gelation of organic fluids by anthraquinone-steroid-based molecules: structural features influencing the properties of gels*, Langmuir, 1996. 12: p. 1474–1482.

[122] He, P., Liub, J., Liua, K., Dinga, L., Yana, J., Gaoa, D., and Y., Fang, *Preparation of novel organometallic derivatives of cholesterol and their gel-formation properties*, Colloid Surface A, 2010. 362: p. 127–134.

[123] Gronwald, O., Snip, E., and S., Shinkai, *Gelators for organic liquids based on self-assembly: a new facet of supramolecular and combinatorial chemistry*, Current Opinion in Colloid & Interface Science, 2002. 7: p. 148-156.

[124] Dey, T., Kim, D.A., and A.G., Marangoni, "Ethylcellulose oleogels", in: *Edible oleogels: structure and health implications*, Marangoni, A.G., Garti, N., Eds., AOCS Press, Urbana, 2011.

[125] Laredo, T., Barbut, S., and A.G., Marangoni, *Molecular interactions of polymer oleogelation*, Soft Matter, 2011. 7: p. 2734–2743.

[126] Smith, D.K., "Molecular Gels – Nanostructured Soft Materials", in: *Organic nanostructures*, Atwood, J.L., Steed, J.W., Eds., Wiley-VCH Verlag GmbH & Co. KGaA, Weinheim, 2008.

[127] Terech, P., Ostuni, E., and R.G., Weiss, *Structural study of cholesteryl anthraquinone-2-carboxylate (CAQ) physical organogels by neutron and X-ray small angle scattering*, The Journal of Physical Chemistry, 1996. 100: p. 3759-3766.

[128] Abdallah, D.J., Sirchio, S.A., and R.G., Weiss, *Hexatriacontane organogels. The first determination of the conformation and molecular packing of a low-molecular-mass organogelator in its gelled state*, Langmuir, 2000. 16: p. 7558-7561.

[129] Rogers, M.A., Wright, A.J., and A.G., Marangoni, *Crystalline stability of self-assembled fibrillar networks of 12-hydroxystearic acid in edible oils*, Food Research International, 2008. 41: p. 1026–1034.

[130] Palui, G., Garai, A., Nanda, J., Nandi, A.K., and A., Banerjee, *Organogels from different self-assembling new dendritic peptides: morphology, rheology, and structural investigations*, The Journal of Physical Chemistry B, 2010, 114, 1249–1256.

[131] Duffy, N., Blonk, H.C.G., Beindorff, C.M., Cazade, M., Bot, A., and G.S.M.J.E., Duchateau, *Organogel-Based Emulsion Systems, Micro-Structural Features and Impact on In Vitro Digestion*, Journal of the American Oil Chemists' Society, 2009. 86: p. 733–741.

[132] Shchipunov, Y.A., and E.V., Shumilina, *Lecithin bridging by hydrogen bonds in the organogel*, Material Science and Engineering: C, 1995. 3: p. 43–50.

[133] Suzuki, M., Nanbu, M., Yumoto, M., Shiraib, H., and K., Hanabusa, *Novel dumbbell-form low-molecular-weight gelators based on L-lysine: their hydrogelation and organogelation properties*, New Journal of Chemistry, 2005. 29: p. 1439–1444.

[134] Kamikawa, Y., and T., Kato, *Color-Tunable Fluorescent Organogels: Columnar Self-Assembly of Pyrene-Containing Oligo(glutamic acid)s*, Langmuir, 2007. 23: p. 274–278.

[135] Rao, M.A., *Rheology of Fluid and Semisolid Foods: Principles and Applications*, 2nd *ed*., Springer, New York, 2007.

[136] Rogers, M.A., Wright, A.J., and A.G., Marangoni, *Nanostructuring fiber morphology and solvent inclusions in 12-hydroxystearic acid/canola oil organogels*, Current Opinion in Colloid & Interface Science, 2009. 14: p. 33–42.

[137] Lopez-Martinez, A., Morales-Rueda, J., Dibildox-Alvarado, E., Charo-Alonso, M., Marangoni, A., and J., Toro-Vazquez, *Comparing the crystallization and rheological behavior of organogels developed by pure and commercial monoglycerides in vegetable oil*, Food Research International, 2014. 64: p. 946-957.

[138] Chopin-Doroteo, M., Morales-Rueda, J.A., Dibildox-Alvarado, E.,Charó-Alonso, M.A., de la Peña-Gil, A., and J.F., Toro-Vazquez, *The Effect of Shearing in the Thermo-mechanical Properties of Candelilla Wax and Candelilla Wax–Tripalmitin Organogels*, Food Biophysics, 2011. 6: p. 359–376.

[139] Tang, D., ang A.G., Marangoni, *Modeling the rheological properties and structure of colloidal fat crystal networks*, Trends in Food Science & Technology, 2007. 18: p. 474-483.

[140] Van den Tempel, M., *Mechanical properties of plastic disperse systems at very small deformation*, Journal of Colloid Science, 1961. 16: p. 284-296.

[141] Van den Tempel, M., *Rheology of concentrated suspensions*, Journal of Colloid and Interface Science, 1979. 71: p. 18-20.

[142] Vreeker, R., Hoekstra, L.L., den Boer, D.C., and W.G.M., Agterof, *The fractal nature of fat crystal networks*, Colloids and Surfaces, 1992. 65: p. 185-189.

[143] Mandelbrot, B.B., *The fractal geometry of nature*, Freeman, New York, 1982.

[144] Marangoni, A.G., *The nature of fractality in fat crystal networks*, Trends in Food Science & Technology, 2002. 13: p. 37–47.

[145] Shih, W.H., Shih, W.Y., Kim, S.I., Liu, J., and I.A., Aksay, *Scaling behavior of the elastic properties of colloidal gels*, Physical Review A, 1990. 42: p. 4772-4779.

[146] Narine, S.S., and A.G., Marangoni, *Mechanical and structural model of fractal networks of fat crystals at low deformation*, Physical Review E, 1999. 60: p. 6991-7000.

[147] Awad, T.S., Rogers, M.A., and A.G., Marangoni, *Scaling behavior of the elastic modulus in colloidal networks of fat crystals*, Journal of Physical Chemistry B, 2004. 108: p. 171-179.

[148] Toro-Vazquez, J.F., Dibildox-Alvaradoa, E., Charó-Alonso, M., Herrera-Coronado, V., and C.A., Gómez-Aldapa, *The Avrami Index and the Fractal Dimension in Vegetable Oil Crystallization*, Journal of the American Oil Chemists' Society, 2002. 79: p. 855-866.

[149] Lopes da Silva, J.A., Gonçalves, M.P., and M. A., Rao, *Kinetics and thermal behaviour of the structure formation process in HMP/sucrose gelation*, International Journal of Biological Macromolecules, 1995. 17: p. 25-32.

[150] Lopes da Silva, J.A., and M.A., Rao, "Rheological Behavior of Food Gel Systems", in *Rheology of Fluid and Semisolid Foods, Principles and Applications*, Aspen Publishers Inc., Gaithersburg, 1999.

[151] Lupi, F.R., Gabriele, D., Facciolo, D., Baldino, N., Seta, L., and B., de Cindio, *Effect of organogelator and fat source on rheological properties of olive oil-based organogels*, Food Research International, 2012. 46: p. 177–184.

[152] Lapasin, R., and S., Pricl, *Rheology of industrial polysaccharides: Theory and applications*, 1st *ed*., Blackie Academic and Professional, Glasgow, 1995.

[153] Tung, C.Y., and P.J., Dynes, *Relationship between viscoelastic properties and gelation in thermosetting systems*, Journal of Applied Polymer Science, 1982. 27: p. 569–574.

[154] Winter, H.H., and F., Chambon, *Analysis of linear viscoelasticity of a cross-linking polymer at the gel point*, Journal of Rheology, 1986. 30: p. 367-382.

[155] Winter, H.H., Morganelli, P., and F. Chambon, *Stoichiometry effects on rheology of model polyurethanes at the gel point*, Macromolecules, 1988. 21: p. 532-535.

[156] Winter, H.H., and M., Mours, *Rheology of Polymers Near Liquid-Solid Transitions*, Advances in Polymer Science, 1997. 134: p. 165-234.

[157] Hughes, N.E., Marangoni, A.G., Wright, A.J., Rogers, M.A., and J.W.E., Rush, *Potential food applications of edible oil organogels*, Trends in Food Science & Technology, 2009. 20: p. 470-480.

[158] Carretti, E., Dei, L., and R.G., Weiss, *Soft matter and art conservation. Rheoreversible gels and beyond*, Soft Matter, 2005. 1: p. 17-22.

[159] Rogers, M.A., Wright, A.J., and A.G., Marangoni, *Engineering the oil binding capacity and crystallinity of self-assembled fibrillar networks of 12-hydroxystearic acid in edible oils*, Soft Matter, 2008. 4: p. 1483-1490.

[160] Elliger, C.A., Guadagni, D.G., and C.E., Dunlap, *Thickening action of hydroxystearates in peanut butter*, Journal of the American Oil Chemists' Society, 1972. 49: p. 536–537.

[161] Marty, S., Baker, K., Dibildox-Alvarado, E., Rodrigues, J. N., and A.G., Marangoni, *Monitoring and quantifying of oil migration in cocoa butter using a flatbed scanner and fluorescence light microscopy*, Food Research International, 2005. 38: p. 1189-1197.

[162] Bot, A., Veldhuizen, Y.S.J., den Adel, R., and E.C., Roijers, *Non-TAG structuring of edible oils and emulsions*, Food Hydrocolloids, 2009. 23: p. 1184–1189.

[163] Hu, J., *Adaptive and Functional Polymers, Textiles and their Applications*, Imperial College Press, Singapore, 2011.

[164] Fukasawa, J.-I., Tsutsumi, H., and A., Ishida, *New oil-gelling agents for cosmetics: formation mechanism of oil gels*, International Journal of Cosmetic Science, 1989. 11: p. 153-165.

[165] Martinez, M.R., Benavides, M.M., Hernandez, M.M., and V.G., Lara, *Influence of the concentration of a gelling agent and the type of surfactant on the rheological characteristics of oleogels,* Il Farmaco, 2003. 58: p. 1289-1294.

[166] Villalobos-Hernandez, J., and C., Muller-Goymann, *Novel nanoparticulate carrier system based on carnauba wax and decyl oleate for the dispersion of inorganic sunscreens*

in aqueous media, European Journal of Pharmaceutics and Biopharmaceutics, 2005. 60: p. 113-122.

[167] Kirilov, P., Rum, S., Gilbert, E., Roussel, L., Salmon, D., Abdayem, R., Serre, C., Villa, C., Haftek, M., Falson, F., and F., Pirot, *Aqueous dispersions of organogel nanoparticles - potential systems for cosmetic and dermo-cosmetic applications*, International Journal of Cosmetic Science, 2014. 36: p. 336-346.

[168] Morales, M., Gallardo, V., Clares, B., and M., Garcia, *Study and description of hydrogels and organogels as vehicles for cosmetic active ingredients*, Journal of Cosmetic Science, 2009. 60: p. 627-636.

[169] Stortz, T.A., and A.G., Marangoni, *The replacement for petrolatum: thixotropic ethylcellulose oleogels in triglyceride oils*, Green Chemistry, 2014. 16: p. 3064–3070.

Chapter 2: rheological and microstructural characterisation of raw materials

Abstract

A complete characterisation, from a rheological, thermal and structural point of view, of various oils, fats and organogelators was carried out. Three different vegetable oils (sunflower oil, virgin and extra-virgin olive oil) have been analysed, as well as a vegetal fat, cocoa butter. Moreover, two potential organogelators were characterised: Myverol 18-04K, a commercial mixture of monoacylglycerols of fatty acids, and policosanol, a natural extract composed of primary long-chain fatty alcohols. The rheological behaviour of raw materials under cooling was studied performing both Dynamic Temperature Ramp Tests and Step Shear Rate Temperature Ramp Tests (at $1s^{-1}$ and $100s^{-1}$). Furthermore, DSC and NMR (for SFC determination) tests were carried out. When crystallisation was observed, the temperature of crystallisation onset was determined using all the techniques of analysis (rheology, DSC, NMR). Finally, FT-IR spectra at room temperature were collected, allowing the intrinsic characteristics of each material to be highlighted.

All the raw materials studied in the present Chapter were then used to produce more complex systems (organogels, structured emulsions, bigels), that will be described in the following chapters.

2.1 Introduction

Fats are an important component of our diet. The role played by fats in material functionality, flavour perception, texture and health characteristics is mainly due to their physical properties. Therefore, an understanding of these physical properties is relevant from scientific, technological and medical perspectives [1]. Fats and oils are complex multi-component mixtures of triacylglycerols (TAGs), hence the physical properties of fat materials are governed by a complex joint of various structural levels beginning with triglyceride molecules [1].

The unsaturation of the fatty acids is one of the key factors that determines the physical and nutritional functionality of TAGs. In fact, the only difference between a fat and an oil is that a fat is solid at room temperature (25°C) while oil is liquid. Oils, such as olive or

78

sunflower oil, contain a greater proportion of mono- and poly-unsaturated fatty acids, while fats like cocoa butter and palm fat, contain a greater proportion of saturated fatty acids [1].

One of the main key features of fats is that they are polycrystalline materials [2]. If a TAG melt is cooled below the crystallisation temperature of the highest melting TAG, the melt becomes undercooled, therefore the highest-melting TAG becomes super-saturated within a metastable region with respect to the liquid phase in which it is dissolved [1]. The understanding of crystallisation of TAGs is crucial for both research and industrial uses. Therefore, the main characteristics of TAG crystallisation phenomena will be overviewed in the following sections.

2.1.1 Crystallisation behaviour of TAGs

The crystallisation behaviour of TAGs in terms of crystallisation rate, crystal morphology, crystal sizes and their network is directly influenced by polymorphism which is, in turn, influenced by molecular structure itself and by several external factors (temperature, pressure, solvent, rate of crystallisation, impurities, etc.) [2].

Depending on the super-saturation of the melt, TAGs can crystallise into one of three predominant forms upon cooling, α, β' and β, in ascending order of melting point, density and stability [1, 3]. Each one of these polymorphs can form directly from the melt. Nevertheless, homotropic polymorphic transformations from a less stable to a more stable solid phase will take place in time. Figure 2.1 shows a schematic representation of TAG polymorphs. The three polymorphs are based on sub-cell structures, which define the cross-sectional packing modes of the aliphatic chain [2].
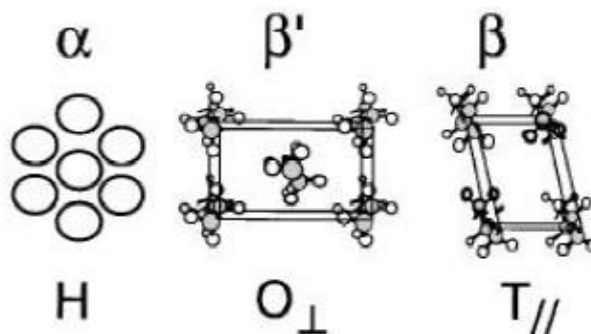
Figure 2.1 Polymorphism of triacylglicerols [2].

TAG nucleation into a specific polymorphic form can be understood using activation energy arguments. The energy of activation to form the α polymorph is much lower than the activation energy to form the β'or β forms [1]. Hence, the formation of α polymorph will be kinetically favoured even though it has the lowest thermodynamic stability [4].

As an example, Figure 2.2 shows the crystallisation behaviour of tripalmitoylglycerol (PPP), a fat model substance [2, 5]. Molecular structures of the three forms of PPP are the disordered aliphatic chain conformation in α, the intermediate packing in β' and the most dense packing in β, with decreasing values of the Gibbs free energy, *G*. The combined effects of the molecular structures and the rate of crystallisation lead to an amorphous-like crystal morphology for α form, tiny bulky shape for β' form and needle shape for β [2].
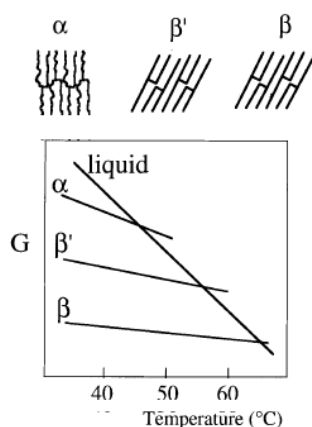
Figure 2.2 Structure models and Gibbs energy-temperature relationship of three polymorphs of PPP [2].

Generally speaking, it has been shown that fat crystallisation is dominated by nucleation processes [1]. Crystal number and size, spatial distribution of mass and crystal surface characteristics are greatly determined by the nucleation rate. When TAG crystals nucleate, molecules adopt the so-called "tuning fork" or "chair" conformations upon packing into a crystalline lattice (see Figure 2.3). Since in the solid state the fatty acid hydrocarbon chains are generally in an extended conformation, a molecular asymmetry is observed which results in the formation of TAG crystalline lamellae upon crystallisation [1].
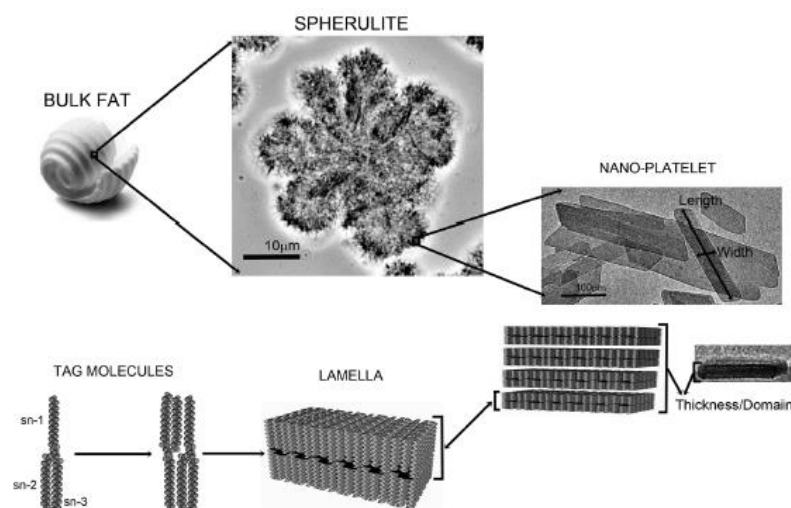
Figure 2.3 Structural hierarchy of TAG crystal network [1].

The nucleation of TAGs is quickly followed by crystalline growth. At the mesoscale level (length scales within the micrometre range), crystals aggregates show several different habits (sherulites, needle-like crystals, micro-platelets, disordered crystal aggregates, spherical crystal aggregates, fractal-like aggregates, etc.). Despite the differences in morphologies, crystalline aggregates exhibit some common features, for example the crystalline mass in a network of these crystals is always distributed in a fractal fashion [1].

Nevertheless, it should be taken into account that fats from natural sources are complex mixtures of different types of TAGs. Therefore, complicated behaviour of melting, crystallisation, crystal morphology and aggregation of the real-fat systems are partly due to the physical properties of the component TAGs, and more importantly due to the phase behaviour of the mixtures [2]. The complex behaviour of real TAG mixtures has been extensively studied recently, using various techniques (synchrotron radiation X-ray diffraction, FT-IR spectroscopy, differential scanning calorimetry and optical observation) [1, 2, 6, 7].

2.1.1.1 Crystallisation behaviour of cocoa butter

Cocoa butter is an outstanding example of polymorphic fat, in fact, according to proper crystallisation and ageing conditions, different crystal forms are obtained, which exhibit characteristic melting points (see Table 2.1) and X-ray diffraction patterns [8, 9, 10]. The polymorphism of cocoa butter has often been discussed in the literature because it is

related to the organoleptic and physical characteristics of chocolate or other food products (snap, moulding contraction, gloss and blooming during storage) [10].

Polymorph	Melting point [°C]
γ (I)	14.9-16.1
α (II)	17.0-23.2
β'_2 (III)	22.8-27.1
β'_1 (IV)	25.1-27.4
β_2 (V)	31.3-33.2
β_1 (VI)	33.8-36.0

Table 2.1 Melting point of the different polymorphic forms of cocoa butter [10].

Nevertheless, no uniform nomenclature is available in the literature for cocoa butter polymorphs. Cocoa butter polymorphism is commonly described in terms of six different polymorphic forms, noted from I to VI in increasing order of melting points and stability, according to the nomenclature of Wille and Lutton [10, 11]. Other authors named cocoa butter polymorphs as γ, α, β_1', β_2', β_1 and β_2 [11]. Schenk and Peschar [12] unified the different polymorph in γ, α, β', β(V) and β(VI). In fact, the existence of some polymorphs is debated. According to some authors, Form III corresponds to a mixture of Forms II and IV and is not a separate crystalline form. In the same way, Form I could be a phase mixture and Form VI can result from phase separation within a solid solution [10].

2.1.1.2 Crystallisation behaviour of monoglycerides

The liquid-crystal and fully crystalline structures of pure monoglycerides were first described by Larsson in 1966 [13] and then reviewed by Larsson himself [14] and Krog [15]. The polymorphic behaviour of monoglycerides involves the following phase sequence on cooling: isotropic fluid, lamellar and alpha-crystalline phases [16]. Initially, the behaviour of pure saturated asymmetric monoglycerides (1-MAG) has been extensively studied [17, 18]. There are generally three polymorphs for these monoglycerides, called sub-α, α and β [17]. Monoglycerides crystallise directly in the α polymorph which can transform into a more stable β form during storage at ambient temperatures. When monoglycerides in the α form are cooled 35–50°C below the crystallisation point of the α polymorph, they undergo a polymorphic transition to a reversible sub-α polymorph [15, 17]. The sub-α polymorph contains a β' sub-cell and is less stable than the α form.

For some 1-MAG compounds, such as 1-mono-stearoyl-*rac*-glycerol, a further sub-α form has been detected (called sub-α_2) at temperature lower than 0°C [18]. A β' polymorphic form is only formed through quick crystallisation using specific solvents and is not observed by thermal analysis techniques such as differential scanning calorimetry [17, 19]. For commercial monoglycerides, containing also small amounts of other components like diglycerides and triglycerides, no β' polymorph could be detected [15, 17]. Commercial mixture of MAGs typically show a polymorphic behaviour different from pure MAG, according to the composition of the mixture [18].

In contrast to the asymmetric 1-monoglycerides, different studies have described that the symmetric 2-monoglycerides (also named β-monoglycerides) do not exhibit polymorphism and are only characterized by a melting point which is lower than the melting point of the corresponding asymmetric isomers [19, 17].

2.1.1.3 Crystallisation behaviour of vegetable oils

It is well known that vegetable oils are liquid at room temperature. The arrangement of TAGs in the solid and liquid states depends on a balance between the organizing influence of the attractive interactions between the molecules and the disorganizing influence of the thermal energy [20]. For the majority of industrial and commercial uses, the crystallisation of vegetable oils is unwanted. Nevertheless, palm oil is widely used in the food and cosmetic industry because it is cheap and its high melting fractions can be easily crystallised and separated through fractionation [21]. Extra-virgin olive oil is the major edible vegetable oil in Mediterranean countries, mainly due to its beneficial health effects [22]. Olive oil is always used as liquid oil and the eventual presence of crystalline aggregates (which can form at temperature lower than 4-5°C) is one of the primary causes of consumer dissatisfaction. Solid derivatives of olive oil, such as waxes and butters, are obtained by catalytic hydrogenation of olive oil and employed as viscosity modifiers in cosmetics [23].

2.2 Materials and methods

2.2.1 Samples ingredients

In the present work, three vegetable oils were characterised: virgin olive oil (De Santis, Italy), sunflower oil (De Santis, Italy), both supplied by a local supermarket, and extra-virgin olive oil (kindly supplied by Gabro S.r.l., Italy). According to the manufacturers,

virgin olive oil is mainly composed of mono-unsaturated fatty acids (about 75%$_{w/w}$), the rest being saturated (about 15%$_{w/w}$) and poly-unsaturated (about 10%$_{w/w}$), whereas extra-virgin olive oil contains about 72%$_{w/w}$ of mono-unsaturated fatty acids, 14%$_{w/w}$ of poly-unsaturated and 14%$_{w/w}$ of saturated fatty acids. Instead, sunflower oil is composed of 12%$_{w/w}$ of saturated fatty acids, 32%$_{w/w}$ of mono-unsaturated and 56%%$_{w/w}$ of poly-unsaturated fatty acids.

A natural source of saturated fats, cocoa butter (kindly supplied by Icam S.p.A., Italy), were characterised. According to the manufacturers data, cocoa butter (see Table 2.2) is mainly composed of saturated (56–68%$_{w/w}$) and mono-unsaturated (31–38%$_{w/w}$) fats and a low amount of poly-unsaturated fats (2–4%$_{w/w}$).

Fatty acid	Composition [%$_{w/w}$]
Stearic acid	32-37
Oleic acid	30-37
Palmitic acid	23-30
Linoleic acid	2-4
Arachidic acid	<1
Palmitoleic acid	<1

Table 2.2 Average composition of cocoa butter.

The thermal and structural properties of two different potential organogelators were studied: a commercial mixture of monoglycerides of fatty acids (Myverol 18-04K, Kerry Group, Ireland, referred to as "Myverol" throughout the chapter) and policosanol (A.C.E.F., Italy), a mixture of primary fatty alcohols, extracted from rice bran wax. According to the manufacturers, Myverol is roughly composed of 50%$_{w/w}$ monopalmitin (C$_{16:0}$) and 50%w/w monostearin (C$_{18:0}$). The fatty alcohol composition of policosanol (according to the manufacturers) is listed in Table 2.3.

Fatty alcohol	Composition [%$_{w/w}$]
1-Tetracosanol (C$_{24}$)	1-9
1-Hexacosanol (C$_{26}$)	3-35
1-Octacosanol (C$_{28}$)	60-69
1-Triacontanol (C$_{30}$)	5-20
1-Dotriacontanol (C$_{32}$)	0.1-10
1-Tertatriacontanol (C$_{34}$)	0.1-10

Table 2.3 Fatty alcohol composition of policosanol.

Composition and identified of tested materials are listed in Table 2.4.

Sample ID	Virgin Olive Oil [%$_{w/w}$]	Sunflower Oil [%$_{w/w}$]	Extra Virgin Olive Oil [%$_{w/w}$]	Cocoa Butter [%$_{w/w}$]	Myverol [%$_{w/w}$]	Policosanol [%$_{w/w}$]
VO	100	-	-	-	-	-
EVO	-	-	100	-	-	-
SO	-	100	-	-	-	-
CB	-	-	-	100	-	-
M	-	-	-	-	100	-
P	-	-	-	-	-	100

Table 2.4 Samples ID and composition.

2.2.2 Rheological characterisation

All samples were characterised with a controlled strain rheometer ARES-RFS (TA Instruments, USA), equipped with a parallel plate geometry (ϕ=50mm, gap=1±0.1mm) and a Peltier system (±0.1°C) acting under the lower plate. All raw materials were analysed using the same temperature conditions employed for organogels (see Chapters 3 and 4). Therefore, samples were poured on the lower plate of the rheometer (preheated at 70°C) and a controlled cooling rate of 1°C/min was applied during rheological measurements.

A rheological characterisation based on both Small Amplitude Oscillation Tests (SAOTs) and Step Rate Temperature Ramp Tests (SRTRTs) was carried out. Time Cure Tests were performed in linear viscoelastic conditions from 70°C to 0°C with a constant frequency of 1Hz. Preliminary Strain Sweep Tests were carried out at different temperatures from the temperature of sample preparation down to 0°C, in order to

investigate the potential changes in linear viscoelastic conditions at decreasing temperature. For each Strain Sweep Test, the material was cooled down to the desired temperature using a cooling rate of 1°C/min and applying the minimum strain within the instrument limits. Then, Strain Sweep Tests were performed at the desired temperature. Finally, Time Cure Tests were carried out applying different constant strain values in different temperature ranges, with the aim of guaranteeing the linear viscoelastic conditions in the whole temperature range investigated.

When crystallisation phenomena were observed during Time Cure Tests, the onset of crystallisation temperature (T_{co}) was calculated following the procedure described by Lupi et al. [24]: T_{co} was estimated as the temperature at which a strong and sharp increase of the complex modulus G^* (corresponding to a sudden decrease of loss tangent) was observed. The first derivative of the complex modulus with respect to the temperature was evaluated for each curve using a forward numerical method. The ratio R was obtained dividing the derivative values by the moving average of all the derivatives from starting temperature up to the current value. Then, the onset of crystallisation was chosen as the temperature value after which the ratio R increased by at least one order of magnitude. This procedure allowed potential errors in calculating T_{co} to be minimised, owing to the fact that data are often scattered at high temperatures and near the temperature at which the complex modulus began to increase.

In addition, Step Rate Temperature Ramp Tests (SRTRTs) at two different constant shear rates ($1s^{-1}$ and $100s^{-1}$) were performed, decreasing the temperature from 70°C to 0°C. In agreement with the procedure already described for oscillatory tests, the onset of crystallisation $T_{co,s}$ was estimated as the temperature at which a strong change in the slope of the viscosity curve was observed. The ratio R was calculated dividing the first derivative of the viscosity with respect to the temperature at each point by the moving average of all derivatives from starting temperature up to the current value. $T_{co,s}$ was then evaluated as the temperature at which R increased by at least one order of magnitude.

2.2.3 Thermal analysis

For all samples, the crystallisation and melting thermograms were recorded using a Mettler Toledo Model DSC822e (Mettler Toledo, Switzerland). Samples (≈5-10mg) were sealed in aluminium pans, heated at 70°C for 20min and then cooled to 0°C (or lower temperature, for vegetable oils) at a rate of 1°C/min (similarly to the rheological tests), recording the heat flux as a function of temperature. After 1min at the minimum

temperature, the material was heated up to 70°C using the same thermal ramp. As reported in the literature [25], the onset of crystallisation temperature ($T_{co, DSC}$) was estimated as the temperature corresponding to the beginning of the first exothermic peak, while the temperature of melting of each polymorph (T_M) was considered as the temperature corresponding to the peak of the melting endotherm.

2.2.4 Spectroscopic analysis

The solid fat content (SFC) of all investigated raw materials was determined by nuclear magnetic resonance with a Minispec mq20 (Bruker, Germany) [26]. In order to apply the same thermal history then used for organogels (Chapters 3 and 4), samples were preheated at 70°C and poured into NMR tubes. The temperature control was performed with an external water bath (RC 20, LAUDA-Brinkmann LP., USA) that provided an average cooling rate of approximately 1°C/min. Hence, SFC was measured at different temperature values upon cooling. Therefore, SFC values were plotted versus temperature obtaining curves very similar to the SRTRTs. Even for NMR analysis, the onset of crystallisation temperature ($T_{co, NMR}$) was evaluated as the temperature at which a sudden increase in the slope of the *SFC* curve as a function of temperature was observed.

Furthermore, infrared absorption spectra were recorded employing a Nicolet iS-10 FT-IR spectrometer (Thermo Scientific, USA) equipped with a Smart iTX ATR sampling accessory. All spectra were recorded at room temperature within the range of wavenumber between 400 and 4000cm^{-1}.

2.3 Results and discussion

2.3.1 Characterisation of vegetable oils and fats

2.3.1.1 Virgin olive oil

As predictable for a vegetable oil, Time cure tests on sample VO (see Figure 2.4) showed a liquid-like behaviour in almost all of the temperature range investigated. A change in complex modulus curve slope, can be observed at around 5.68±0.22°C, corresponding to a sharp decrease of the phase angle and indicating the beginning of crystallisation phenomena.
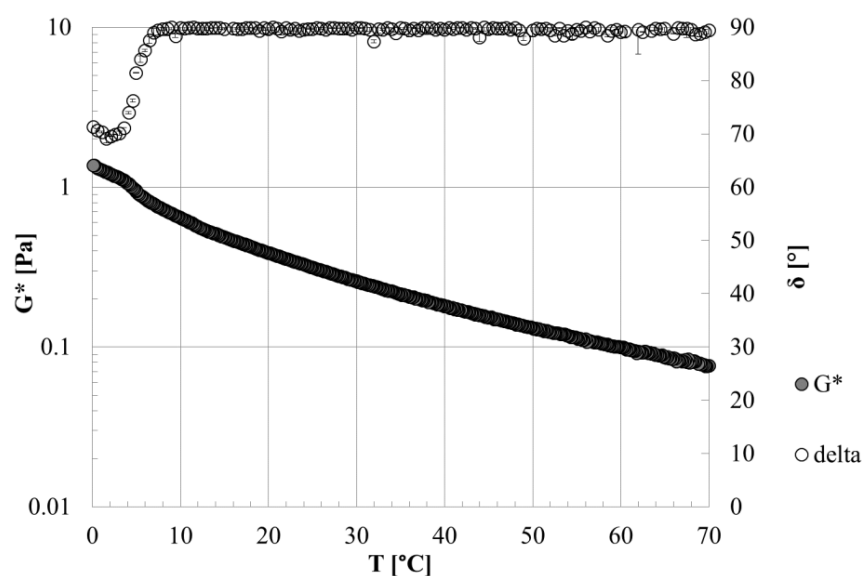
Figure 2.4 Time cure test for sample VO.

Figure 2.5 shows results obtained from SRTRT, evidencing that shear rate influences virgin olive oil crystallisation and delays its onset when high shear rate values are applied. In fact, in agreement with the literature [27], the onset of crystallisation was identified at 4.41±0.22°C at a shear rate of $1s^{-1}$, whereas no crystallisation was observed, within the temperature range investigated, at a shear rate of $100s^{-1}$. In this case, the viscosity increase can be ascribed only to kinetic effects. Indeed, it is well known that moderate shear rates promote crystal nucleation, as a result of a decrease in entropy and an increase in super-cooling, however, high shear rates can damage crystals or inhibit their formation [28].
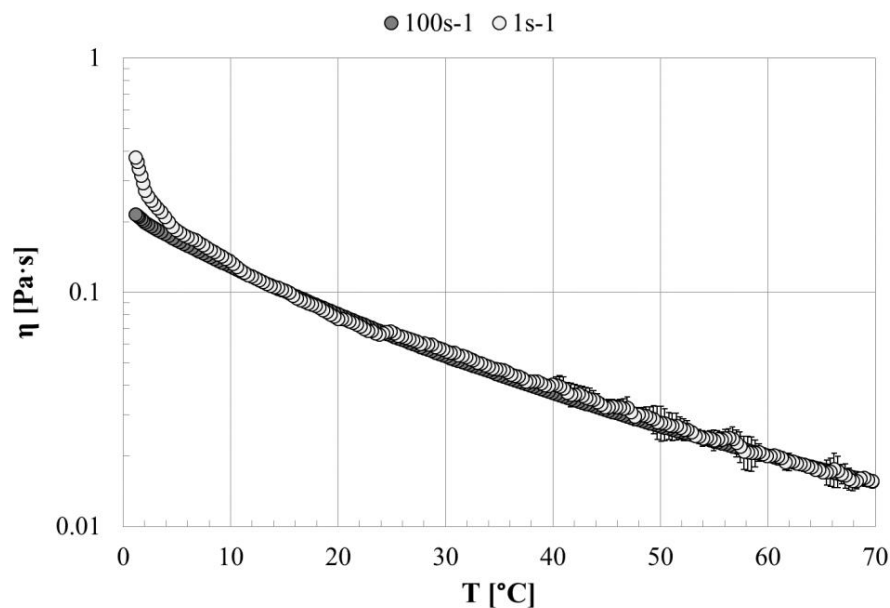
Figure 2.5 SRTRT for sample VO.

NMR measurements on virgin olive oil upon cooling evidenced that SFC was equal to zero in the whole temperature range investigated (from 70°C to 10°C). Virgin olive oil samples were stored at 4°C and 25°C, respectively, for 10 days and SFC values were recorded every 24h. Since VO is liquid at room temperature [29], SFC values at 25°C remained at zero upon ageing, whereas crystallisation occurred at 4°C: SFC values began to increase after 48h and continued to increase upon ageing (see Figure 2.6).
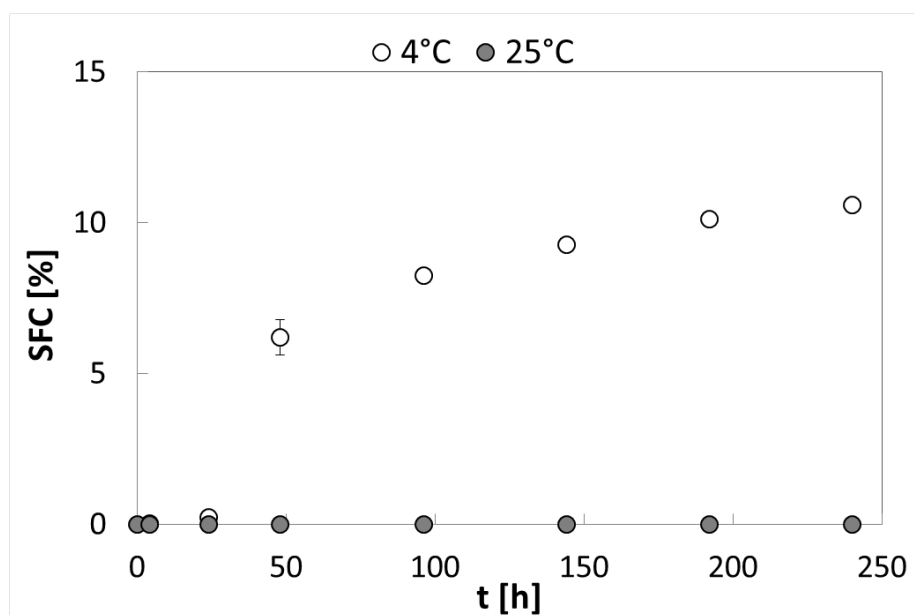
Figure 2.6 SFC as a function of time for sample VO.

The whole FT-IR spectrum between 400 and 4000 cm^{-1} represents the combination of many constituents of oil whereas the region between 1400 and 1800cm^{-1} mostly represents the combination of C–H bending, C=O stretching and C=C stretching [30]. As already reported in the literature, triglycerides are dominant in VO spectrum (see Figure 2.7). The major peaks that represent triglyceride functional groups were observed around 2922cm^{-1} and 2853cm^{-1} (symmetric and asymmetric stretching vibration of the aliphatic CH$_2$ group), 1743cm^{-1} (ester carbonyl functional group of triglycerides), 1465cm^{-1} (bending vibrations of the CH$_2$ and CH$_3$ aliphatic groups), 1238cm^{-1} and 1163cm^{-1} (stretching vibration of the C=O ester groups) and 709cm^{-1} (C–H bending) [30, 31]. In addition, peaks at 1700cm^{-1} (free fatty acids shoulder), 1418cm^{-1} (rocking vibrations of CH bonds of *cis*-disubstituted olefins), 1377cm^{-1} (bending vibrations of CH$_2$ groups), 722cm^{-1} (overlapping of the CH$_2$ rocking vibration and the out-of-plane vibration of *cis*-disubstituted olefins) were detected [31]. Finally, VO spectrum exhibited a band at around 3005cm^{-1}, assigned to the C-H stretching vibration of *cis*-double bond (=CH), that is specific for each vegetable oil: virgin and extra-virgin olive oil contains a high proportion of oleic acyl groups, therefore this peak appears at around 3005-3006cm^{-1}, whereas for other vegetable oils this peak is shifted to higher wavenumbers [31].
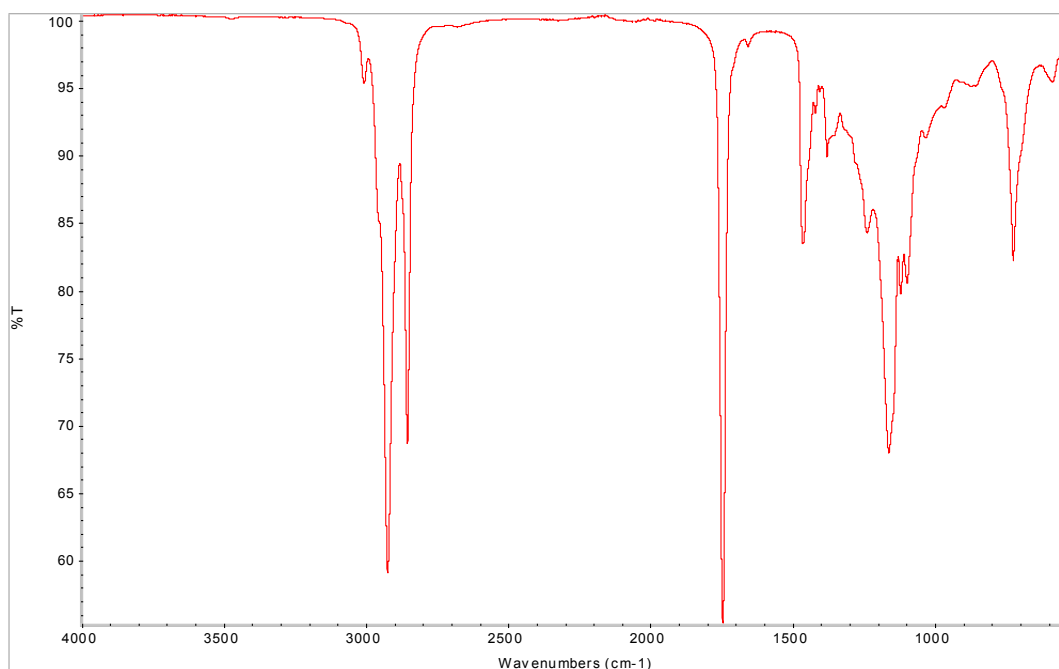
Figure 2.7 FT-IR spectrum for sample VO.

2.3.1.2 Extra-virgin olive oil

The rheological characterisation of sample EVO evidenced a liquid-like behaviour in all the temperature range considered. A small inflection in the phase angle curve during the Time Cure Test (Figure 2.8) was observed at almost 2.25±0.30°C, probably owing to crystal nucleation. As stated before, extra-virgin olive oil contains a lower amount of saturated fats in comparison to virgin olive oil, and this could explain the lower crystallisation temperature value estimated for sample EVO. Similarly, a slight change in the viscosity curve slope occurred at around 3.54±0.45°C (see Figure 2.9) when the lowest shear rate ($1s^{-1}$) was applied.
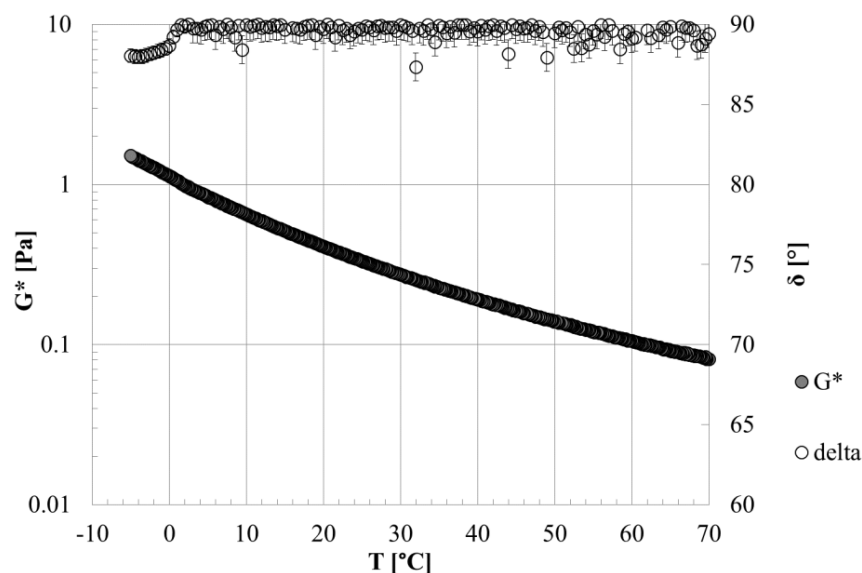
Figure 2.8 Time cure test for sample EVO.
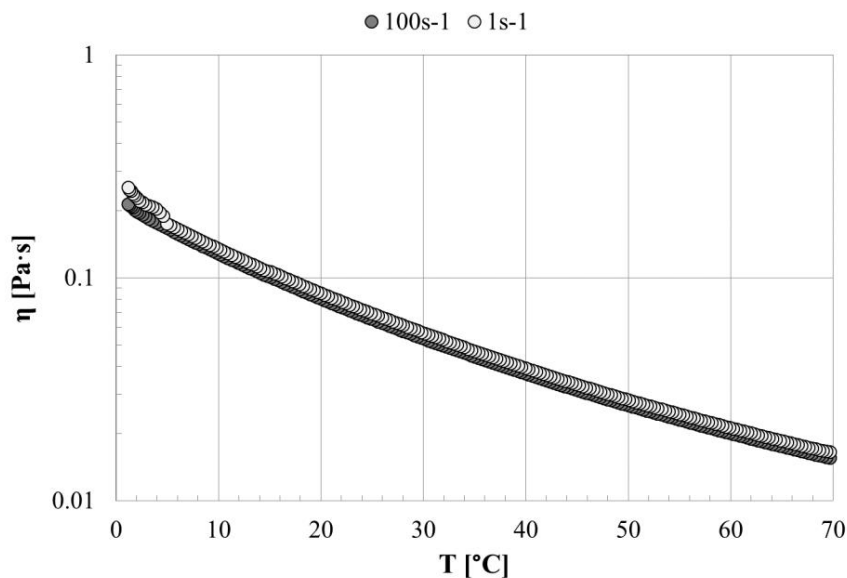
Figure 2.9 SRTRT for sample EVO.

The cooling DSC thermogram of sample EVO showed a single exothermic peak at -10.12±0.25°C, even though a small exothermic peak seems to begin at around -28.03±0.31°C, whereas the melting curve exhibited a broad peak with a shoulder at low temperatures and a further peak at -7.32±0.24°C (see Figure 2.10). The presence of two peaks in the melting thermogram indicates that extra-virgin olive oil is not characterised by a sharp melting point but rather by two distinct melting ranges, which suggests the occurrence of a miscibility gap. A miscibility gap occurs when the individual triglycerides in a complex system are unable to form a continuous range of mixed crystals, rather exhibiting mixtures of crystals of varying compositions and in varying states of crystallisation [32].
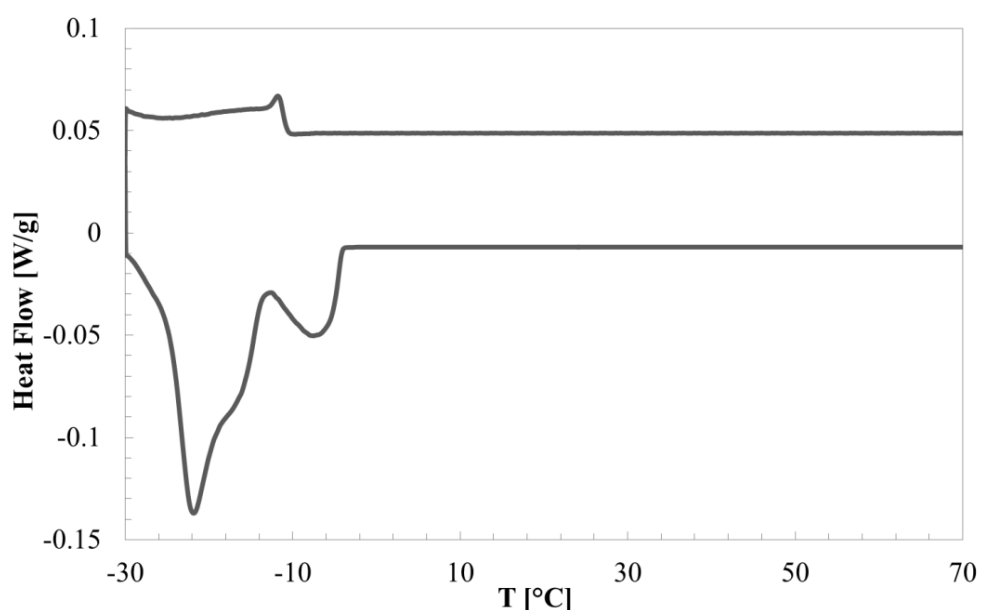
Figure 2.10 DSC thermogram for sample EVO.

As already observed for virgin olive oil, SFC values of sample EVO were found to be at zero in the temperature range investigated (10-70°C).

The FT-IR spectrum of sample EVO (Figure 2.11) is qualitatively very similar to the VO spectrum described in the previous section, with the characteristic extra-virgin olive oil peak at 3005cm^{-1}. The specific position of this peak is often used to detect potential adulteration of extra-virgin olive oil with other vegetable oils [31].
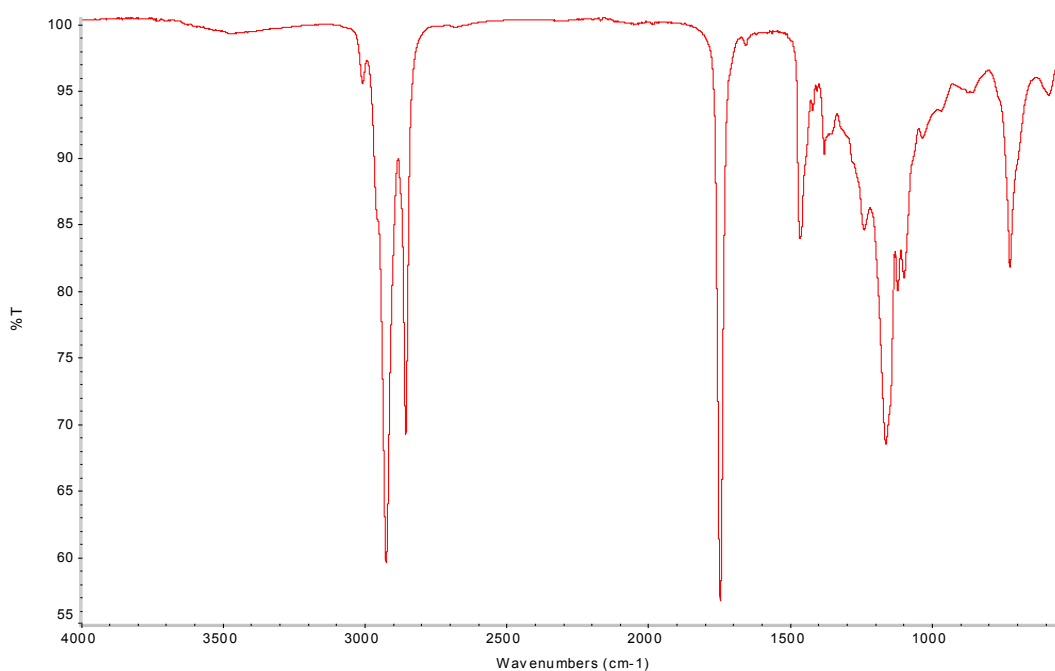
Figure 2.11 FT-IR spectrum for sample EVO.

2.3.1.3 Sunflower oil

It is known that sunflower oil crystallises at very low temperatures [33], and, in fact, this is confirmed by both the Time Cure Test (Figure 2.12) and SRTRT (Figure 2.13), according to which a liquid-like behaviour in the analysed temperature range is evidenced, with complex modulus and viscosity increasing at decreasing temperature only owing to kinetic effects. Similarly, SFC was found to be at zero during NMR tests.
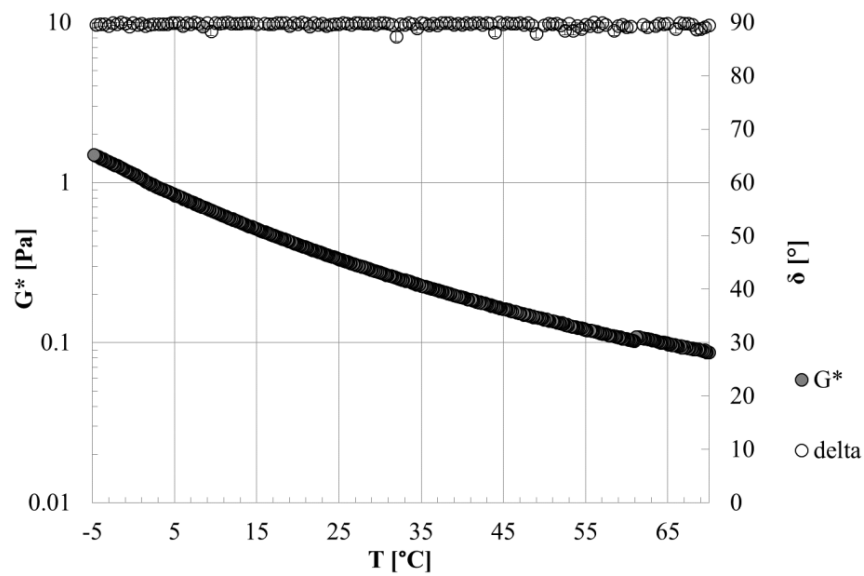
Figure 2.12 Time Cure Test for sample SO.
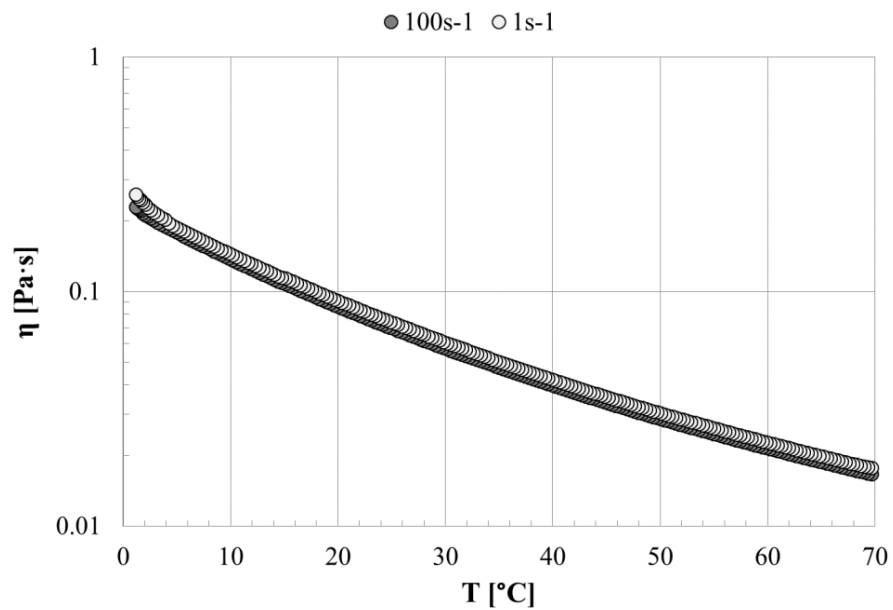
Figure 2.13 SRTRT for sample SO.

The DSC cooling thermogram of sample SO showed a single exothermic peak at around -15.25±0.48°C and a broad melting peak (beginning at -28±0.18°C and ending at -4.98±0.31°C), as it can be appreciated in Figure 2.14.
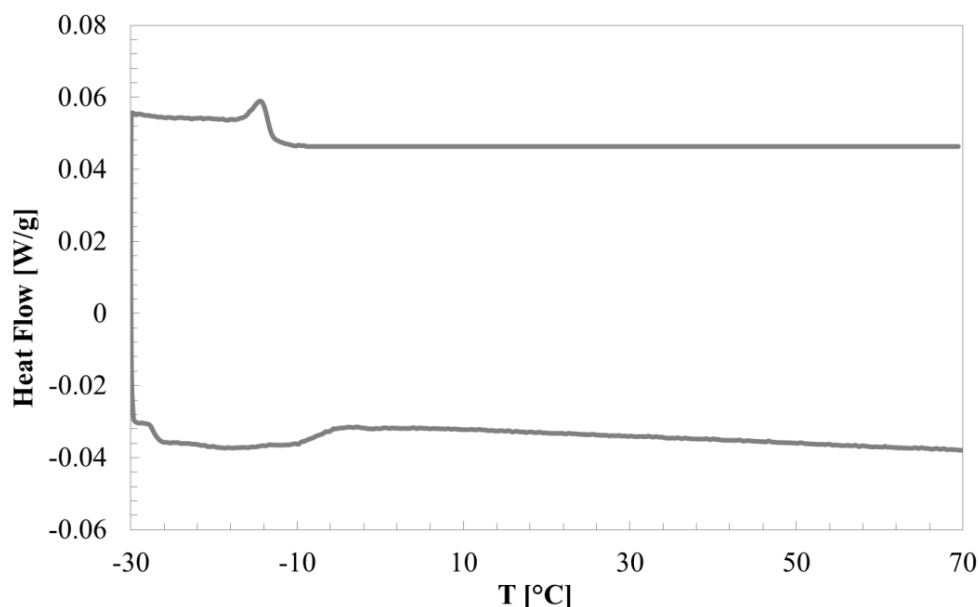
Figure 2.14 DSC thermogram for sample SO.

The FT-IR spectrum of sample SO (see Figure 2.15) exhibited the typical trend observed for vegetable oil and already discussed in the previous sections. However, it is worth noticing that the low-energy peak appeared at $3009 cm^{-1}$ in SO spectrum, whereas VO and EVO spectra both evidenced this peak at $3005 cm^{-1}$. This difference is attributable to the differences in vegetable oil composition, in fact sunflower oil contains a higher proportion of linolenic or linoleic acyl groups whereas extra-virgin olive oil consists of a higher proportion of oleic acyl groups [31].
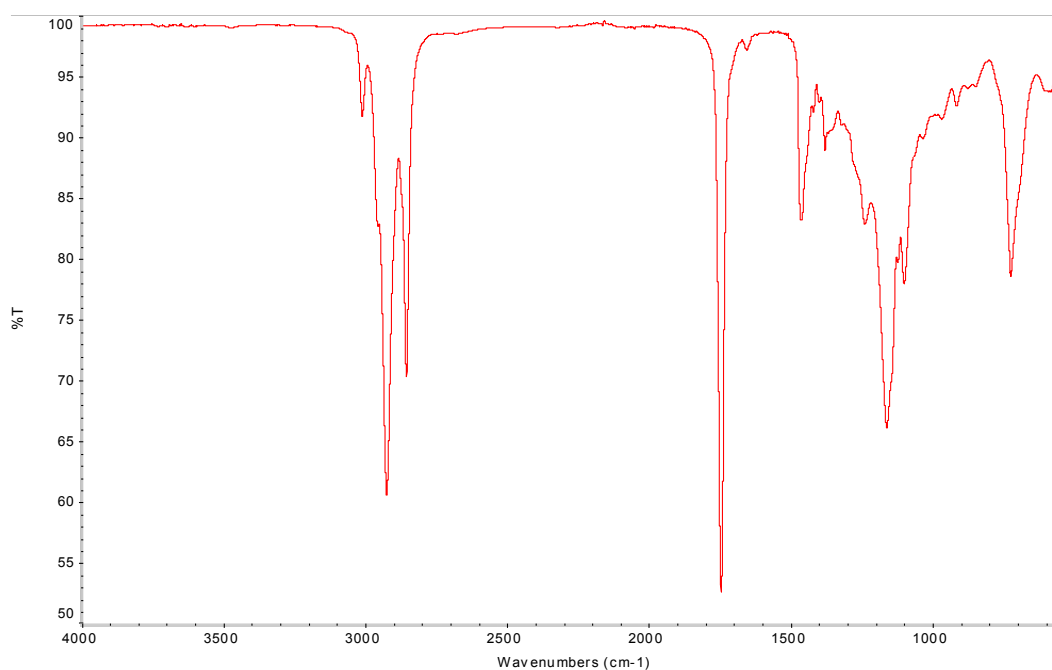
Figure 2.15 FT-IR spectrum for sample SO.

2.3.1.4 Cocoa butter

Figure 2.16 shows Time Cure Test for sample CB, evidencing that at high temperature cocoa butter is in the molten phase and exhibits a liquid-like behaviour. In fact, the loss tangent is always greater than unity and the complex modulus G^* increases with decreasing temperature only for kinetic effects. At around 20.54±0.51°C the onset of crystallisation is observed, with a sharp change in the complex modulus curve due to the potential crystallisation of the cocoa butter in the α form [34, 12].
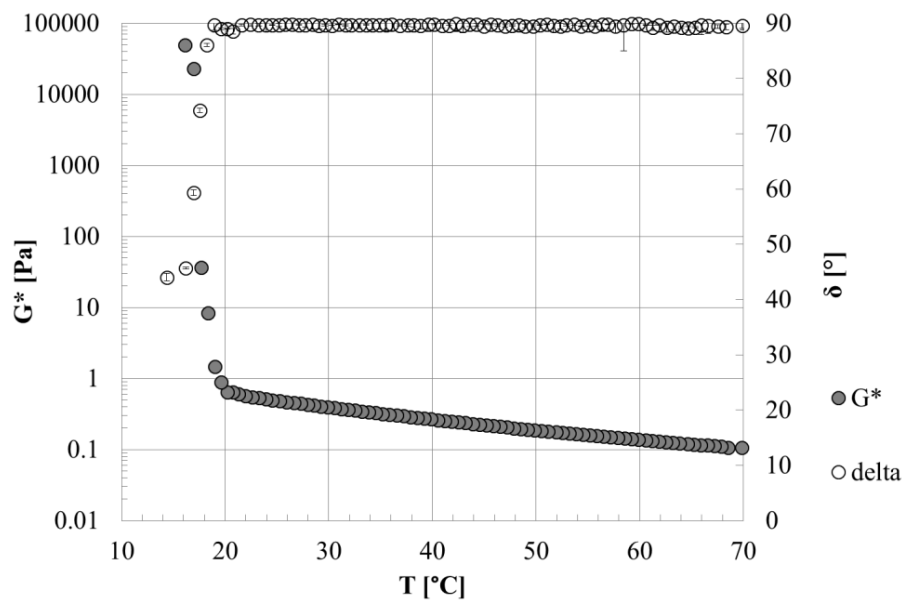
Figure 2.16 Time Cure Test for sample CB.

SRTRTs confirmed that cocoa butter is in the molten state from 70°C to approximately 20°C and the viscosity increases only for kinetic effects (Figure 2.17). In agreement with oscillatory tests, a sharp change in the viscosity slope is observed at around 20.61±0.35°C, owing to crystallisation phenomena. At the lowest shear rate ($1s^{-1}$), a further change in slope was detected at almost 15°C, as already observed by Lupi et al. [35], which can be probably attributed to the shear-dependent formation of either β′ or β crystals.
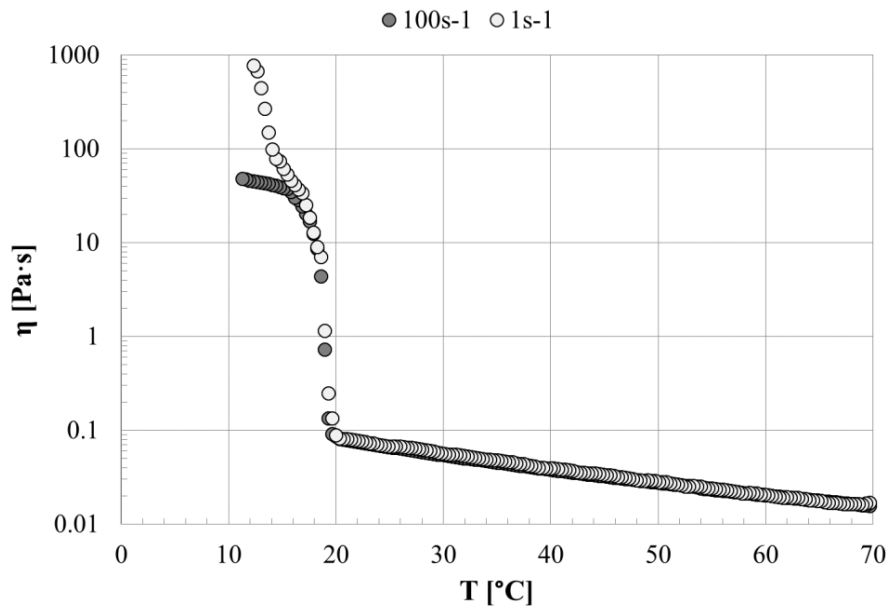
Figure 2.17 SRTRT for sample CB.

Cocoa butter is known to crystallise between 19°C and 23°C, when either a moderate or fast cooling rate are applied [36]. The DSC thermogram for sample CB (Figure 2.18) exhibited a broad peak at around 19.78±0.58°C, indicating the crystallisation from the melt to α polymorph. Polymorphic transition from α to β' form takes place during cooling or upon ageing [36]. The melting curve showed a broad peak with two shoulders, suggesting the presence of different polymorphs.
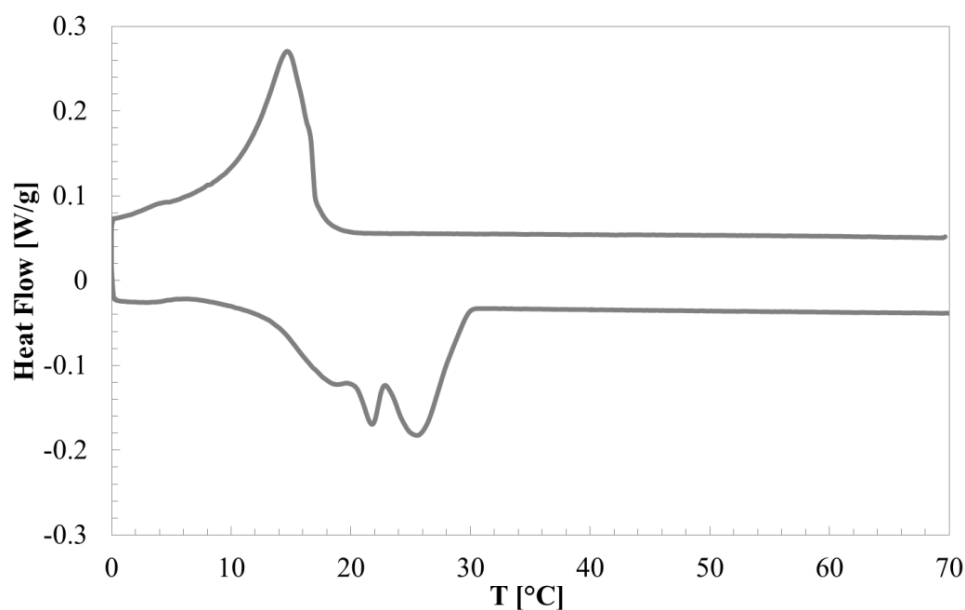
Figure 2.18 DSC thermogram for sample CB.

The onset of crystallisation temperature estimated from rheological and thermal analysis was confirmed by NMR tests. As depicted in Figure 2.19, the SFC curve as a function of temperature showed a sharp change in slope at almost 20.74±0.33°C, associated with the beginning of crystallisation.
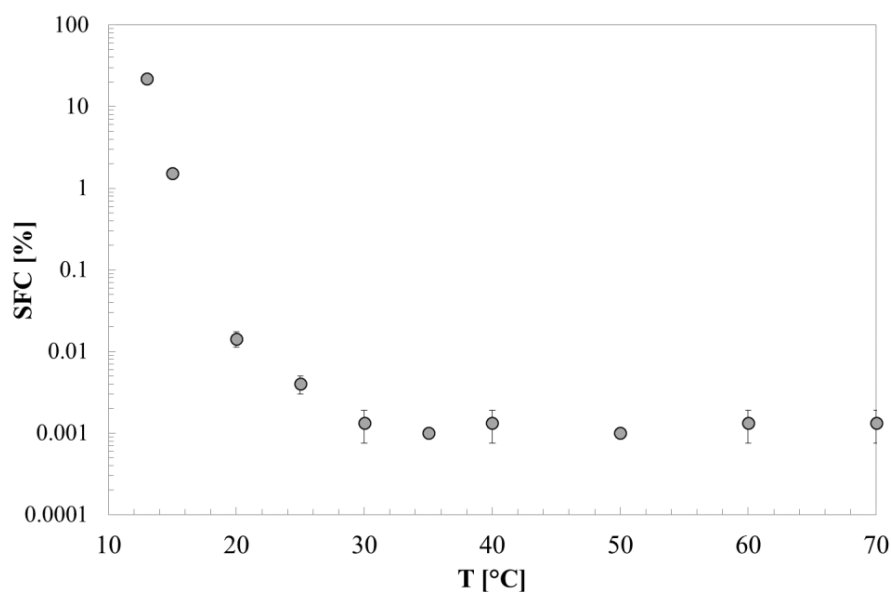
Figure 2.19 SFC as a function of temperature for sample CB.

2.3.2 Characterisation of organogelators

2.3.2.1 Myverol 18-04 K

The DSC thermogram of Myverol 18-04 K is shown in Figure 2.17. Myverol is a commercial mixture of monostearin and monopalmitin (50:50), therefore its thermal behaviour is in agreement with those of other commercial mixture of monoglycerides studied in the literature [17, 18]. The cooling thermogram showed two endothermic peaks, at 66.72±0.15°C and 15.04±0.19°C, respectively, corresponding to the crystallisation in the lamellar form and the polymorphic transition into sub-α form. A similar behaviour has been observed in commercial food-grade mono-stearoyl glycerol products composed of 92%w/w 1-mono-stearoyl glycerol and 5% w/w 1-mono-palmitoyl glycerol [16], 40% w/w 1-mono-stearoyl glycerol and 60% w/w 1-mono-palmitoyl-glycerol [17] and 38% w/w 1-mono-stearoyl glycerol, 54% w/w 1-mono-palmitoyl-glycerol and 8% w/w free fatty acids [18]. It has been shown that 1-mono-stearoyl glycerol and 1-mono-palmitoyl-glycerol often co-crystallise developing a mixed lamellar structure [18]. Upon further cooling, the aliphatic tails of mixed lamellar structure crystallised developing the sub-α phase that originates the second observed exothermic peak. These mesophases melted at 65.02±0.43°C and 16.64±0.31°C, respectively (Figure 2.20). A further endothermic peak appeared at high temperature (68.91±0.15°C), probably indicating the presence of a more stable polymorph (β' or β).
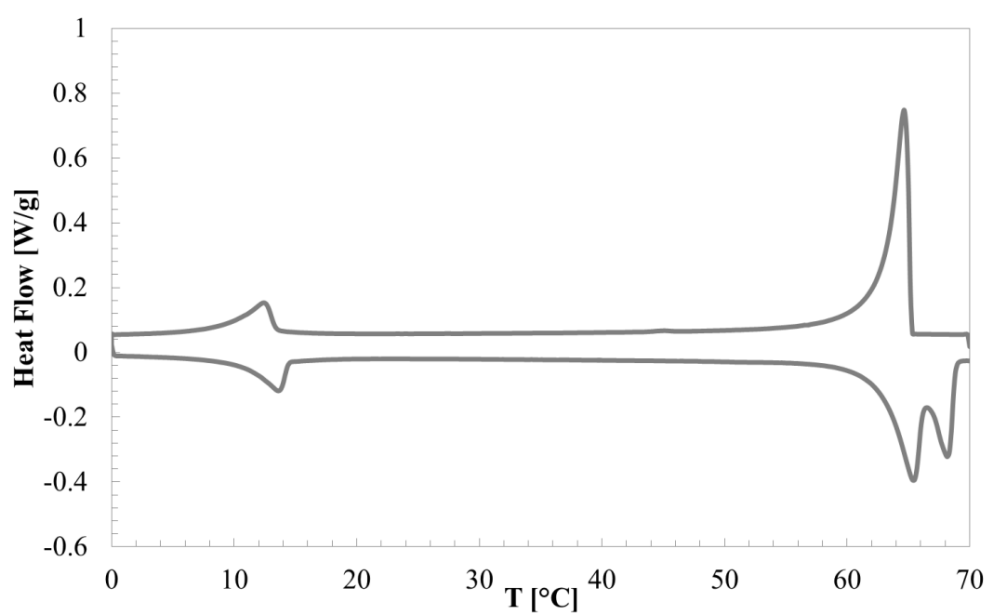
Figure 2.20 DSC thermogram for sample M.

Upon cooling, SFC showed a very sharp increase at 67.11±0.21°C, indicating the beginning of crystallisation (see Figure 2.21). At lower temperature, SFC rapidly reached values close to 100%.
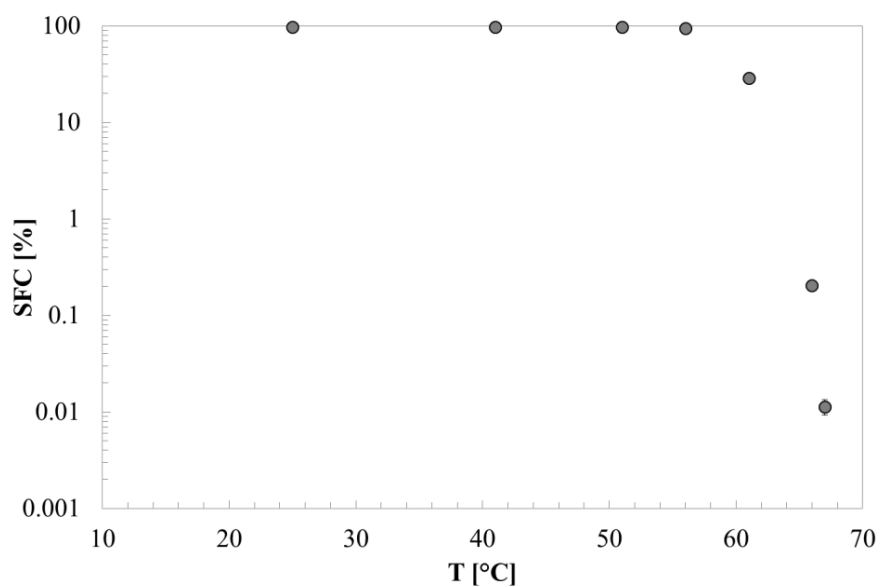
Figure 2.21 SFC as a function of temperature for sample M.

FT-IR spectrum of sample M (Figure 2.22) showed the behaviour already described for other vegetable fats in previous sections. However, a clear twin-peak (3300 and 3240cm^{-1})

appeared in the low-energy region. This peak is attributed to the hydrogen bond between alcohol (2-OH and 3-OH) and ester (C=O) groups, respectively [37].
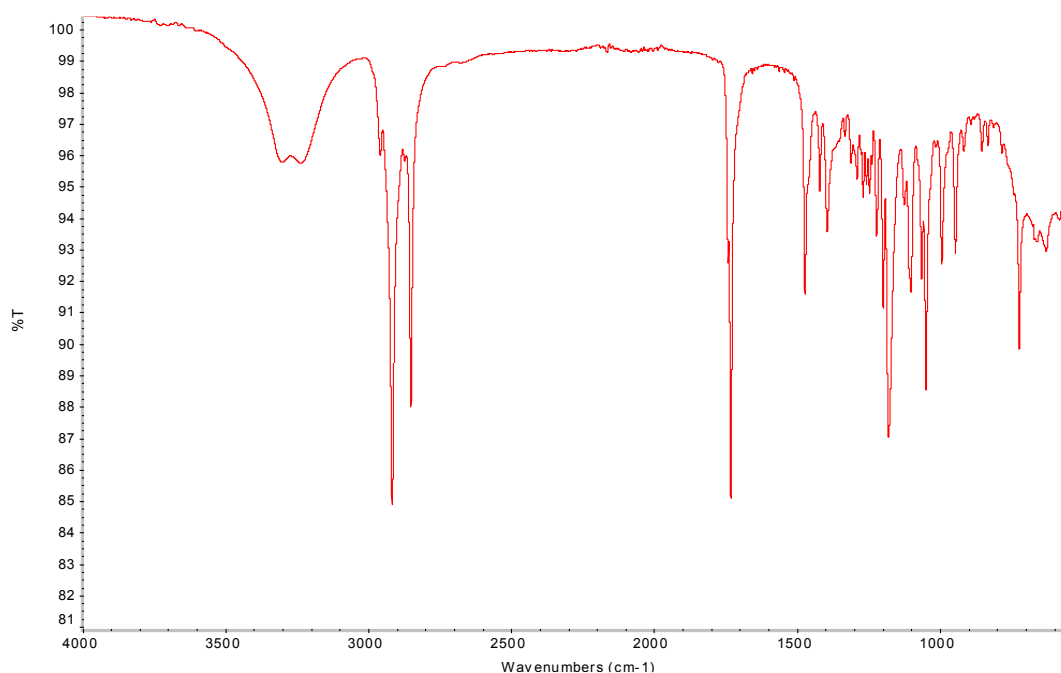
Figure 2.22 FT-IR spectrum for sample M.

2.3.2.2 Policosanol

Although policosanol is a complex mixture of different primary fatty alcohols, the DSC thermogram shown in Figure 2.23 exhibited only two exothermic peaks upon cooling. In agreement with the literature [38], exothermic peaks appeared at 80.14±0.21°C and 58.23±0.18°C, whereas melting peaks were observed at 59.45±0.27°C and 81.49±0.17°C, associated with the potential presence of α and γ typical polymorphs of fatty alcohols [39].
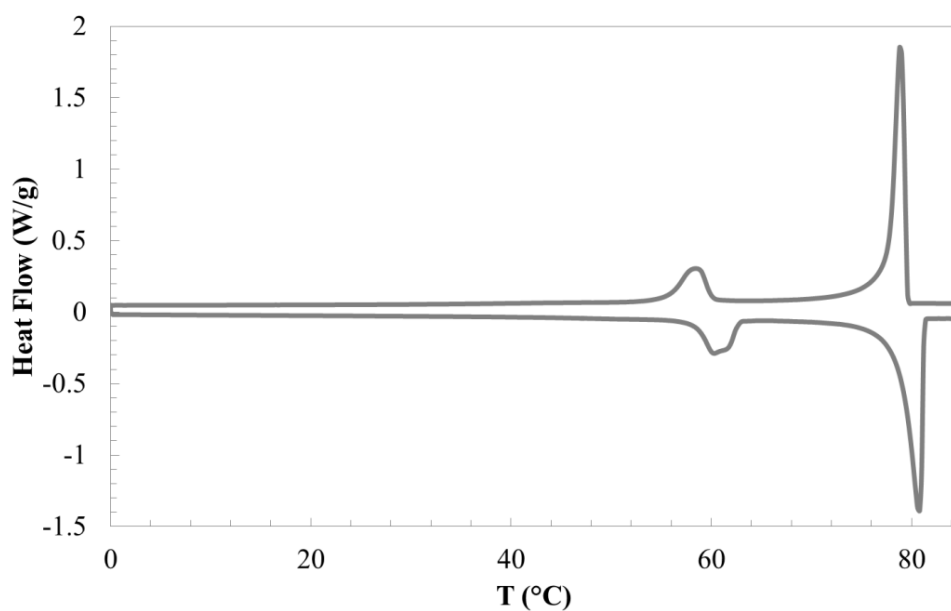
Figure 2.23 DSC thermogram for sample P.

The SFC curve as a function of temperature for sample P (Figure 2.24) showed a sharp change in its slope at around 82.13±0.31°C, owing to crystallisation phenomena.
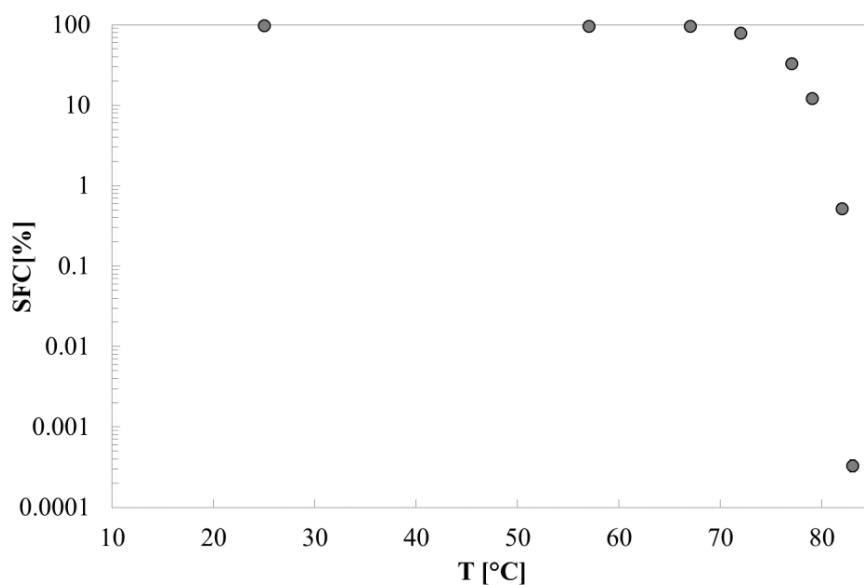
Figure 2.24 SFC as a function of temperature for sample P.

Policosanol FT-IR spectrum (Figure 2.25) showed some typical peaks observed for fats: 2955 and 2915cm^{-1} (symmetric and asymmetric stretching vibration of the aliphatic CH_2 group), 1470 cm^{-1} (bending vibrations of the CH_2 and CH_3 aliphatic groups), 1378cm^{-1}

(bending vibrations of CH_2 groups), whereas the peak at 3291 cm^{-1} indicates the presence of hydrogen bonds between OH groups [27], typical of organic alcohols.
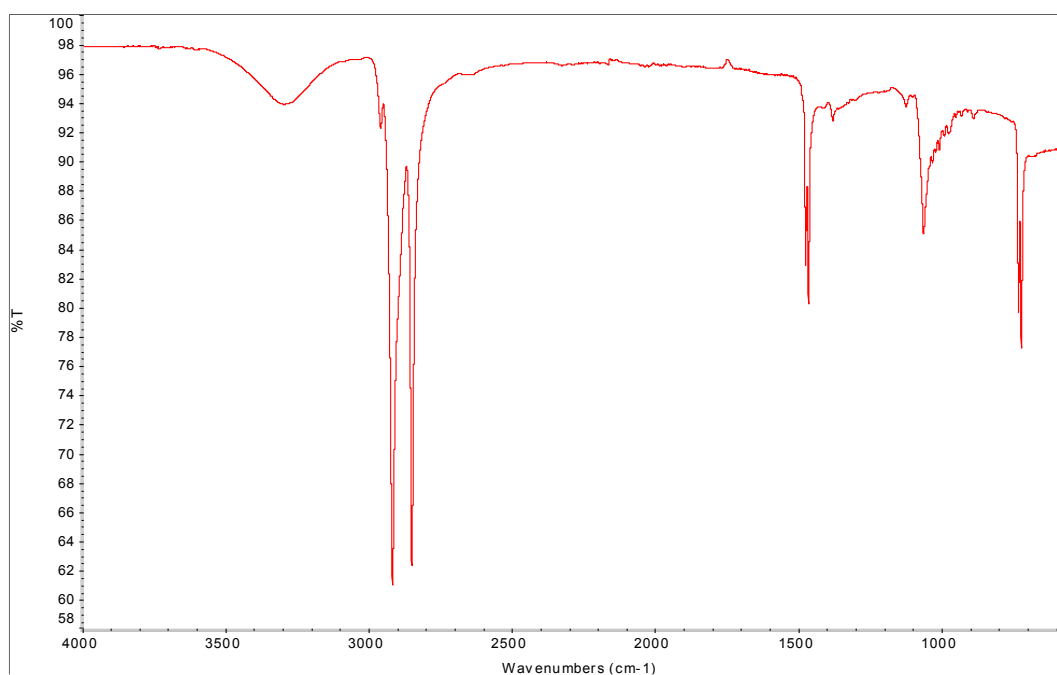
Figure 2.25 FT-IR spectrum for sample P.

Conclusions

Three vegetable oils, cocoa butter and two potential organogelators were studied. Rheological characterisation evidenced that the shear rate influenced virgin olive oil crystallisation: a crystallisation onset was individuated at 5.68±0.22°C during oscillatory tests and at 4.41±0.22°C during SRTRTs at 1s^{-1}, whereas no crystallisation was observed when a shear rate of 100s^{-1} was applied. For both extra-virgin olive oil and sunflower oil no crystallisation phenomena were detected in the investigated temperature range (0-70°C. For extra-virgin olive oil a slight increase in the viscosity curve slope was observed at around 2.25±0.30°C when the lowest shear rate was applied, probably owing to crystallisation phenomena promoted by the moderated applied shear rate. The estimated temperature of crystallisation onset was confirmed by thermal and spectroscopic analysis. SFC at room temperature was at zero for all the investigated vegetable oils; however, it increased significantly upon ageing at 4°C for virgin olive oil. FT-IR spectra evidenced the key features of vegetable oils, with a specific peak at 3009cm^{-1} for sunflower oil and at 3005cm^{-1} for virgin and extra-virgin olive oil, indicating that the former contains a higher

proportion of linolenic or linoleic acyl groups whereas the latter contain a higher proportion of oleic acyl groups.

For cocoa butter, a temperature of crystallisation onset of 20.5±0.5°C was estimated from rheological tests and confirmed by DSC and NMR measurements. Moreover, SRTRTs evidenced that a potential α→β' polymorphic transition occurred at around 15°C under the application of moderate shear rate.

Thermal analysis of Myverol 18-04K showed that it crystallised initially in the α form (66.72±0.15°C) and at low temperature (15.04±0.19°C) a polymorphic transition into sub-α form took place. The presence of two endothermic peaks at high temperature in the melting curve suggested the presence of highly stable polymorphs (β' or β). FT-IR analysis denoted the presence of hydrogen bonds between alcohol (2-OH) and ester (C=O) groups of the organogelator, respectively.

Despite the complexity of policosanol composition, its DSC thermogram exhibited only two exothermic and two endothermic peaks, suggesting the presence of two different polymorphs (probably α and γ typical polymorphs of fatty alcohols). Moreover, quite strong hydrogen bonds between OH groups were detected through FT-IR analysis.

References

[1] Marangoni, A.G., Acevedo, N., Maleky, F., Co, E., Peyronel, F., Mazzanti, G., Quinn, B., and D., Pink, *Structure and functionality of edible fats*, Soft Matter, 2012. 8: p. 1257-1300.

[2] Sato, K., *Crystallization behaviour of fats and lipids - a review*, Chemical Engineering Science, 2001. 56: p. 2255-2265.

[3] Larsson, K., *Classification of glyceride crystal forms*, Acta Chemica Scandinavia, 1966. 20: p. 2255-2260.

[4] Marangoni, A.G., *Fat Crystal Networks*, *1st ed*., Marangoni, A.G., Ed., Marcel Dekker, New York, 2005.

[5] Hernqvist, L., "Crystal structures of fats and fatty acids", in *Crystallization and polymorphism of fats and fatty acids*, Garti N. and K. Sato, Eds., Marcel Dekker, New York, 1988.

[6] Ueno, S., Minato, A., Yano, J., and K., Sato, *Synchrotron radiation X-ray diffraction study of polymorphic crystallization of SOS from liquid phase*, Journal of Crystal Growth, 1999. 198/199: p. 1326-1329.

[7] Minato, A., Yano, J., Ueno, S., Smith, K., and K., Sato, *FT-IR study on microscopic structures and conformations of POP-PPO and POP-OPO molecular compounds*, Chemistry and Physics of Lipids, 1997. 88: p. 63-71.

[8] Aronhime, J.S., Sarig, S., and N., Garti, *Reconsideration of Polymorphic Transformations in Cocoa Butter Using the DSC*, Journal of the American Oil Chemists Society, 1988. 65: p. 1140-1143.

[9] Chapman, G.M., Akehurst, E.E., and W.B., Wright, *Cocoa butter and confectionery fats*. *Studies using programmed temperature X-ray diffraction and differential scanning calorimetry*, Journal of the American Oil Chemists Society, 1971. 48: p. 824-830.

[10] Loisel, C., Keller, G., Lecq, G., Bourgaux, C., and M., Ollivon, *Phase Transitions and Polymorphism of Cocoa Butter*, Journal of the American Oil Chemists Society, 1998. 75: p. 425-439.

[11] Fessas, D., Signorelli, M., and A., Schiraldi, *Polymorphous transitions in cocoa butter – a quantitative DSC study*, Journal of Thermal Analylis and Calorimetry, 2005. 82: p. 691-702.

[12] Schenk, H., and R., Peschar, *Understanding the structure of chocolate*, Radiation Physics and Chemistry, 2005. 71: p. 829-835.

[13] Larsson, K., *The crystal structure of the L-1-monoglyceride of 11-bromoundecanoic acid*, Acta Crystallographica, 1966. 21: p. 267–272.

[14] Larsson, K., *Lipids - Molecular Organisation, Physical Functions and Technical Applications*, Oily Press, Dundee, 1994.

[15] Krog, N., *Crystallization Processes in Fats and Lipid Systems*, Marcel Dekker, New York, 2001.

[16] Chen, C.H., Van Damme, I., Terentjev, *Phase behavior of C18 monoglyceride in hydrophobic solutions*, Soft Matter, 2009. 5: p. 432–439.

[17] Vereecken, J., Meeussen, W., Foubert, I., Lesaffer, A., Wouters, J., and K., Dewettinck, *Comparing the crystallization and polymorphic behaviour of saturated and unsaturated monoglycerides*, Food Research International, 2009. 42: p. 1415–1425.

[18] López-Martínez, A., Morales-Rueda, J.A., Dibildox-Alvarado, E., Charó-Alonso, M.A., Marangoni, A.G., and J.F., Toro-Vazquez, *Comparing the crystallization and rheological behavior of organogels developed by pure and commercial monoglycerides in vegetable oil*, Food Research International, 2014. 64: p. 946–957.

[19] Hagemann, J.W., "Thermal behaviour and polymorphism of acylglycerides", in *Crystallization and polymorphism of fats and fatty acids*, Garti N. and K. Sato, Eds., Marcel Dekker, New York, 1988.

[20] McClements, D.J., "Emulsion ingredients", in *Food Emulsions: Principles, Practices, and Techniques*, CRC Press, Boca Raton, 2004.

[21] Zaliha, O., Chong, C.L., Cheow, C.S., Norizzah, A.R., and M.J., Kellens, *Crystallization properties of palm oil by dry fractionation*, Food Chemistry, 2004. 86: p. 245–250.

[22] Calligaris, S., Sovrano, S., Manzocco, L., and M.C., Nicoli, *Influence of Crystallization on the Oxidative Stability of Extra Virgin Olive Oil*, Journal of Agricultural and Food Chemistry, 2006. 54: p. 529-535.

[23] Azbar, N., Bayram, A., Filibeli, A., Muezzinoglu, A., Sengul, F., and A., Ozer, A Review of Waste Management Options in Olive Oil Production, Critical Reviews in Environmental Science and Technology, 2004. 34: p. 209-247.

[24] Lupi, F.R., Gabriele, D., Facciolo, D., Baldino, N., Seta, L., de Cindio, B., *Effect of organogelator and fat source on rheological properties of olive oil-based organogels*, Food Research International, 2012. 46: p. 177–184.

[25] Toro-Vazquez, J.F., Morales-Rueda, J.A., Dibildox-Alvarado, E., Charó-Alonso, M., Alonzo-Macias, M., and M.M., González-Chávez, *Thermal and textural properties of organogels developed by candelilla wax in safflower oil*, Journal of the American Oil Chemists' Society, 2007. 84: p. 989–1000.

[26] Blake, A.I., Co, E.D., and A.G., Marangoni, *Structure and Physical Properties of Plant Wax Crystal Networks and Their Relationship to Oil Binding Capacity*, Journal of the American Oil Chemists' Society, 2014. 91: p. 885-903.

[27] Lupi, F.R., Gabriele, D., and B., de Cindio, *Effect of Shear Rate on Crystallisation Phenomena in Olive Oil-Based Organogels*, Food and Bioprocess Technology, 2012. 5: p. 2880-2888.

[28] Walstra, P., Kloek, W., and T., van Vliet, "Fat crystal networks", in *Crystallization processes in fats and lipid systems*, Garti N. and Sato K., Eds., Marcel Dekker, New York, 2001.

[29] Ghotra, B.S., Dyal, S.D., and S.S., Narine, *Lipid shortenings: A review*, Food Research International, 2002. 35: p. 1015–1048.

[30] Yang, H., Irudayaraj, J., and M.M., Paradkar, *Discriminant analysis of edible oils and fats by FTIR, FT-NIR and FT-Raman spectroscopy*, Food Chemistry, 2005. 93: p. 25–32.

[31] Vlachos, N., Skopelitis, Y., Psaroudaki, M., Konstantinidou, V., Chatzilazarou, A., and E., Tegou, *Applications of Fourier transform-infrared spectroscopy to edible oils*, Analytica Chimica Acta, 2006. 573–574: p. 459–465.

[32] Jansen, M., and J., Birch, *Composition and stability of olive oil following partial crystallization*, Food Research International, 2009. 42: p. 826–831.

[33] Dian, N.L.H.M., Sundram, K., and N.A., Idris, *DSC Study on the Melting Properties of Palm Oil, Sunflower Oil, and Palm Kernel Olein Blends Before and After Chemical Interesterification*, Journal of the American Oil Chemists' Society, 2006. 83: p. 739-745.

[34] Lupi, F.R., Gabriele, D., Facciolo, D., Baldino, N., Seta, L., de Cindio, B., *Effect of organogelator and fat source on rheological properties of olive oil-based organogels*, Food Research International, 2012. 46: p. 177–184.

[35] Lupi, F.R., Gabriele, D., and B., de Cindio, *Effect of Shear Rate on Crystallisation Phenomena in Olive Oil-Based Organogels*, Food and Bioprocess Technology, 2012. 5: p. 2880-2888.

[36] Foubert, I., Fredrick, E., Vereecken, J., Sichien, M., and K., Dewettinck, *Stop-and-return DSC method to study fat crystallization*, Thermochimica Acta, 2006. 471: p. 7–13.

[37] Chen, C.H., and E.M., Terentjev, *Aging and Metastability of Monoglycerides in Hydrophobic Solutions*, Langmuir, 2009. 25: p. 6717-6724.

[38] Martínez, L., Uribarri, E., and A., Laguna, *Characterization and Compatibility Studies between Policosanol, a New Hypocholesterolemic Drug, and Tablet Excipients Using Differential Scanning Calorimetry (DSC)*, Archiv der Pharmazie, 1999. 332: p. 439–441.

[39] Gandolfo, F.G., Bot, A., and E., Flöter, *Phase diagram of mixtures of stearic acid and stearyl alcohol*, Thermochimica Acta, 2003. 404: p. 9-17.

Chapter 3: rheological and microstructural analysis of MAG organogels

Abstract

The rheological and microstructural properties of MAG (monoacylglycerols)/virgin olive oil organogels were investigated using different techniques. Both Step Shear Rate Temperature Ramp Tests (at $1s^{-1}$ and $100s^{-1}$) and Dynamic Temperature Ramp Tests were carried out with a cooling rate of 1°C/min, allowing the temperature of crystallisation onset (T_{co}) to be determined. Furthermore, a gelation temperature (T_g), analysed in a temperature ramp test in correspondence to a phase angle equal to 45°, was observed even at a Myverol mass fraction of 0.001. No significant differences between the two critical temperatures T_{co} and T_g were encountered for a Myverol fraction higher than 0.034. The temperature of crystallisation onset was determined also by using different techniques besides rheology. In fact, this thermo-rheological parameter was evaluated also by DSC and NMR, and an empirical equation was proposed to fit the experimental T_{co} values as a function of the organogelator fraction. DSC and FT-IR analysis were performed in order to investigate the microstructure of MAG/olive oil gels. SFC was determined by NMR spectroscopy and a fractal model was used to relate rheological properties to the microstructure of the system. Moreover, the average rate of SFC increase and the average structure development rate of tested samples were determined and related to the organogelator fraction. The stability of MAG/olive oil organogels was studied recording SFC values and DSC thermograms after one week of storage, indicating the potential formation of stable β polymorphs during ageing. In addition, the effect of the nature of the vegetable oil on the rheological and structural features of MAG organogels was investigated: micro-photographs were taken at different temperatures during rheological tests, showing the presence of a close-packed crystal network especially in the system containing sunflower oil. Finally, the effect of the addition of a natural, vegetable fat containing a high amount of saturated fats, cocoa butter, on the rheological and microstructural properties of MAG gels was studied. Also for these samples, a rheological, DSC and NMR characterisation were carried out and the fractal model was used to fit experimental storage modulus data (G') as a function of the volume fraction of solids.

3.1 Introduction

Edible oil organogels (or oleogels) produced with MAG are one of the most promising alternatives for designing new hardstocks without the addition of structured fats. As an example, MAG oleogels could be used for producing healthy food products as substitutes for butter, owing to both their mechanical stability and their biocompatibility [1]. Concentrated mixtures of MAG in edible oils form cream-like materials widely used both in personal care products and in food industries [1]. In addition, the absence of water allows MAG/edible oil gels to be not susceptible to microbial infection, thus these systems can be stored at room temperature without any addition of preservatives. Moreover, some authors also investigated the possibility of using MAG structures to control the aroma release in low-fat foods [2, 3]. Calligaris et al. [4] showed that the structured multi-lamellar phases in MAG/oil/water organogels affected the partition of aroma evidencing the capability to entrap lipophilic compounds within the MAG/oil shells.

3.1.1 Crystalline structure of MAG gels

As stated in Chapter 1, MAGs are among the rare systems capable of self-assembling both in aqueous and organic phases. In fact, aqueous solutions of MAG form different liquid crystalline mesophases upon cooling [5]. By decreasing temperature, cubic phases and then bimolecular lamellar phases spaced out by an aqueous phase are formed (Figure 3.1) [6, 7, 5, 8]. Both mesophases are liquid crystals, since they exhibit long-range order, having, on the other hand, hydrocarbon chains in a liquid-like state.
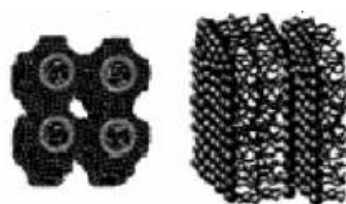
Figure 3.1 Schematic representation of cubic and lamellar MAG structures in water [8].

Crystallisation of the hydrocarbon chains occurs upon further cooling of the liquid crystalline mesophases below the Krafft temperature (i.e. the temperature of demixing from water). Similarly to triacylglycerols, these crystals can pack into one of three typical subcell packings (hexagonal, α, orthorhombic, β', triclinic, β). In the event that α crystals form, the material usually exhibit gel-like properties. In the resulting α-gel, bimolecular

layers are still separated by an aqueous phase and the hydrocarbon chains possess rotational mobility [5, 1]. It has been shown that over time, crystals in the α-gel undergo a polymorphic phase transition to form β crystals, which leads to the expulsion of the water between the bimolecular layers and the formation of the so-called coagel [5]. Indeed, on a long time-scale, the D- and L- isomers of chiral MAG gradually separate within crystalline bilayers, leading to full expulsion of water [9]. Because of the tendency of the material to expel the water between the MAG bilayers, usually no more than 25%$_{w/w}$ of water can be dispersed in crystalline MAG phase [5, 10, 11].

The phase behaviour of MAG in hydrophobic solvents in less studied. In ternary MAG/oil/water systems, the presence of water usually dominates the behaviour of structuring MAG [9, 12]. Because of the difference in hydrogen bonding pattern, MAG/hydrophobic solvents show a different phase behaviour with respect to the aqueous systems [1]. In the hydrophobic environment, below the isotropic-lamellar transition, the inverse lamellar phase is formed, with aliphatic tails on the outside of the bilayer (Figure 3.2) [1, 9]. In this configuration, the hydrophilic head groups are compressed in the middle of the bilayer and tend to adopt a 2-D close-packed conformation (2-D hexagonal lattice) [9]. Owing to the unique size ratio between the glycerol head and the lateral area of the aliphatic chain, the inverse lamellar bilayers have a very definite hexagonal plane ordering [1]. The uniqueness of these systems lies in the fact that the size of the glycerol head almost exactly matches the spacing of this rotator phase lattice. Since the 2-D ordering is promoted by compressing the glycerol heads inside the bilayers, the ordering occurs immediately on entering the lamellar phases, in contrast to aqueous systems where a significant decrease in temperature is required to form the α-crystalline state. Therefore, the inverse lamellar phase behaves macroscopically as a gel, unlike the usual complex-fluid rheological behaviour of lamellar systems [9].

Upon cooling of the inverse lamellar phase below its crystallisation point, the hexagonal lateral packing of the extended molten chains transforms into a crystalline form, similar to the sub-α crystals of pure MAG (Figure 3.2). The alkyl chains tend to arrange in parallel sheets [1, 9].
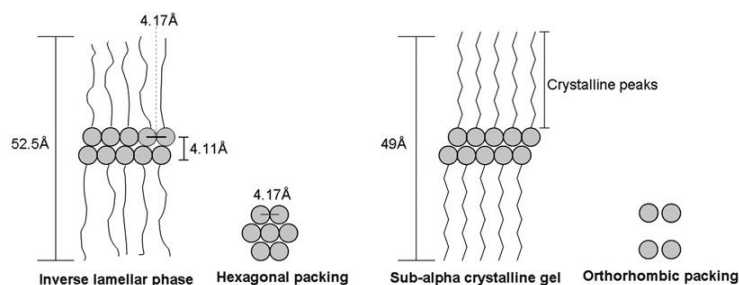
Figure 3.2 Schematic shown of the inverse lamellar phase and sub-α crystals [9].

Da Pieve et al. [13] analysed MAG/cod liver oil gels using a polarizing light microscope and showed a needle-like morphology of MAG crystals. Kesselman and Shimoni [14] confirmed this result for MAG/olive oil gels and reported the formation of additional spherulitic or rosette-like microstructure using corn oil, instead of olive oil, as the solvent (Figure 3.3). It has been suggested that the type of oil could influence the microstructural features of MAG crystals. According to Co and Marangoni [5], the differences in MAG crystal morphology can be attributed to the presence of a large number of impurities in virgin olive oil rather than any intrinsic difference between the triacylglycerols of the two oils (virgin olive oil and corn oil).
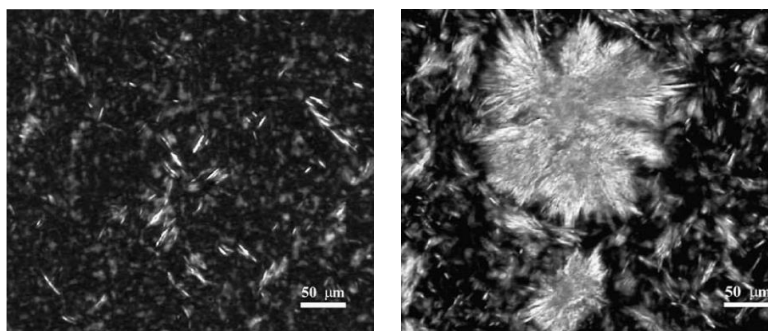
Figure 3.3 Polarized light microscopy of MAG/olive oil (left) and MAG/corn oil (right) gels [14].

3.1.2 Thermo-mechanical properties of MAG oleogels

Chen et al. [9] characterised monostearin/hazelnut oil gels, showing that the temperature at which the inverse lamellar phases were formed increased at increasing MAG concentration, whereas the temperature at which the sub-α form was observed did not change with an increase in the MAG concentration.

Ojijo et al. [15] studied the effect of MAG concentration and cooling rate on the properties of MAG/olive oil gels. The temperature of the onset of structure formation, final G' values and gel hardness were found to increase with increasing MAG concentration. At

a concentration lower than the critical gelation value, *G''* was found to be higher than *G'* at low frequencies and vice versa at high frequencies. At higher MAG concentrations, a true gel behaviour was observed. The effect of cooling rate on the evolution of the *G'* was also described by the same authors. At high cooling rates, the profile of *G'* over temperature was monotonic, while at low cooling rates, the *G'* temperature profile exhibited inflection points. This result was associated with the formation of a secondary structure, in particular with the co-crystallisation of the α and the β crystal polymorphs. The presence of secondary structural elements yielded to the formation of a more elastic network structure [15].

The same authors [15] also studied the effect of the application of shear on MAG/olive oil gels. It has been shown that the application of shear in lamellar phases of MAG results in the formation of unusual structures such as multi-lamellar vesicles. The formation and the subsequent crystallisation of these structures can result in gelling structures with different morphologies from gels developed under no-shear conditions [5, 15].

Da Pieve et al. [13] showed that the application of higher shear rates during structuring of MAG/cod liver oil organogels resulted in a lower *G'* and a loss of oil binding capacity. It was found that the application of increasing steady shear caused the formation of spherical crystalline particles, instead of platelet crystals, with lower structuring capability. It was also found that the application of shear resulted in an increase of the crystalline domain size, as demonstrated by the application of Scherrer equation (often used in the literature to estimate the size of particles of crystals from X-ray diffraction data) [5, 13].

After gel formation, the microstructure of MAGs in different phases changes with time, leading to significant variation of the organogel physical properties. Chen and Terentjev [1] studied ageing and stability of monostearin/hazelnut oil organogels. It was found that during ageing the network structure broke down into isolated β-crystal clusters dispersed in the continuous oil phase. Hence, the lamellar network framework broke down and phase separation between MAG crystals and the solvent occurred. As a result, the material lost its intrinsic gel rheological properties. Using infrared spectroscopy, Chen and Terentjev [1] demonstrated the coexistence of 3- and 2-OH hydrogen bonding in the initial stages of ageing, whereas 2-OH hydrogen bonding was predominant and led to the separation of D- and L-isomers of MAG after further ageing.

Figure 3.4 schematically shows and sums up the phase behaviour of MAG in hydrophobic solvents: upon cooling, MAG initially self-assemble into inverse lamellar phases from the isotropic fluid, further cooling results in the formation of sub-α crystals,

whereas on ageing, 2-OH hydrogen bonds between polar glycerol head groups form and lead to the formation of the more stable β crystalline polymorph with tri-clinical packing.
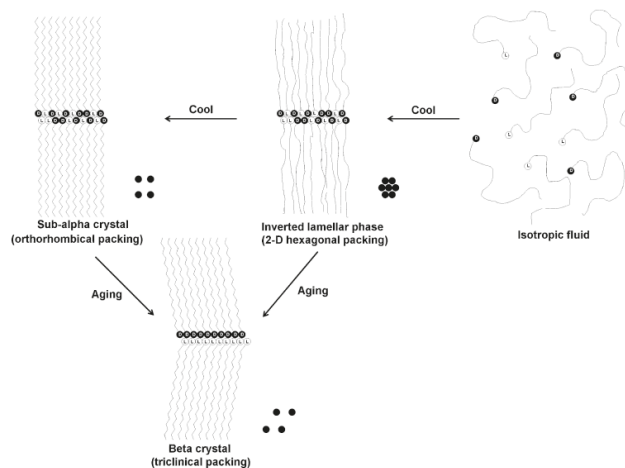
Figure 3.4 Schematic representation of MAG structures in hydrophobic solvents and their behaviour on ageing [1].

3.1.3 Properties of oleogels from MAG mixtures

Chen and Terentjev [16] investigated the effect of mixtures of different MAGs on the formation of oleogels. At a given concentration of MAG, a 1:1 mixture of monostearin and monopalmitin formed the inverse lamellar phase at a temperature higher than the value at which monostearin alone forms the same phase; this effect was observed only at low MAG concentrations. On the contrary, the temperature at which the sub-α crystals form, was found to be lower for the mixture than the value detected for pure monostearin. Changes in the ratio of monostearin to monopalmitin did not result in any difference in the temperature of lamellar phase formation. However, varying the relative ratio of monostearin and monopalmitin resulted in the decrease of the temperature at which the sub-α phase was formed. This result was more noticeable for a 1:1 ratio of monostearin to monopalmitin [16, 5]. Lòpez-Martìnez et al. [17] compared the properties of organogels formed from a commercial mixture of MAG (mainly composed of 37.7%$_{w/w}$ C_{18} and 54.0%$_{w/w}$ C_{16}) to those of a pure MAG (C_{18}), showing that organogels containing mixed MAG exhibited higher values of both the storage modulus *G'* and the SFC. In addition, the constituent units of the network structure were composed of smaller crystal in systems containing mixed MAG. Commercial MAG organogels developed β crystals, directly from the inverse lamellar phase or during ageing through a polymorphic transition, that can be responsible of the eventual collapse of the 3-D network.

Within this framework, the aim of the present work is the rheological, thermal and microstructural analysis of MAG/olive oil oleogels for potentially different uses in food. The investigation of the rheological characteristics of organogels produced with a commercial mixture of MAG as the organogelator was carried out by using Small Amplitude Oscillation Tests (SAOTs), with the aim of studying the effect of the gelator concentration on both the transition temperatures (the onset of crystallisation, T_{co}, and the onset of gelation, T_g). Step Rate Temperature Ramp Tests (SRTRTs), at different shear rates, were also performed, in order to evaluate the effect of the applied shear rate on the viscosity and the transition temperature of MAG gels. Different techniques (NMR, DSC, as well as rheology) were used to evaluate the onset of crystallisation temperature, since this parameter plays an important role in detecting the potential industrial uses of structured materials. Furthermore, the influence of the type of vegetable oil on the rheological properties and the microstructure of the gels was also investigated. Finally, the effect of the addition of cocoa butter was studied. This vegetal fat, rich in natural saturated components, can act as a thickening agent for structured lipid phases. The addition of low amounts of cocoa butter does not affect the healthiness of the final product, since it has been demonstrated that it has a neutral effect on cholesterol levels [18].

3.2 Materials and methods

3.2.1 Samples ingredients and preparation

The majority of the investigated organogels were produced with a commercial virgin olive oil (De Santis, Italy) as the solvent and a mixture of monoglycerides of fatty acids (with an equal mass fraction of monopalmitin and monostearin; the trade name is Myverol 18-04K, (Kerry Group, Ireland, referred to as "Myverol" throughout the chapter) as the organogelator. Therefore, in order to study the effect of the type of vegetable oil, samples GM and EM (see Table 3.1) were prepared using sunflower oil (De Santis, Italy) and extra virgin olive oil (Gabro S.r.l., Italy) respectively as the solvent, without changing the organogelator mass fraction (0.03). With the aim of studying the effects of Myverol concentration on crystallisation and gelation phenomena in olive oil based organogels, the organogelator fraction was ranged between 0.001 and 0.50. OBM samples (see Table 3.1) contained cocoa butter (Icam S.p.A., Italy), in addition to olive oil and monoglycerides. In this work, low amounts of cocoa butter were used with a view to investigating low-

saturated-fat systems, suitable for healthy applications. The composition of all raw materials was already described in Chapter 2. All samples were prepared adding the right amount of organogelator, and in some cases cocoa butter, contemporary to the oil [19, 20], previously warmed up to 70°C in a water bath thermostatically controlled by a plate heater (VELP Scientifica, Italy). The system was continuously mixed using a laboratory stirrer (RW 20, IKA, Germany) and maintained at the temperature of preparation until tests were performed.

Sample ID	Virgin Olive Oil [%$_{w/w}$]	Sunflower Oil [%$_{w/w}$]	Extra Virgin Olive Oil [%$_{w/w}$]	Myverol [%$_{w/w}$]	Cocoa Butter [%$_{w/w}$]	B/O [-]
OM1	99.9	-	-	0.1	-	-
OM2	99.5	-	-	0.5	-	-
OM3	99.0	-	-	1.0	-	-
OM4	98.5	-	-	1.5	-	-
OM5	96.6	-	-	3.4	-	-
OM6	90	-	-	10	-	-
OM7	70	-	-	20	-	-
OM8	50	-	-	30	-	-
OM9	97	-	-	3	-	-
EM	-	-	97	3	-	-
GM	-	97	-	3	-	-
OBM1	94.0	-	-	2	4	0.04
OBM2	86.3	-	-	10	3.7	0.04
OBM3	76.7	-	-	20	3.3	0.04
OBM4	67.1	-	-	30	2.9	0.04
OBM5	57.6	-	-	40	2.4	0.04
OBM6	94.3	-	-	3.4	2.3	0.02
OBM7	85.2	-	-	3.4	11.4	0.13
OBM8	92.9	-	-	3.4	3.7	0.04
OBM9	48.1	-	-	50	1.9	0.04
OBM10	93.7	-	-	2.5	3.8	0.04

Table 3.1 Samples ID and composition. B/O is the ratio between cocoa butter and olive oil.

3.2.2 Rheological characterisation

All samples were analysed with a controlled strain rheometer ARES-RFS (TA Instruments, USA), equipped with a parallel plate geometry (ϕ=50mm, gap = 1±0.1mm). Organogels are highly temperature-dependent materials, therefore the temperature of the lower plate was carefully controlled by a Peltier system (±0.1°C). The samples were poured on the lower plate of the rheometer (preheated at the temperature of sample preparation) and the rheological properties of the material were measured cooling the sample in the rheometer cell, with a controlled cooling rate of 1°C/min.

For all samples a rheological characterisation based on Small Amplitude Oscillation Tests (SAOTs) was carried out. Time cure tests were performed in linear viscoelastic conditions from 70°C to 10°C with a constant frequency of 1Hz. Lower final temperatures (0°C) were adopted for samples exhibiting a lower temperature of crystallisation onset. Preliminary strain sweep tests were carried out according to the procedure described in Chapter 2 and then Time cure tests were performed applying different constant strain values in different temperature ranges, in order to always guarantee the linear viscoelastic conditions.

Two parameters, T_{co} and T_g, were estimated from the analysis of the obtained Time cure tests. The onset of crystallisation temperature (T_{co}) was calculated following the procedure described by Lupi et al. [20], already reported in Chapter 2. In particular, T_{co} was estimated as the temperature at which a sharp increase of the complex modulus G^* was observed.

The gelation point (T_g) was identified at the crossover between dynamic moduli, where the loss tangent is unity and, thus, the phase angle is 45°, according to a simplified criterion often used in the literature [20, 21, 22].

For each sample, an average structure development rate (SDr) was also evaluated. According to the definition given by Lopes da Silva et al. [23], the average SDr in the time interval between t_1 and t_2 is equal to:

$$SDr_{av} = \frac{1}{t_1 - t_2} \int_{t_1}^{t_2} \left(\frac{dG'}{dt}\right) dt \qquad (3.2.1)$$

In the present work, the initial time t_1 was considered as the time at which the temperature is equal to T_{co} during time cure tests, whereas t_2 corresponds to the time at which the temperature value of T_{25} is reached, where $T_{25} = T_{co} - 25$. Therefore, the average SDr was calculated as shown in Eq. 3.2.2:

$$SDr_{av} = \frac{1}{t(T_{co}) - t(T_{25})} \int_{t(T_{co})}^{t(T_{25})} \left(\frac{dG'}{dt}\right) dt \qquad (3.2.2)$$

The first derivative of the elastic modulus *G'* with respect to the time was calculated for each curve obtained from time cure tests using a forward numerical method and the integral between two consecutive points was evaluated using the trapezoidal rule. The value of *SDr* was then evaluated as the sum of all the integrals previously calculated.

Moreover, the flow behaviour of gels was investigated performing Step Rate Temperature Ramp Tests (SRTRTs) at two different constant shear rates ($1s^{-1}$ and $100s^{-1}$), decreasing the temperature from 70°C to 10°C. In agreement with the procedure already used for oscillatory tests, the onset of crystallisation $T_{co,s}$ was estimated as the temperature at which a strong change in the slope of the viscosity curve was observed (see Chapter 2).

In order to investigate the effect of the kind of vegetable oil on the microstructural and rheological properties of Myverol organogels, Temperature ramp tests and SRTRTs at the constant shear rate of $1s^{-1}$ were carried out on samples EM, GM and OM9 using a stress-controlled HAAKE MARS III rheometer (Thermo Fisher Scientific, Germany) equipped with the RheoScope module (222-1912). Images were recorded at different temperature levels during rheological measurements.

3.2.3 Thermal analysis

The crystallisation and melting thermograms of samples OM4, OM5, OM7, EM, GM, OBM1, OBM4, OBM6, OBM7, OBM8 were obtained using a Mettler Toledo Model DSC822e (Mettler Toledo, Switzerland), according to the procedure described in Chapter 2. As elsewhere reported [24], the onset of crystallisation temperature ($T_{co, DSC}$) was calculated as the temperature corresponding to the beginning of the first exothermic peak, while the temperature of melting of each polymorph (T_M) was individuated as the temperature corresponding to the peak of the melting endotherm.

In order to investigate the stability of the analysed samples and their potential polymorphic transitions, DSC measurements were repeated after 1 week of storage at two different temperatures (4°C and 25°C). Samples were sealed in aluminium pans, held at 4°C or 25°C for 15 min and then heated up to 100°C at 1°C/min, with the aim of detecting the possible presence of high melting polymorphs. After 1min at 100°C, samples were cooled down (at 1°C/min) to 0°C, so as to verify the thermo-reversibility of the investigated organogels.

3.2.4 Spectroscopic analysis

The solid fat content of Myverol organogels was measured by low-frequency nuclear magnetic resonance (Minispec mq20, Bruker, Germany) [25]. In this case, organogel formation was promoted directly in NMR tubes using the same thermal history as for the rheological and thermal characterisation. Temperature was controlled with an external water bath (RC 20, LAUDA-Brinkmann LP., USA). SFC was therefore measured at different temperature values during gel formation.

Even for spectroscopy, the onset of crystallisation temperature ($T_{co, NMR}$) was evaluated as the temperature at which a sharp increase in the slope of the *SFC* versus temperature was observed. Moreover, the average rate of SFC increase (*SFCr*) between T_{co} and T_{25} was estimated as reported in Eq. 3.2.3:

$$SFCr = \frac{1}{t(T_{co})-t(T_{25})} \int_{t(T_{co})}^{t(T_{25})} \left(\frac{dSFC}{dt}\right) dt \qquad (3.2.3)$$

In the present work, the fractal model proposed by Tang and Marangoni [26] is used to relate the rheological properties of Myverol organogels to their microstructure. According to the fractal model, the non-linear relationship between storage modulus *G'* and the volumetric fraction of solids *Φ* in fat crystal networks can be expressed as follows:

$$G' = \lambda \Phi^{1/(3-D)} \qquad (3.2.4)$$

where λ is a constant dependent on the strength of the interactions between fat crystal flocs and *D* is the fractal dimension of the network [28]. The storage modulus measured during temperature ramp tests was related to the volume fraction of solids calculated as follows:

$$\Phi = \frac{SFC/100}{\frac{SFC}{100}+\left(1-\frac{SFC}{100}\right)\left(\frac{\rho_M}{\rho_O}\right)} \qquad (3.2.5)$$

where SFC is the mass fraction of solids measured using NMR, ρ_M is the density of Myverol ($970 kg/m^3$ at room temperature, experimentally estimated), ρ_O is the density of virgin olive oil ($920 kg/m^3$ at room temperature, according to the literature [27]).

Infrared absorption spectra were recorded using a Nicolet iS-10 FT-IR spectrometer (Thermo Scientific, USA) equipped with a Smart iTX ATR sampling accessory. Samples were prepared at 70°C according to the procedure previously described and allowed to cool at room temperature. Then, spectra were recorded at room temperature. With the aim of investigating gel stability and detecting potential changes in the characteristics of hydrogen bonding, FT-IR measurements were repeated after one week of storage at room temperature.

A statistical analysis was used to evaluate the significance of potential differences between two comparable data. The commercial software Statgraphics Centurion XV (Statpoint Technologies Inc., Warrenton) was used to carry out such analysis using *t-student* test. Differences among parameters were considered significant with an interval of confidence of 90% (*p*=0.1).

3.3 Results and discussion

3.3.1 Effect of MAG concentration on the rheological properties of virgin olive oil-based gels

All the investigated MAG/olive oil samples showed the same rheological behaviour during Time cure tests. As an example, Figure 3.5 shows the complex modulus, G^*, and the phase angle, δ, for sample OM4. It can be observed that, at high temperature ($T>T_{co}$), the mixture is completely molten and, as a consequence, a pure viscous behaviour is found, as confirmed by low values of the complex modulus and δ nearly 90°. In this temperature region, the complex modulus increases with decreasing temperature only because of kinetic effects. At the T_{co} value, a sudden increase in the complex modulus curve slope can be observed, while the phase angle starts to decrease, indicating the beginning of the crystallisation phenomena. Cooling down the sample, interactions between crystalline aggregates tend to form and to extend over the whole system, resulting in the formation of a 3-D crystalline gel network. The temperature (T_g) at which the phase angle is 45° (or, similarly, at the G'-G'' crossover, where loss tangent is unity) was identified as the gelation point. At lower temperature ($T<T_g$), the system behaves as a solid-like gel material. A further slope change in both curves of G^* and δ can be observed at approximately 15°C, indicating a potential second transition. This variation in the rheological properties will be discussed in more detail in the next paragraph, comparing rheological results with those obtained from thermal and spectroscopic analysis.

Aiming at investigating the crystallisation and gelation phenomena promoted by the oganogelator, the rheological behaviour of systems containing low amounts of Myverol (samples OM1-OM3) was studied.
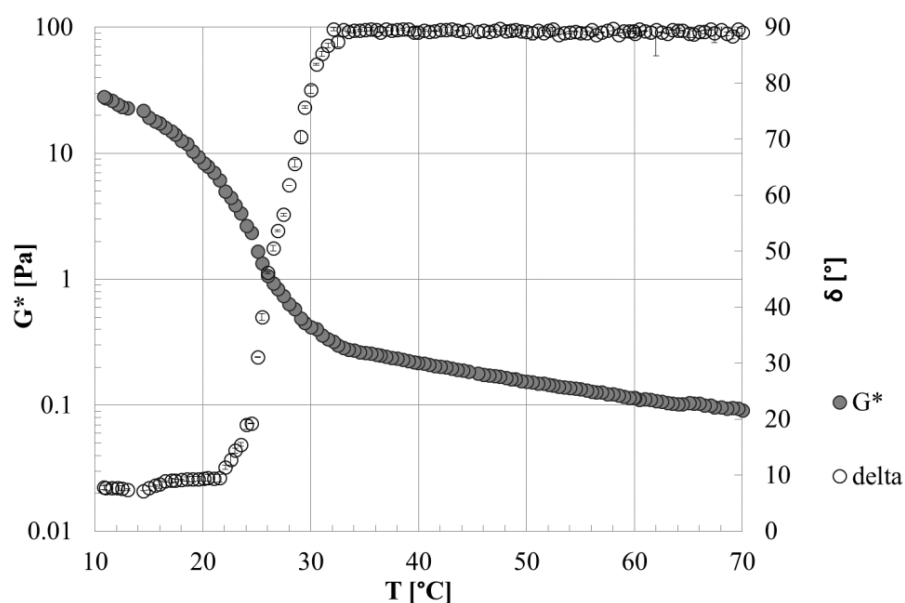
Figure 3.5 Time cure test for sample OM4.

As shown in Figure 3.6, the onset of crystallisation results in a sharp decrease of δ and tends to be shifted to higher temperature values when the MAG fraction is increased. Even though very low fractions of organogelator were investigated, the crossover between loss and storage modulus ($\delta=45°$) could be always detected for all the samples analysed, indicating that the minimum organogelator mass fraction required for gelation (approachable to a sort of percolation concentration) is very small (ranging between 0 and 0.001). Nevertheless, it has to be pointed out that the results obtained can be affected by the applied operating conditions. Lupi et al. [20] analysed similar systems using a cooling rate of 5°C/min and the minimum Myverol fraction required for crystallisation was found to range between 0.001 and 0.005, whereas gelation could be found only when the organogelator fraction was higher than a critical concentration ranging between 0.01 and 0.015. In addition, it is worth noticing that for OM1-OM3 samples, the gelation temperature is lower than room temperature, which makes these systems unsuitable for many uses in the food industry.
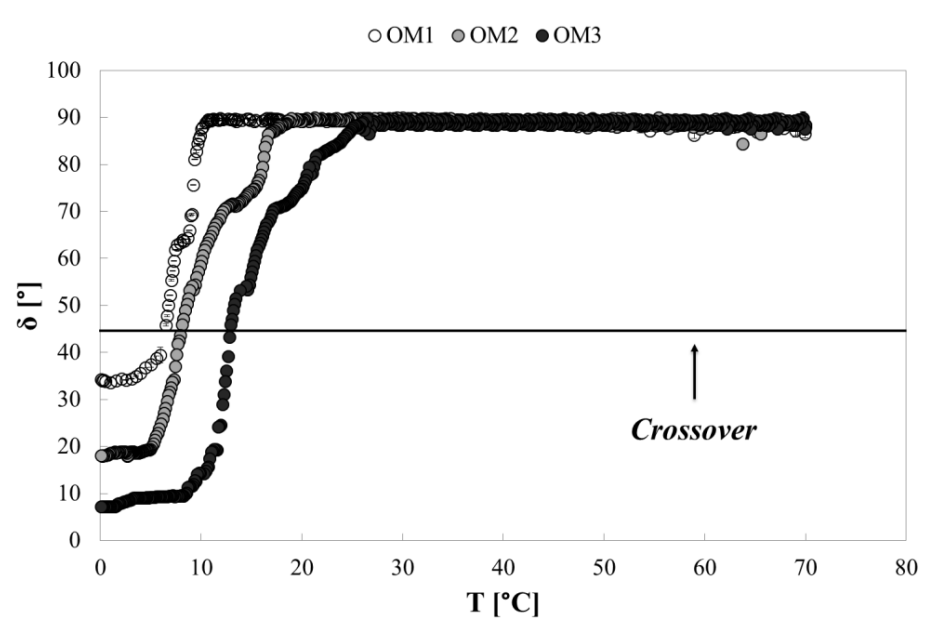
Figure 3.6 Phase angle versus temperature for OM1-OM3 samples.

The estimated T_{co} and T_g values for OM samples are listed in Table 3.2. The results obtained evidence that both T_{co} and T_g increase with increasing Myverol concentration, with an asymptotic trend of T_{co} at high organogelator concentrations. Higher MAG concentrations cause a higher degree of super-saturation, resulting in an increase of the temperature of crystallisation onset. In addition, as already reported in the literature [17], as the organogelator concentration decreases the MAG/vegetable oil system requires higher super-cooling to develop a gel.

Moreover, it is worth noticing that for Myverol concentrations lower than 0.034 the onset of crystallisation begins at a higher temperature with respect to T_g, denoting that at the T_{co} crystal nucleation and aggregation occur, whereas at lower temperatures (starting from T_g) interconnections among aggregates begin to develop, leading to a 3-D crystalline network structure.

Increasing the Myverol fraction, the difference between T_{co} and T_g decreases and starting from a Myverol fraction of at least 0.034 (sample OM5) no significant difference is encountered between the two critical temperatures (see Table 3.2 and Figure 3.7). The degree of super-saturation obtained for a Myverol fraction larger than this critical threshold promotes interactions among aggregates and allows the formation of long-scale interconnections together with crystallisation phenomena.

Sample ID	T_{co} [°C]	T_g [°C]	$T_{co,s}$ (1s^{-1}) [°C]	$T_{co,s}$ (100s^{-1}) [°C]
OM1	10.75±0.10	7.48±1.95	8.33±0.50	8.96±0.25
OM2	18.02±0.09	8.14±0.07	18.07±0.75	18.05±0.25
OM3	27.67±0.54	10.91±0.09	28.20±0.26	27.51±0.25
OM4	32.55±0.29	25.55±0.09	32.92±0.01	32.75±0.25
OM5	43.73±0.11	42.64±0.02	42.41±0.03	43.02±0.85
OM6	55.18±0.05	53.75±0.02	54.95±0.10	55.01±0.19
OM7	61.76±0.06	59.46±0.03	61.03±0.11	60.98±0.24
OM8	61.14±0.25	59.61±0.04	61.45±0.13	61.22±0.18
OM9	42.79±0.25	29.80±0.02	42.55±0.32	42.05±0.29

Table 3.2 T_{co} and T_g for OM samples. $T_{co,s}$(1s^{-1}) and $T_{co,s}$(100s^{-1}) indicate the onset of crystallisation temperature estimated from SRTRTs at a constant shear rate of 1s^{-1} and 100s^{-1}, respectively.
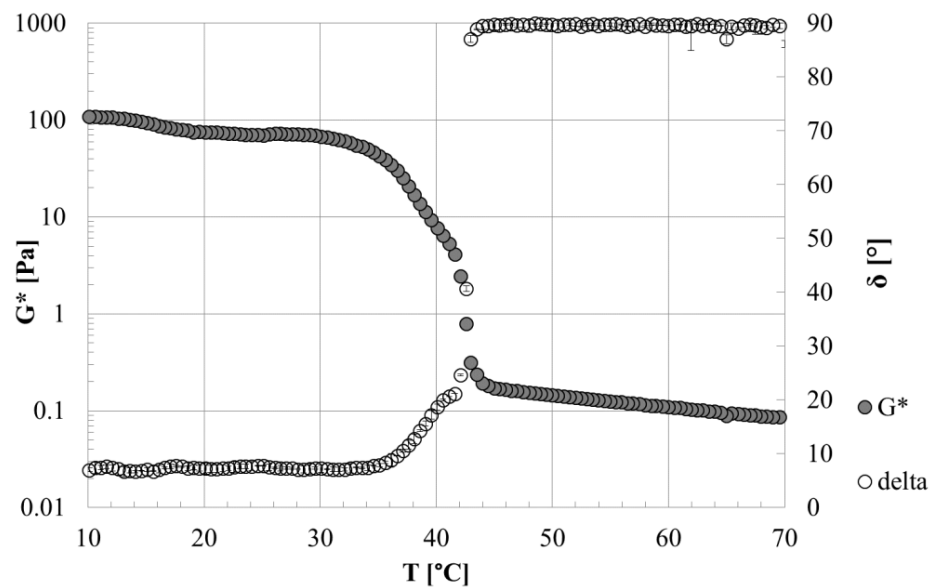
Figure 3.7 Time cure test for sample OM5.

As far as the flow behaviour of MAG organogels is concerned, the viscosity curve showed the same trend for all investigated samples during SRTRTs. As an example, Figure 3.8 shows the results obtained for the OM4 system. At high temperature ($T>T_{co,s}$), a liquid-like behaviour, with viscosity independent of the applied shear rate, is observed. Cooling down the material ($T=T_{co,s}$), a sudden change in the viscosity curve slope indicates the beginning of crystallisation phenomena. At lower temperature ($T<T_{co,s}$), the flow behaviour is greatly determined by the shear rate applied. At the highest shear rate, a

lowering in the viscosity values is observed. Da Pieve et al. [13] demonstrated that the introduction of shear during organogel formation affects the structure of the system at different levels (nano, micro and macro levels) significantly. They found that the application of high shear rates hindered the formation of well-organized structures, instead of promoting the formation of smaller clusters. At high shear rates, the crystallisation regime favours nucleation over growth. Although the presence of small crystals usually yields high viscosity values, it should be taken into account that the application of high shear rates could partially destroy the crystalline network structure during its formation, resulting in the observed decrease of the viscosity values.

It is worth noticing that two further slope changes can be observed at the lowest shear rate ($1s^{-1}$). A similar behaviour was already described in the literature [28, 29] and it was attributed to microstructural changes due to polymorphic transitions. Lupi et al. [28] suggested that crystallisation initially occurs in the α-crystalline polymorph, then it proceeds through α-crystals nucleation and their partial/complete polymorphic transition into β' crystals and finally the formation and growth of crystalline aggregates results in the development of a network structure.
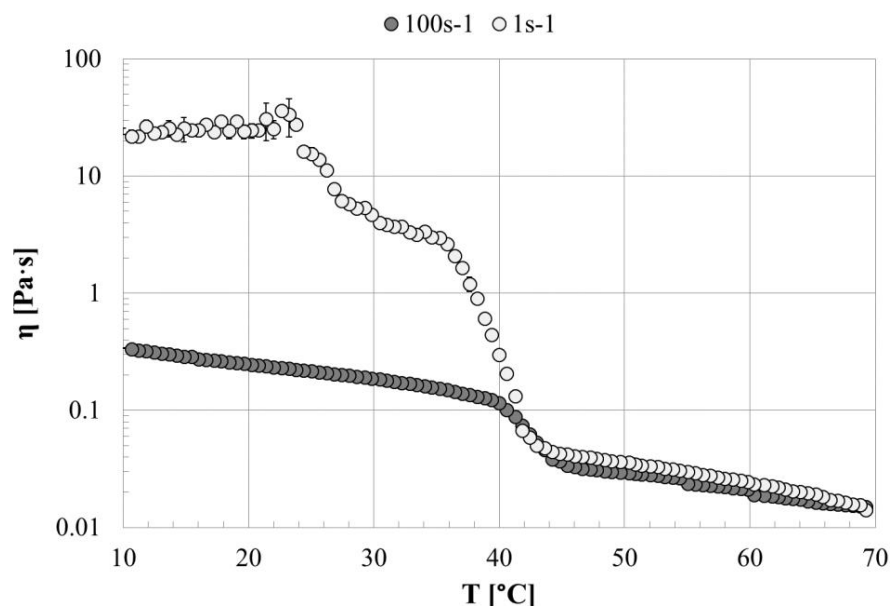
Figure 3.8 Step Rate Temperature Ramp Test at $1s^{-1}$ and $100s^{-1}$ for sample OM4.

The temperature of crystallisation onset is not determined by the applied shear rate for all the OM samples investigated (see Table 3.2). Furthermore, it should be noted that the temperature of crystallisation onset is independent of the kinematic conditions employed,

for Myverol fractions of at least 0.005. Indeed, no significant difference can be detected between the temperature of crystallisation onset calculated from oscillatory tests and from SRTRTs.

3.3.2 Thermal and structural analysis of MAG organogels

3.3.2.1 DSC analysis

The cooling DSC thermogram showed the same trend for all MAG/olive oil samples investigated. As an example, Figure 3.9 shows the results obtained for the pure organogelator and the OM5 sample. The crystallisation of Myverol showed two exothermic peaks (starting at 65.97±0.08°C and 14.05±0.03°C), as already reported in the literature for commercial mixtures of MAGs [17]. All samples studied exhibited the same behaviour upon cooling: the high-temperature peak corresponds to the crystallisation phenomena already detected through rheological analysis, whereas the low-temperature peak appears at approximately 15°C for all samples. The second transition temperature (very close to the sub-α transition temperature of pure MAGs) was found to be independent of the organogelator concentration.
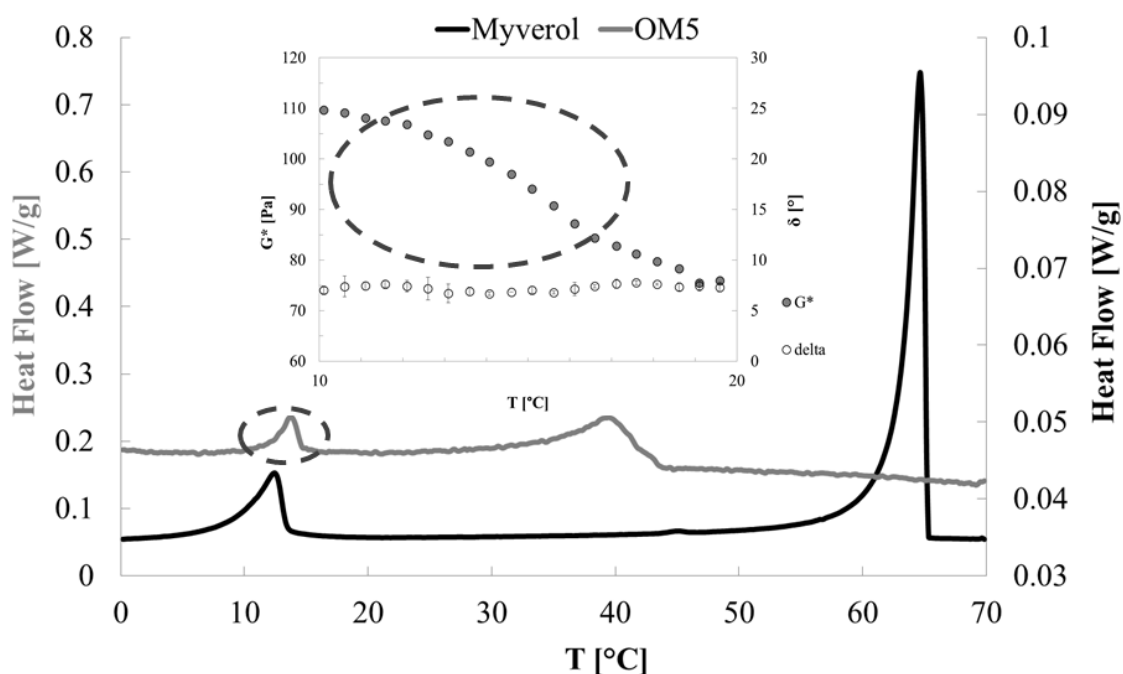
Figure 3.9 Cooling DSC thermograms of pure Myverol and sample OM5.

Chen et al. [9] observed a similar behaviour for monostearin/hazelnut oil organogels. They suggested that the high-temperature transition corresponded to the formation of the inverse lamellar phase, whereas the low-temperature transition represented the Krafft temperature at which the aliphatic chains crystallise in the lamellae.

For all Myverol/olive oil samples considered the first transition peak appears at the same temperature (T_{co}) at which a sudden increase in the complex modulus was found in the Time cure tests, indicating the beginning of crystallisation phenomena. It seems reasonable to assume that the first transition peak corresponds to the self-assemble of the organogelator into the inverse lamellar phase as a precursor of crystal growth and aggregation. The low-temperature peak (corresponding to a moderate change in the slope of the complex modulus curve in Time cure tests) indicates the polymorphic transition into a crystalline form, analogous to the sub-α crystals observed for pure MAGs.

Figure 3.10 shows the cooling and heating thermogram for pure organogelator and for OM4, OM5 and OM7 samples. It can be noticed that all samples show the same behaviour upon cooling, as stated before. On the contrary, the melting thermogram is similar for all OM samples only at low temperature. All curves exhibit an endothermic peak at low temperatures (around 10°C for all samples), corresponding to the melting of sub-α structures. At higher temperature, the melting thermogram (i.e. results obtained when the sample is subjected to a heating ramp) of samples containing low amount of MAGs (OM4 and OM5) shows a single broad peak, whereas two consecutive endotherms can be observed for sample OM7 and for the pure organogelator, indicating the melting of two different structures. According to some authors [15], high MAG concentrations cause a high degree of super-saturation and, as a consequence, crystal nucleation can occur in both α and β polymorphs.
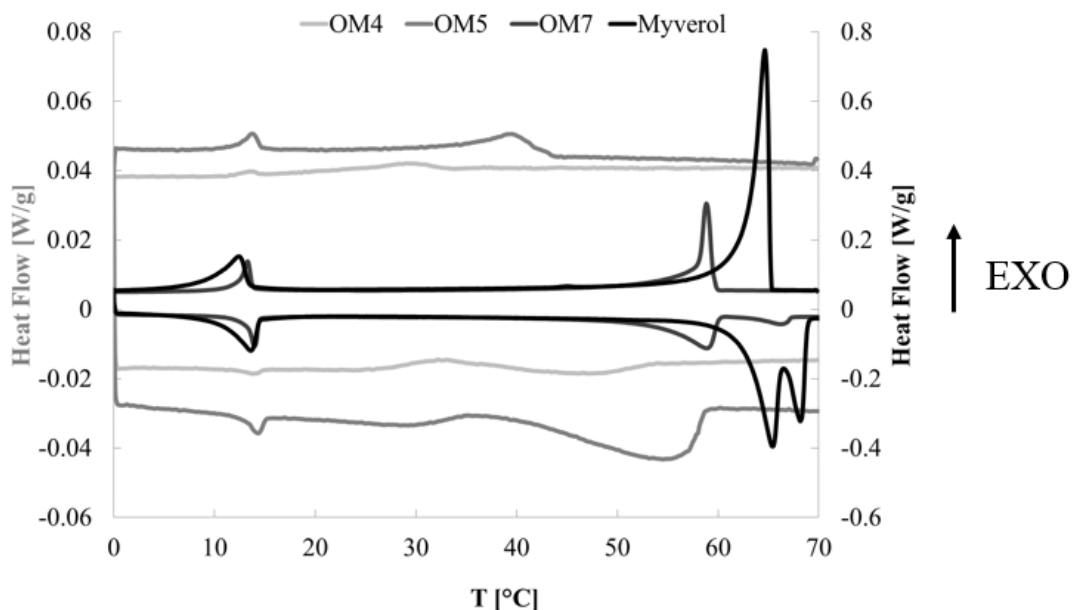
Figure 3.10 DSC thermograms of OM4, OM5 and OM7 samples and pure Myverol.

3.3.2.2 FT-IR analysis

In order to describe better the microstructure of Myverol/olive oil organogels, FT-IR spectra were recorded at room temperature, immediately after gel formation. The low-energy region from 3000 to 4000 cm^{-1} is particularly interesting because it corresponds to the OH-stretching modes [17]. Figure 3.11 shows spectra recorded for samples OM4, OM5 and OM7. In the low-energy region, a small inflection can be detected in the OM4 spectrum, whereas a broad peak appear in the OM5 and OM7 spectra. For the OM7 spectrum, it can be observed that this is split into two smaller peaks. The "twin" absorption peak corresponds to the 2-OH and 3-OH intermolecular hydrogen bonding between organogelator molecules [1]. Figure 3.11 shows a dominant absorption peak in the OM7 spectrum and a single peak in the OM5 spectrum at around 3350cm^{-1}, corresponding to 3-OH groups bonded with hydrogen bonds [1]. The lower-energy "twin" peak of the OM7 spectrum at around 3250cm^{-1} corresponds to 2-OH hydrogen bonding. The 2-OH hydrogen bonding decreases the vibration frequency of molecules, resulting in the band shift towards a lower wavenumber [1]. The coexistence of 3-OH and 2-OH hydrogen bonding was already observed by Chen and Terentjev [1] during ageing of MAG/hazelnut oil organogels. They associated the presence of 2-OH hydrogen bonding with the formation of the stable β crystal polymorph.

The results obtained suggest the formation of a single structure (the inverse lamellar phase) in the OM5 system and the coexistence of two structures (lamellar structures and β crystals) in the OM7 system, at room temperature. This is in agreement with results obtained from DSC analysis, as discussed above.
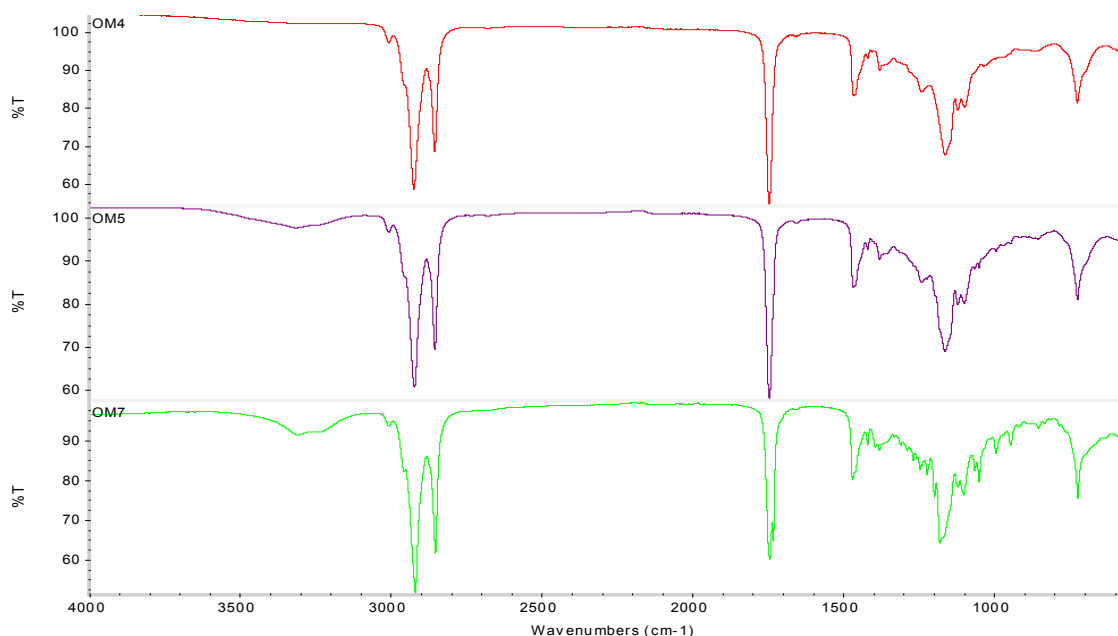
Figure 3.11 FT-IR spectra for OM4, OM5 and OM7 samples.

3.3.3 Determination of SFC and application of fractal model

The SFC of MAG/olive oil systems increased with decreasing temperature, as can be appreciated in Figure 3.12. The trend of the SFC curve is very similar to the above-mentioned behaviour of the complex modulus during temperature ramp tests: at high temperature ($T>T_{co,NMR}$), the SFC is almost constant and values are very close to zero. At the onset of crystallisation ($T=T_{co,NMR}$) a sharp increase in the SFC can be detected, followed by a transition region, and, finally, a plateau can be observed for further reduction in temperature.
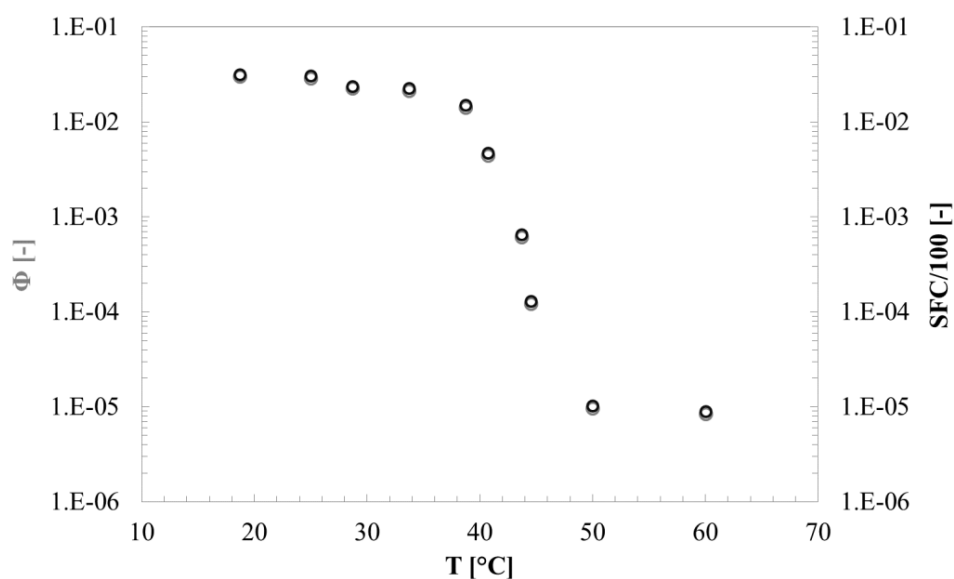
Figure 3.12 SFC and volumetric fraction of solids (Φ) versus temperature, for sample OM5.

It is worth noticing that the SFC value at the plateau is very close to the mass fraction of organogelator of the system. Blake et al. [25] defined the "theoretical SFC" for organogels containing varying concentrations of waxes, assuming ideal solubility of the organogelator in the oil. The "theoretical SFC" can be determined by multiplying the fraction of the organogelator by the measured solids content of the neat organogelator added to the system. Values obtained for the Myverol organogels investigated are listed in Table 3.3. The theoretical values are slightly higher than experimental values measured at T_{25} ($T_{25}=T_{co}-25$), as already reported in the literature [25]. This result suggests slight Myverol solubility in liquid olive oil. Indeed, an organogelator should be neither too soluble nor insoluble in a solvent in order to achieve a proper balance of gelator/gelator interactions and gelator/solvent interactions [5, 25].

Sample	SFC$_{th}$ [%]	SFC (T_{25}) [%]
OM5	3.29	3.19±0.03
OM6	9.67	9.01±0.01
OM7	29.00	28.89±0.11
OM8	48.34	48.08±0.07
OM9	2.90	2.67±0.01

Table 3.3 Theoretical (SFC$_{th}$) and measured SFC at T_{25} for OM5-OM9 samples.

SFC has been measured at different temperature lower than T_{co}, which are:

$T_{10}=T_{co}-10$

$T_{15}=T_{co}-15$

$T_{25}=T_{co}-25$.

For all samples investigated, the SFC was found to be directly proportional to the organogelator mass fraction (see Figure 3.13):

$$\frac{SFC}{100} = aX_M \tag{3.3.1}$$

where $a(T_{10})=0.89\pm0.04$, $a(T_{15})=0.96\pm0.05$ and $a(T_{25})=0.97\pm0.05$.
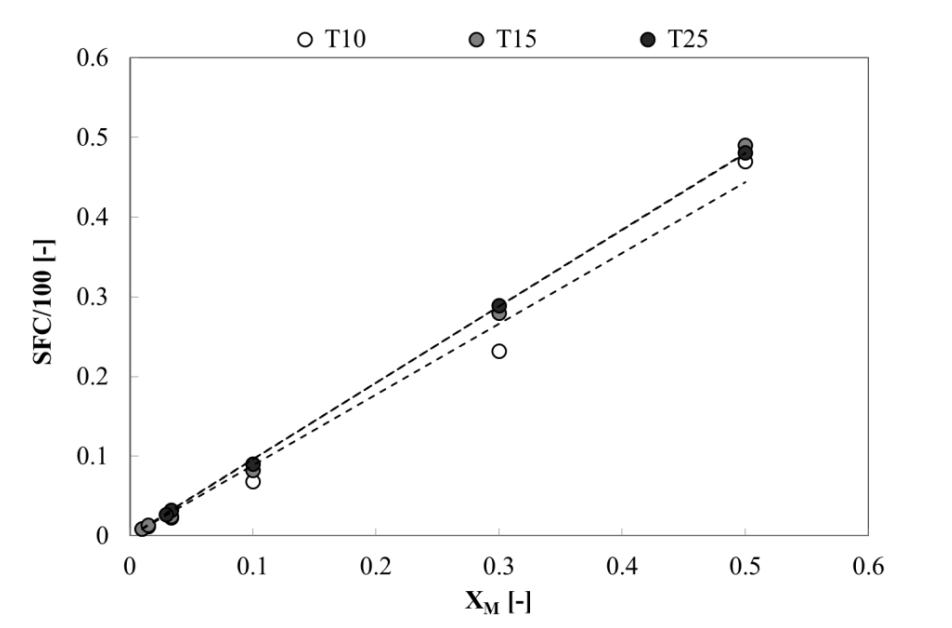
Figure 3.13 SFC versus Myverol fraction at different temperature levels.

The calculated values of the volume fraction of solids Φ (Eq. 3.2.5) for OM5 sample are shown in Figure 3.12. G' data were related to the volume fraction of solids according to Equation 3.2.4 (fractal model). Fitting parameters for the fractal model at two different temperature levels (T_{10} and T_{15}) are shown in Table 3.3.2:

Temperature	λ [Pa]	D [-]
T_{10}	82702±7550	2.74±0.02
T_{15}	119372±8914	2.74±0.02

Table 3.4 Fitting parameters of Eq. 3.2.4.

It is worth noticing that parameter λ increases with increasing the distance from T_{co}, whereas the fractal dimension remains constant upon cooling. Therefore, the decrease in temperature results in an increase of the strength of links between crystal aggregates but no significant changes in the spatial distribution of crystals within the network can be detected.

From Figure 3.14, it can be seen that the fractal model seems to fit the experimental trend in a satisfying way.
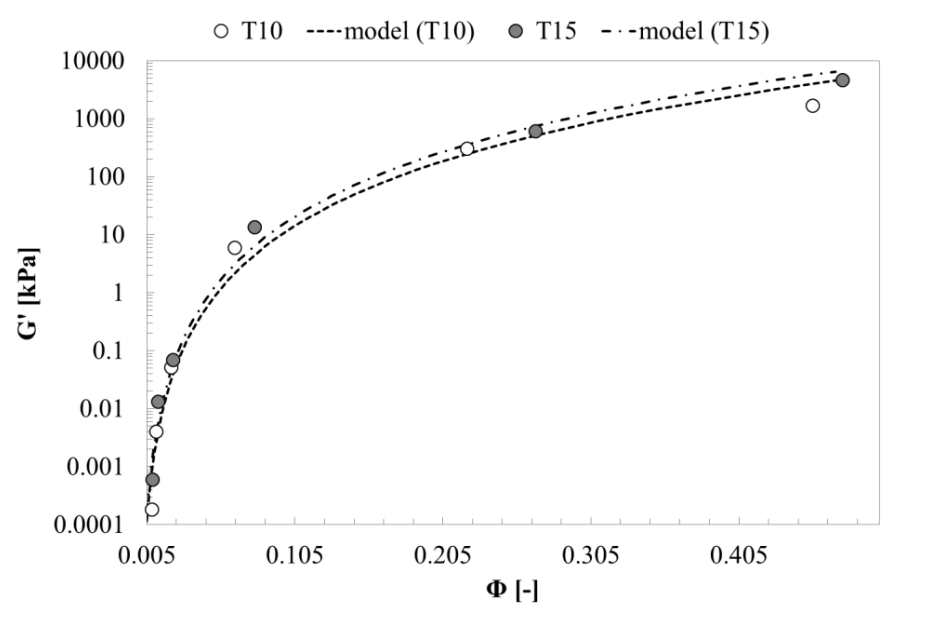
Figure 3.14 Application of fractal model.

The original fractal model was further modified by Tang and Marangoni [26], by substituting the apparent volume fraction of solids Φ with the effective volume fraction Φe of stress-loading solids. The final equation of the modified fractal model is:

$$G' = \lambda \left(1 - e^{-k\Phi^b} \right)^{1/(3-D)} \tag{3.3.2}$$

Owing to the limited amount of experimental data available and the high number of parameters included in the model, it was not possible to fit data with the modified fractal model. Nevertheless, using the fractal dimension estimated with the original fractal model, the fitting parameters λ, k and b of Eq. 3.3.4 were calculated. Figure 3.15 and 3.16 show the fitting of experimental data using both the original and the modified fractal model. It can be observed that both models fit the experimental data quite well; however, the

modified fractal model seems to fit better the experimental trend at intermediate and high volume fractions.
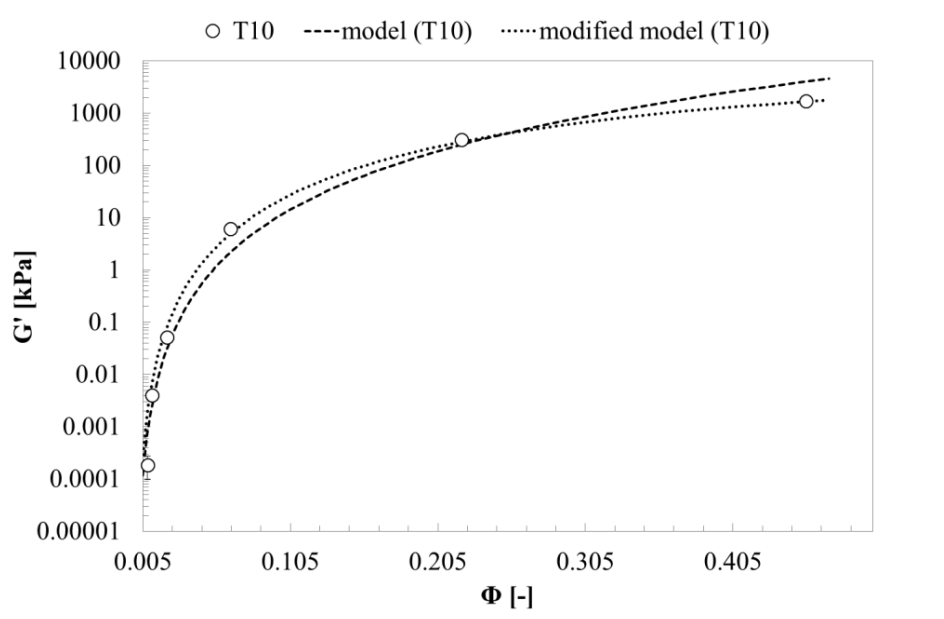
Figure 3.15 Fractal model and modified fractal model at T$_{10}$.
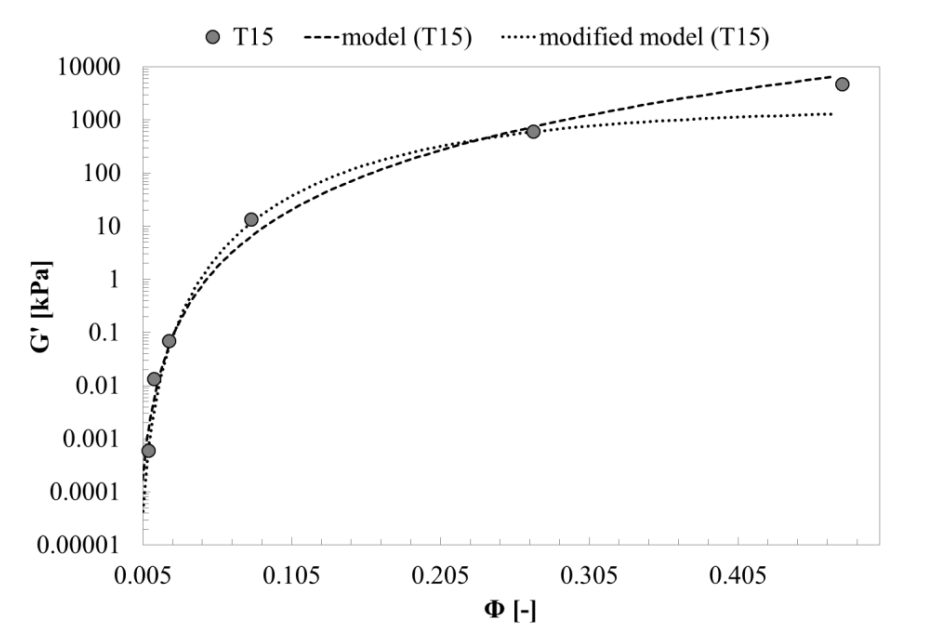
Figure 3.16 Fractal model and modified fractal model at T$_{15}$.

3.3.4 Interpretation of thermo-rheological parameters and structure development rate

The onset of crystallisation temperature (calculated from the rheological characterisation, DSC and NMR analysis) is reported in Table 3.5 and in Figure 3.17. It is worth noticing that no significant differences can be appreciated between T_{co} values estimated using different techniques (see Table 3.5).

Sample	T_{co} [°C]	$T_{co,DSC}$ [°C]	$T_{co,NMR}$ [°C]
OM1	10.75±0.10		
OM2	18.02±0.09		
OM3	27.67±0.54		28.11±0.23
OM4	32.55±0.29	32.81±0.21	32.93±0.12
OM5	43.73±0.11	43.72±0.30	44.02±0.11
OM6	55.18±0.05		55.51±0.39
OM7	61.76±0.06	61.71±0.21	61.68±0.44
OM8	61.14±0.25		61.62±0.28
OM9	42.79±0.25	42.35±0.08	41.99±0.35

Table 3.5 Temperature of crystallisation onset for OM samples, calculated from rheological SAOTs (T_{co}), from DSC analysis ($T_{co,DSC}$) and from NMR measurements ($T_{co,NMR}$).

At high organogelator fractions, experimental results exhibited an asymptotic trend of T_{co} as a Myverol fraction function, indicating a saturation effect. The following simple empirical equation can be adopted to explain the relationship between T_{co} and the Myverol fraction X_M:

$$T_{co} = \frac{A \cdot X_M}{B + X_M} \tag{3.3.3}$$

where A=62.81±0.54°C and B=0.013±0.001.

There again, it could be of interest to relate the onset of crystallisation temperature T_{co} to the microstructure of the system. The asymptotic trend observed for T_{co} at high organogelator fraction is qualitatively similar to the behaviour of the storage modulus G' as a function of the volume fraction of solids Φ, well described by the modified fractal model (Eq. 3.3.2). Therefore, the empirical equation 3.3.6 can be proposed to fit T_{co} results:

$$T_{co} = A' \left(1 - e^{-B'X_M^C}\right)^{1/(3-D)} \tag{3.3.4}$$

where the fractal dimension D has already been estimated from rheological data (G' versus Φ), whereas $A'=64.20\pm2.34°C$, $B'=6.058\pm0.676$ and $C=0.282\pm0.021$.
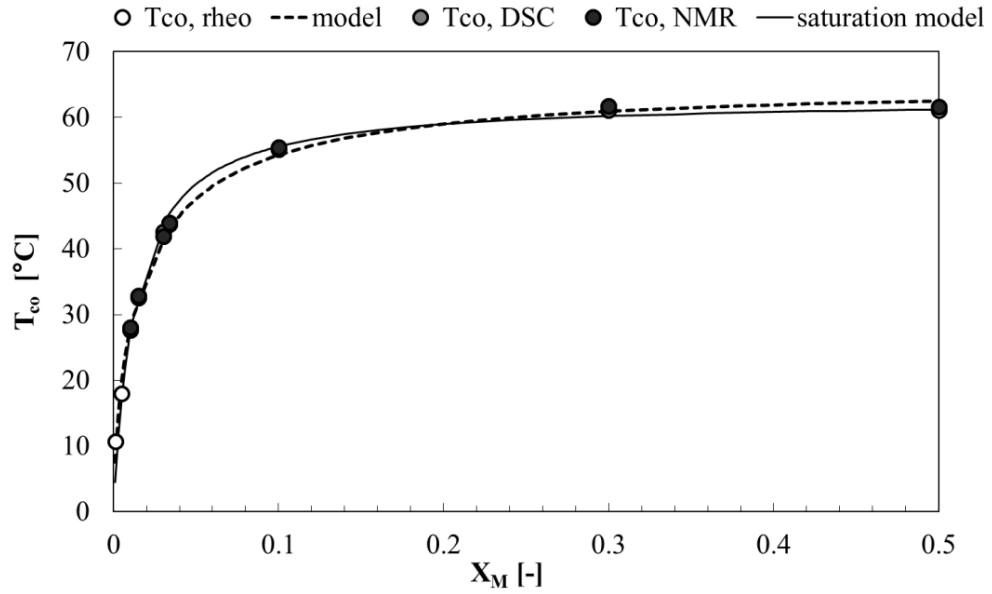
Figure 3.17 *T_{co}* as a function of Myverol fraction and data fitting with both modified fractal model (Eq. 3.3.6) and saturation model (Eq. 3.3.5).

In order to investigate the influence of MAG concentration on the rate of network development, for each sample both the average rate of SFC increase (*SFCr*) and the average rate of structure development (*SDr*) were estimated. On the one hand, the *SFCr*, calculated from NMR data, provides an indirect measurement of the rate of crystal mass increase during cooling of Myverol/olive oil systems. As shown in Figure 3.18, it was found that the *SFCr* increases at increasing Myverol fraction and the following empirical equation is proposed to fit the results obtained:

$$SFCr = a'X_M \tag{3.3.5}$$

with $a'=0.078\pm0.001s^{-1}$ ($R^2=0.99$).
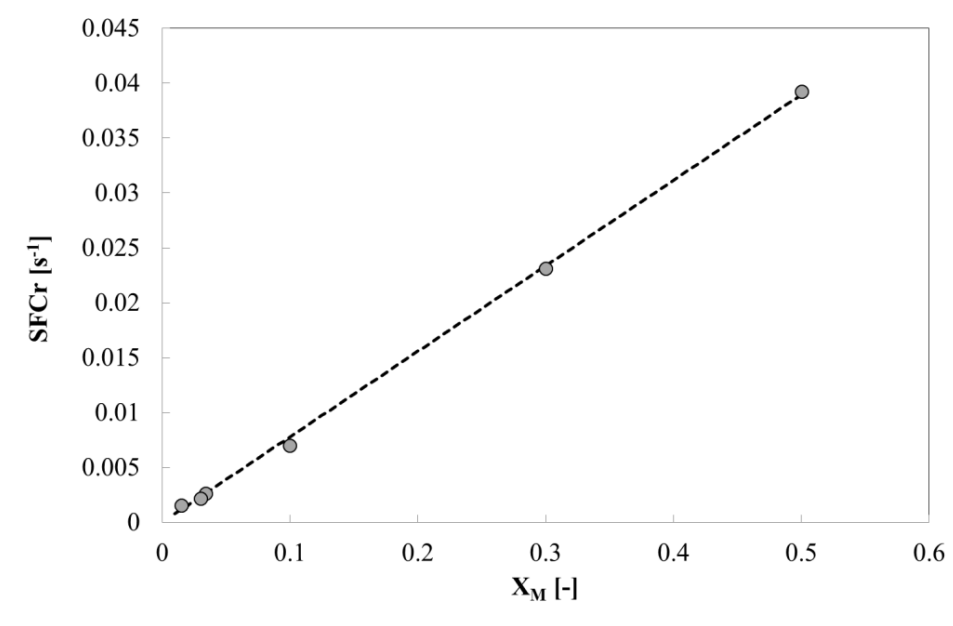
Figure 3.18 Rate of SFC increase (SFCr) as a function of Myverol fraction and data fitting with Eq. 3.3.5.

On the other hand, the average *SDr*, calculated from rheological analysis, provides information on the rate of elastic modulus increase during cooling of self-assembling structuring agents. The changes observed in rheological properties during Temperature ramp tests are closely related to changes in the system microstructure, occurring upon cooling. Therefore, it seems reasonable to relate the *SDr* estimated from rheological analysis to the above-mentioned fractal structure of the systems investigated, according to Eq. 3.3.6:

$$SDr = \lambda' X_M^{1/(3-D)} \qquad (3.3.6)$$

where λ'=85400±3100Pa/s, whereas the fractal dimension has already been estimated (*D*=2.74).
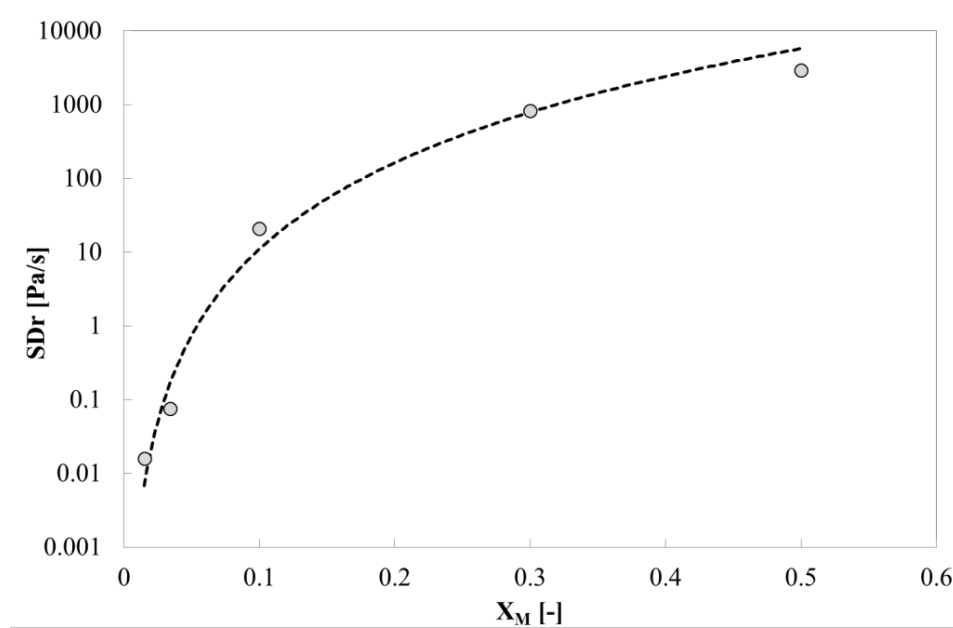
Figure 3.19 Structure development rate (*SDr*) as a function of Myverol fraction and data fitting with Eq. 3.3.8.

3.3.5 Ageing and stability of MAG/olive oil organogels

With the aim of investigating Myverol/olive oil gel stability and potential micro-structural changes occurring during ageing, SFC values were recorded every 24 h for 10 days; OM samples were stored at two different temperatures (4°C and 25°C, respectively). As an example, Figure 3.20 shows the results obtained for sample OM5. At the lowest temperature, it can be observed that a sharp increase in SFC values occurs after the first day of storage and then a further small increase can be detected. On the contrary, at room temperature the SFC remains almost constant, although a limited decrease is observed after 2-3 days of storage, indicating a partial instability of the system. It should be pointed out that SFC values at 4°C are well above the maximum theoretical value because of olive oil crystallisation, as shown for olive oil SFC measurements in Chapter 2.
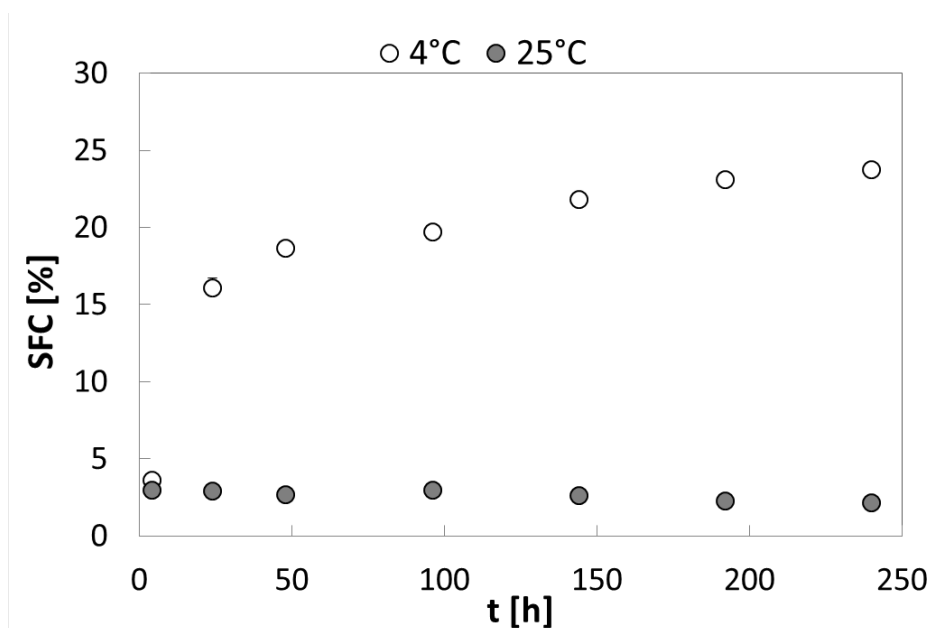
Figure 3.20 SFC as a function of time for sample OM5.

After one week of storage of OM samples at 4°C and 25°C respectively, DSC thermograms were recorded. The results for sample OM5 are shown in Figure 3.21 and compared with the thermogram obtained just after sample preparation ($t=t_0$). It can be seen that the two peaks displayed in the melting thermogram of the fresh sample coalesced into one broad peak shifted to higher temperatures. This result suggests the formation of a high-melting polymorph during ageing, indicating the partial or complete transition of lamellar structures and sub-α crystals into the β form. Moreover, it is worth noticing that all cooling thermograms in Figure 3.21 show the same behaviour, denoting the complete thermo-reversibility of the investigated systems.
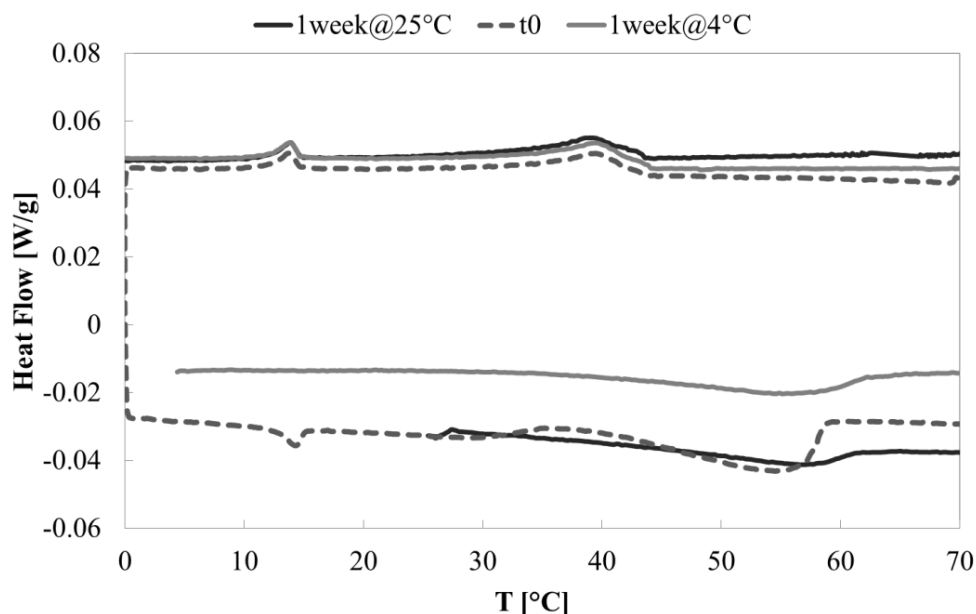
Figure 3.21 DSC thermograms of OM5 sample just after preparation (*t0*), after 1 week of storage at 25°C (*1week@25°C*) and after 1 week of storage at 25°C (*1week@4°C*).

3.3.6 Effect of the solvent on structural and rheological properties

The effects of the kind of vegetable oil used as the solvent were investigated for samples prepared at a constant Myverol fraction (0.03, samples EM, OM9, GM). During Temperature ramp tests, the complex modulus and the phase angle curves showed the same behaviour already described in the previous sections for OM samples. Interestingly, the temperature of crystallisation onset was found not to be significantly affected by the kind of vegetable oil (see Table 3.6). Lupi et al. [20] obtained similar results, showing that, above a critical organogelator concentration, the temperature of crystallisation onset was not determined by the composition of the oil phase. On the contrary, it can be observed that the temperature of gelation of the OM9 system (prepared with virgin olive oil) is lower than the gelation point exhibited by EM and GM samples (containing extra-virgin olive oil and sunflower oil, respectively).

In order to describe better the influence of the solvent on the rheological properties of the organogel, G^* and δ at T_5, T_{10}, T_{15} and T_{25} were compared (Figure 3.22 and 3.23). Sample GM exhibits the highest values of the complex modulus at temperature values slightly lower than T_{co}; however, differences between G^* values of all samples become less evident at $T=T_{25}$.

Sample	T_{co} [°C]	$T_{co,DSC}$ [°C]	$T_{co,NMR}$ [°C]	T_g [°C]
EM	42.77±0.21	41.73±0.09	41.58±0.24	33.36±0.35
OM9	42.51±0.29	42.35±0.08	42.48±0.17	29.79±0.02
GM	41.97±0.54	42.03±0.13	42.11±0.23	34.07±0.45

Table 3.6 Temperature of crystallisation onset, calculated from rheological SAOTs (T_{co}), from DSC analysis ($T_{co,DSC}$) and from NMR measurements ($T_{co,NMR}$) and temperature of gelation (T_g) for EM, OM9, GM samples.

The same trend was observed for the phase angle (with GM showing the lowest values). Therefore, it seems that solvent mainly affects the rate of structure formation, whereas the consistency and the solid-like behaviour of Myverol organogel at low temperature, far enough from the onset of crystallisation, are slightly influenced by the type of oil.
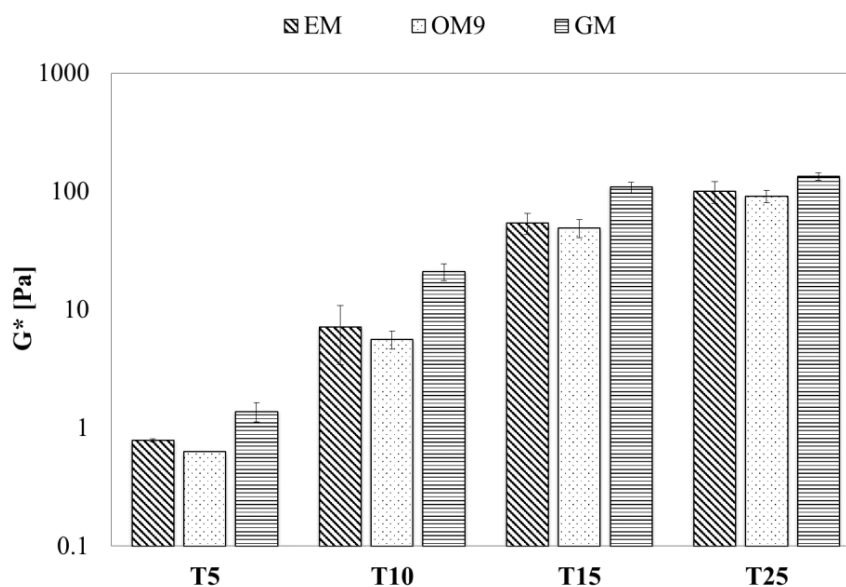
Figure 3.22 Complex modulus G^* at different temperature levels for EM, OM9 and GM samples.
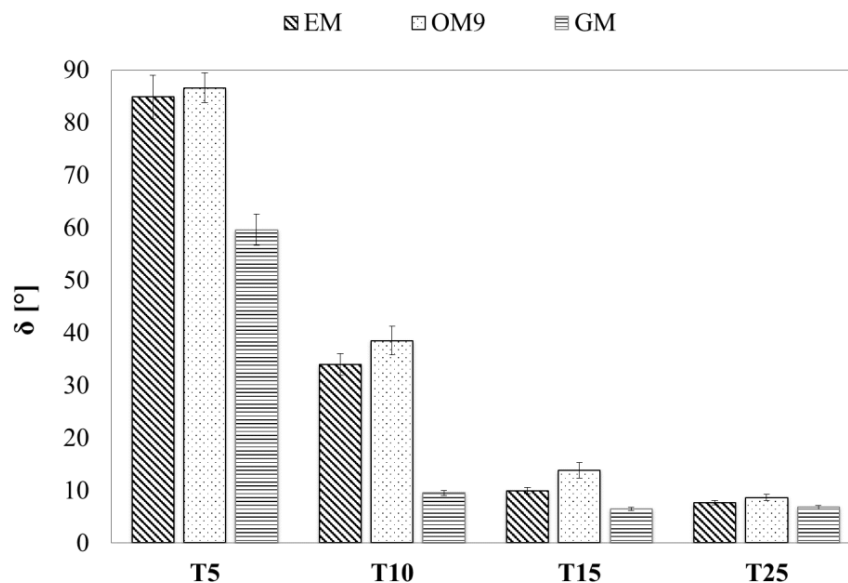
Figure 3.22 Complex modulus *G** at different temperature levels for EM, OM9 and GM samples.

The trend observed for the rheological properties *G** and δ was confirmed by the results obtained for *SFCr* and *SDr* (Figures 3.24 and 3.25): the system containing sunflower oil (GM) showed the highest value of the average *SFCr* (although differences are very small) and of the *SDr*, whereas the gel prepared with virgin olive oil (OM9) exhibited the lowest values of both parameters.
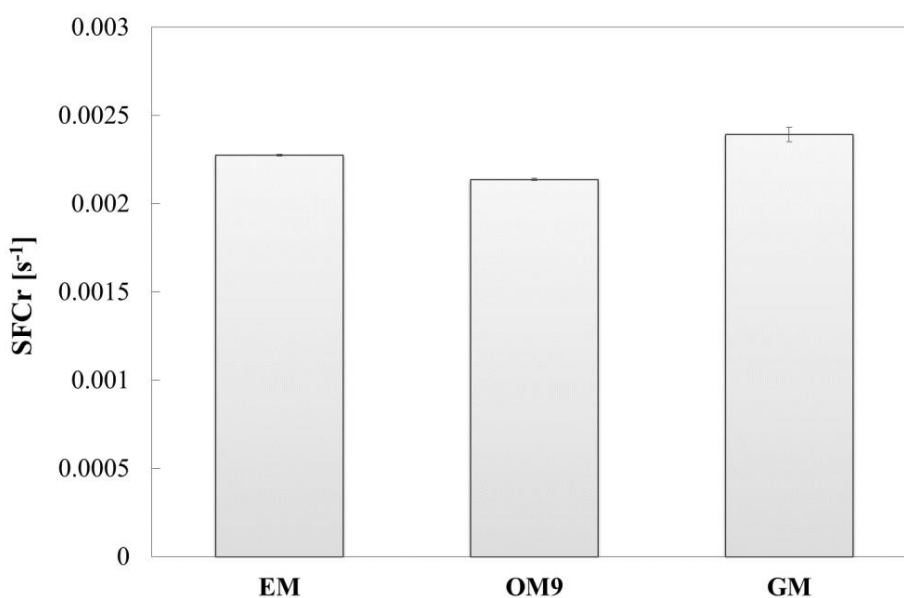
Figure 3.23 Rate of SFC increase (*SFCr*) for GM, EM and OM9 samples.
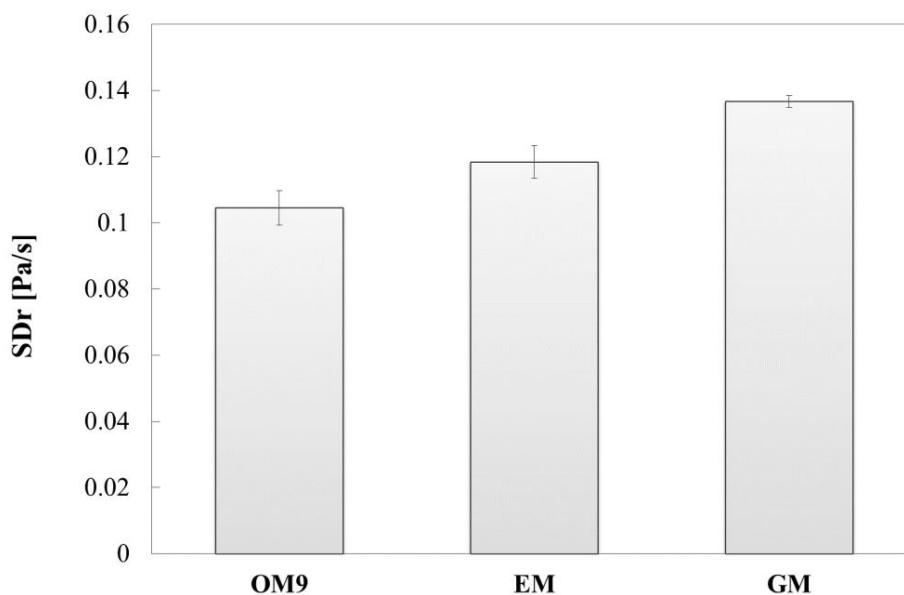
Figure 3.24 Structure development rate (*SDr*) for GM, EM and OM9 samples.

In agreement with results obtained in other works [17], the highest $G*$ values observed for sample GM could be partly explained by the higher crystal mass (resulting in higher SFC values at a defined distance from the onset of crystallisation). Nevertheless, it is well known that the type of oil could influence the microstructural formation of the MAG network, owing to the formation of different crystalline structures [5].

With the aim of investigating the possible changes in the microstructure of Myverol organogels produced with different vegetable oils, both SRTRTs (at a constant shear rate of $1s^{-1}$) and Temperature ramp tests were carried out using a RheoScope Module, in order to observe changes in microscopic structure of tested samples during rheological measurements. Figure 3.25 shows the complex modulus and the phase angle for the sample EM during Time cure test (the different temperatures at which images were recorded have been highlighted within the plot).
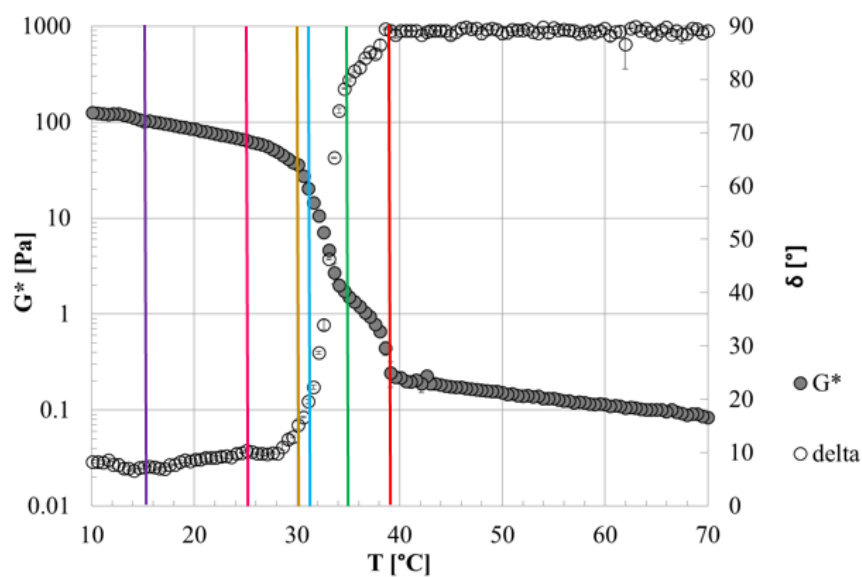
Figure 3.25 Time cure test for sample EM. Coloured lines correspond to the different micro-photographs shown in Figure 3.26.
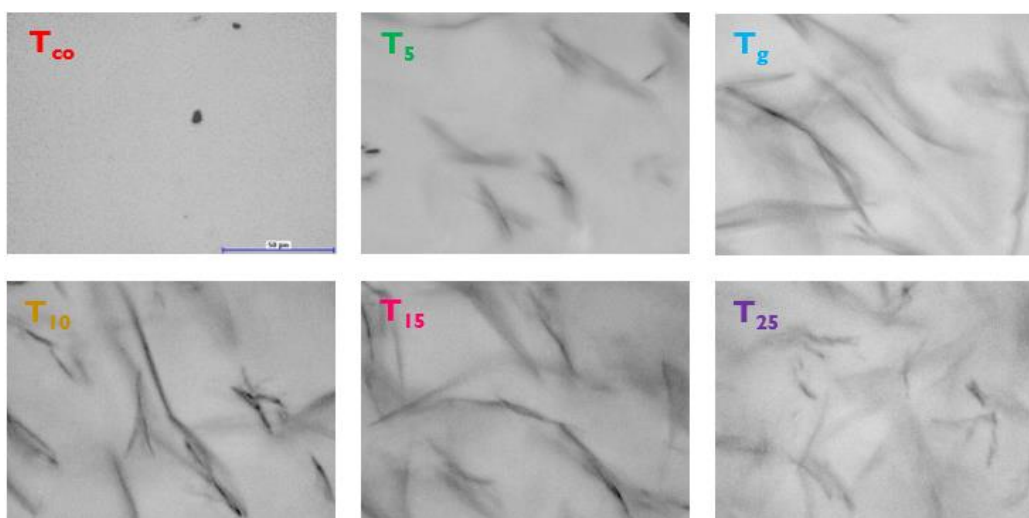
Figure 3.26 Micro-photographs of sample EM during Time cure test (Figure 3.25) at different temperatures (control bar is 50µm).

At the same temperatures, images were taken also for GM and OM9 samples. The results are shown in Figures 3.28 and 3.30.
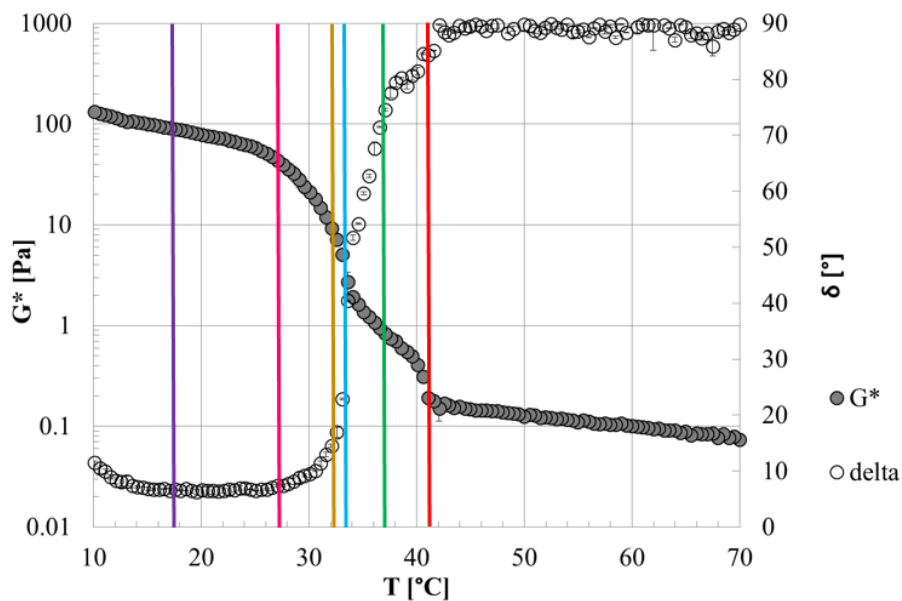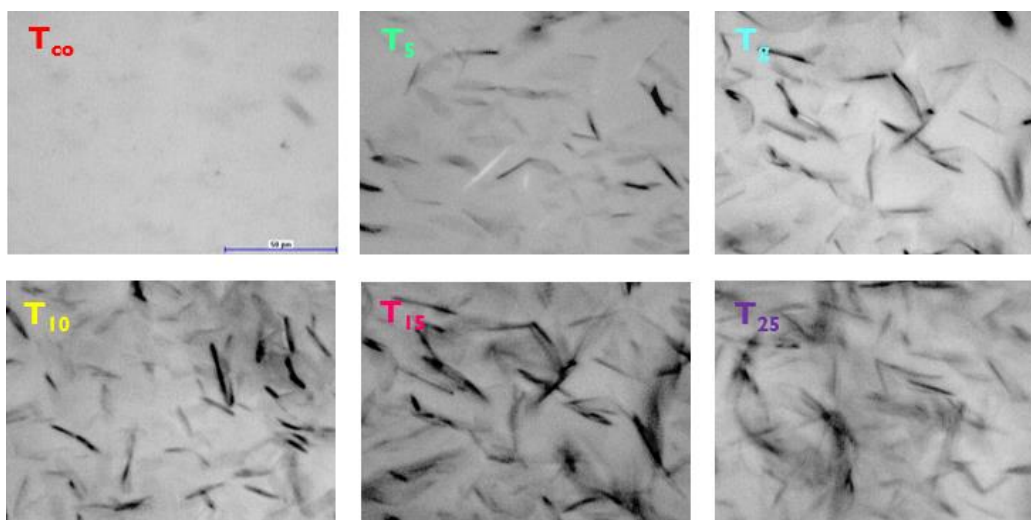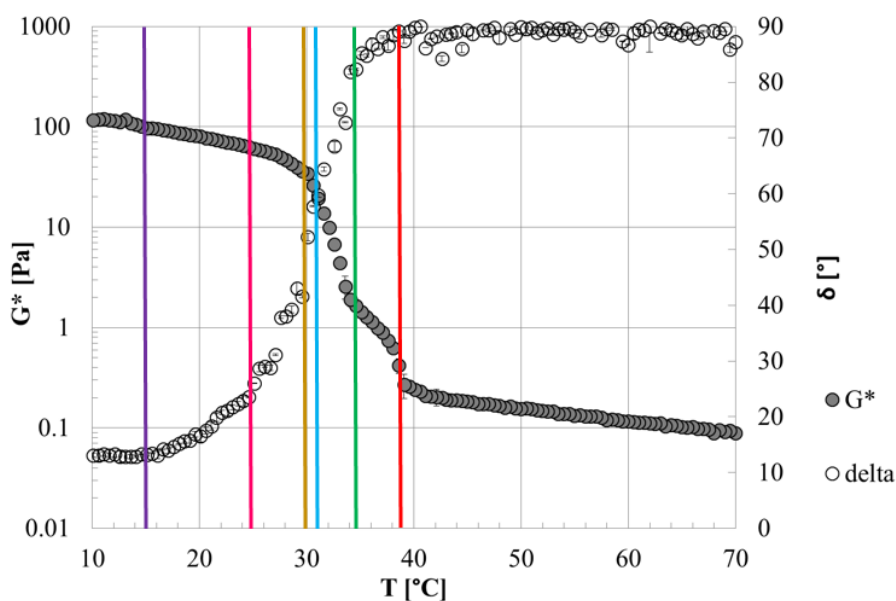
Figure 3.27 Time cure test for sample GM. Coloured lines correspond to the different micro-photographs shown in figure 3.28.

Figure 3.28 Micro-photographs of sample GM during Time cure test at different temperatures (control bar corresponds to 50μm).

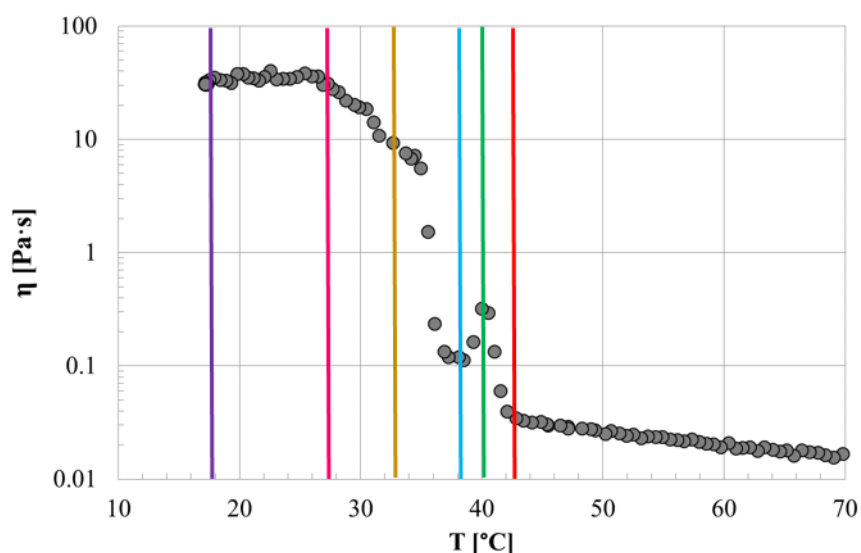**Figure 3.29 Time cure test for sample OM9. Coloured lines correspond to the different micro-photographs shown in figure 3.30.**
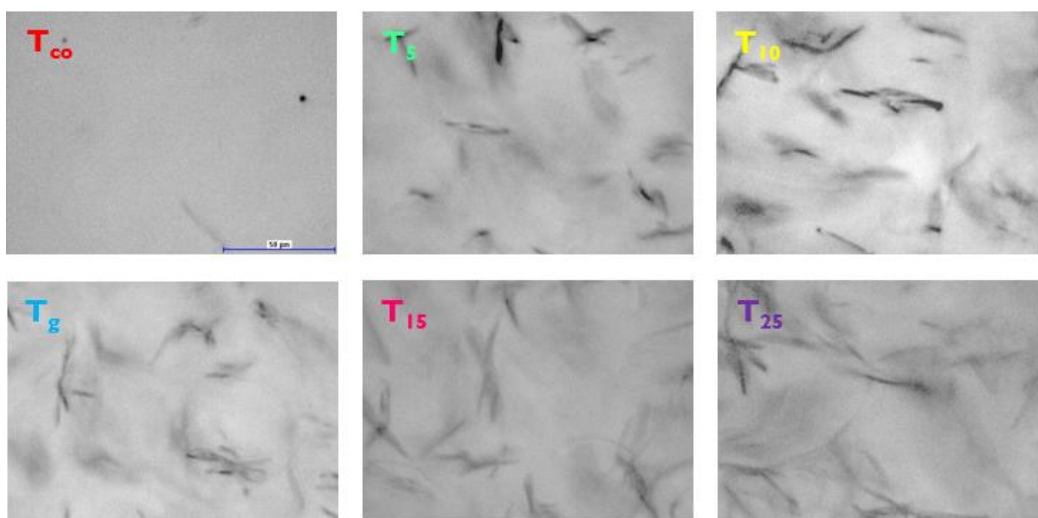
Figure 3.30 Micro-photographs of sample OM9 during Time cure test at different temperatures (control bar corresponds to 50μm).

For all tested samples, only small crystal nuclei can be observed at $T=T_{co}$. At lower temperature, microphotographs show crystals with needle-like shape, similar to those observed by Kesselman and Shimoni [14] in MAG/olive oil oleogels and by López-Martínez et al. [17] in MAG/sunflower oil organogels. Nevertheless, the three investigated organogels exhibit some differences in their microstructure. In sample OM9 and especially in sample EM, for $T \leq T_g$ crystals seem to grow along a single dimension, resulting in the formation of a network composed of fibre-like aggregates. At the same distance from the

onset of crystallisation (for $T \leq T_g$), the system containing sunflower oil (GM) is characterised by the presence of a larger number of smaller crystals, arranged in a close packed network structure. In agreement with the literature [17], the three-dimensional crystal organisation developed by smaller crystals would provide a larger surface area and, as a consequence, a more efficient organization for oil entrapment in the GM organogel. This resulted in a more consistent and structured organogel with respect to those produced with virgin or extra-virgin olive oil.

Figure 3.31 shows the results obtained from the SRTRT (at a constant shear rate of 1 s^{-1}) for the EM sample. The temperatures at which micro-photographs were recorded for all the investigated samples are highlighted.

Figure 3.31 SRTRT at 1s^{-1} for sample EM. Coloured lines correspond to the different micro-photographs shown in Figure 3.32.
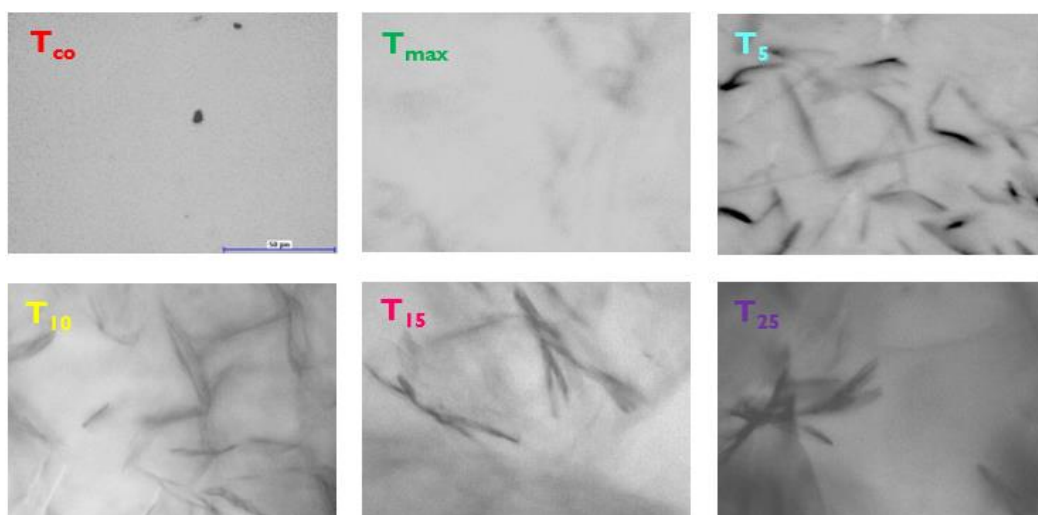
Figure 3.32 Microphotographs of sample EM during SRTRT (at 1s^{-1}) at different temperatures (control bar corresponds to 50μm).
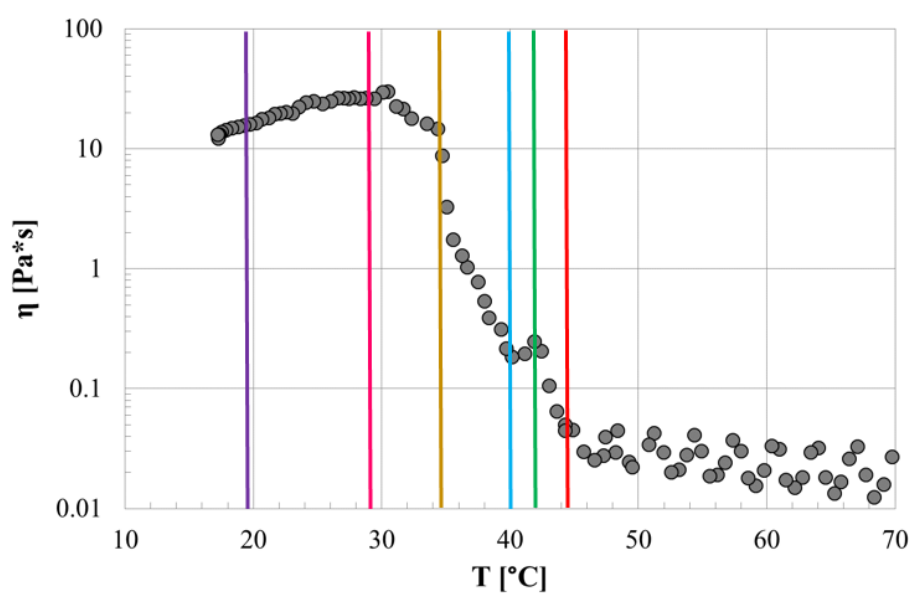

Figure 3.33 SRTRT at 1s^{-1} for sample GM. Coloured lines correspond to the different micro-photographs shown in Figure 3.34.
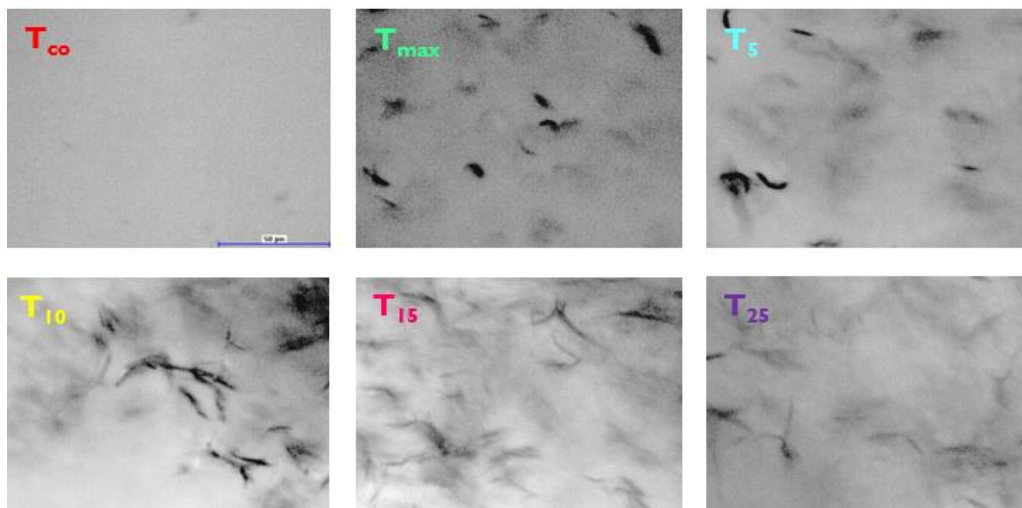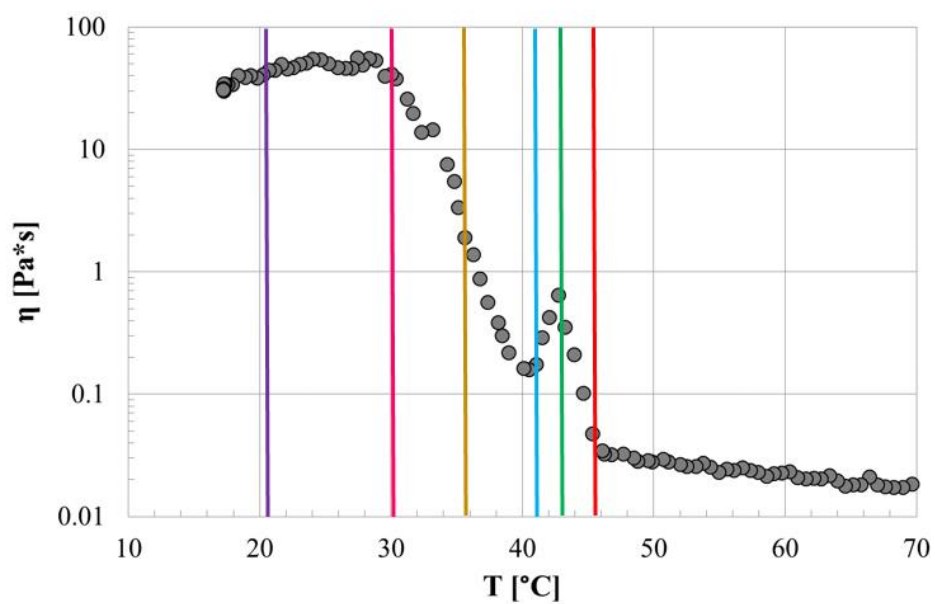
Figure 3.34 Micro-photographs of sample GM during SRTRT (at 1s⁻¹) at different temperatures (control bar corresponds to 50μm).

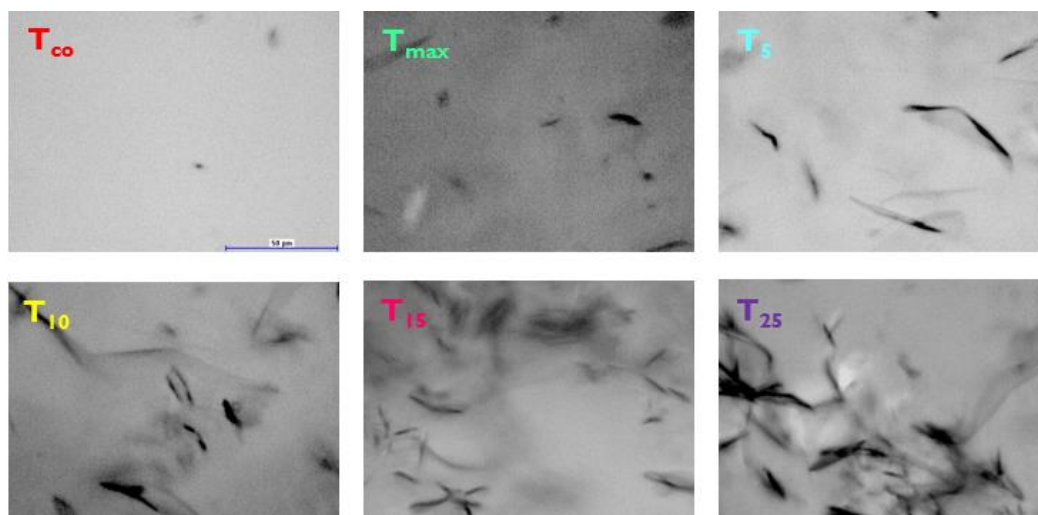**Figure 3.35 SRTRT at 1s⁻¹ for sample OM9. Coloured lines correspond to the different micro-photographs shown in Figure 3.36.**

Figure 3.36 Micro-photographs of sample OM9 during SRTRT (at 1s^{-1}) at different temperatures (control bar corresponds to 50μm).

As already observed during oscillatory tests, small and random crystals are formed at $T=T_{co}$. At a slightly lower temperature, a maximum trend in the viscosity curve can be found, being the peak of the maximum at temperature corresponding to $T=T_{max}$.

At $T=T_{max}$ the images show the initial formation of needle-like crystals and probably a partial breakage of the structures during formation due to the applied shear rate. At even lower temperature ($T_5 \leq T \leq T_{10}$), needle-like crystals seem to grow in length and begin to interact among each other, resulting in the formation of an interconnected crystalline structure. At temperature levels far enough from the onset of crystallisation (i.e. T_{15}, T_{25}), the effect of the applied shear rate is more evident. It is well-known from the literature that the application of shear modifies the habits of MAG crystals [13]. In particular, the application of shear hinders the formation of well-organized platelet structures, instead of promoting the random clustering of crystals domains into spherical assemblies [13]. The images recorded at $T=T_{25}$ show the formation of random flocs composed of needle-like crystals, especially for the OM9 and EM systems. It is worth noticing that the OM9 sample exhibits the lowest rate of network development, as already observed from oscillatory tests. At $T=T_{10}$, the presence of a well-interconnected network structure for both GM and EM systems is evidenced, whereas sample OM9 exhibits random crystalline aggregates at the same temperature. Nevertheless, at the lowest temperature level ($T=T_{25}$) OM9 shows the largest and best-defined crystal flocs, suggesting that the microstructure of MAG organogels produced with virgin olive oil is highly affected by the shear rate applied.

In addition to optical and rheological characterisation, thermal and spectroscopic analysis were carried out. Figure 3.33 shows the obtained DSC thermograms. The cooling thermogram of EM, GM and OM9 samples shows the same trend with two peaks mentioned previously for OM samples, indicating the isotropic/lamellar phases transition at high temperature and the polymorphic transition into sub-α crystals upon cooling. Conversely, differences in the slope of the three melting thermograms at high temperature can be appreciated, suggesting the presence of different structures.
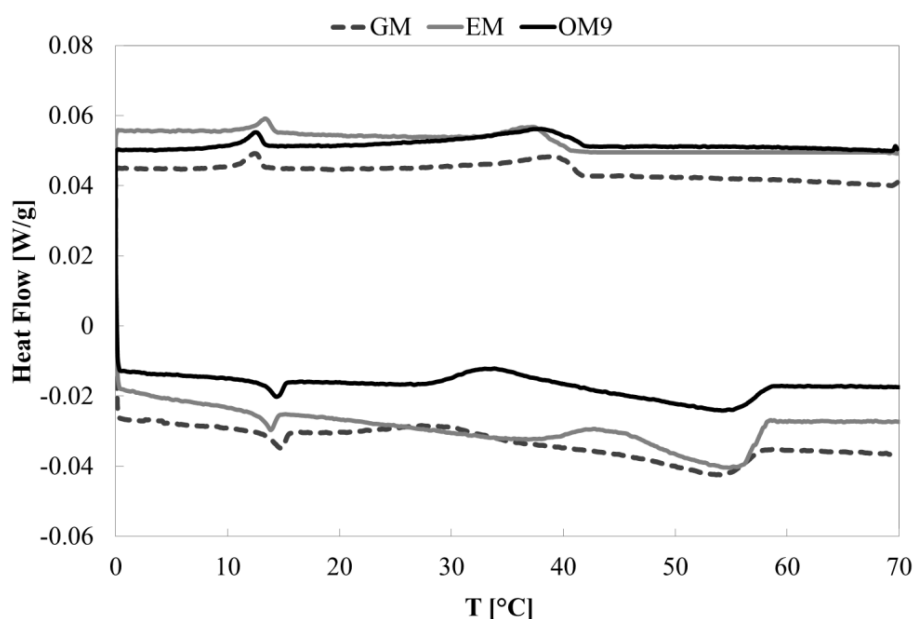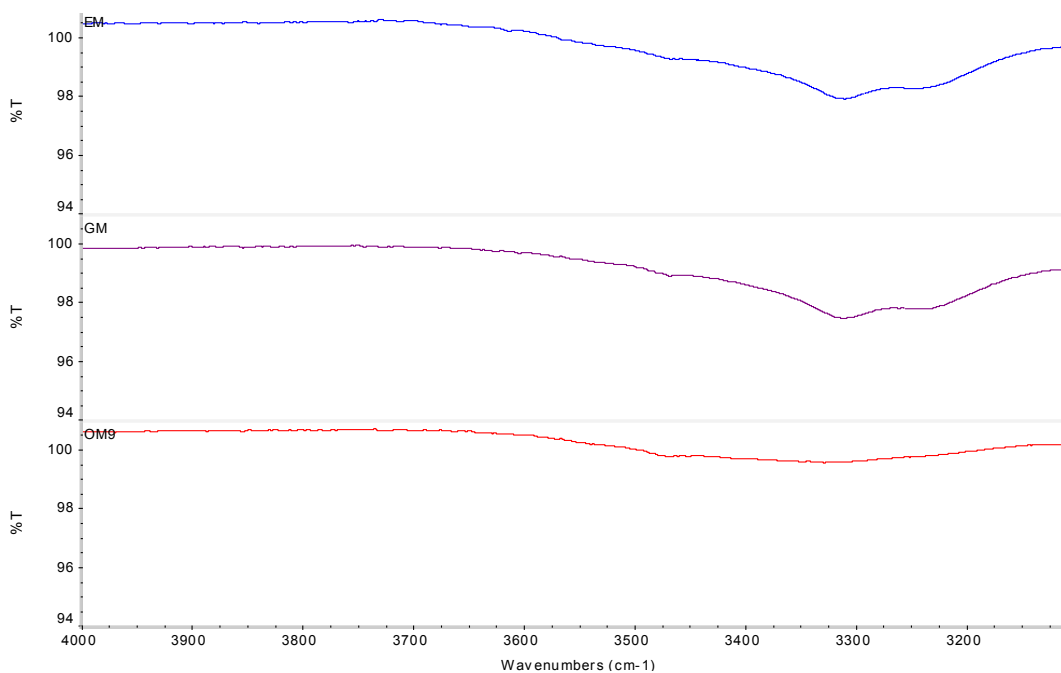

Figure 3.33 DSC thermograms for GM, EM and OM9 samples.

FT-IR spectra were recorded at room temperature immediately after the gel formation. The investigation was focused on the low-energy region corresponding to the OH-stretching modes (from 3000 to 4000cm^{-1}). The results are shown in Figure 3.34.
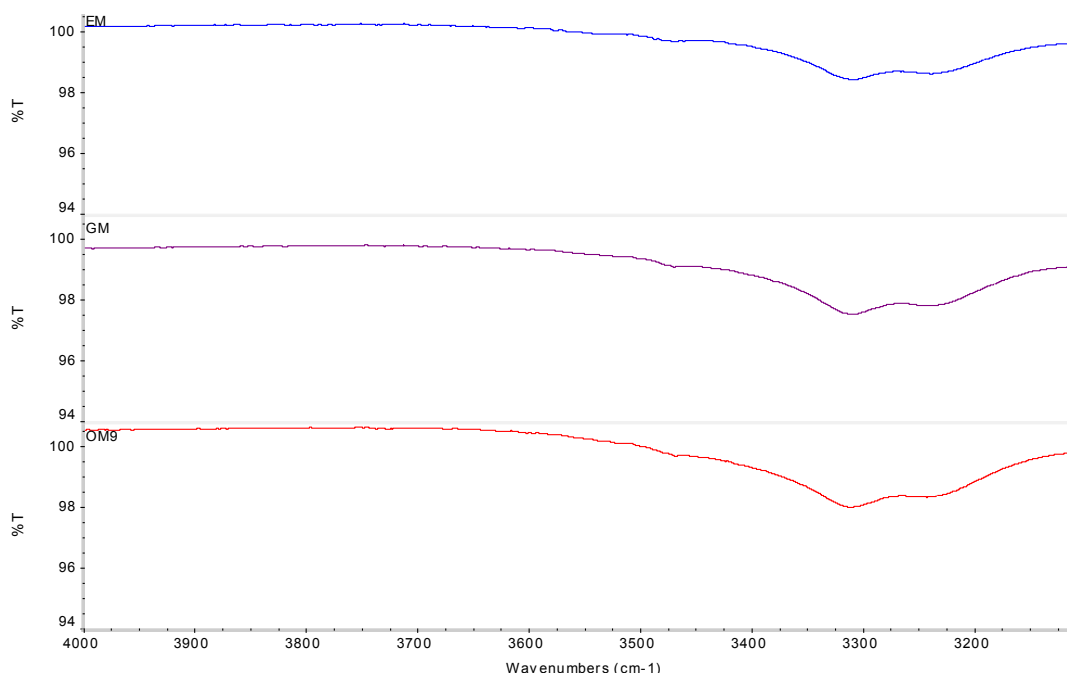
Figure 3.34 FT-IR spectra in the low-energy region for EM (blue line), GM (purple line) and OM9 (red line) samples.

The OM9 spectrum exhibits a single broad peak, while a "twin" absorption peak can be detected in both EM and GM spectra, corresponding to the above-mentioned 2-OH and 3-OH hydrogen bonding. The coexistence of 3-OH and 2-OH hydrogen bonding indicates the presence of two different structures, presumably lamellar structures and β crystals. López-Martínez et al. [17] observed the presence of β crystals in oleogels prepared with commercial MAGs as the organogelator and sufflower oil as the solvent. They suggested that the β polymorph could crystallize directly from the inverse lamellar phase upon cooling or it could be the result of a polymorphic transition from the sub-α phase [17]. Since FT-IR spectra were recorded at a temperature higher than the onset of sub-α polymorph crystallisation (i.e. at room temperature), it seems reasonable to propose that β crystals formed directly from inverse lamellar structures. It is worth noticing that the presence of stable 2-OH hydrogen bonding in organogels produced with virgin olive oil was observed only at Myverol fractions higher than 0.034, as reported in the previous sections.

Therefore, it can be speculated that the kind of vegetable oil strongly affects the state of hydrogen bonding in Myverol organogels. In addition to the results obtained from the optical analysis, the more elastic network structure observed for GM and EM samples could be explained by the formation of secondary structural elements [5, 15]. Indeed, the

presence of mixed crystals have implications in the three-dimensional microstructure of the organogel and, therefore, in its rheological properties [17]. Hence, the presence of the stable 2-OH hydrogen bonding led to an increased capability of network development, evidenced by higher gelation point and *SDr* values for EM and GM samples.

After one week of storage at room temperature, the coexistence of 3-OH and 2-OH hydrogen bonding was observed also in the OM9 organogel, produced with virgin olive oil (see Figure 3.35). It is worth noticing that Chen and Terentjev [1] demonstrated that 2-OH hydrogen bonding became predominant in MAG/hazelnut oil organogels after five days of storage, resulting in destabilisation phenomena of the gel (i.e. the breakage of lamellar network and the sedimentation of aggregates). Results obtained in the present work (see Figure 3.35) evidence the presence of both 2-OH and 3-OH hydrogen bonding still after one week of storage, denoting a higher stability of the systems investigated regarding sedimentation phenomena.

Figure 3.35 FT-IR spectra in the low-energy region for EM (blue line), GM (violet line) and OM9 (red line) samples, after one week of storage at room temperature.

3.3.7 Effect of the addition of saturated fats

Temperature ramp tests on OBM samples were performed, with the aim of understanding better the role of cocoa butter (a vegetal source of natural saturated compounds) in crystallisation and gelation phenomena of Myverol organogels and its

effect on the final rheological properties. As an example, Figure 3.36 shows results obtained for the OBM1 system. All MAG/cocoa butter/olive oil organogels studied exhibited the same rheological behaviour already described for MAG/olive oil systems, with a pure viscous behaviour at high temperature ($T>T_{co}$), a sharp increase of the complex modulus at $T=T_{co}$ and a solid-like behaviour at low temperature ($T<T_g$).
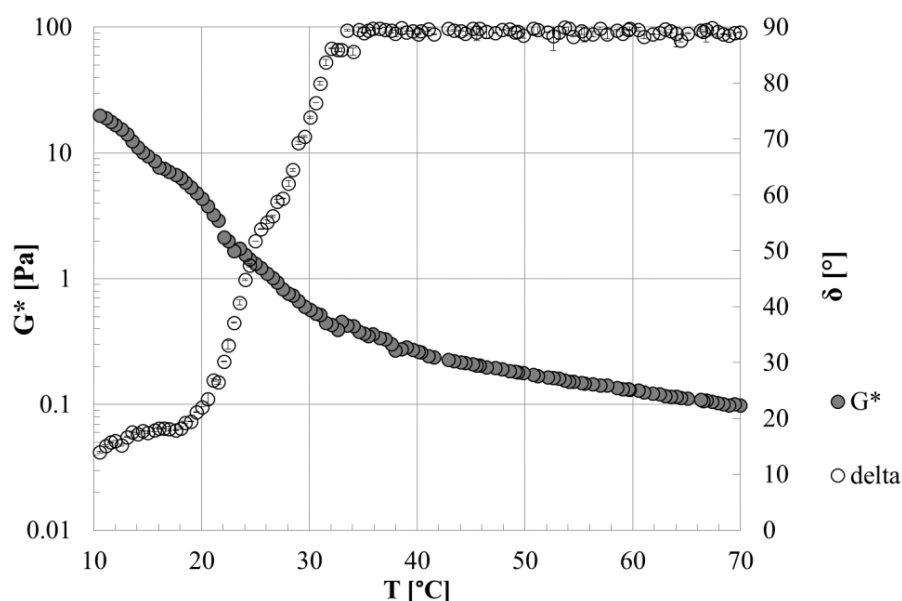

Figure 3.36 Time cure test for sample OBM1.

The calculated values of T_g and T_{co} from rheological, thermal and spectroscopic analysis are listed in Table 3.6. It can also be observed that no significant differences are evident for systems containing cocoa butter between T_{co} and T_g values for Myverol fractions higher than the critical value of 0.034. Moreover, comparing these results with those reported in Table 3.2, above the critical threshold of X_M=0.034, the two critical temperatures are affected only by the organogelator content, independently of the composition of the oil phase.

Sample ID	T_{co} [°C]	T_g [°C]	$T_{co,DSC}$ [°C]	$T_{co,NMR}$ [°C]
OBM1	35.71±0.93	22.48±0.78	36.52±0.22	35.11±0.22
OBM2	53.60±0.18	52.92±0.12		53.40±0.25
OBM3	59.54±0.11	58.04±0.08		59.77±0.24
OBM4	60.85±0.05	59.68±0.01	58.67±0.36	60.51±0.25
OBM5	60.07±0.12	59.80±0.02		60.23±0.46
OBM6	44.09±0.17	42.96±0.93	44.01±0.22	43.79±0.18
OBM7	43.31±0.30	42.65±0.87	43.33±0.15	43.28±0.22
OBM8	42.94±0.05	42.55±0.24	43.31±0.18	42.79±0.18
OBM9	61.05±0.25	59.07±0.31		60.84±0.24
OMB10	39.76±0.23	31.22±0.72		40.07±0.19

Table 3.6 Gelation temperature (T_g) and onset of crystallisation temperature for OBM samples, calculated from rheological SAOTs (T_{co}), DSC analysis ($T_{co,DSC}$) and NMR ($T_{co,NMR}$).

This is in agreement with results obtained by Lupi et al. [20], who studied the rheological behaviour of similar systems subjected to a faster cooling rate.

The influence of the organogelator concentration on the structural features of systems containing a fixed cocoa butter/olive oil ratio (B/O=0.04) was also investigated. Experimental results from DSC analysis (Figure 3.37) evidenced the same behaviour upon cooling, while at high Myverol concentration (sample OBM4) the high-temperature peak of the melting thermogram is split into two smaller peaks, owing to the presence of two structures, as observed for OM systems.
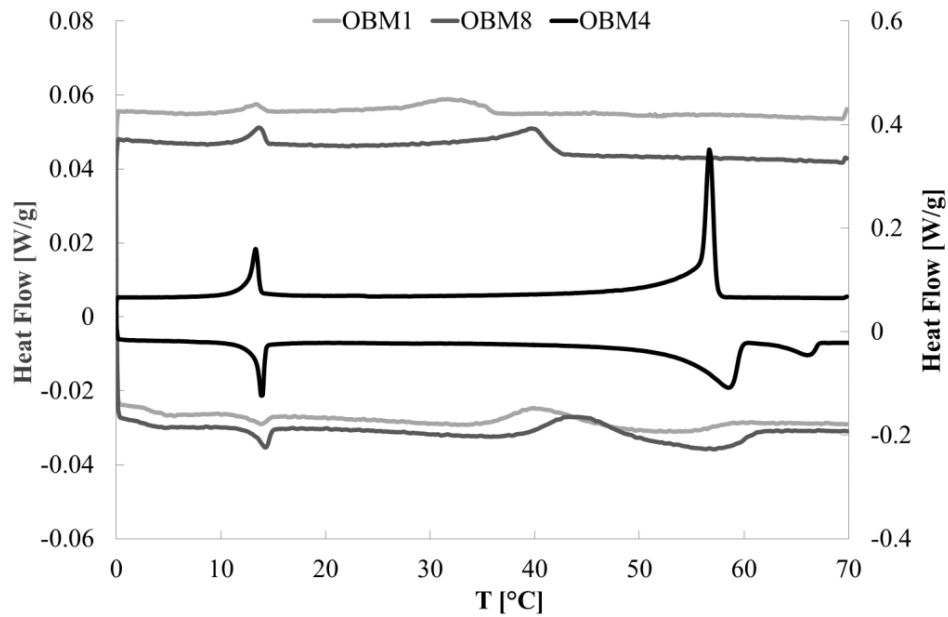
Figure 3.37 DSC thermograms of OBM1, OBM8 and OBM4 samples.

The SFC was measured at different temperature levels upon cooling for all OBM systems. The trend of the SFC as a function of temperature was found to be qualitatively similar to that described for OM samples. The plateau value of the SFC curve was slightly higher than the theoretical value for all samples (see Table 3.7) due to the crystallisation of cocoa butter, except for the OBM6 system, produced with the lower cocoa butter/olive oil ratio (B/O=0.02).

The fractal model was used to relate the storage modulus *G'* of OBM samples at the fixed B/O=0.04 to the microstructure of the system (Eq. 3.3.2). The volume fraction of solids *Φ* was calculated according to Equation 3.3.3 and parameters *λ* and *D* were estimated at two different temperatures, T_{10} and T_{15} (with $\lambda(T_{10})$=12.06·10^4±5.90·10^3Pa, $D(T_{10})$=2.76±0.02, $\lambda(T_{15})$=13.46·10^4±6.60·10^3Pa and $D(T_{15})$=2.76±0.01).

It is worth noticing that *D* remains constant upon cooling as already observed for OM systems.

Sample	B/O [-]	SFC_{th} [%]	SFC (T_{25}) [%]
OBM1	0.04	1.93	1.99±0.01
OBM2	0.04	9.67	9.80±0.01
OBM3	0.04	19.33	19.44±0.03
OBM4	0.04	29.00	29.11±0.03
OBM5	0.04	38.67	38.71±0.01
OBM6	0.02	3.29	3.17±0.01
OBM7	0.13	3.29	4.30±0.04
OBM8	0.04	3.29	3.75±0.01
OBM9	0.04	48.33	48.46±0.05
OBM10	0.04	2.42	2.59±0.01

Table 3.7 Theoretical (SFC_{th}) and measured SFC at T_{25} for OBM samples.

At both temperature levels, λ values are higher than the values estimated for OM samples, indicating an increased strength of the links between crystal flocs because of the addition of cocoa butter. Figures 3.38 and 3.39 shows the fitting of data with the original fractal model (Eq. 3.3.3) and the modified fractal model (Eq. 3.3.4 with D=2.76).
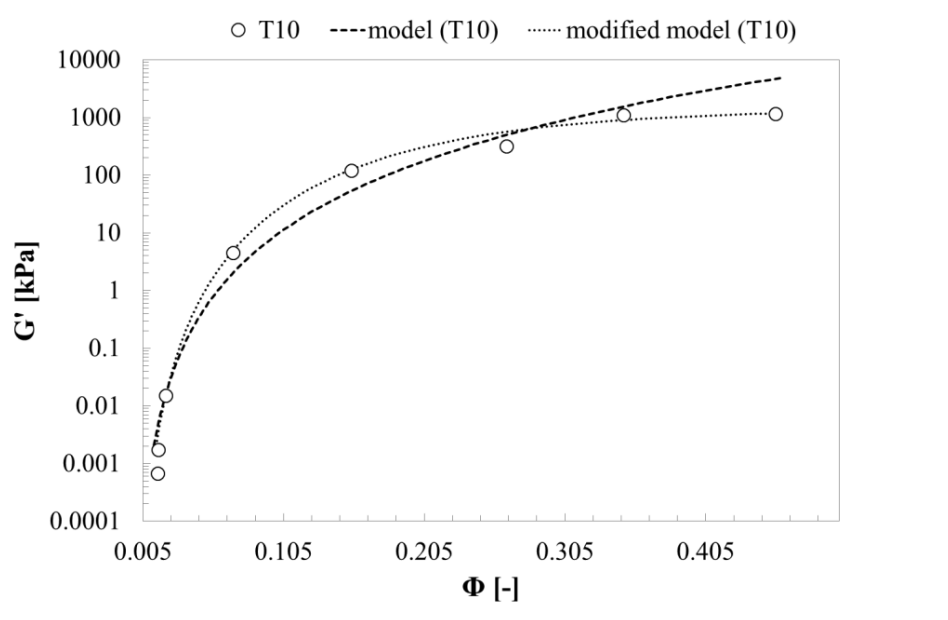

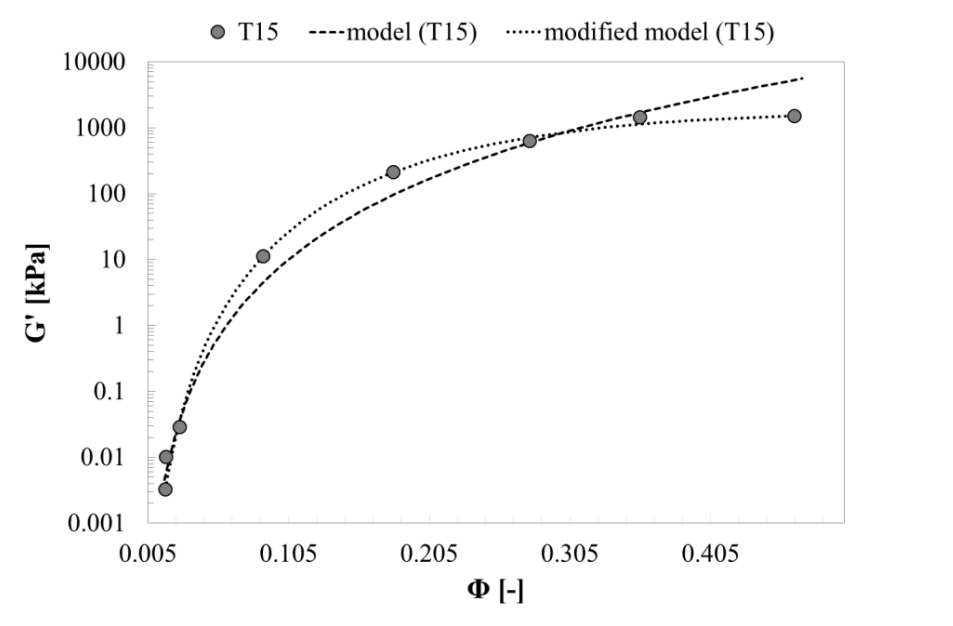**Figure 3.38 Fractal model and modified fractal model at T_{10} for OBM samples with B/O=0.04.**

Figure 3.39 Fractal model and modified fractal model at T$_{15}$ for OBM samples with B/O=0.04.

The average *SFCr* and *SDr* of OBM samples (B/O=0.04) were calculated and related to the organogelator fraction according to Equation 3.3.7 and 3.3.8 (see Figure 3.40 and 3.41), respectively. Parameter *a'* of Eq.3.3.7 for OBM samples was found to be higher than the value estimated for OM samples (*a'$_{OBM}$*=0.086±0.001s^{-1}, *a'$_{OM}$*=0.078±0.001 s^{-1}), indicating an increased rate of SFC increase due to the higher content of saturated fats. However, the estimated value of *λ'* for OBM systems is lower than the value found for OM samples (*λ'$_{OBM}$*=79778±1774Pa/s, *λ'$_{OM}$*=85391±3088Pa/s). Probably the complexity of the oil phase composition (containing cocoa butter, Myverol and olive oil) led to a reduction in the network formation rate. In addition, *SDr* data were fitted using the following empirical equation, derived from the modified fractal model:

$$SDr = \lambda'' \left(1 - e^{-B''X_M^{C''}}\right)^{1/(3-D)} \tag{3.3.9}$$

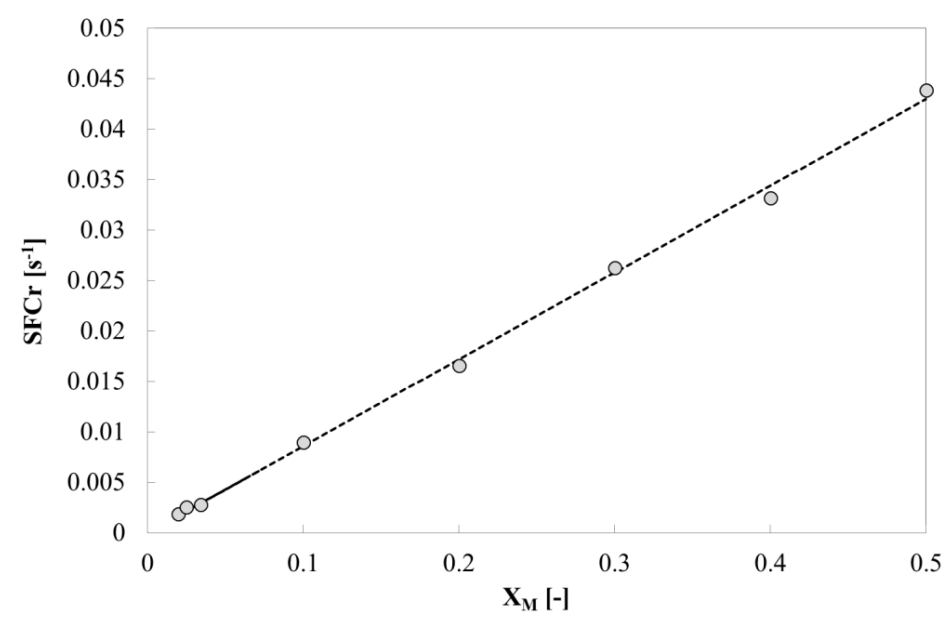which seems to data fit better at high Myverol fractions (see Figure 3.41).

Figure 3.40 Rate of SFC increase (*SFCr*) as a function of Myverol fraction and data fitting with Eq.3.3.7 for OBM samples with B/O=0.04.
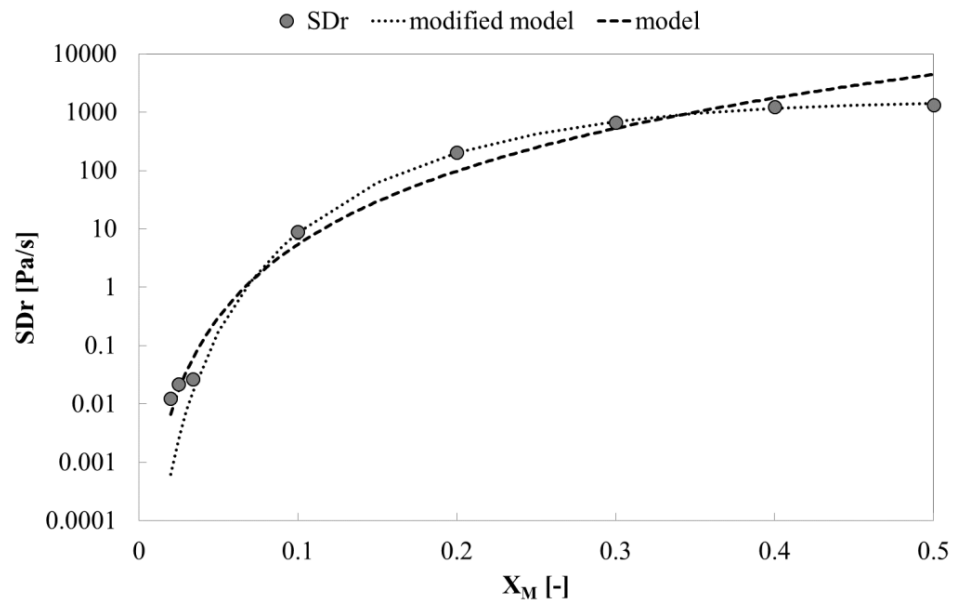

Figure 3.41 Structure development rate (*SDr*) as a function of Myverol fraction and data fitting with Eq.3.3.8 (model) and Eq.3.3.9 (modified model) for OBM samples with B/O=0.04.

The trend observed for T_{co} is very similar to that described for the OM samples, therefore Equation 3.3.5 and 3.3.6 were employed to fit experimental data. Both empirical models fit the experimental trend very well.
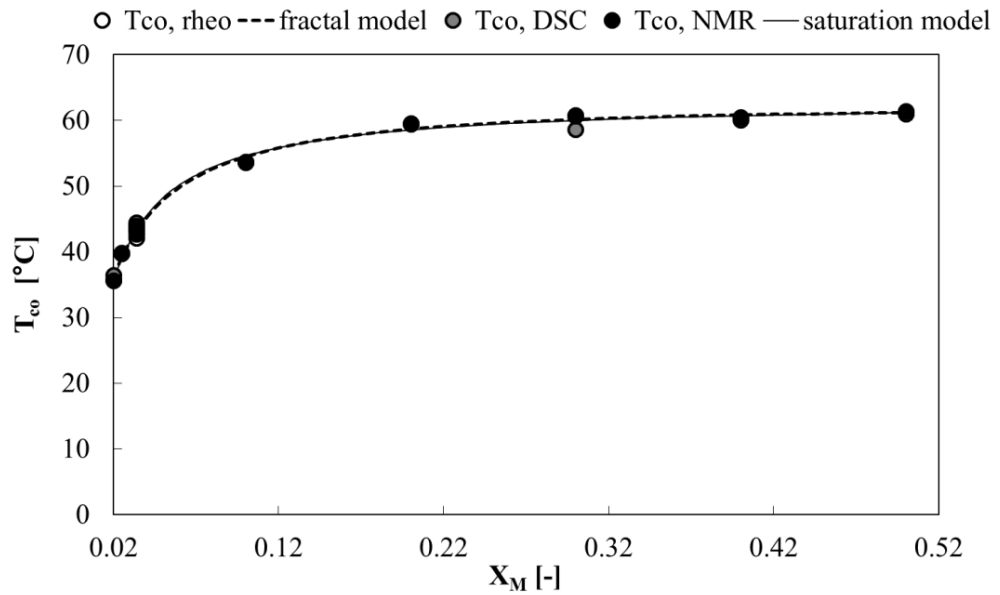
Figure 3.42 T_{co} as a function of Myverol fraction and data fitting with both modified fractal model (Eq. 3.3.6) and saturation model (Eq. 3.3.5) for OBM samples.

The effect of the cocoa butter/olive oil ratio on the rheological properties (G^* and δ) at different temperature levels was investigated for samples prepared with a constant Myverol fraction of 0.034 (see Figure 3.43 and 3.44).
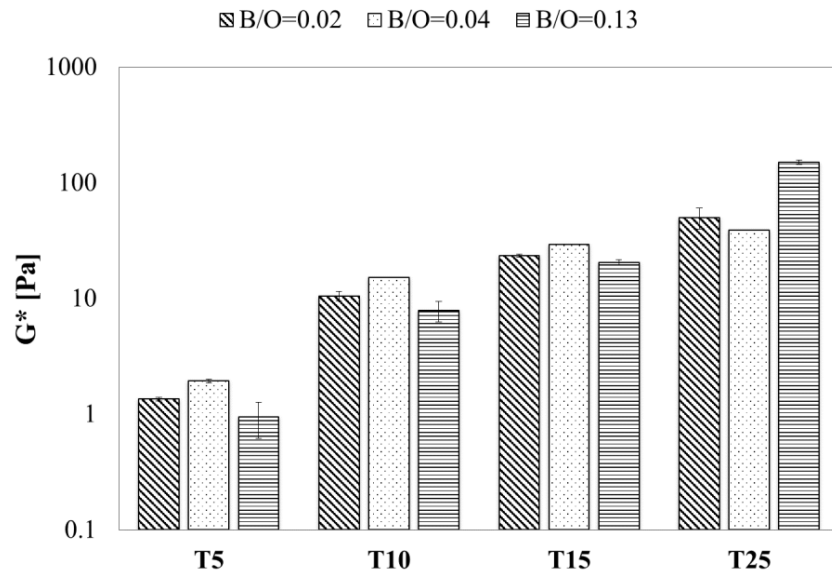

Figure 3.43 Complex modulus G^* at different temperature levels as a function of the B/O ratio.
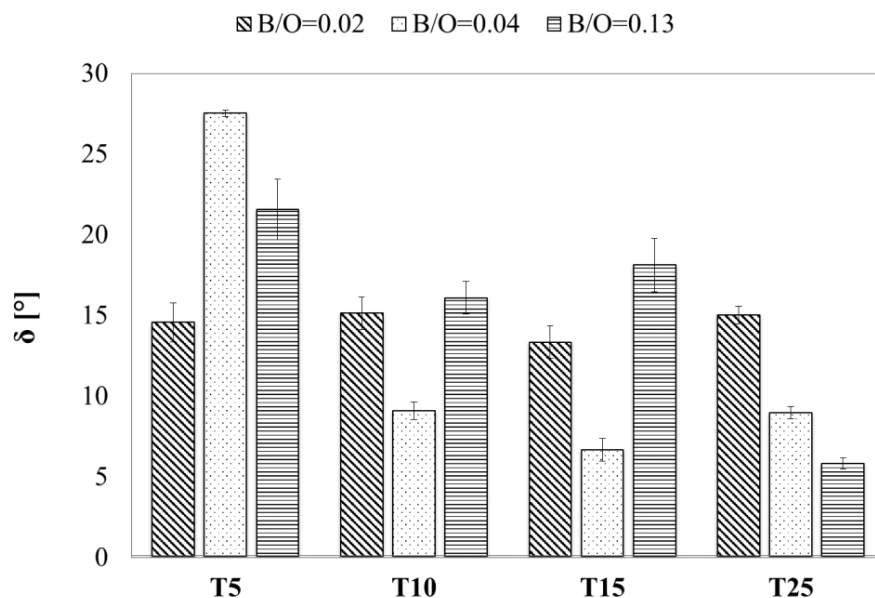
Figure 3.44 Phase angle δ at different temperature levels as a function of the B/O ratio.

The system containing the highest B/O ratio (B/O=0.13) shows lower values of the complex modulus and higher values of the phase angle at low temperature levels, but, when a temperature far enough from the onset of crystallisation is reached, a more consistent and structured network is formed. As already observed for the results concerning the *SDr*, the addition of cocoa butter seems to slow down the structuring processes. Nevertheless, when more time is available, a more structured material is obtained with increasing B/O ratio. The presence of a sort of "annealing" time due to high B/O ratio was already observed by Lupi et al. [20].

Results obtained from DSC analysis (Figure 3.45) evidence the same crystallisation behaviour for all samples produced with different B/O ratios, even though a small peak can be detected at around 3°C in the OBM7 (B/O=0.13) cooling thermogram, probably owing to the formation of cocoa butter polymorphs. The presence of this polymorph resulted in a different initial melting behaviour of the OBM7 system. After one week of storage at 25°C, only a single peak can be detected in the melting thermogram of the three samples, as observed for OM samples. At the highest B/O ratio (B/O=0.13), the melting thermogram exhibits a broader peak, shifted to higher temperature values, indicating the presence of more stable polymorphs and/or a higher mass of solids.

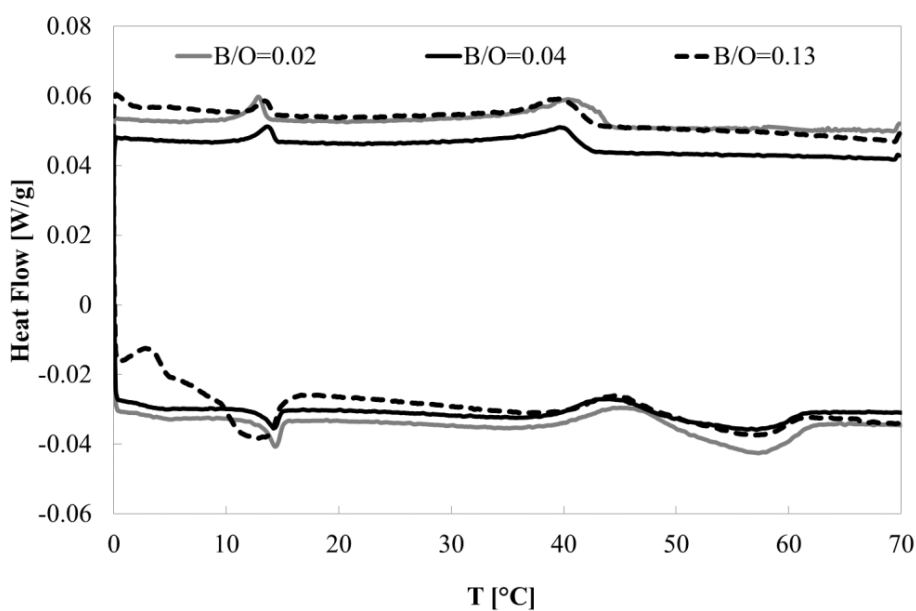**Figure 3.45 DSC thermograms at different B/O ratio with a constant Myverol fraction of 0.034.**
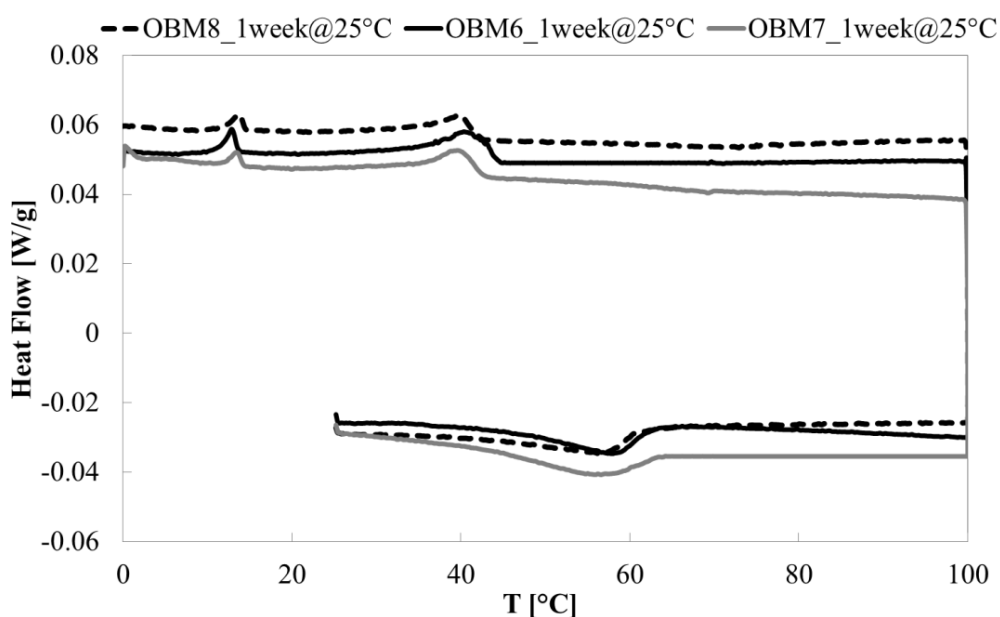

Figure 3.46 DSC thermograms at different B/O ratio with a constant Myverol fraction of 0.034, after one week of storage at 25°C.

Conclusions

Organogels based on virgin olive oil and a commercial mixture of MAGs were prepared and studied by using a rheological, thermal and spectroscopic analysis, in order to

determine the mechanical properties, the transition temperature and the microstructure of the systems.

Both Temperature ramp tests and SRTRTs at a constant cooling rate of 1°C/min evidenced the capability of Myverol to structure olive oil at mass fractions as low as 0.001. The onset of crystallisation temperature (T_{co}) and the gelation temperature (T_g) did not significantly differ for a Myverol critical mass fraction of 0.034, indicating that, at an organogelator fraction high enough, the processes of crystal nucleation and growth and the formation of long scale interconnection occur at the same time. T_{co} was found to be independent of the applied kinematic conditions when a Myverol concentration of 0.005 was exceeded.

The DSC cooling thermograms showed two exotherms: the high-temperature peak indicates the beginning of crystallisation phenomena and the formation of inverse lamellar structures, while the low-temperature peak (displayed for all samples at around 15°C) corresponds to a polymorphic transition into sub-α crystals. Both the melting DSC thermograms and the FT-IR spectra in the low energy region evidenced the formation of two different structures (presumably inverse lamellar structure and β crystals) at high Myverol concentrations. The presence of intermolecular hydrogen bonds was found to be crucial for MAG organogel formation. The interactions involved in organogel formation will be further discussed in Chapter 4, dealing with olive oil based organogels produced with a different organogelator.

The SFC of the samples investigated was measured at different temperatures upon cooling showing the same behaviour observed for the complex modulus during Temperature ramp tests. At temperature levels far enough from the T_{co} (T_{10}, T_{15} and T_{25}), SFC was found to be proportional to the mass fraction of the organogelator. The volume fraction of solids at a constant distance from the onset of crystallisation was calculated and related to the storage modulus *G'* according to a fractal model. It was found that the strength of the interactions among the flocs constituting the network increased increasing the distance from the crystallisation onset, whereas the fractal dimension of the network remained constant upon cooling.

No significant difference was observed between the values of the temperature of crystallisation onset estimated using different techniques (rheology, DSC and NMR). A saturation model and also an empirical equation based on the modified fractal model were proposed to relate this thermo-rheological parameter to the organogelator fraction. Both the average rate of SFC increase (*SFCr)* and the average structure development rate (*SDr)*

were calculated. It was observed that the *SFCr* was directly proportional to the Myverol fraction, whereas, owing to the fractal structure of the considered systems, an empirical equation based on the fractal model was proposed to fit the *SDr* values as a function of the organogelator concentration.

After one week of storage at 4°C, Myverol/olive oil organogels showed a significant increase in the SFC owing to olive oil crystallisation, whereas samples stored at 25°C exhibited a slight instability. The DSC melting thermogram of samples stored at the two different temperatures of 4 and 25°C showed a single broad peak, suggesting that the polymorphic transition into β crystals occurred during ageing.

The organogels produced with different vegetable oils (virgin, extra-virgin and sunflower oil) at a constant Myverol fraction of 0.03 showed the same temperature of crystallisation onset, whereas some differences in the gelation point and in the structure development rate were detected. The system containing sunflower oil exhibited the highest capability of network development (in terms of structure development rate) and also the highest consistency. Micro-photographs recorded during Temperature ramp tests evidenced that the Myverol/sunflower oil network was composed of a larger number of small needle-like crystals, whereas samples prepared with virgin and extra-virgin olive oil were characterised by the presence of long fibre-like aggregates. Moreover, the Myverol/virgin olive oil system was found to be highly sensitive to the shear rate applied, showing the formation of large spherical flocs at low temperature. FT-IR spectra evidenced the coexistence of 2-OH and 3-OH hydrogen bonding in samples produced with extra-virgin olive oil and sunflower oil, whereas the presence of more stable structures (suggested by the 2-OH peak) was observed in the sample containing only virgin olive oil after one week of storage at room temperature.

Finally, the effect of cocoa butter addition, a vegetal and natural source of saturated fats rich in stearic acid, was investigated. Systems produced with the addition of cocoa butter showed the same rheological behaviour as MAG/olive oil samples and the T_{co} was found to be independent of the composition of the oil phase when a Myverol fraction of 0.034 was exceeded. At a constant cocoa butter/olive oil ratio of 0.04, storage modulus data were well fitted by a fractal model. Empirical equations similar to those adopted for bi-component systems were proposed to fit T_{co}, *SFCr* and *SDr* data as a function of the organogelator concentration. When the cocoa butter/olive oil ratio was varied, an initial slowdown of the structure development was observed at high B/O ratio, followed by an increase in consistency and structuring at temperature levels far enough from the crystallisation onset.

All the results obtained, such as T_{co} and T_g, as well as the relationship between rheological and microstructural properties or the effect of the solvent and saturated fat content within the organogel, can be helpful in designing new products and/or structured emulsions with controlled properties.

References

[1] Chen, C.H., and E.M., Terentjev, *Aging and Metastability of Monoglycerides in Hydrophobic Solutions*, Langmuir, 2009. 25: p. 6717-6724.

[2] Dassanayake, L.S.K., Kodali, D.R., and S., Ueno, *Formation of oleogels based on edible lipid materials*, Current Opinion in Colloid & Interface Science 16 (2011) 432–439

[3] Phan, V.A., Liao, Y.C., Antille, N., Sagalowicz, L., Robert, F., and N., Godinot, *Delayed volatile compound release properties of self-assembly structures in emulsions*, Journal of Agricultural and Food Chemistry, 2008. 56: p. 1072–1077.

[4] Calligaris, S., Da Pieve, S., Arrighetti, G., and L., Barba, *Effect of the structure of monoglyceride–oil–water gels on aroma partition*, Food Research International, 2010. 43: p. 671–677.

[5] Co, E.D., and A.G., Marangoni, *Organogels: An Alternative Edible Oil-Structuring Method*, Journal of the American Chemical Society, 2012. 89: p. 749-780.

[6] Krog, N., and K., Larsson, *Phase behaviour and rheological properties of aqueous systems of industrial distilled monoglycerides*, Chemistry and Physics of Lipids, 1968. 2: p. 129–143.

[7] Larsson, K., and N., Krog, *Structural properties of lipid–water gel phase*, Chemistry and Physics of Lipids, 1973. 10: p. 177–180.

[8] Sagalowicz, L., Leser, M.E.,Watzke, H.J., and M., Michel, *Monoglyceride self-assembly structures as delivery vehicles*, Trends in Food Science & Technology, 2006. 17: p. 204–214.

[9] Chen, C.H., Van Damme, I., Terentjev, *Phase behavior of C18 monoglyceride in hydrophobic solutions*, Soft Matter, 2009. 5: p. 432–439.

[10] Brokaw, G.Y., and W.C., Lyman, *The behaviour of distilled monoglycerides in the presence of water*, Journal of the American Oil Chemists' Society, 1958. 35: p. 49–52.

[11] Marangoni, A.G., Idziak, S.H.J., Vega, C., Batte, H., Ollivon, M., Jantzi, P.S., and W.E., Rush, *Encapsulation-structuring of edible oil attenuates acute elevation of blood lipids and insulin in humans*, Soft Matter, 2007. 3: p. 183–187.

[12] Batte, H.D., Wright, A.J., Rush, J.W., Idziak, S.H.J., and A.G., Marangoni, *Effect of processing conditions on the structure of monostearin–oil–water gels*, Food research international, 2007. 40: p. 982–988.

[13] Da Pieve, S., Calligaris, S., Co, E., Nicoli, M.C., and A.G., Marangoni, *Shear nanostructuring of monoglyceride organogels*, Food Biophysics, 2010. 5: p. 211–217.

[14] Kesselman, E., and E., Shimoni, *Imaging of oil/monoglyceride networks by polarizing near-field scanning optical microscopy*, Food Biophysics, 2007. 2: p. 117–123.

[15] Ojijo, N.K.O., Neeman, I., Eger, S., and E., Shimoni, *Effects of monoglyceride content, cooling rate and shear on the rheological properties of olive oil/monoglyceride gel networks*, Journal of the Science of Food and Agriculture, 2004. 84: p. 1585–1593.

[16] Chen, C.H., and E.M., Terentjev, "Monoglycerides in oils", in: *Edible oleogels: structure and health implications*, Marangoni, A.G., and N., Garti, Eds., AOCS Press, Urbana, 2011.

[17] López-Martínez, A., Morales-Rueda, J.A., Dibildox-Alvarado, E., Charó-Alonso, M.A., Marangoni, A.G., and J.F., Toro-Vazquez, *Comparing the crystallization and rheological behavior of organogels developed by pure and commercial monoglycerides in vegetable oil*, Food Research International, 2014. 64: p. 946–957.

[18] Salas, J.J., Bootello, M.A., Martínez-Force, E., and R., Garcés, *Production of stearate-rich butters by solvent fractionation of high stearic–high oleic sunflower oil*, Food Chemistry, 2011. 124: p. 450–458.

[19] Garti, N., Binyamin, H., and A., Aserin, *Stabilization of water-in-oil emulsions by submicrocrystalline α-form fat particles*, Journal of the American Oil Chemists' Society, 1998. 75: p. 1825–1831.

[20] Lupi, F.R., Gabriele, D., Facciolo, D., Baldino, N., Seta, L., de Cindio, B., *Effect of organogelator and fat source on rheological properties of olive oil-based organogels*, Food Research International, 2012. 46: p. 177–184.

[21] Lapasin, R., and S., Pricl, *Rheology of industrial polysaccharides: Theory and applications, 1st ed*., Blackie Academic and Professional, Glasgow, 1995.

[22] Tung, C.Y., and P.J., Dynes, *Relationship between viscoelastic properties and gelation in thermosetting systems*, Journal of Applied Polymer Science, 1982. 27: p. 569–574.

[23] Lopes da Silva, J.A., Gonçalves, M.P., and M. A., Rao, *Kinetics and thermal behaviour of the structure formation process in HMP/sucrose gelation*, International Journal of Biological Macromolecules, 1995. 17: p. 25-32.

[24] Toro-Vazquez, J.F., Morales-Rueda, J.A., Dibildox-Alvarado, E., Charó-Alonso, M., Alonzo-Macias, M., and M.M., González-Chávez, *Thermal and textural properties of organogels developed by candelilla wax in safflower oil*, Journal of the American Oil Chemists' Society, 2007. 84: p. 989–1000.

[25] Blake, A.I., Co, E.D., and A.G., Marangoni, *Structure and Physical Properties of Plant Wax Crystal Networks and Their Relationship to Oil Binding Capacity*, Journal of the American Oil Chemists' Society, 2014. 91: p. 885-903.

[26] Tang, D., and A.G., Marangoni, *Modeling the rheological properties and structure of colloidal fat crystal networks*, Trends in Food Science & Technology, 2007. 18: p. 474-483.

[27] Lopes, I.M.G. and M.G., Bernardo-Gil, *Characterisation of acorn oils extracted by hexane and by supercritical carbon dioxide*, European Journal of Lipid Science and Technology, 2005. 107: p. 12–19.

[28] Lupi, F.R., Gabriele, D., and B., de Cindio, *Effect of Shear Rate on Crystallisation Phenomena in Olive Oil-Based Organogels*, Food and Bioprocess Technology, 2012. 5: p. 2880-2888.

[29] Tarabukina, E., Jego, F., Haudin, J.-M., Navard, P., and E., Peuvrel-Disdier, *Effect of shear on the rheology and crystallization of palm oil*, Journal of Food Science, 2009. 74: p. 405–416.

Chapter 4: rheological and microstructural characterisation of policosanol organogels

Abstract

In this chapter, the ability of policosanol (a well-known food-grade nutraceutical mixture of fatty alcohols) to allow the gelation of different vegetable oils has been investigated. In particular, the rheological and microstructural characteristics of policosanol/virgin olive oil organogels were evaluated at different policosanol concentrations, using different techniques. The rheological properties of samples were investigated with Small Amplitude Oscillation Tests. In particular, the onset of crystallisation temperature (T_{co}) and the gelation temperature (T_g) were estimated by carrying out Dynamic temperature ramp tests (Time Cure), whereas the rheological characteristics of samples at room temperature were studied with Frequency sweep tests. It was found that crystallisation occurred for a policosanol mass fraction higher than 0.001, whereas the critical threshold mass fraction for gelation ranged between 0.003 and 0.005. The onset of crystallisation temperature of samples was also evaluated with thermal and spectroscopic techniques such as DSC and NMR, and an empirical equation was proposed to fit experimental data as a function of the policosanol fraction. DSC was also applied to investigate the microstructure of policosanol/olive oil organogels, together with FT-IR characterisation. NMR spectroscopy allowed SFC to be measured, and a fractal model was adopted in order to relate rheological properties to the microstructure of the material. The average rate of SFC increase and the average structure development rate were calculated and related to the organogelator fraction. The potential changes in rheological and structural characteristics of policosanol organogels were studied measuring SFC values, DSC thermograms and FT-IR spectra after one week of storage.

Furthermore, organogels containing different vegetable oils were prepared at a constant policosanol fraction (0.03) and studied through rheological, optical and thermal analysis.

The majority of the results dealing with the rheological analysis of policosanol/olive oil organogels has already been published in an international scientific journal (Lupi, F.R., Gabriele, D., Greco, V., Baldino, N., Seta, L., and B., de Cindio, *A rheological*

characterisation of an olive oil/fatty alcohols organogel, Food Research International, 2013. 51: p. 510–517).

Finally, the thermo-rheological properties of olive oil-based organogels produced with mixtures of organogelators (containing policosanol and glyceryl stearate) were investigated.

4.1 Introduction

Fatty alcohols have been recently studied as potential edible oil organogelators. Schaink et al. [1] investigated the gelling capabilities of a mixture of stearic acid and stearic alcohol in sunflower oil. The lowest organogelator concentration, at which the network formation was observed, was found to be around $3.5\%_{w/w}$, whereas the lowest threshold of the gelator mass fraction which was found to allow the crystallisation, was $1.5\%_{w/w}$. The authors demonstrated the presence of a distinct maximum in hardness and G' (in linear conditions) values for the mixture with a concentration ratio acid:alcohol 3:7. Microscopy revealed that the shape of the organogel crystals varied significantly with the composition of the structuring mixture. When only one of the structurants was present, crystals showed a plate-like morphology. In particular, crystals formed when stearyl alcohol was the only organogelator exhibited a foliated (mica-like) crystal habit (see Figure 3.1e). On the contrary, when both stearic alcohol and stearic acid were used as organogelators, crystals were found to be needle shaped (Figure 3.1d). The crystals of the best structuring ratio (3:7 acid:alcohol) on average showed the smallest size. This probably explains why these organogels had the largest G' and the highest hardness.
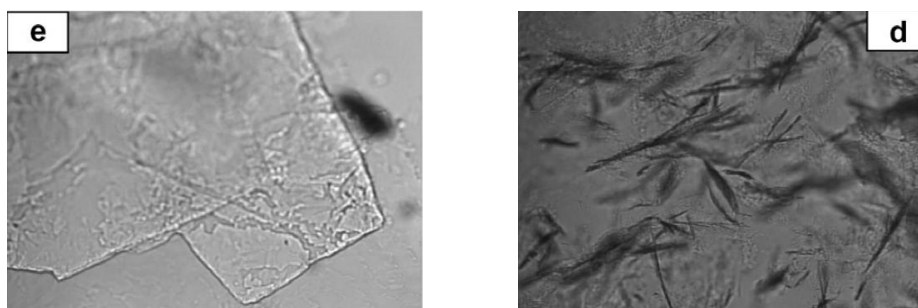
Figure 4.1 Microscopy images of organogels produced with $5\%_{w/w}$ of: d) a stearic acid:stearic alcohol mixture (3:7), e) stearic alcohol [1].

Gandolfo et al. [2] studied the oil-structuring potential of homologous series of fatty alcohols and fatty acids with chain lengths ranging from 16 to 22 carbons, showing that both n-alcohols and n-fatty acids had the potential to structure sunflower oil at concentrations as low as 2%w/w. Moreover, they observed that n-alcohols yielded more easily to the formation of harder products than fatty acids at the same concentration. Polarised light microphotographs of the organogel containing 5%w/w steric alcohol showed the presence of a large fractured agglomerate of platelet-like crystals of about 1800μm.
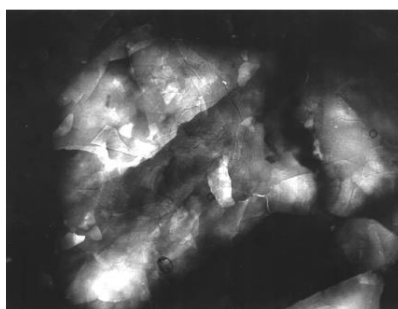
Figure 4.2 Microphotograph of 5%w/w stearic alcohol in sunflower oil after 1day at 5°C [2].

Gansolfo et al. [2] showed that the type of vegetable oil had no significant effect on the structure. When a mixture of both fatty acids and fatty alcohols was used as gelling agent the ratio between acid and alcohol proved to be a major influence on the structure hardness obtained. Also in this work, a synergetic effect for stearic alcohol:stearic acid=7:3 mixture was observed. The authors suggested that the predominant mechanism explaining the synergetic effect in the stearyl alcohol/stearic acid system in oil was the increase in nucleation rate due to the lowering of the interfacial energy.

Daniel and Rajasekharan [3] studied the ability of various fatty compounds such as long-chain fatty acids, fatty alcohols, wax esters and dicarboxylic acids (with carbon chain lengths of 10 to 31) to gel vegetable oils. Fatty alcohols were found to be capable of gelling plant oils although the minimum organogelator concentration required for gelation was higher than the value estimated for the equivalent fatty acids.

An indirect application of fatty alcohols for oil structuration is the addition of waxes extracted from vegetable sources [4, 5, 6]. Blake et al. [5] compared the microstructural, thermal and rheological properties and oil binding capacity of organogels produced with different plant-derived waxes. The small sizes of the microstructural particles observed in Candelilla wax (a mixture of high-melting alkanes, sterols, fatty alcohols, fatty acids and

waxy esters extracted from Yerba evergreen shrub, *Euphorbia cerifera*) organogels, as well as their higher fractal dimension, resulted in a higher oil-binding capacity and consistency compared to rice bran, sunflower and Carnauba waxes.

In the present work, some vegetable oils were structured with a plant-extracted mixture of primary fatty alcohols, commercially named "policosanol". This food-grade additive can be extracted from different vegetable sources, such as sugar cane wax, beeswax, rice bran and wheat germ [7]. Policosanol is a mixture of fatty primary alcohols with an aliphatic chain in the range of 20–36 carbons, mainly composed of docosanol (C22), tetracosanol (C24), hexacosanol (C26), octacosanol (C28), and triacontanol (C30) [8].

Previous studies demonstrated that policosanol exerts several positive effects on human health, most of all in the prevention and treatment of cardiovascular diseases without major adverse effects [9, 10, 11, 12]. In particular, Xu et al. [9] investigated the long-term effects of dietary octacosanol (the main component of policosanol) on plasma lipids, showing that dietary octacosanol significantly reduced the levels of plasma triacylglycerols by approximately 70% after 5 weeks. According to the literature, octacosanol should be able to decrease lipid levels [9], lowering the LDL (low density lipoprotein) in blood [10]. In addition, in the last few years, policosanol has been used as an ergogenic product to enhance athletic performance [9, 13].

Although many interesting works dealing with the potential nutraceutical properties of policosanol have been published, the potential capabilities of this natural extract to gel vegetable oils have never been investigated. In the present work, the investigation of rheological and microstructural characteristics of organogels produced with policosanol (mainly composed of octacosanol) as the organogelator and a virgin olive oil as the organic solvent was carried out. The main aim of the investigation was the characterisation of gels obtained with different amounts of policosanol, aiming at better understanding the role of this organogelator. The rheological characterisation was carried out by using both Small Amplitude Oscillation Tests (SAOTs) and Step Rate Temperature Ramp Tests (SRTRTs). Furthermore, the effect of the process temperature applied during the preparation of the samples on rheological characteristics was evaluated. The onset of crystallisation temperature (T_{co}) was evaluated for each organogel, whereas a gelation temperature (T_g), evidencing the formation of a three-dimensional network, was observed for samples having a gelator concentration larger than a critical threshold. In addition to rheology, other techniques (DSC, NMR) were used to estimate the onset of crystallisation temperature.

Moreover, the effect of the kind and botanical source of vegetable oil on the rheological and microstructural features of policosanol organogels was studied.

4.2 Materials and methods

4.2.1 Samples ingredients and preparation

Most of the samples investigated were prepared by using a commercial virgin olive oil (De Santis, Italy) as the solvent and policosanol from rice bran wax and mainly composed of octacosanol ($60\%_{w/w}$) (A.C.E.F., Italy), as the organogelator. The detailed composition of all raw materials was reported in Chapter 2. As described in Table 4.1, the policosanol mass fraction was ranged between 0.001 and 0.55 in order to investigate the role of this organogelator on crystallisation and gelation mechanisms. With the aim of analysing the influence of the kind and botanical source of the vegetable oil, EP and GP systems were produced with extra virgin olive oil (Gabro S.r.l., Italy) and sunflower oil (De Santis, Italy) respectively as the solvent, with a constant policosanol fraction of 0.03 (see Table 4.1).

Sample ID	Virgin Olive Oil [$\%_{w/w}$]	Sunflower Oil [$\%_{w/w}$]	Extra Virgin Olive Oil [$\%_{w/w}$]	Policosanol [$\%_{w/w}$]
OP1	99.9	-	-	0.1
OP2	99.7	-	-	0.3
OP3	99.5	-	-	0.5
OP4	99	-	-	1
OP5	98	-	-	2
OP6	95	-	-	5
OP7	85	-	-	15
OP8	70	-	-	30
OP9	45	-	-	55
OP10	97	-	-	3
OP11	96.4	-	-	3.4
OP12	97.5	-	-	2.5
EP	-	-	97	3
GP	-	97	-	3

Table 4.1 Samples ID and composition.

The oil, poured in a glass beaker, was preheated up to the desired temperature of preparation in a thermostatically-controlled water bath (plate heater VELP Scientifica, Italy) and then mixed (RW 20, IKA, Germany) with the proper amount of policosanol. All samples were stored at the preparation temperature until tests were performed and then cooled down with a controlled thermal ramp within the instruments during rheological and microstructural measurements.

With the aim of investigating the effect of the preparation temperature, samples containing a policosanol fraction of 0.01, 0.02 and 0.03 were prepared adding the proper amount of organogelator to the oil previously warmed up to the different temperatures of 70°C, 85°C and 97°C. All other samples were prepared at 85°C. Compositions and identifiers of tested samples are listed in Table 4.1.

After a complete characterisation of both MAG organogels (shown in Chapter 3) and policosanol organogels, the ability of mixtures of organogelators to allow the gelation of olive oil was studied. In addition to olive oil/policosanol (OP samples) and olive oil/glyceryl stearate organogels (OG samples), OGP samples were prepared using mixtures of policosanol and glyceryl stearate, following the same preparation procedure already described for policosanol organogels. As reported in Table 4.2, the total mass fraction of organogelators was varied, keeping the ratio between policosanol and glyceryl stearate mass fraction within the mixtures always at 1.

Sample ID	Virgin Olive Oil [%$_{w/w}$]	Glyceryl Stearate [%$_{w/w}$]	Policosanol [%$_{w/w}$]
OP13	96	-	4
OP14	93.2	-	6.8
OP15	92	-	8
OP16	87.5	-	12.5
OG1	96.6	3.4	-
OG2	96	4	-
OG3	93.2	6.8	-
OG4	92	8	-
OG5	87.5	12.5	-
OGP1	96.6	1.7	1.7
OGP2	96	2	2
OGP3	93.2	3.4	3.4
OGP4	84	8	8
OGP5	75	12.5	12.5

Table 4.2 Samples ID and composition.

4.2.2 Rheological characterisation

A controlled stress rheometer DSR-200 (Rheometric Scientific, U.S.A.), equipped with a parallel plates geometry (ϕ=40mm, gap 1±0.1 mm), was used to characterise all samples. The temperature of the lower plate was controlled (±0.1°C) by a Peltier effect system. In order to control the thermal history for all tests carefully, the warm organogel was poured on the lower plate of the rheometer previously heated up to the desired temperature of preparation.

For all samples a rheological characterisation based on Small Amplitude Oscillation Tests (SAOTs) was carried out. Preliminary Stress sweep tests were performed at different temperatures from the preparation value (70°C, 85°C or 97°C) down to 20°C, approximately every 10°C to investigate the potential changes in linear viscoelastic conditions as a function of temperature. In the range of temperatures where presumably a microstructural transition was expected, a higher number of Stress sweep tests was performed in order to describe better the change of the linear viscoelastic region during crystallisation and/or gelation. For each Stress sweep test, the sample was cooled down in

the rheometer cell from the preparation temperature to the desired value using a cooling rate of 1°C/min and applying the minimum stress within the instrument limits.

Then, Time cure tests were carried out at the constant frequency of 1Hz, cooling the sample from the preparation temperature down to 20°C with a cooling rate of 1°C/min. Lower final temperatures (0°C) were adopted for samples exhibiting a lower temperature of crystallisation onset. The applied stress was modified for each test during cooling in order to adapt its value to changes in the material structure, always guaranteeing the linear viscoelastic conditions.

In accordance with a procedure elsewhere adopted in the literature [14] and already described in Chapter 2, the onset of crystallisation temperature was estimated as the temperature at which a sudden increase of the complex modulus $G*$ and a sharp decrease of the loss tangent during Time cure tests was observed.

In accordance with a simplified criterion, the gelation value was identified as the crossover between dynamic moduli or, in the same way, as the temperature at which the loss tangent is equal to unity and, therefore, the phase angle δ is 45°.

For all samples, the average structure development rate between T_{co} and T_{25} was calculated according to the procedure described in Chapter 3 (Equation 3.2.2) [15].

Rheological properties of selected samples (OP3, OP4, OP5, OP12 and OP10) were further investigated at 25°C performing Frequency sweep tests in linear conditions. With the aim of carefully controlling the thermal history of all the samples, a Temperature ramp test in linear conditions was performed down to 25°C, following the procedure previously described, and after a rest period of 100s (to guarantee that equilibrium conditions were obtained) Frequency sweep test was performed.

In addition, Temperature ramp tests and SRTRTs (in the temperature range between 85°C and 20°C) at the fixed shear rate of $1s^{-1}$ were performed for samples produced with different vegetable oils (EP, GP and OP10) using a stress-controlled HAAKE MARS III rheometer (Thermo Fisher Scientific, Germany) equipped with the RheoScope module (222-1912). Images were recorded at different temperature levels during rheological tests.

4.2.3 Thermal analysis

The cooling and heating thermograms of the most interesting samples (OP4, OP6, OP8, OP11, OP10, EP and GP) were measured using a Mettler Toledo Model DSC822e (Mettler Toledo, Switzerland), following the procedure reported in Chapter 2. In agreement with the

literature [16], the temperature of crystallisation onset ($T_{co,DSC}$) was individuated as the temperature corresponding to the beginning of the first exothermic peak in the cooling thermogram, whereas the melting temperature of each polymorph (T_M) was estimated as the temperature corresponding to the peak of the melting endotherm.

The aging and stability of selected samples was investigated through DSC measurements (according to the procedure reported in Chapter 3) after 1 week of storage at 4°C and 25°C.

4.2.4 Spectroscopic analysis: NMR and FT-IR

The solid fat content of policosanol organogels was determined by pulsed nuclear magnetic resonance (NMR) using a Minispec mq20 (Bruker, Germany), controlling sample temperature with a RC 20 water bath (LAUDA-Brinkmann LP., USA) [17]. During NMR measurements, samples were subjected to the same thermal history adopted during rheological tests (cooling rate of 1°C/min). Moreover, the onset of crystallisation temperature ($T_{co,NMR}$) and the average rate of SFC increase ($SFCr$) were estimated as already described in Chapter 3 (see Equation 3.2.3).

The fractal model proposed by Tang and Marangoni [18] was applied in order to relate the elastic modulus G' of the investigated samples to the volume fraction of solids Φ:

$$G' = \lambda \Phi^{1/(3-D)} \tag{4.2.1}$$

It is worth noticing that a modified fractal model was proposed by the same authors [18] in order to describe an apparent change in the fractal dimension D over a large range of solids fraction:

$$G' = \lambda \left(1 - e^{-k\Phi^b}\right)^{1/(3-D)} \tag{4.2.2}$$

The volume fraction of solids Φ for samples produced with virgin olive oil was calculated as follows:

$$\Phi = \frac{SFC/100}{\frac{SFC}{100} + \left(1 - \frac{SFC}{100}\right)\left(\frac{\rho_P}{\rho_O}\right)} \tag{4.2.3}$$

where SFC is the fraction of solids measured using NMR (i.e. the mass fraction of solids, according to the literature [5]), ρ_P is the density of policosanol (960kg/m^3 at room temperature, experimentally calculated), ρ_O is the density of virgin olive oil (920g/m^3 at room temperature, according to the literature [19]).

FT-IR measurements were performed using a Nicolet iS-10 FT-IR spectrometer (Thermo Scientific, USA) equipped with a Smart iTX ATR sampling accessory. All samples were prepared at 85°C following the procedure described in Paragraph 4.2.1 and absorption spectra were recorded immediately after cooling at room temperature. For selected samples, FT-IR spectra were recorded again after one week of storage at room temperature, in order to investigate potential changes in the microstructure of tested materials.

A statistical analysis was used to evaluate the significance of potential differences between two comparable data. The commercial software Statgraphics Centurion XV (Statpoint Technologies Inc., Warrenton) was used to carry out this analysis using a *t-student* test. Differences among parameters were considered significant with an interval of confidence of 90% (p=0.1).

4.3 Results and discussion

4.3.1 Rheological characterisation of policosanol/olive oil organogels

4.3.1.1 Effect of the preparation temperature

The temperature of sample preparation could affect the final properties of organogels, in fact, the gelator should be added to the oil at a temperature higher than its melting point in order to achieve a good solubility [20]. Starting from these considerations, a preliminary analysis on the influence of the preparation temperature on rheological properties of policosanol/olive oil organogels was carried out. According to the literature [21], the melting temperature of pure policosanol ranges between 80°C and 82°C according to the potential differences in composition due to the raw material characteristics. In the present work, a melting temperature of 81.5±0.2°C was estimated through DSC analysis, as already reported in Chapter 2. Hence, samples OP4, OP5 and OP10 were prepared at three different temperatures (70°C, 85°C and 97°C), lower and higher than the estimated melting point, in an attempt to find the preparation temperature more suitable for the characteristics of this organogelator.

Time cure tests were performed in order to investigate samples produced in different conditions and their characteristics were compared in terms of complex modulus *G** and phase angle *δ*, as shown in Figures 4.3, 4.4 and 4.5. The results obtained evidenced significant similarities with the rheological behaviour of organogels made with different

orgenogelators (see Chapter 3). At high temperatures, the system was in the molten state and it exhibited phase angle values at approximately 90° and very low values of complex modulus. It is worth noticing that the large deviations often observed for data at high temperatures are due to instrument limits when the measurement of very low viscous systems is needed. Cooling the sample down to the critical temperature T_{co}, G^* showed a sudden increase, contemporarily with phase angle decrease, indicating the beginning of crystallisation. At lower temperature, the system behaved as a solid-like gel material.

As far as sample OP4 is concerned (see Figure 4.3), no significant differences in G^* values could be detected when the sample was prepared at 85°C or 97°C whereas slight differences during the transition region arose when the sample was prepared at 70°C. The phase angle seems to be more affected by the preparation temperature even though the greatest differences were observed, also in this case, when the sample prepared at 70°C is compared to the others.

When samples produced with higher amounts of policosanol (OP5 and OP10) are considered, no differences were observed for both G^* and δ values at all investigated preparation temperatures (see Figure 4.4 and 4.5). It should be noted that very scattered data of the phase angle were obtained for sample OP10 at low temperature, owing to the relevant consistency of the sample.

Therefore, it can be concluded that, even for very low policosanol concentration, the preparation temperature does not affect the organogel properties in a relevant way when a threshold value of 85°C is exceeded. As a consequence, in the present work all samples were prepared at 85°C, in order to ensure the complete melting of the organogelator and, at the same time, to minimise the oxidative phenomena of the vegetable oil (promoted by high temperature) as much as possible [22].
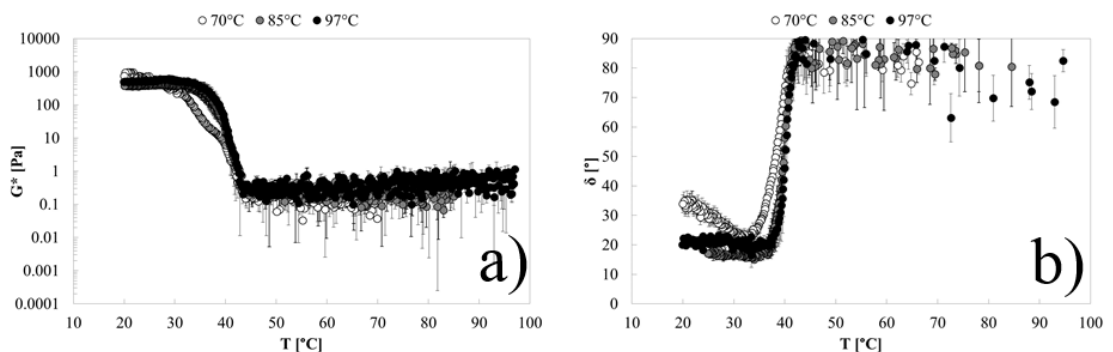

Figure 4.3 G^* (a) and δ (b) from temperature ramp tests for sample OP4 prepared at 70, 85 and 97°C.
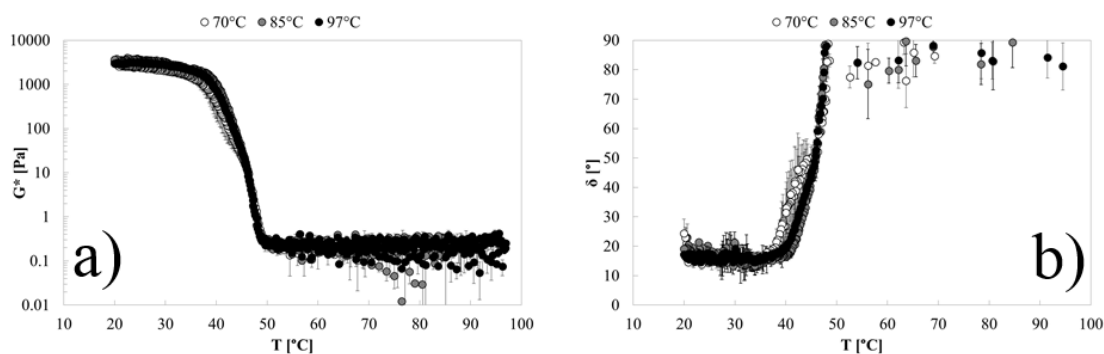
Figure 4.4 G^* (a) and δ (b) from temperature ramp tests for sample OP5 prepared at 70, 85 and 97°C.
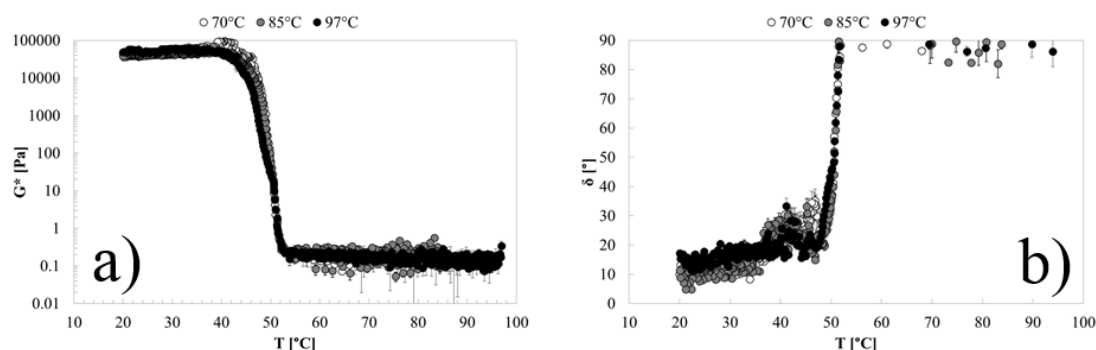

Figure 4.5 G^* (a) and δ (b) from temperature ramp tests for sample OP10 prepared at 70, 85 and 97°C.

4.3.1.2 Effect of policosanol concentration

With the aim of studying the crystallisation and gelation phenomena induced by policosanol, samples produced with low concentrations of organogelator (OP1-OP4) were investigated. As shown in Figure 4.6, the phase angle of sample OP1 did not exhibit relevant changes in the whole temperature region investigated. A similar behaviour can be observed for sample OP2, even though a more regular trend can be evidenced at the onset of crystallisation, because of the increase in elasticity caused by crystal formation. Nevertheless, quite large values of the phase angle were measured, indicating a liquid-like behaviour.

On the contrary, when policosanol mass fraction is at least 0.005 (sample OP3), the crossover between loss and storage modulus (δ=45°) can be observed at the temperature value (T_g) of 26±1°C, indicating the formation of a 3-D network. Hence, it seems that between 0.003 and 0.005 there is a critical value of the policosanol mass fraction defining the transition between an unlinked suspension of policosanol and fat crystalline aggregates

and a gelled material with interconnected unities. The final solid-like behaviour of the system was found to be determined by the organogelator amount, as evidenced by the different trends in the phase angle observed for samples OP3 and OP4.

Therefore, for samples with a policosanol fraction higher than 0.005, both critical temperatures T_{co} and T_g were evaluated.
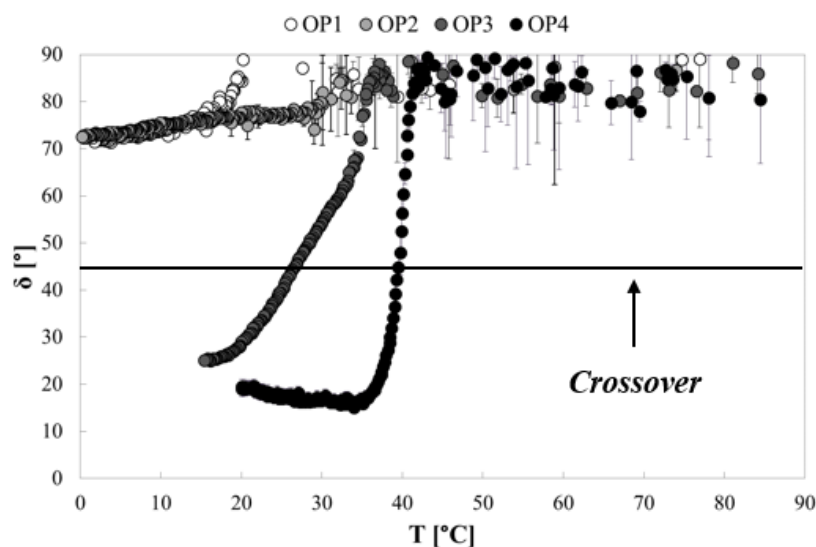

Figure 4.6 Phase angle δ for OP1, OP2, OP3 and OP4 samples.

The estimated values are listed in Table 4.3. It can be noticed that, when increasing the organogelator concentration, the difference between the two critical temperatures became smaller. Moreover, the temperature of gelation was significantly different from the temperature of crystallisation onset up to a policosanol mass fraction of 0.025, whereas if a fraction of at least 0.03 was added to the organogel no differences were encountered between the two critical temperatures.

This range is very close to that described in Chapter 3 for MAG organogels and found elsewhere in the literature [14].

Sample ID	T_{co} [°C]	T_g [°C]
OP1	21.7±0.9	-
OP2	34.2±0.4	-
OP3	38.2±0.1	26±1
OP4	42.4±0.4	39.5±0.3
OP5	47.7±0.1	45.6±0.3
OP6	56.5±0.3	54±1
OP7	65.7±0.1	64.0±0.8
OP8	72.5±0.5	71.6±0.7
OP9	76.7±0.1	76.3±0.1
OP10	52.0±0.3	50.1±3
OP11	53.8±0.2	51.9±0.4
OP12	50.3±0.5	49.4±0.1

Table 4.3 T_{co} and T_g values for OP samples.

4.3.1.3 Frequency sweep tests

Frequency sweep tests at 25°C were carried out on selected policosanol organogels. In order to guarantee a controlled thermal history, all samples were cooled down to the final temperature on the rheometer plate at a constant cooling rate of 1°C/min. Figure 4.7 and 4.8 show the obtained results for samples OP3, OP4, OP5, OP12 and OP10 (produced, respectively, with policosanol fractions of 0.005, 0.01, 0.02, 0.025 and 0.03) in terms of complex modulus G^* and phase angle δ, respectively. Sample OP3, containing the lowest amount of policosanol, exhibited a different behaviour from other samples, showing a significant dependence of complex modulus on frequency and a liquid-like behaviour (phase angle higher than 45°) for all tested frequencies.

On the other hand, all other samples were characterised by an almost constant value of the complex modulus (increasing with increasing policosanol concentration) and a very low phase angle. Hence, it can be concluded that they exhibited a typical strong gel behaviour [23].

These results are in agreement with data obtained from Temperature ramp tests: the policosanol fraction of 0.005 (sample OP3) represents the threshold value for gelation, with a gelation temperature of almost 26.1±0.9°C, very close to the temperature adopted in

Frequency sweeps. Therefore, being in a transition condition, sample OP3 behaved as a concentrated suspension of crystalline aggregates not yet gelled, whereas all other samples, containing policosanol fraction larger than the critical value of 0.005, exhibited a real strong gel behaviour.

It is worth noticing that the rheological properties of policosanol/olive oil organogels seem suitable for potential uses as alternatives to commercial saturated fats. Dynamic moduli of samples OP12 and OP10 (containing, respectively, a policosanol fraction of 0.025 and 0.03) were found to be quite close to the values observed for traditional commercial products (*G'* of butter at 1Hz and 20°C between 10^4 and $3 \cdot 10^5$ Pa [24] and *G'* of margarine between $2.5 \cdot 10^4$ and $5 \cdot 10^6$ Pa [25, 26]). Commercial fats are usually water in oil emulsions, in which policosanol organogels could represent the potential continuous structured oil phase. Nevertheless, the investigated policosanol/olive oil organogels at relatively low organogelator concentrations evidenced rheological properties close to those of the final product.

As far as the phase angle is concerned (see Figure 4.8), it can be observed that at increasing policosanol concentration, the structuring level remained almost constant, whereas the consistency (related to the complex modulus at 1Hz, Figure 4.7) increased. These results suggest that it is possible to design different materials suitable for fat replacement and with a controlled "consistency" by changing the amount of organogelator.
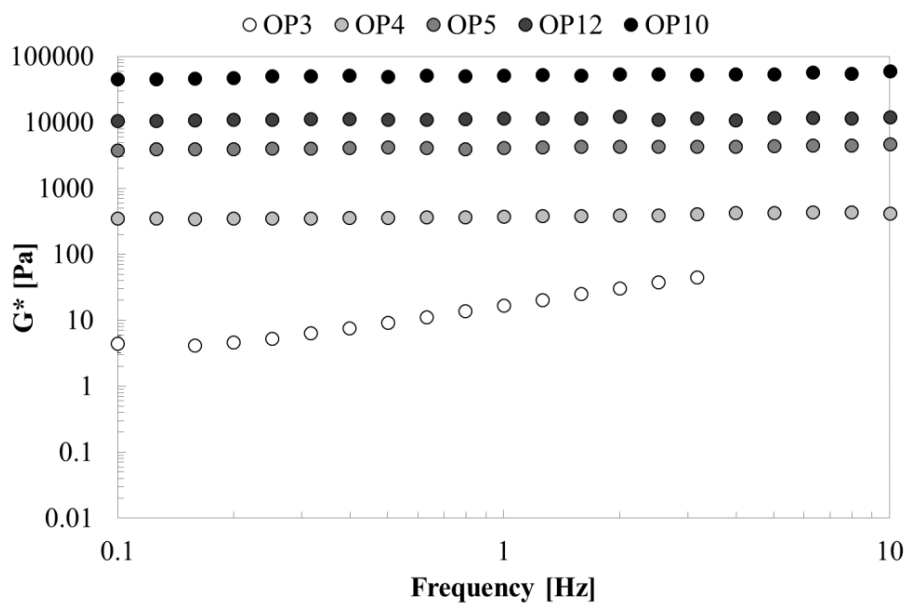

Figure 4.7 Frequency sweep tests for samples OP3, OP4, OP5, OP12 and OP10 in terms of complex modulus.
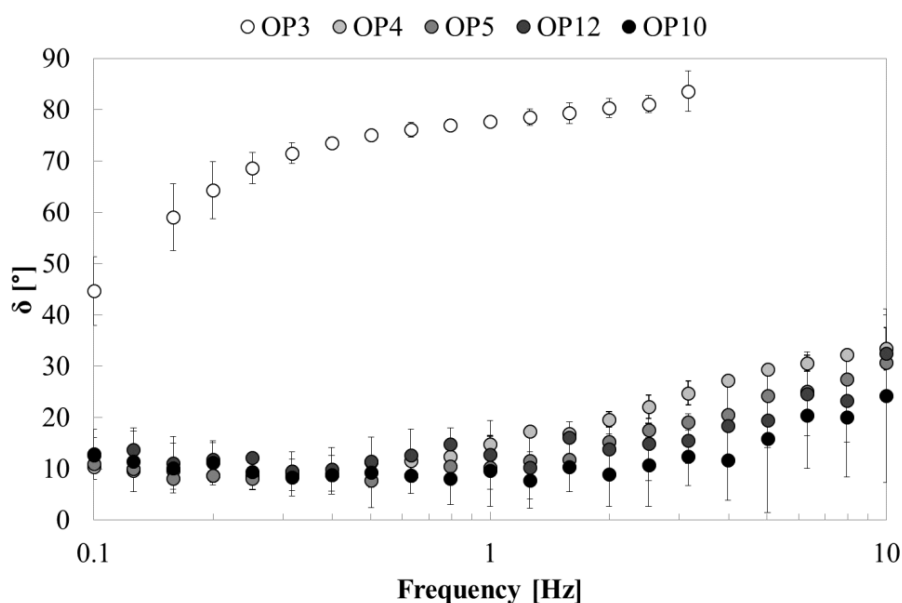
Figure 4.8 Frequency sweep tests for samples OP3, OP4, OP5, OP12 and OP10 in terms of phase angle δ.

4.3.2 Thermal and structural analysis of policosanol organogels

4.3.2.1 DSC analysis

Figure 4.9 shows the DSC thermogram of selected OP samples (produced with low, intermediate and high policosanol fractions). The three cooling and melting curves exhibited clearly different behaviour. The crystallisation of OP4 sample (X_P=0.01) showed one small exothermic peak, followed by a small endothermic peak during melting. The transition peak observed upon cooling appeared at the same temperature at which a sudden change in the slope of G^* curve was found during Temperature ramp test (T_{co}), evidencing the beginning of crystallisation phenomena.

The thermogram of sample OP6 (X_P=0.05) exhibited only one exothermic peak with a shoulder during cooling and one broad melting peak upon heating. The behaviour of sample OP6 is very similar to that found by Toro-Vazquez et al. [16] for a 3%$_{w/w}$ Candelilla wax in safflower oil organogel: the peak present in both the cooling and heating thermograms was associated with the gelation and melting of Candellilla wax components, mainly hentriacontane (a long-chain alkane hydrocarbon with the structural formula $CH_3(CH_2)_{29}CH_3$). Similarly, the shoulder-peak observed in OP6 cooling thermogram could be related to the crystallisation of policosanol components, especially octacosanol ($C_{28}H_{58}O$). On the other hand, Gandolfo et al. [27] reported that the peak with a shoulder

182

observed in stearyl alcohol DSC thermogram, corresponded to a solid-solid phase transition between the α and γ typical polymorphs of fatty alcohols. Hence, the peak found in OP6 cooling thermogram could also be due to a polymorphic transition of fat crystals.
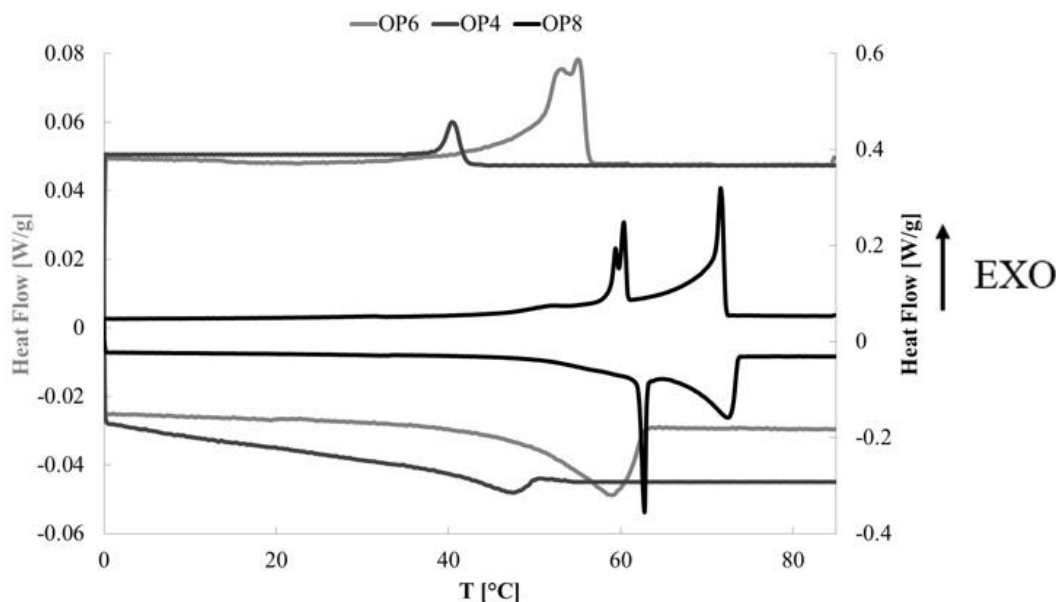

Figure 4.9 DSC thermograms for OP4, OP6 and OP8 samples.

The behaviour of OP8 (X_P=0.30) sample was found to be more complex in comparison to other samples. A narrow exothermic peak can be observed at high temperature in the cooling thermogram followed by a smaller peak with a shoulder, whereas the melting thermogram evidenced a narrow and then a broad endothermic peak. Unexpectedly, the DSC thermogram of OP8 sample was found to be qualitatively very similar to that of C_{32}-alkane (dotriacontane, $C_{32}H_{66}$) reported by Morales-Rueda et al. [28] and Tozaki at al. [29]. The two exothermic peaks in the dotriacontane thermogram were associated with the development of a rotator phase from the melt and the transition from the rotator phase to crystal, respectively, while the first endothermic peak in the melting region was associated with a solid-solid transition from the crystalline to the rotator phase and the second peak to the transition from the rotator to the liquid phase [28, 29, 30]. In addition, Morales-Rueda et al. [28] investigated a dispersion of 3%$_{w/w}$ C_{32} in safflower oil, obtaining results similar to those found in this work for organogels prepared with low policosanol fractions. Therefore, it seems that at high organogelator fractions the thermal behaviour of

organogels is mainly due to the longest-chain components of policosanol, whereas at low policosanol fractions a less complex behaviour is observed.

4.3.2.2 FT-IR analysis

In order to investigate the potential formation of hydrogen bonds, samples were allowed to cool at room temperature and immediately after gel formation ($t=t_0$) FT-IR spectra were recorded. Figure 4.10 shows the results obtained for samples OP2, OP6 and OP8. According to the literature, intermolecular hydrogen bonds should appear as medium-intensity bands in the 3550-3450cm^{-1} wavenumber range [31]. OP2 and OP6 spectra did not evidence the presence of any intermolecular hydrogen bonds. It is worth noticing that sample OP2 was prepared with a policosanol fraction of 0.003, lower than the critical threshold for gelation (X_P=0.005). On the contrary, sample OP6 was produced with a policosanol fraction of 0.05, well above the minimum policosanol concentration required for gelation. Nevertheless, no intermolecular hydrogen bonding was detected in the OP6 spectrum, therefore it can be concluded that the presence of hydrogen bonds was not the main "driving force" for policosanol organogel formation.
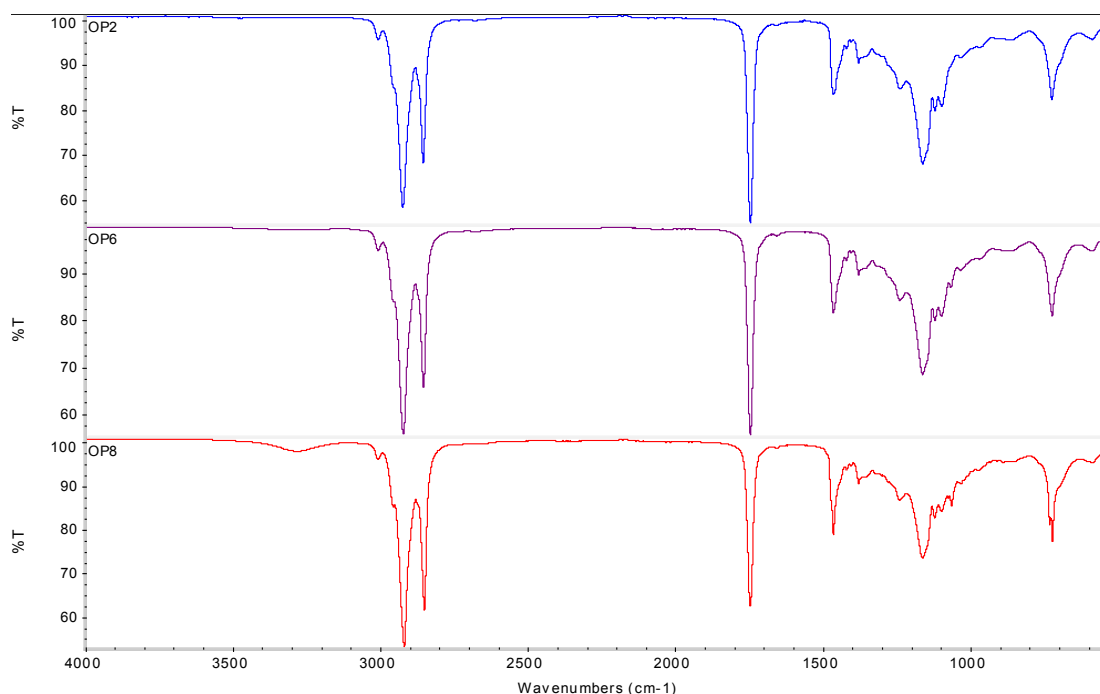

Figure 4.10 FT-IR spectra for OP2, OP6 and OP8 samples at $t=t_0$.

Sample OP8 (X_P=0.30) exhibited a different behaviour, with a small peak at around 3300cm^{-1}. This peak can be associated with the presence of weak intermolecular hydrogen

bonds [31]. Hence, the formation of hydrogen bonds as interactions among policosanol molecule aggregates can be observed only at high organogelator concentrations.

As stated before, even though no intermolecular hydrogen bonds were detected for sample OP6, this sample was prepared with a policosanol fraction much higher than the critical threshold required for gelation. Therefore, other kinds of intermolecular interactions may be responsible for organogel formation. Van der Waals forces play an important role in organogelation phenomena, especially for organogelators characterised by long alkyl chains [32]. It should be taken into account that policosanol is a mixture of long-chain fatty alcohols, hence it seems reasonable to propose that policosanol organogel formation is driven by van der Waals interactions. Suzuki et al. [32] showed that van der Waals interactions shifted the absorption bands of symmetric and anti-symmetric CH_2 streching vibrational modes to lower wavenumbers. For sample OP2 (no organogel formation) the above-mentioned bands appeared at $2922cm^{-1}$ and $2853cm^{-1}$, whereas for sample OP6 peaks were observed at $2920cm^{-1}$ and $2851cm^{-1}$ and for sample OP8 at $2917cm^{-1}$ and $2848cm^{-1}$. The lower wavenumber shift revealed a decrease in the fluidity of the alkyl chains [32], confirming the organisation of the alkyl groups via van der Waals interactions.

In the previous Chapter, it was shown that Myverol organogel formation is highly dependent on the formation of hydrogen bonds between organogelator molecules, whereas policosanol organogels are formed mainly through van der Waals interactions. For organogelation, the suitable balance of hydrogen bonding and van der Waals interactions is needed [32]. From the results obtained in the present work, it can be concluded that although the Myverol chain length is small (C_{16}-C_{18}) intermolecular hydrogen bonds allow Myverol organogels to be formed, and, on the other hand, even though policosanol organogels do not show the presence of hydrogen bonds, van der Waals interactions between long chain fatty alcohols allow policosanol organogels to be formed.

4.3.3 Determination of SFC and application of fractal model

The SFC of policosanol/olive oil systems increased with decreasing temperature, following the same trend observed for the complex modulus G^* during Temperature ramp tests. As an example, Figure 4.11 shows results obtained for sample OP11. It can be seen that at temperatures higher than the crystallisation onset ($T>T_{co,NMR}$) SFC was almost zero; a significant increase of SFC occurred as soon as the $T_{co,NMR}$ was reached and, finally, at

lower temperatures an almost constant trend was found. For each sample, the volume fraction of solids Φ was calculated according to Equation 4.2.3. Results for sample OP11 are depicted in Figure 4.11.
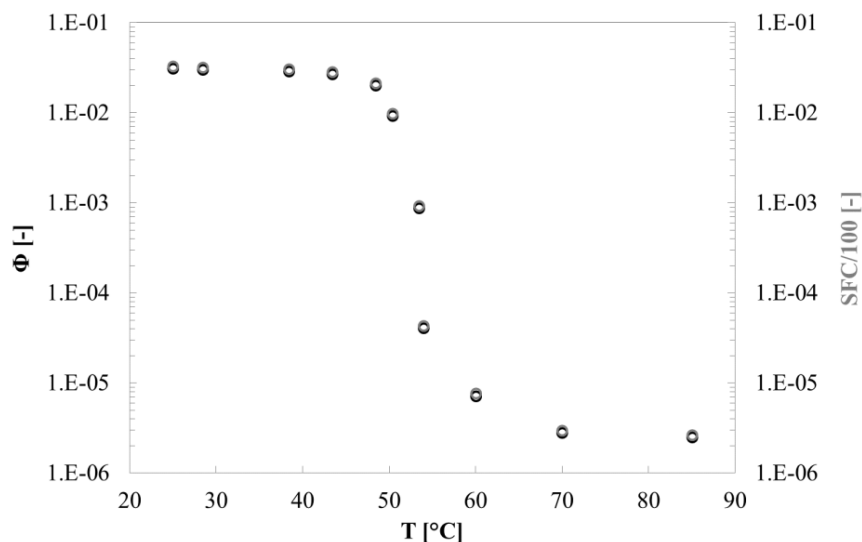

Figure 4.11 SFC and volumetric fraction of solids (Φ) versus temperature, for sample OP11.

As already discussed in Chapter 3 for organogels produced with a different organogelator, the plateau value of the SFC curve was found to be almost equal to the mass fraction of organogelator and it was slightly lower than the "theoretical SFC value" defined by Blake et al. [5]. In Table 4.4, the "theoretical SFC" (SFC_{th}) is compared to the experimental value measured within the plateau region, at the temperature level T_{25} ($T_{25}=T_{co,NMR}-25$).

Sample	SFC$_{th}$ [%]	SFC (T$_{25}$) [%]
OP2	0.29	0.27±0.01
OP3	0.49	0.46±0.11
OP4	0.97	0.95±0.01
OP5	1.96	1.82±0.01
OP6	4.87	4.51±0.01
OP7	14.60	14.21±0.04
OP8	29.21	29.04±0.01
OP9	53.54	52.41±0.15
OP10	2.92	2.68±0.01
OP11	3.31	3.20±0.01
OP12	2.43	2.25±0.01

Table 4.4 Theoretical (SFC$_{th}$) and measured SFC at T$_{25}$ for OM5-OM9 samples.

In order to obtain results independent of potential kinetic effects, data at a fixed distance from the onset of crystallisation were used, therefore SFC was measured at the following temperatures:

$T_{10}=T_{co}-10$

$T_{15}=T_{co}-15$

$T_{25}=T_{co}-25$.

As shown in Figure 4.12, the SFC was found to be directly proportional to policosanol mass fraction at all investigated temperatures:

$$\frac{SFC}{100} = aX_P \qquad (4.3.1)$$

where *a(T$_{10}$)=0.80±0.11*, *a(T$_{15}$)=0.93±0.07* and *a(T$_{25}$)=0.95±0.05*.
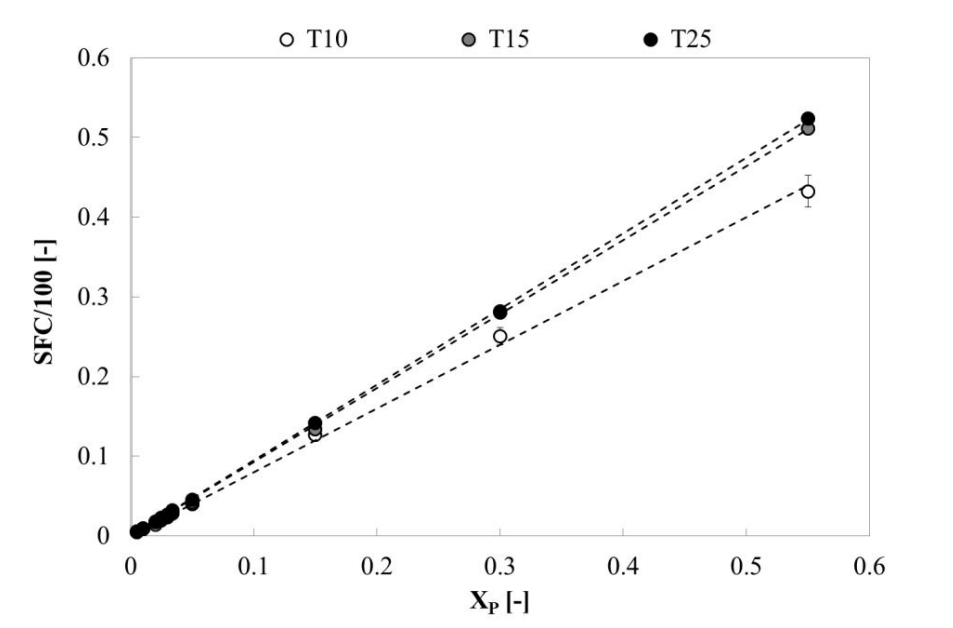
Figure 4.12 SFC versus policosanol fraction at different temperature levels.

In addition, rheological data were related to the volume fraction of solids Φ. The non-linear relationship observed between the storage modulus G' and Φ is well explained by the fractal model (Equation 4.2.1), as can be appreciated in Figures 4.13 and 4.14.
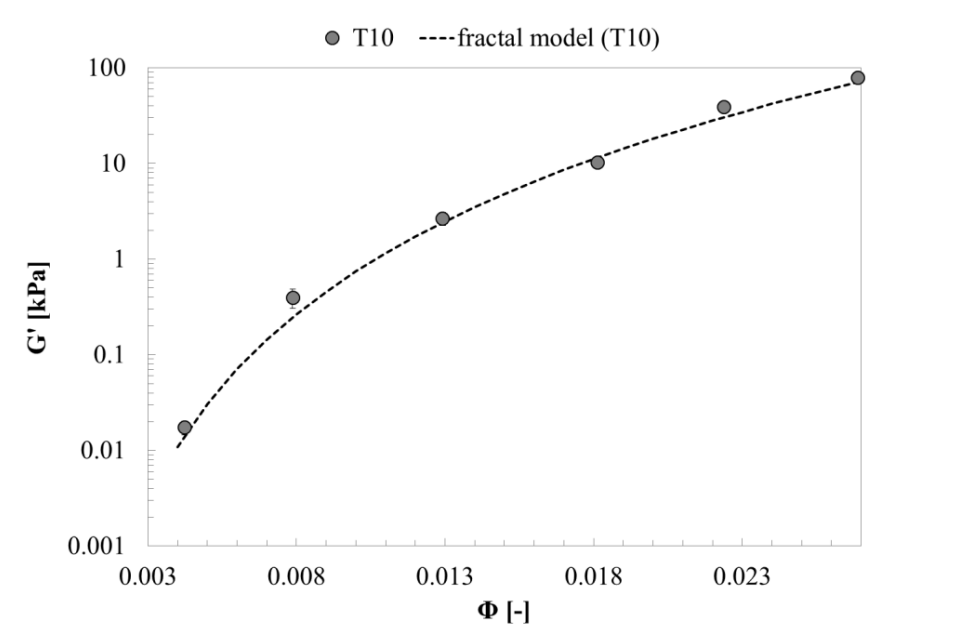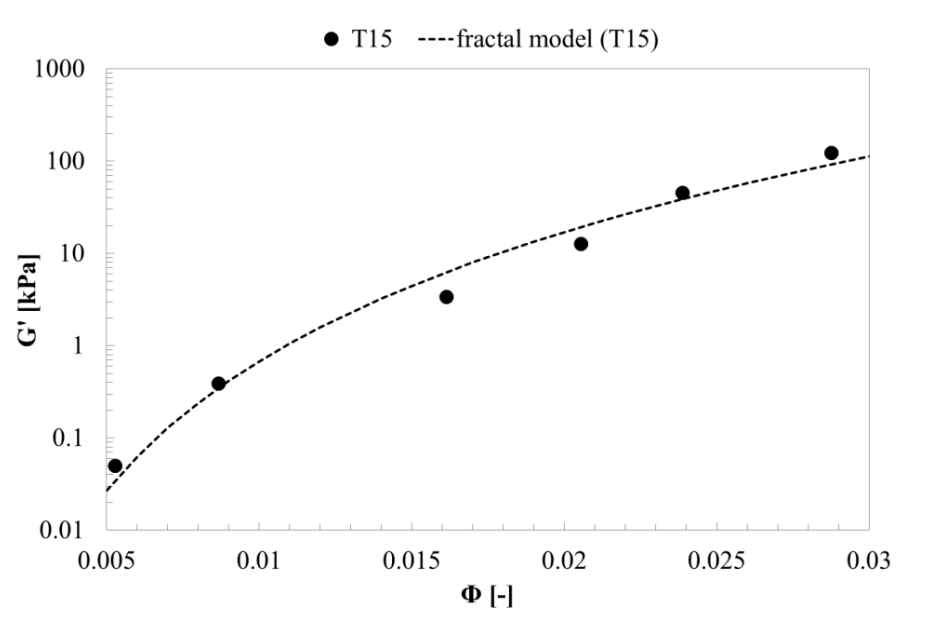

Figure 4.13 Application of fractal model at T$_{10}$.

Figure 4.14 Application of fractal model at T$_{15}$.

The "original fractal model" considered in the present work, was chosen because of the limited range of policosanol fractions added to the samples, for which a storage modulus could be detected. The fitting parameters obtained are reported in table 4.5:

Temperature	λ [Pa]	D [-]
T$_{10}$	$1.22 \cdot 10^9 \pm 6.11 \cdot 10^7$	2.78 ± 0.01
T$_{15}$	$1.36 \cdot 10^9 \pm 5.43 \cdot 10^7$	2.78 ± 0.02

Table 4.5 Fitting parameters of Eq. 4.2.1.

As already observed for MAG/olive oil organogels (Chapter 3), the parameter λ increased with decreasing temperature, while an almost constant value of D was found, indicating that, according to the model, the microstructure of the network did not change significantly during the cooling process. The estimated λ values at both temperatures were very high, evidencing the formation of a network with strong interactions between interconnecting unities.

4.3.4 Interpretation of thermo-rheological parameters and structure development rate

As reported in Table 4.6, no significant difference was encountered between T_{co} values calculated through different techniques of analysis (rheology, DSC and NMR).

Sample	T_{co} [°C]	$T_{co,DSC}$ [°C]	$T_{co,NMR}$ [°C]
OP1	21.7±0.9		
OP2	34.2±0.4		34.7±0.3
OP3	38.2±0.1		38.6±0.4
OP4	42.4±0.4	42.7±0.1	42.2±0.3
OP5	47.7±0.1		47.1±0.4
OP6	56.5±0.3	57.0±0.2	56.9±0.2
OP7	65.7±0.1		65.1±0.6
OP8	72.5±0.5	73.0±0.1	72.3±0.4
OP9	76.7±0.1		76.2±0.4
OP10	52.0±0.3		52.3±0.5
OP11	53.8±0.2	53.6±0.1	53.4±0.3
OP12	50.3±0.5		50.8±0.2

Table 4.6 Temperature of crystallisation onset for OP samples, calculated from rheological Temperature ramp tests (T_{co}), from DSC analysis ($T_{co,DSC}$) and from NMR measurements ($T_{co,NMR}$).

The behaviour of T_{co} with increasing policosanol fraction is qualitatively similar to that found for other organogelators (see Chapter 3), with an asymptotic trend at high organogelator fractions. As already discussed in Chapter 3, looking for a potential relationship between T_{co} and X_P, it seems reasonable to relate the thermo-rheological parameter T_{co} to the fractal microstructure of the system. Even though little data was available for the storage modulus G', a greater amount of data was available for the temperature of crystallisation onset, therefore an empirical equation qualitatively similar to the "modified fractal model" (Equation 4.2.2) has been proposed:

$$T_{co} = A' \left(1 - e^{-B'X_P^C}\right)^{1/(3-D)} \tag{4.3.2}$$

where the fractal dimension D has already been estimated from rheological data (D=2.78), whereas A=101±8°C, B'=2.90±0.31 and C=0.132±0.011. Data fitting with Equation 4.3.2 is shown in Figure 4.15.
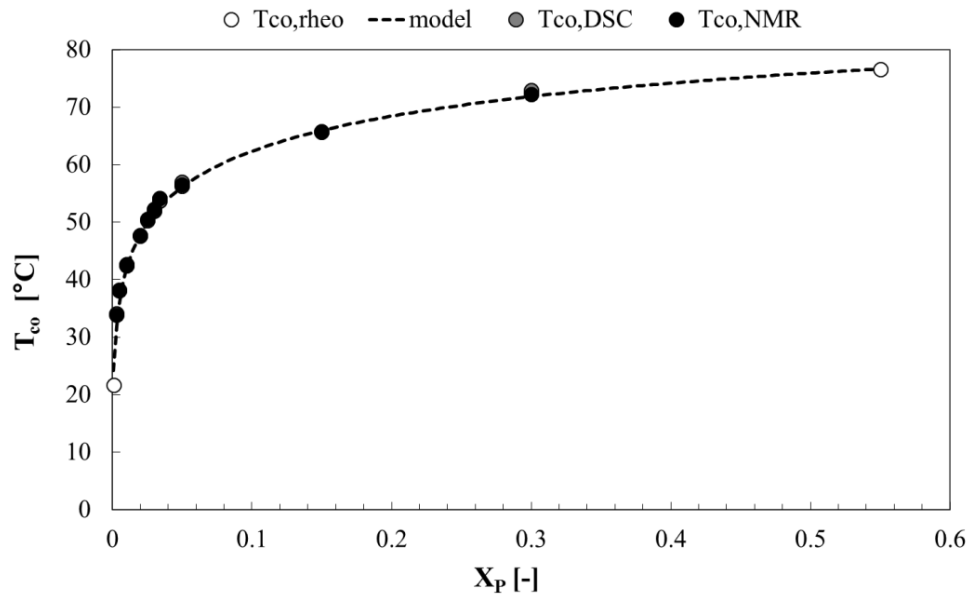
Figure 4.15 *T_{co}* as a function of policosanol fraction and data fitting with modified fractal model (Eq. 4.3.2).

In order to investigate the influence of policosanol fraction on the rate of structure development, the average rate of SFC increase (*SFCr*) and the average rate of structure development (*SDr*) were calculated for all samples, according to Equation 3.2.3 and 3.2.2, respectively. As already observed for MAG organogels (Chapter 3), the *SFCr* was found to be directly proportional to the policosanol fraction (see Figure 4.16):

$$SFCr = a'X_P \qquad (4.3.3)$$

where *a'*=0.085±0.002 s^{-1} (with *R^2*=0.99).

The average *SDr*, estimated from rheological measurements, is related to the rate of storage modulus increase upon cooling of the systems investigated. As discussed before for *T_{co}*, the *SDr* calculated from rheological characterisation has been related to the fractal microstructure of policosanol organogels, as follows:

$$SDr = \lambda'X_P^{1/(3-D)} \qquad (4.3.4)$$

where *λ'*=4.12·10^8±4.21·10^{6}Pa/s, whereas the fractal dimension has already been estimated from rheological data (*G'* versus *Φ*, *D*=2.78). Although little data was available, the proposed empirical equation seems to fit the experimental trend quite well (Figure 4.17).
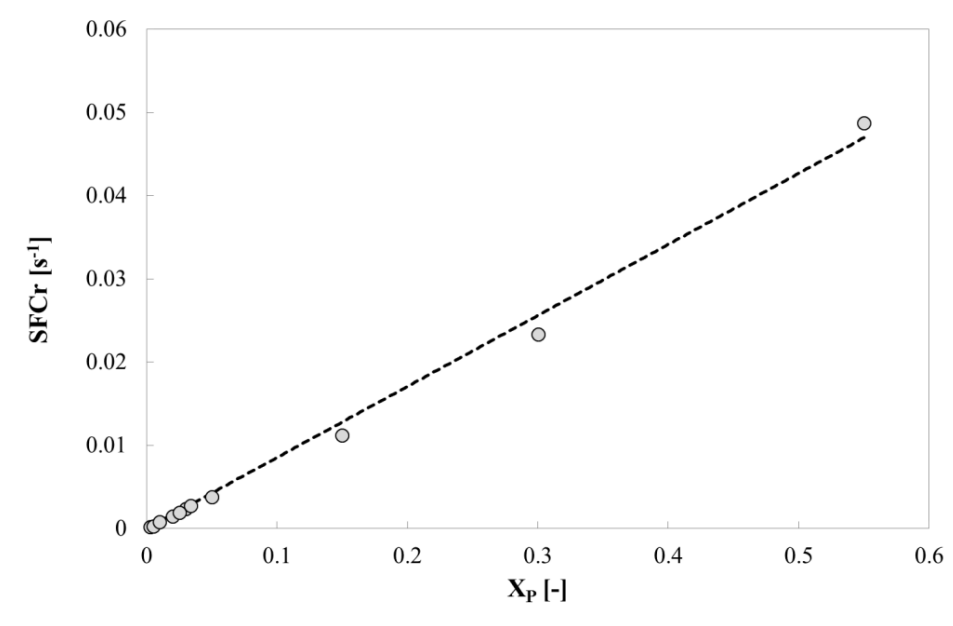
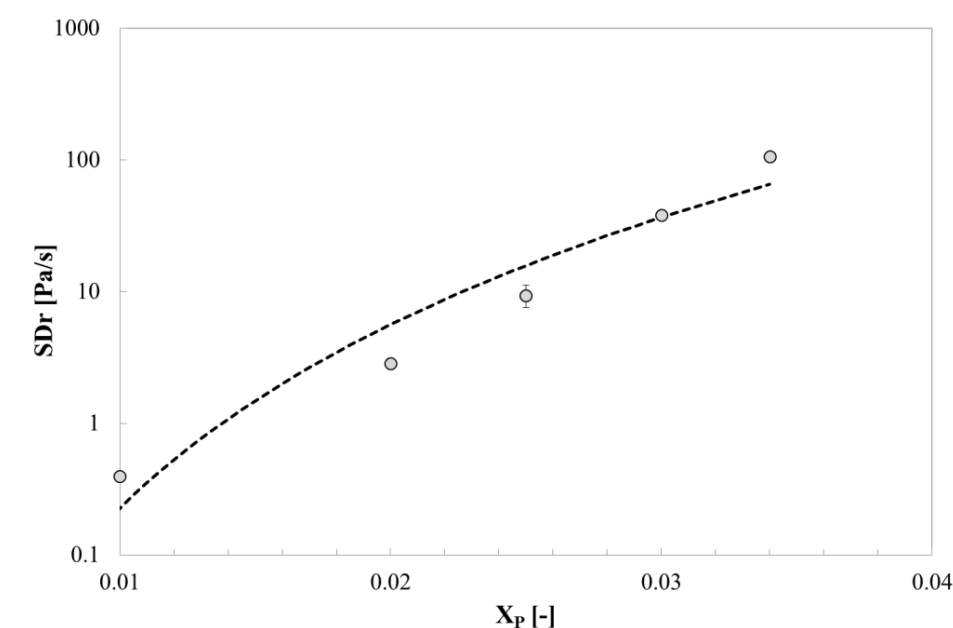**Figure 4.16 Rate of SFC increase (*SFCr*) as a function of policosanol fraction and data fitting with Eq. 4.3.3.**

Figure 4.17 Structure development rate (*SDr*) as a function of policosol fraction and data fitting with Eq. 4.3.4.

4.3.5 Aging of policosanol/olive oil organogels

With the aim of investigating potential changes in the microstructural and rheological properties of policosanol organogels, rheological, NMR, DSC and FT-IR measurements were repeated after one week of storage at two different temperatures (4°C and 25°C,

respectively). Figure 4.18 shows FT-IR spectra of samples OP2, OP6 and OP8 after one week of storage at room temperature. It can be seen that a small and broad peak arose in the OP6 spectrum at around $3450cm^{-1}$, whereas the peak at $3300cm^{-1}$ already observed in OP8 spectrum at $t=t_0$ did not show any relevant changes. No peaks are detectable in the low-energy region for sample OP2. Therefore, it seems that upon aging no hydrogen bonds formed in systems containing a low amount of policosanol, whereas weak intermolecular hydrogen bonding formed at intermediate concentrations and remained stable at high policosanol fractions.
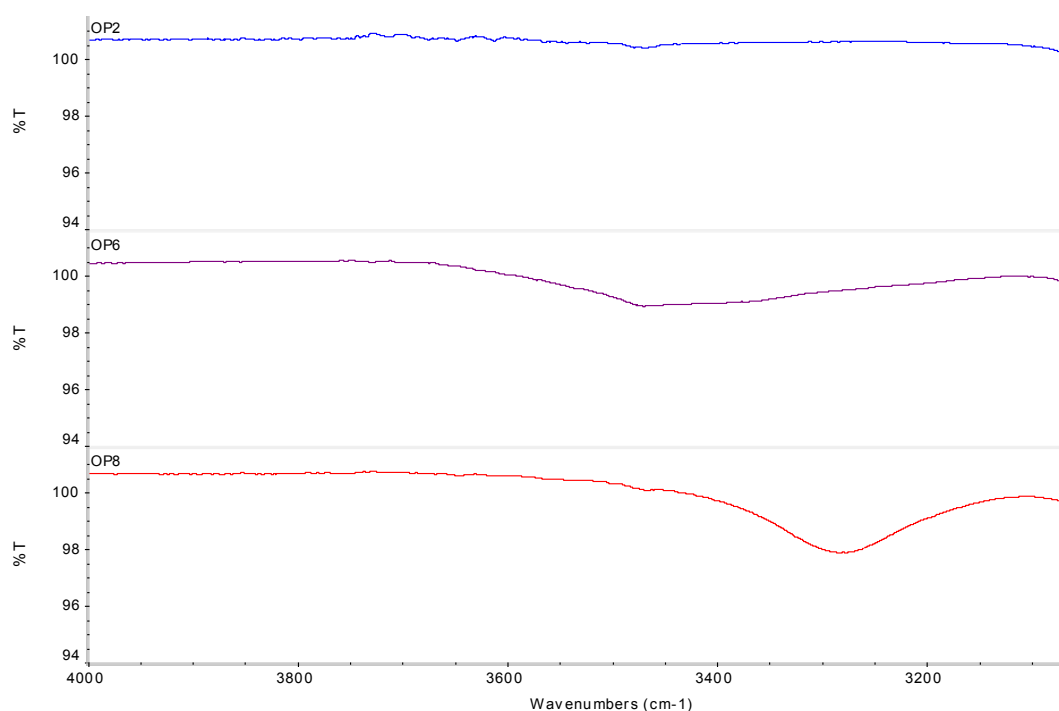
Figure 4.18 FT-IR spectra for OP2, OP6 and OP8 samples at *t=1week*.

SFC measurements were carried out every 24h for 10 days during storage at 4°C and 25°C. Results for sample OP10 are shown in Figure 4.19. At the lowest storage temperature, an increase in the SFC can be appreciated within the first 4 days and then values remained almost constant. It is worth noticing that the final plateau value is well above the maximum theroretical SFC mentioned above since crystallisation of olive oil took place at 4°C (see SFC measurements on olive oil, Chapter 2). On the contrary, at room temperature SFC values did not show any significant change, indicating a good stability of the systems investigated.
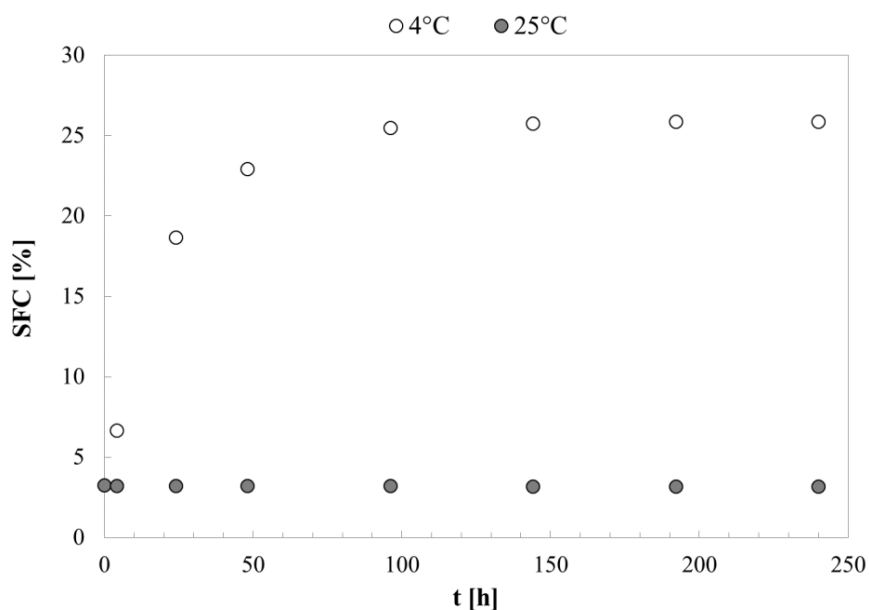
Figure 4.19 SFC as a function of time for sample OP10.

After one week of storage at 4°C and 25°C respectively, DSC thermograms were recorded. Figure 4.20 evidences that the melting peak became broader and shifted to higher temperatures after storage, suggesting the potential formation of stable polymorphs upon aging. Cooling thermograms recorded at $t=t_0$ and at $t=1week$ at both storage temperatures exhibited the same trend, indicating that policosanol organogels are completely thermo-reversible.
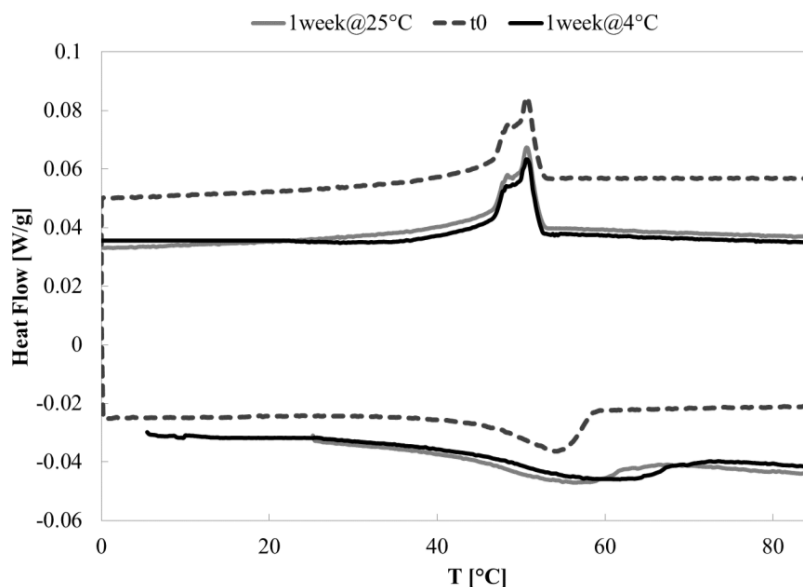

Figure 4.20 DSC thermograms of OP10 sample just after preparation (*t0*), after 1week of storage at 25°C (*1week@25°C*) and after 1week of storage at 25°C (*1week@4°C*).

Although small differences were detected through DSC analysis, G^* and phase angle values of sample OP10 after one week of storage at room temperature did not exhibit any significant changes, as can be seen from Figure 4.21. This suggests that small changes in microstructural characteristics of crystalline gels, like LMW organogels, do not correspond automatically to a modification of rheological parameters.
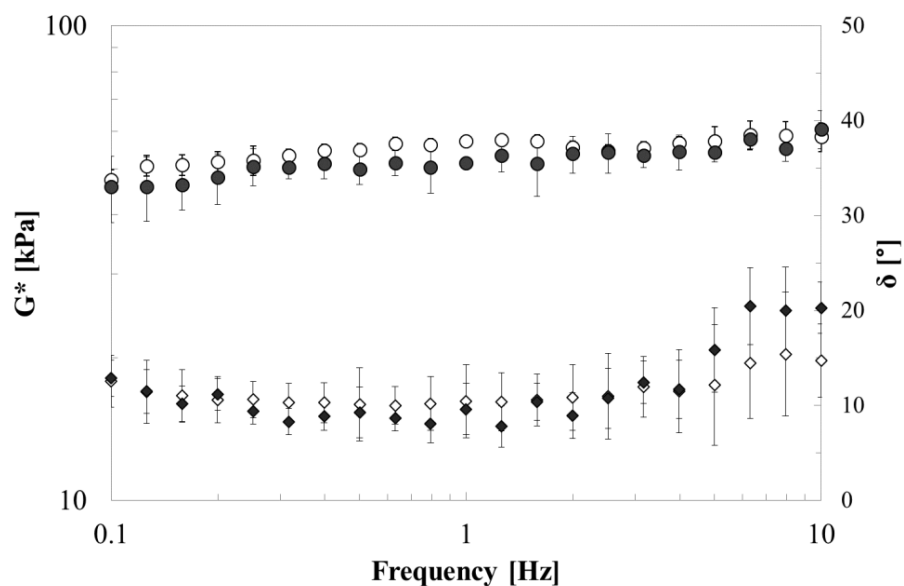

Figure 4.21 Frequency sweep test for sample OP10 at *t=t0* (full symbols) and *t=1week* (open symbols). *G** (circles) and δ (diamonds) versus frequency are shown.

4.3.6 Effect of the solvent on structural and rheological properties

The effects of the different vegetable oils used to produce organogels on their microstructural and rheological characteristics was investigated for samples prepared at a constant policosanol fraction of 0.03 (OP10, EP and GP). The vegetable oil used as the solvent did not affect the temperature of crystallisation onset, as evidenced in Table 4.7. Furthermore, at the policosanol fraction investigated, T_{co} is almost equal to T_g, therefore the three samples did not show any significant differences also in the gelation point.

Sample	T_{co} [°C]	$T_{co,DSC}$ [°C]	$T_{co,NMR}$ [°C]	T_g [°C]
OP10	52.0±0.3	52.2±0.1	52.3±0.5	50.1±0.4
EP	52.4±0.2	52.3±0.1	52.5±0.2	50.5±0.2
GP	52.7±0.3	52.4±0.1	52.9±0.3	50.8±0.4

Table 4.7 Temperature of crystallisation onset, calculated from rheological SAOTs (T_{co}), from DSC analysis ($T_{co,DSC}$) and from NMR measurements ($T_{co,NMR}$) and temperature of gelation (T_g) for EP, OP10, GP samples.

With the aim of studying the potential differences in both the microstructure and the rheological properties of policosanol organogels produced with different vegetable oils, Temperature ramp tests and also SRTRTs (at a constant shear rate of 1s^{-1}) were performed with a RheoScope Module. Figures 4.22, 4.24 and 4.26 show the complex modulus and the phase angle measured during Temperature ramp tests on samples OP10, GP and EP, respectively. The different temperature values at which images were recorded have been highlighted within the plots.

A comparison among the results obtained for the three samples suggested that both the complex modulus and the phase angle did not exhibit any relevant differences among the investigated systems. This is in agreement with results reported by Gandolfo et al. [2]: they demonstrated that the kind of vegetable oil had no great effect on the rheological properties of fatty alcohol organogels.

Figures 4.23, 4.25 and 4.27, show that the crystallisation and gelation processes are very fast: for all tested samples, some small needle-like crystal nuclei can be observed at $T=T_{co}$ and at $T=T_g$ (that is slightly lower than T_{co}) interacting aggregates of fibre-like crystals already formed.
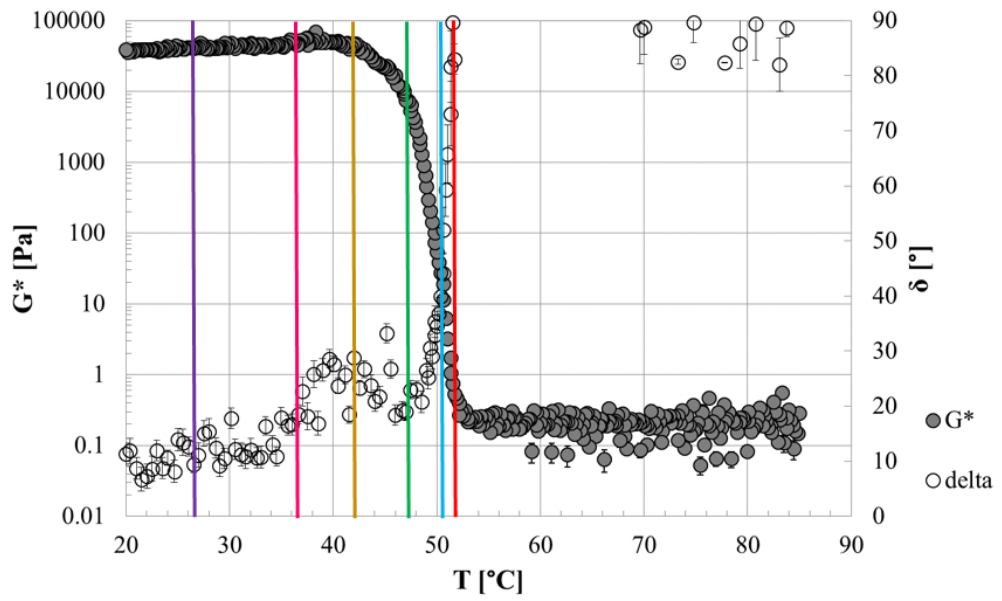
Figure 4.22 Time cure test for OP10 sample. Coloured lines correspond to the different microphotographs shown in Figure 4.23.
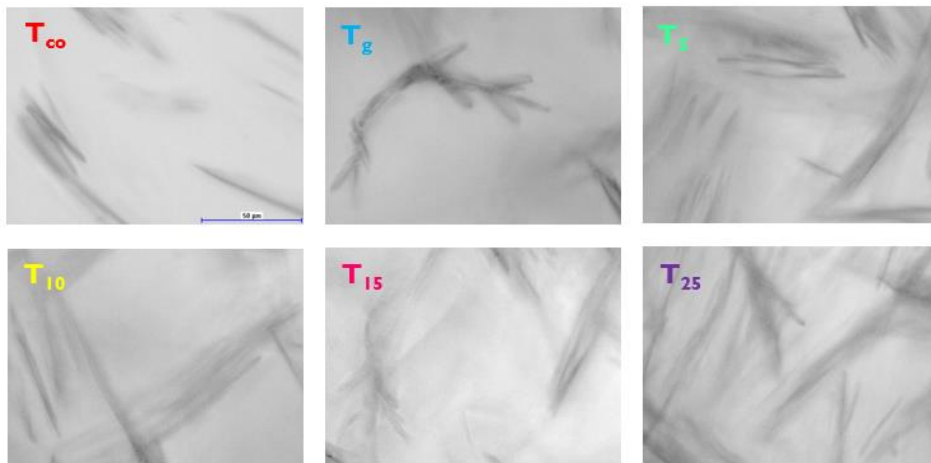

Figure 4.23 Microphotographs of OP10 sample during Time cure test (Figure 4.22) at different temperature levels (control bar is 50µm).
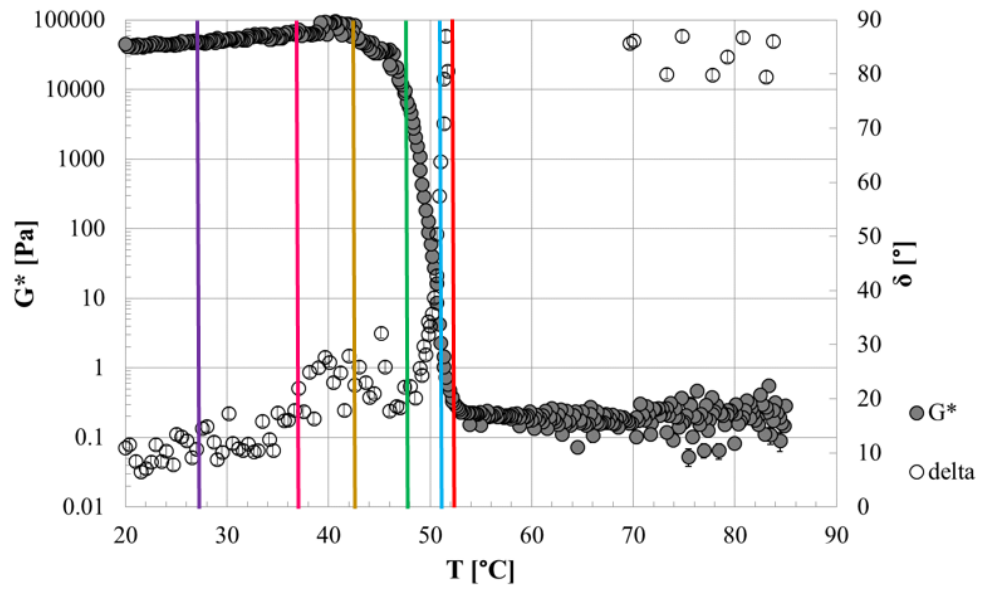
Figure 4.24 Time cure test for GP sample. Coloured lines correspond to the different microphotographs shown in Figure 4.25.
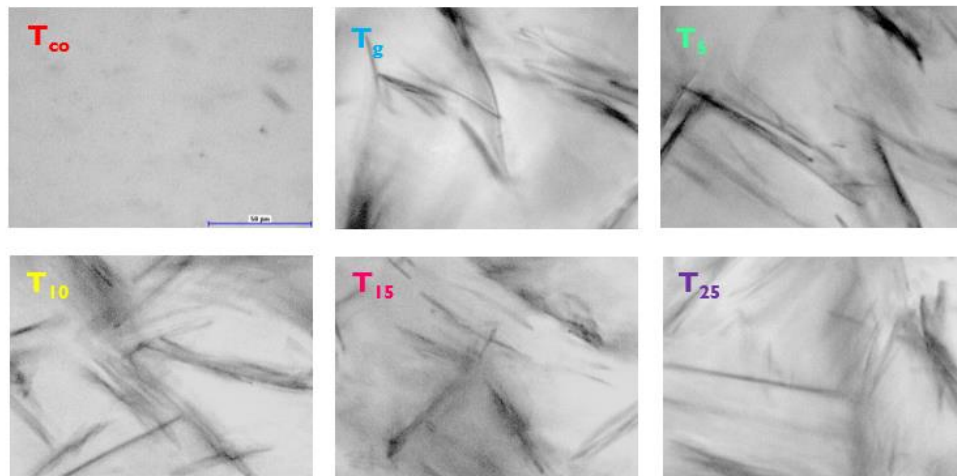

Figure 4.25 Microphotographs of GP sample during Time cure test (Figure 4.24) at different temperature levels (control bar is 50μm).
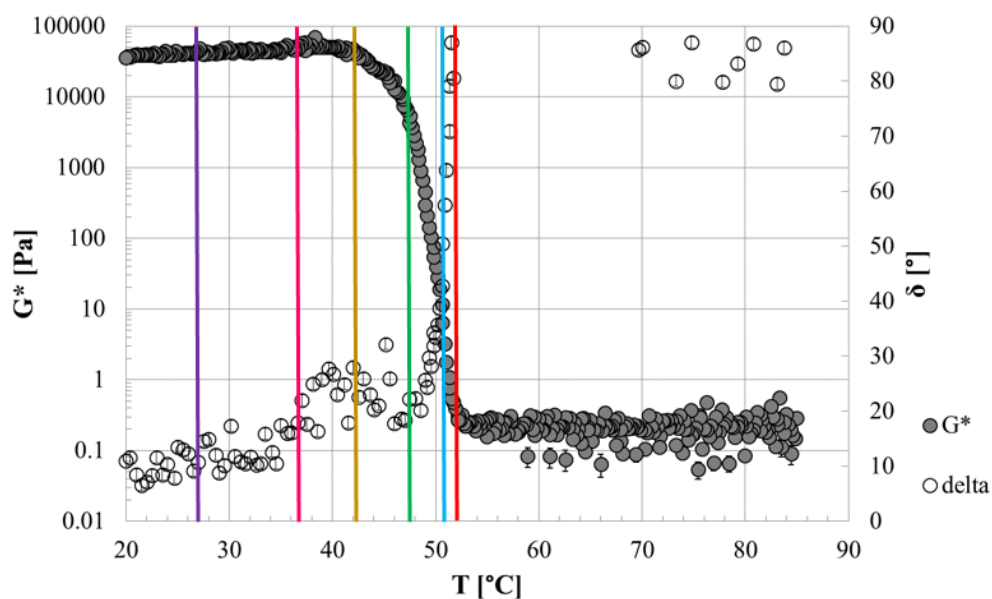
Figure 4.26 Time cure test for EP sample. Coloured lines correspond to the different microphotographs shown in Figure 4.27.
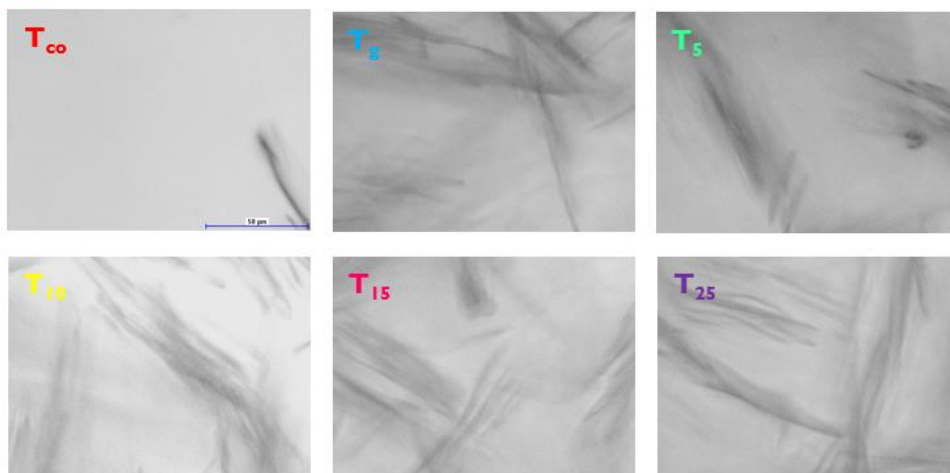

Figure 4.27 Microphotographs of EP sample during Time cure test (Figure 4.26) at different temperature levels (control bar is 50μm).

As far as the flow behaviour of policosanol organogels is concerned, the viscosity curve showed the same trend for all investigated samples during SRTRTs, as can be seen from Figures 4.28, 4.30 and 4.32. At high temperature ($T>T_{co,s}$) viscosity increased with decreasing temperature only because of kinetic effects. When the onset of crystallisation was reached ($T=T_{co,s}$) a sudden change in the viscosity curve slope occurred. At lower temperature ($T<T_{co,s}$), a plateau in the viscosity values was observed. It is worth noticing

that for further reduction in temperature ($T<T_{25}$) viscosity tended to decrease, probably because the applied shear rate caused a partial breakage or slippage of the crystalline network structure.

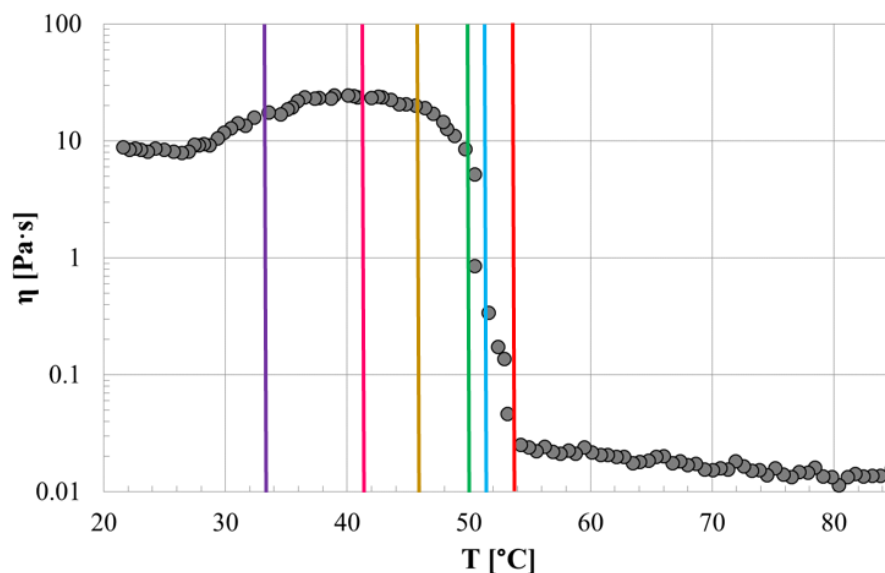**Figure 4.28 SRTRT at 1s⁻¹ for OP10 sample. Coloured lines correspond to the different microphotographs shown in Figure 4.29.**

Figure 4.29 Microphotographs of OP10 sample during SRTRT (at 1s⁻¹) at different temperature levels (control bar corresponds to 50μm).

Figure 4.30 SRTRT at 1s⁻¹ for GP sample. Coloured lines correspond to the different microphotographs shown in Figure 4.31.

Figure 4.31 Microphotographs of GP sample during SRTRT (at 1s⁻¹) at different temperature levels (control bar corresponds to 50μm).

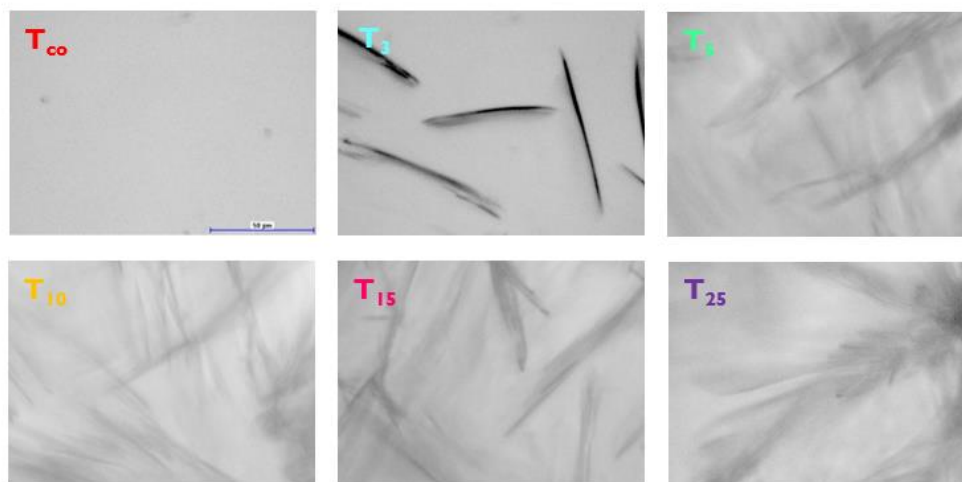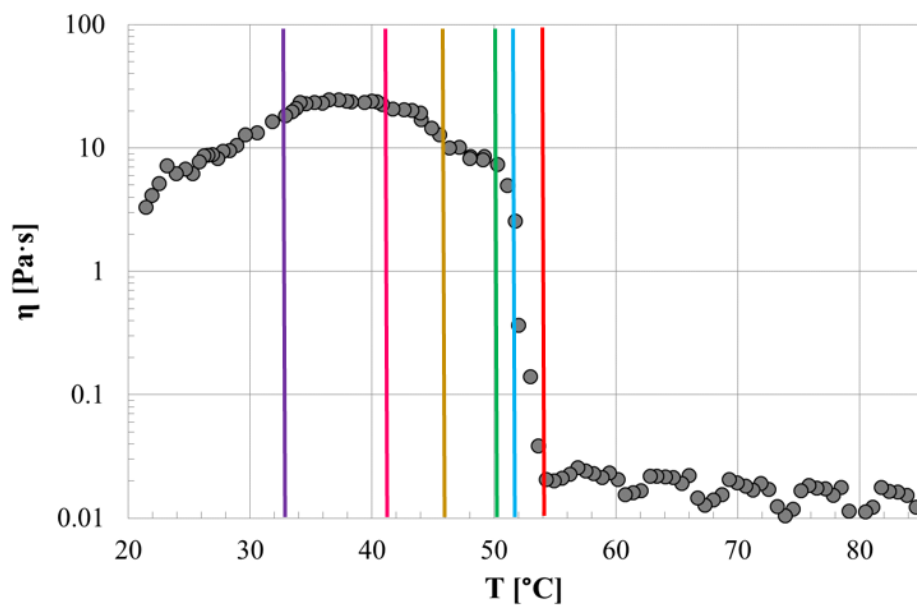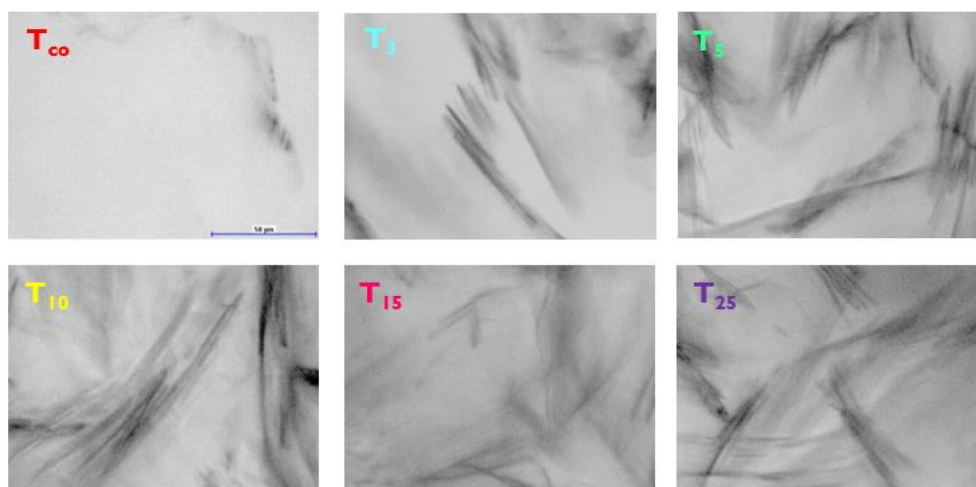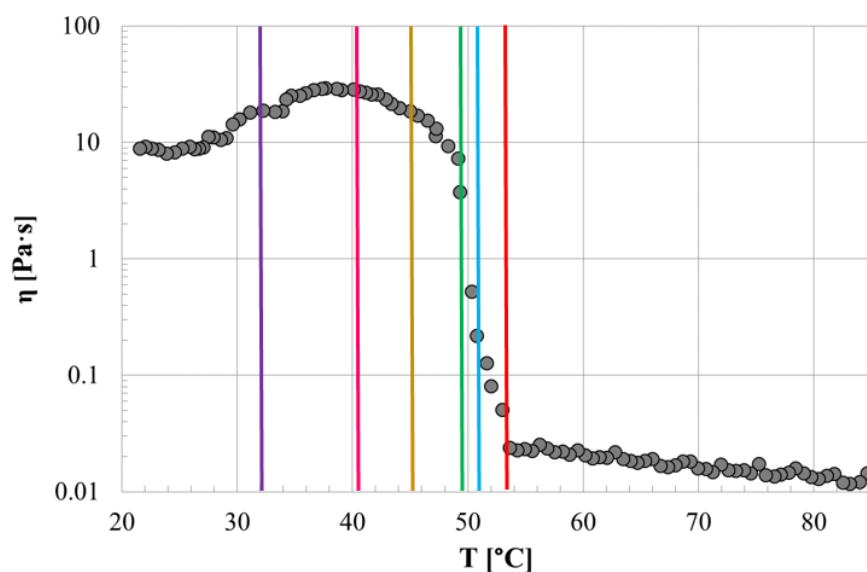**Figure 4.32 SRTRT at 1s⁻¹ for EP sample. Coloured lines correspond to the different microphotographs shown in Figure 4.33.**
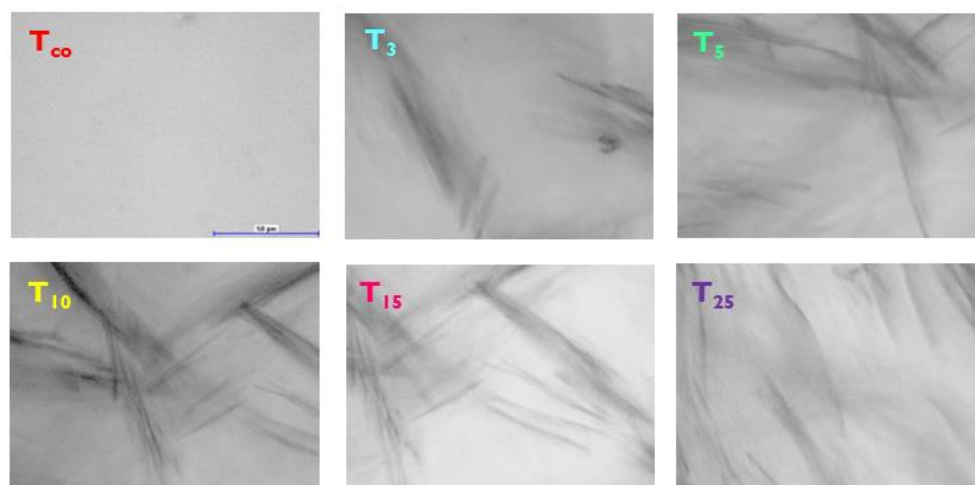
Figure 4.33 Microphotographs of EP sample during SRTRT (at 1s⁻¹) at different temperature levels (control bar corresponds to 50μm).

As already observed during oscillatory measurements, small and random crystalline area formed at $T=T_{co}$. At slightly lower temperature, after a narrow transition region, viscosity tended to reach a plateau value, indicating that crystallisation phenomena were very fast. In fact, images at $T=T_3$ and $T=T_5$ show the formation of long aggregates of fibre-like crystals. At lower temperature ($T_5 \leq T \leq T_{15}$), aggregates seem to grow and interact among each other, resulting in the formation of an interconnected fibrillar network

structure. At even lower temperature ($T=T_{25}$), the effect of the applied shear rate seems to be more evident. The crystalline structure appeared more rarefied, especially for EP and OP10 samples. Nevertheless, it is worth noticing that no significant differences can be appreciated in the morphology of crystalline aggregates of policosanol organogels produced with different vegetable oils.

In agreement with results obtained from optical and rheological characterisation, DSC thermograms and FT-IR spectra of policosanol organogels containing different vegetable oils did not show significant differences (see Figures 4.34 and 4.35, respectively). Only small differences can be detected in the shape of the crystallisation peak (Figure 4.34); however, all investigated samples exhibited a single peak with a shoulder. This behaviour has been already discussed in the previous sections for sample OP6 (Figure 4.9, Paragraph 4.3.2.1).
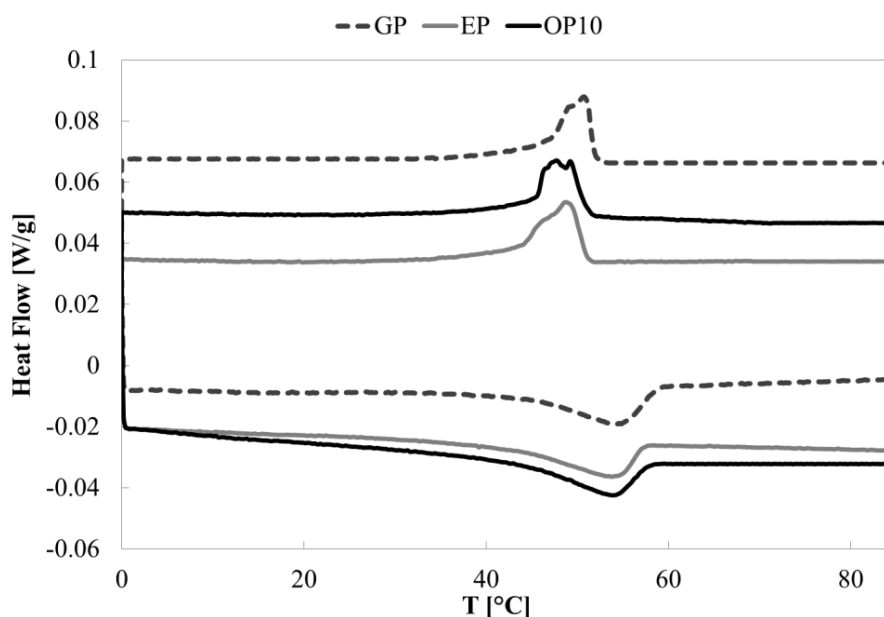
Figure 4.34 DSC thermograms for GP, EP and OP10 samples.

FT-IR spectra were recorded at room temperature immediately after gel formation ($t=t_0$, Figure 4.35) and after one week of storage at 25°C ($t=1week$, Figure 4.36). Only after one week, a very small peak in the low-energy region can be observed in GP, EP and OP10 spectra, probably indicating the formation of weak hydrogen bonds upon aging.
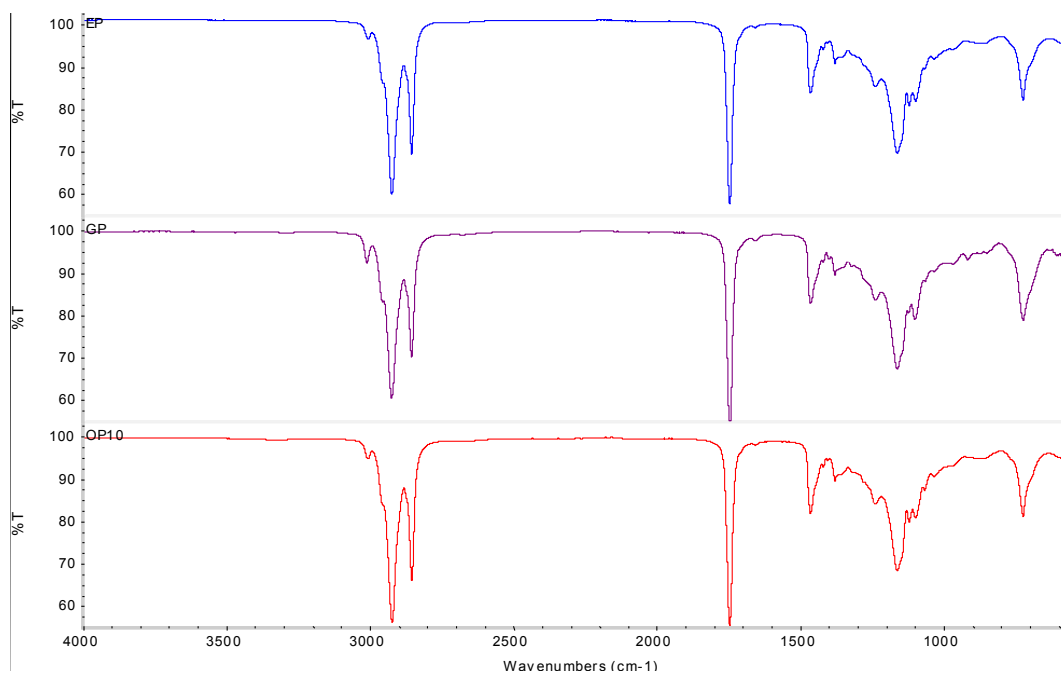
Figure 4.35 FT-IR spectra at *t=t₀* for EP (blue line), GP (purple line) and OP10 (red line) samples.
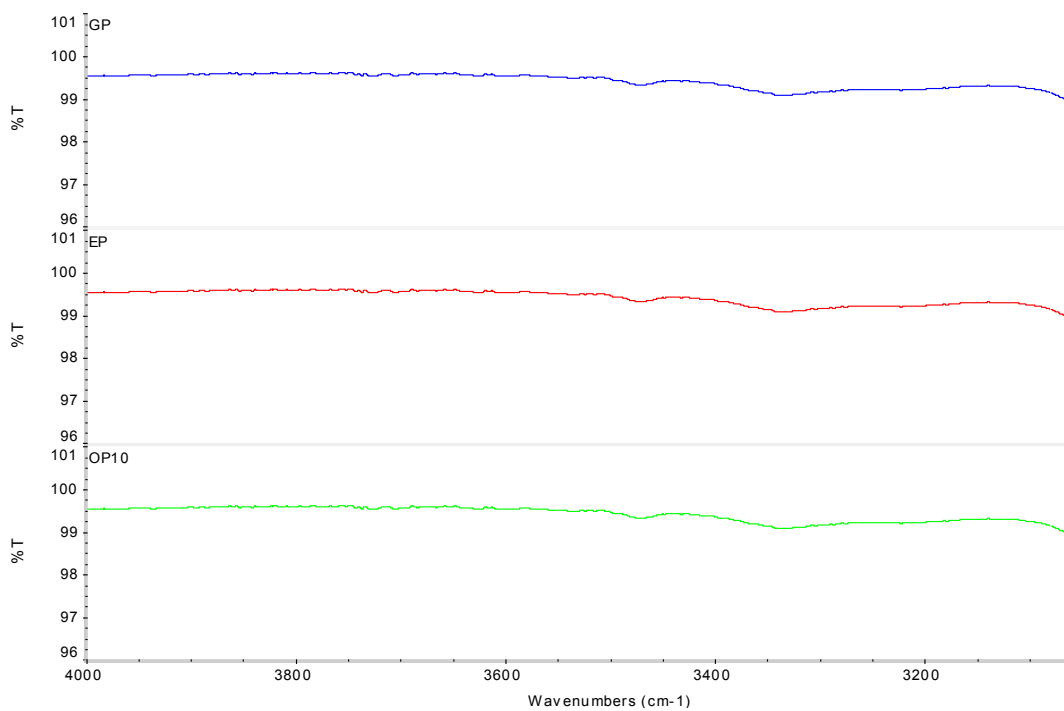
Figure 4.36 FT-IR spectra in the low-energy region at *t=1week* for GP (blue line), EP (red line) and OP10 (green line) samples.

4.3.7 Thermo-rheological properties of mixtures of organogelators

After a complete characterisation of both monoglycerides/olive oil and policosanol/olive oil organogels, organogels produced with mixtures of policosanol and glyceryl stearate were studied. Results obtained in terms of T_{co} are listed in Table 4.8 and shown in Figure 4.37.

Sample ID	T_{co} [°C]
OP13	55.8±0.4
OP14	60.8±0.3
OP15	62.0±0.7
OP16	65.1±0.7
OG1	27.0±0.1
OG2	30.0±0.1
OG3	36.0±0.3
OG4	37.5±0.1
OG5	40.3±0.4
OGP1	46.3±1.0
OGP2	47.5±0.1
OGP3	54.1±0.1
OGP4	61.5±0.7
OGP5	65.3±1.0

Table 4.8 T_{co} values for OP, OG and OGP samples.
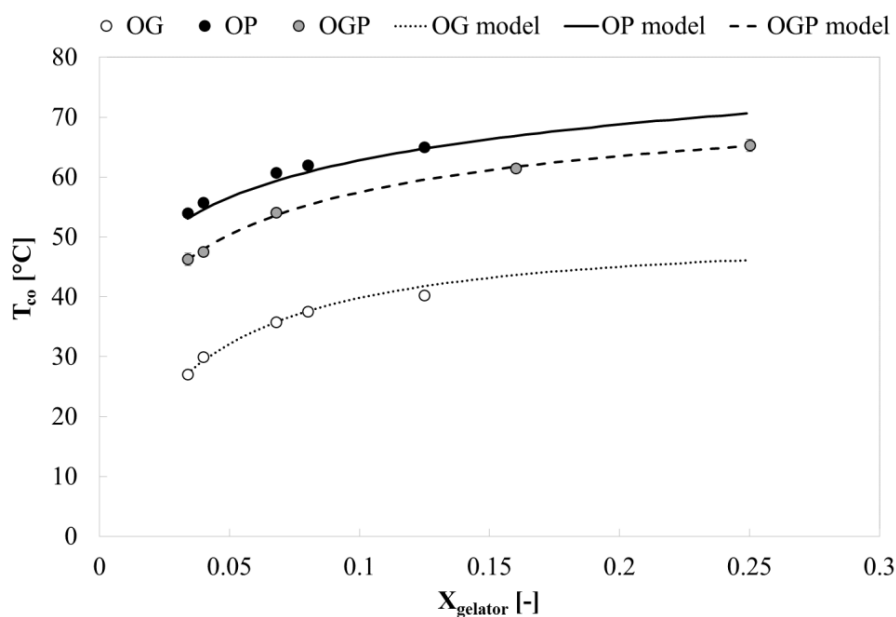
Figure 4.37 T_{co} **as a function of gelator fraction and data fitting with modified fractal model (Eq. 4.3.2).**

Comparing results obtained for pure organogelators, it can be concluded that policosanol is stronger than gyceryl stearate, in fact, the fraction of organogelator being equal, policosanol showed higher T_{co} and G^* values. From T_{co} values reported in Table 4.3 and 4.8, it can be deduced that the temperature of crystallisation onset of each mixture is very close to the value calculated for a policosanol organogel containing the same amount of policosanol that the mixture contains. As an example, samples OGP4 and OP15 were both produced with a policosanol mass fraction of 0.08 and the corresponding values of T_{co} are 61.5±0.7°C and 62.0±0.7°C, respectively. Therefore, it can be concluded that, even though the mixtures were produced with a ratio between policosanol and glyceryl stearate of 1, thermo-rheological properties of mixtures of organogelators were more similar to those of the strongest organogelator within the mixture, that is, policosanol.

A similar result was also obtained applying the fractal model, with the elastic modulus G' and the model curve of mixtures OGP more similar to those of policosanol organogels OP, as shown in Figure 4.38.

Figure 4.38 Application of fractal model at T_{15} for OP, OG and OGP samples.

FT-IR analysis evidenced the presence of weak intermolecular hydrogen bonds, owing to the presence of glyceryl stearate within the mixture (Figure 4.39).

Figure 4.39 FT-IR spectra for OP13 (blue line), OG2 (purple line) and OGP2 (red line) samples.

Conclusions

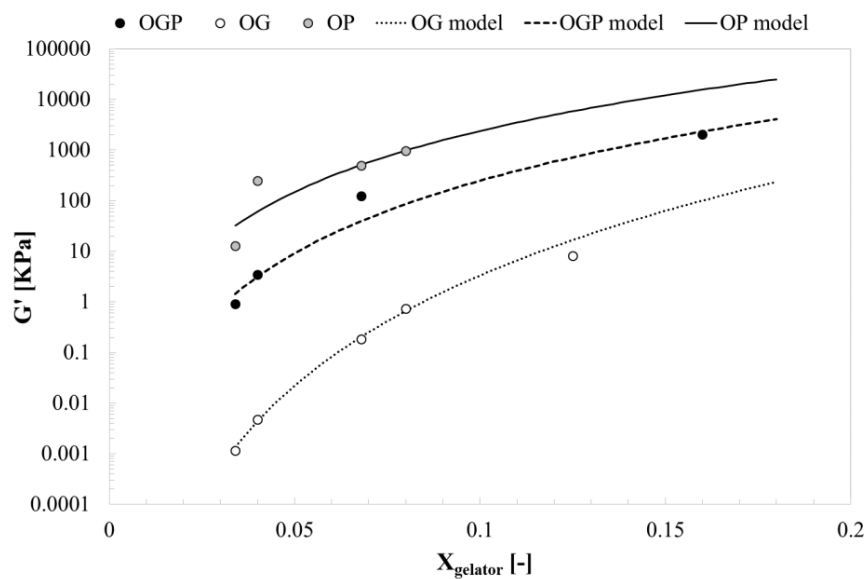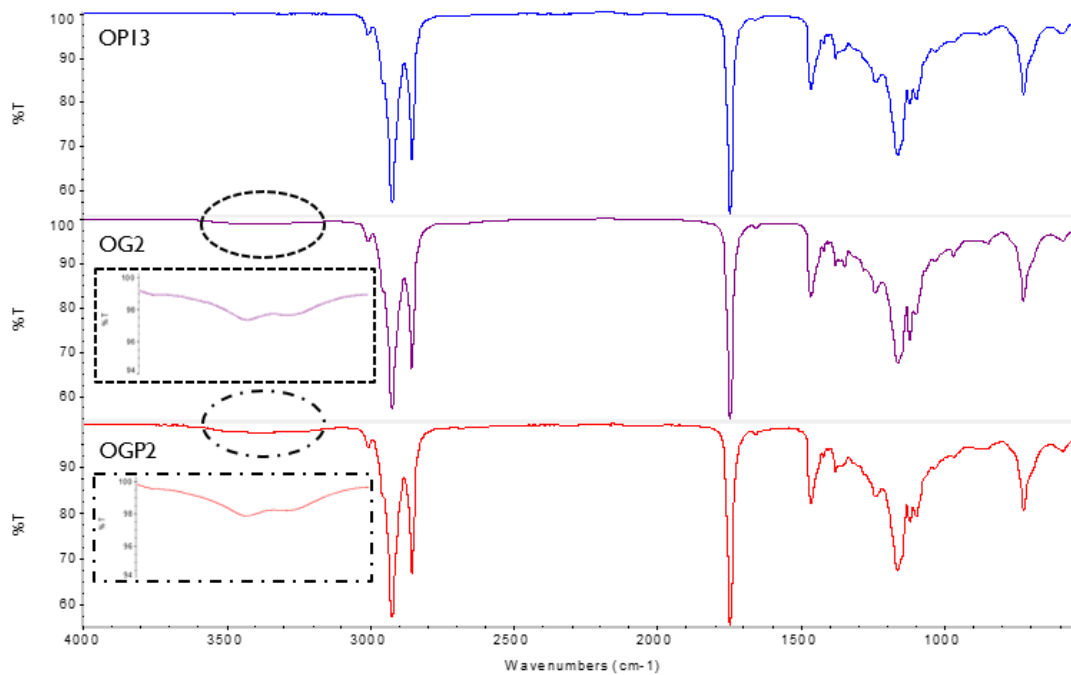Organogels based on virgin olive oil and policosanol, an edible mixture of primary fatty alcohols, were prepared and investigated by using rheological, thermal and spectroscopic methods. The aim was the determination of both mechanical and structural properties. In addition, the phase/mechanical transition temperatures of the investigated systems were estimated.

Rheological measurements evidenced a relevant capability of policosanol to structure olive oil even at low concentrations; in fact, a mass faction as low as 0.001 was able to crystallise oil, whereas a faction ranging between 0.003 and 0.005 was required for its gelation. Also Frequency sweep tests at room temperature evidenced a strong gel behaviour of "cold" organogels, for policosanol mass fractions larger than the critical threshold of 0.005. DSC analysis showed a different behaviour for samples prepared at different policosanol concentrations, with a more complex trend for high policosanol fractions added to the systems. This behaviour was associated with potential polymorphic transitions more evident at high organogelator concentrations. FT-IR spectra in the low-energy region evidenced the formation of very weak hydrogen bonds only at high policosanol fractions and organogel formation was found to be mainly due to van der Waals interactions among organogelator molecules.

The SFC of the investigated samples was measured by NMR spectroscopy at different temperatures and it was found to be directly proportional to the organogelator mass fraction, at low temperatures. Then, the volume fraction of solids at a fixed distance from the onset of crystallisation was calculated and related to rheological properties by using a fractal model. The strength of the links among the aggregates within the network was found to be very high and it increased at decreasing temperature, whereas the fractal dimension remained constant.

Moreover, an equation qualitatively similar to the modified fractal model was proposed to fit the onset of crystallisation values as a function of the organogelator fraction. An empirical equation based on the fractal model was also proposed to relate the average structure development rate (*SDr*) estimated from rheological analysis to the organogelator fraction. On the contrary, the average rate of SFC increase (*SFCr*) was found to be directly proportional to policosanol fraction.

After one week of storage, DSC thermograms and FT-IR spectra suggested that slight differences occurred upon aging, probably with the formation of more stable polymorphs, whereas rheological properties remained almost constant.

The effect of the solvent on the rheological (both oscillatory and flow) and structural properties of policosanol organogels was also investigated. The botanical source and the kind of vegetable oil used as the solvent, did not seem to affect the morphology of crystalline aggregates in a significant way and the final mechanical properties of policosanol organogels.

Finally, mixtures of organogelators in olive oil were studied, as complex systems for both food and cosmetic potential uses. It was found that the thermo-rheological properties of organogels containing mixtures of organogelators were more similar to those of the strongest organogelator within the mixture.

References

[1] Schaink, H.M., van Malssen, K.F., Morgado-Alves, S., Kalnin, D., and E. van der Linden, *Crystal network for edible oil organogels: Possibilities and limitations of the fatty acid and fatty alcohol systems*, Food Research International, 2007. 40: p. 1185–1193.

[2] Gandolfo, F.G., Bot, A., and E., Flöter, *Structuring of Edible Oils by Long-Chain FA, Fatty Alcohols, and Their Mixtures*, Journal of the American Oil Chemists' Society, 2004. 81: p. 1-6.

[3] Daniel, J., and R., Rajasekharan, *Organogelation of Plant Oils and Hydrocarbons by Long-Chain Saturated FA, Fatty Alcohols, Wax Esters, and Dicarboxylic Acids*, Journal of the American Oil Chemists' Society, 2003. 80: p. 417-421.

[4] Co, E.D., and A.G., Marangoni, *Organogels: An Alternative Edible Oil-Structuring Method*, Journal of the American Chemical Society, 2012. 89: p. 749-780.

[5] Blake, A.I., Co, E.D., and A.G., Marangoni, Structure and Physical Properties of Plant Wax Crystal Networks and Their Relationship to Oil Binding Capacity, Journal of the American Oil Chemists' Society, 2014. 91: p. 885-903.

[6] Toro-Vazquez, J. F., Morales-Rueda, J. A., Dibildox-Alvarado, E., Charó-Alonso, M., Alonzo-Macias, M., and M.M., González-Chávez, *Thermal and textural properties of organogels developed by candelilla wax in safflower oil*, Journal of the American Oil Chemists' Society, 2007. 84: p. 989–1000.

[7] Francini-Pesenti, F., Brocadello, F., Beltramolli, D., Nardi, M., and L., Caregaro, *Sugar cane policosanol failed to lower plasma cholesterol in primitive, diet-resistant hypercholesterolaemia: A double blind, controlled study*, Complementary Therapies in Medicine, 2008. 16: p. 61–65.

[8] Irmak, S., Dunford, N. T., and J., Milligan, *Policosanol contents of beeswax, sugar cane and wheat extracts*, Food Chemistry, 2006. 95: p. 312–318.

[9] Xu, Z., Fitz, E., Riediger, N., and M.H., Moghadasian, *Dietary octacosanol reduces plasma triacylglycerol levels but not atherogenesis in apolipoprotein E-knockout mice*, Nutrition Research, 2007. 27: p. 212–217.

[10] Varady, K.A., Wang, Y., and P.J., Jones, *Role of policosanols in the prevention and treatment of cardiovascular disease*, Nutrition Reviews, 2003. 61: p. 376-383.

[11] Menendez, R., Amor, A.M., Gonzalez, R.M., Fraga, V., and R., Mas, *Effect of policosanol on the hepatic cholesterol biosynthesis of normocholesterolemic* rats, Biological Research 1996. 29: p. 253-257.

[12] Kabir, Y., and S., Kimura, *Biodistribution and metabolism of orally administered octacosanol in rats*, Annals of Nutrition and Metabolism, 1993. 37: p. 33-38.

[13] Taylor, J.C., Rapport, L., and G.B., Lockwood, *Octacosanol in human health*, Nutrition, 2003. 19: p. 192-195.

[14] Lupi, F.R., Gabriele, D., Facciolo, D., Baldino, N., Seta, L., de Cindio, B., *Effect of organogelator and fat source on rheological properties of olive oil-based organogels*, Food Research International, 2012. 46: p. 177–184.

[15] Lopes da Silva, J.A., Gonçalves, M.P., and M. A., Rao, *Kinetics and thermal behaviour of the structure formation process in HMP/sucrose gelation*, International Journal of Biological Macromolecules, 1995. 17: p. 25-32.

[16] Toro-Vazquez, J.F., Morales-Rueda, J.A., Dibildox-Alvarado, E., Charó-Alonso, M., Alonzo-Macias, M., and M.M., González-Chávez, *Thermal and textural properties of organogels developed by candelilla wax in safflower oil*, Journal of the American Oil Chemists' Society, 2007. 84: p. 989–1000.

[17] Marangoni, A.G., and D., Rousseau, *The Influence of Chemical Interesterification on the Physicochemical Properties of Complex Fat Systems. 3. Rheology and Fractality of the Crystal Network*, Journal of the American Oil Chemists' Society, 1998. 75: p. 1633-1636.

[18] Tang, D., and A.G., Marangoni, *Modeling the rheological properties and structure of colloidal fat crystal networks*, Trends in Food Science & Technology, 2007. 18: p. 474-483.

[19] Lopes, I.M.G. and M.G., Bernardo-Gil, *Characterisation of acorn oils extracted by hexane and by supercritical carbon dioxide*, European Journal of Lipid Science and Technology, 2005. 107: p. 12–19.

[20] Vintiloiu, A., and J.C., Leroux, *Organogels and their use in drug delivery – A review*. Journal of Controlled Release, 2008. 125: p. 179-192.

[21] de Lucas, A., García, A., Alvarez, A., and I., Gracia, Supercritical extraction of long chain n-alcohols from sugar cane crude wax, Journal of Supercritical Fluids, 2007. 41: p. 267–271.

[22] Pristouri, G., Badeka, A., and M.G., Kontominas, *Effect of packaging material headspace, oxygen and light transmission, temperature and storage time on quality characteristics of extra virgin olive oil*, Food Control, 2010. 21: p. 412–418.

[23] Lopes da Silva, J.A., and M.P., Gocalves, *Rheological study into the ageing process of high methoxyl pectin/sucrose aqueous gels*, Carbohydrate Polymers, 1994. 24: p. 235-245.

[24] Rønholt, S., Kirkensgaard, J.J.K., Pedersen, T. B., Mortensen, K., and J.C., Knudsen, *Polymorphism, microstructure and rheology of butter. Effects of cream heat treatment*, Food Chemistry, 2012. 135: p. 1730–1739.

[25] Vithanage, C.R., Grimson, M.J., and B.G., Smith, *The effect of temperature on the rheology of butter, a spreadable blend and spreads*, Journal of Texture Studies, 2009. 40: p. 346–369.

[26] Lupi, F.R., Gabriele, D., de Cindio, B., Sánchez, M.C., and C., Gallegos, *A rheological analysis of structured water-in-olive oil emulsions*, Journal of Food Engineering, 2011. 107: p. 296–303.

[27] Gandolfo, F.G., Bot, A., and E., Flöter, *Phase diagram of mixtures of stearic acid and stearyl alcohol*, Thermochimica Acta, 2003. 404: p. 9-17.

[28] Morales-Rueda, J.A., Dibildox-Alvarado, E., Charó-Alonso, M.A., Weiss, R.G., and J. F., Toro-Vazquez, *Thermo-mechanical properties of candelilla wax and dotriacontane organogels in safflower oil*, European Journal of Lipid Science and Technology, 2009. 111: p. 207–215.

[29] Tozaki, K., Inaba, H., Hayashi, H., Quan, C., Nemoto, N. and T., Kimura, *Phase transitions of n-$C_{32}H_{66}$ measured by means of high resolution and super-sensitive DSC*, Thermochimica Acta, 2003. 397: p. 155–161.

[30] Wentzel, N., and S.T., Milner, *Crystal and rotator phases of n-alkanes: A molecular dynamics study*, The Journal of Chemical Physics, 2010. 132: p. 1-10.

[31] den Adel, R., Heussen, P.C.M., and A., Bot, *Effect of water on self-assembled tubules in β-sitosterol + γ-oryzanol-based organogels*, Journal of Physics: Conference Series, 2010. doi:10.1088/1742-6596/247/1/012025.

[32] Suzuki, M., Nakajima, Y., Yumoto, M., Kimura, M., Shirai, M., and K., Hanabusa, *Effects of Hydrogen Bonding and van der Waals Interactions on Organogelation Using Designed Low-Molecular-Weight Gelators and Gel Formation at Room Temperature*, Langmuir, 2003. 19: p. 8622-8624.

Chapter 5: rheological analysis of structured W/O emulsions as shortening replacers

Abstract

Margarine and shortenings are W/O structured emulsions. The oily phase is commonly structured by the formation of a saturated fat crystalline network, which entraps water droplets. However, it has been demonstrated that the excessive consumption of saturated fats leads to negative effects owing to increased cholesterol levels in the bloodstream. Moreover, it is worth noticing that the structuration and saturation of oils is traditionally achieved by hydrogenation processes, from which unhealthy *trans* fatty acids can be obtained as by-products.

In the present work, the rheological characterisation of olive oil-based W/O emulsions as potential healthy shortening replacers was carried out. According to the results shown in Chapter 3, the structuration of the oily phase was reached by organogelation, using mono-glycerides of fatty acids as the organogelator molecules and cocoa butter as thickening agent. In particular, the effect of cocoa butter on the thermal stability and the rheological properties of the emulsions was investigated. A microstructural characterisation was performed through contrast phase and optical microscopy. Finally, the effect of the storage conditions on the rheological properties was studied.

5.1 Introduction

In general, fat spreads (butter, margarine or low fat spreads) are water-in-oil (W/O) emulsions, with a fat content of ranging from 80%$_{w/w}$ to 20% $_{w/w}$. The lipid matrix of these emulsions consists of a fat crystalline network [1]. A shell of crystals surrounds the water droplets, preventing them from merging [1, 2]. In fact, the production of shortenings is related to the type of fats and oils used and to the way in which these fats and oils crystallise and form solid networks [3]. Fats have to satisfy both physical functionality and health/nutritional requirements, which are sometimes at odds with each other in terms of the ingredients that are required to deliver specific functionality [3]. The functionality and texture of shortenings are based on the underlying colloidal network of fat crystals that trap

water in this network structure [4]. This fat crystal network (composed of saturated fats) is essential for providing structure to the liquid oil and consequently, without saturated fats, these products could not be formulated [4, 5]. However, the consumption of excessive amounts of saturated fats is considered highly unhealthy and has been found to show negative effects on cholesterol profiles and increase in the incidence of cardiovascular diseases [4, 6]. Many years of epidemiological research have shown that populations consuming diets with high amounts of saturated fatty acids have relatively high levels of serum cholesterol and experience a high prevalence of coronary heart disease [7, 8, 9].

Structuration of liquid vegetable oils is often achieved through catalytic hydrogenation processes, in which the movement of double bonds in the fatty acid carbon chain can lead to the production of *trans* fatty acids as by-products [4]. It has been demonstrated that *trans* fatty acids raise total and LDL cholesterol while lowering HDL cholesterol [10]. *Trans* fatty acids are increasingly the subject of regulation designed to minimise or even eliminate them from the food supply. Accordingly, the food industry must now produce fats with a low or even zero *trans* fatty acid content [6]. Therefore, recently, much research effort has been focused on seeking alternatives to structure liquid oil without the use of saturated and/or *trans* fats, with the aim of formulating soft matter structures with the functionality of fats but with the nutritional profile of liquid oils (low in saturated fats and high in unsaturated fats) [4, 11].

In the following sections, margarine and healthy margarine substitute production will be discussed in further details.

5.1.1 Margarine and shortenings: a state of the art

The term "shortening" refers to the ability of a fat to lubricate, weaken, or shorten the structure of food components, so that they provide desirable textural properties to a food product. As an example, in a baked product, without shortening, gluten and starch particles adhere to each other and give the sensation of hardness and toughness when chewed [3]. In fats such as margarine and shortening, the functional characteristics of natural fat systems have been modified to provide desirable consistency and keeping quality in the final product (baking, confectionery and cooking).

As already mentioned, margarine is a water-in-oil emulsion, containing at least 80%$_\text{w/w}$, often stabilised by a blend of food emulsifiers, lecithin and monoglycerides, and fat crystals [12, 13]. In fact, margarines, as well as butter, whipped cream and ice cream, are

either partially or wholly stabilised by fat crystals present at the water/oil interface [13]. Although the interactions between emulsifiers and fat crystals are not very clear, Garti et al. [12] suggested that fat particles play an important role in the Pickering stabilisation mechanism of the emulsion, whereas emulsifiers are the molecular bridges which facilitate the adsorption of fat crystals at water/oil interface (see Figure 5.1).
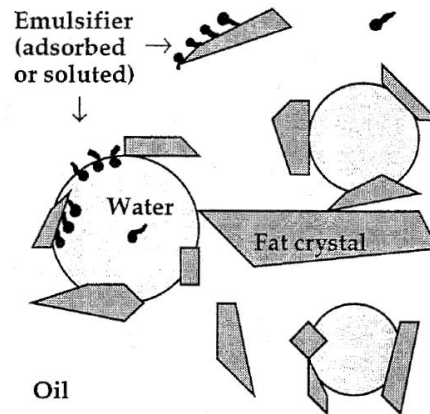

Figure 5.1 Schematic representation of margarine microstructure [12].

The hardness of the fat network and, therefore, of the shortening product is greatly affected by the shape and sizes of crystals and crystal aggregates, which, in turn, are affected by the polymorphic form of fat crystals [3, 14, 15, 16]. Therefore, regarding water-in-oil emulsions, it seems clear that oil phase crystallisation is the most common technique used to increase the hardness of vegetable oils in order to produce shortenings and margarines [17].

The typical method, currently used in food processing industries is the partial hydrogenation of vegetable oils [3]. In 1911 Procter and Gamble Company introduced its hydrogenated shortening, "Crisco", on the market. Since then, hydrogenation was largely employed by all the manufacturers of shortenings or margarine [3]. Hydrogenation is a saturation process: hydrogen is added to the double bonds of unsaturated fatty acids, transforming them to saturated fatty acids, which in turn converts oil into a solid-like fat [3]. The chemical reaction is applied to food industries as partial hydrogenation, by heating vegetable oils in the presence of a metal catalyst and hydrogen. The process of partial hydrogenation produces incomplete saturation of the double bonds, in which some double bonds remain but may move in their positions on the carbon chain, and produces several geometrical and positional isomers, including the above mentioned *trans* fatty acids.

Through hydrogenation, oils such as soybean, safflower, and cottonseed oil, which are rich in unsaturated fatty acids, are converted into margarines and vegetable shortenings [7]. Catalytic hydrogenation is followed by an emulsification step at 100°F (almost 38°C). Then, the emulsion is sent to a "Votator", where it is cooled within two minutes at 45-50°F (almost 7-10°C) by using ammonia at its boiling point. Finally, the emulsion is sent to a second vat, where it continues to crystallise statically [18]. The aim of the last two steps is to obtain a large number of α crystals (quenching step) and convert them into the more stable β' polymorph (static crystallisation) [18].

In fact, for foodstuffs such as margarine, the oil phase should crystallise in the β' form [17, 19]. This polymorphic form possesses smooth mouth-feel, gives hardness to the final margarine and, in addition, traps a large amount of liquid oil because of its spherulitic nature [18, 20, 21]. Furthermore, the β' form is relevant for the production of dough including margarine: β' crystals in dough provide many small bubbles of incorporated air and greater loaf volume, because of their tight lattices [22, 23].

Further innovations in the techniques of margarine processing such as bleaching, deodorisation, fractionation, winterisation, and refining of raw oils and fats, together with the mechanisation of the processing industry, have increased the ability of the industry to meet specific functional and nutritional requirements [3].

5.1.2 Margarine replacers

In recent years, the problem of substituting *trans* fatty acids in margarine and, therefore, the formulation of healthy margarine alternatives has become crucial. Jahanavial [24] proposed the preparation of a healthy margarine mixing at high temperature vegetable oils and hard fats (such as cocoa butter) and using phospholipids as stabilisers.

The first commercial development of a healthy shortening made from a combination of butterfat and vegetable oil was a product named Bregott, in Sweden, containing around $65\%_{w/w}$ milk fat and $15\%_{w/w}$ soybean oil. The manufacturing technique was the same as butter: the cream was pasteurised followed by cooling and oil was mixed in the churn or continuously injected before churning in a continuous butter machine [7].

Among vegetable oils, olive oil, one of the main components of the Mediterranean diet, is widely recognised as healthy and fine food. According to Blanco Muñoz [7], the formulation of an olive-based fat spread could help not only to reduce LDL cholesterol, but also not to raise the ratio of LDL/HDL cholesterol as *trans* fatty acids do. One of the first

companies in Europe that produced a fat spread containing olive oil was Benecol [7]. Other margarines containing olive oil were then introduced to the market; however, they contained low amounts of olive oil (usually no more than 20%$_{w/w}$) [7].

Recently, Patel et al. [4] formulated new structured W/O emulsions, containing shellac/rapeseed oil organogel as continuous structured oily phase. The authors demonstrated that shellac had excellent oleogelation properties (at concentrations as low as 2%$_{w/w}$), therefore they used the extensive network of shellac crystallites as continuous phase to create emulsifier-free, structured W/O emulsions. The authors investigated the ability of shellac oleogels to form W/O emulsions by increasing the ratio between the water and the fat phase while keeping the concentration of shellac fixed at 5%$_{w/w}$ of the total emulsion. Emulsifier-free emulsions (with up to 60%$_{w/w}$ water) that were stable for over 4 months were successfully prepared.

5.1.2.1 Structured emulsions with cocoa butter

The selection of a substitute for *trans* fatty acids requires a consideration of both nutritional factors and food functionality factors. From a nutritional point of view, the most favourable fasting lipid profiles are obtained in response to fats rich in *n*-6 polyunsaturated fatty acids or *cis*-mono-unsaturated fatty acids [6]. While these fatty acids can be substitutes for *trans* fatty acids in frying oils they are not adequate substitutes for trans fatty acids in fats for baking and margarine manufacture since a more solid fat is required [6]. It has been demonstrated that stearic acid has a neutral effect on cholesterol levels [25]; hence, cocoa butter, a vegetable fat rich in stearic acid, could be used to formulate healthy *trans* fat-free margarines.

A detailed discussion of cocoa butter polymorphism is reported in Chapter 2. Figure 5.2 shows a complete scheme of cocoa butter isothermal phase transitions [21].
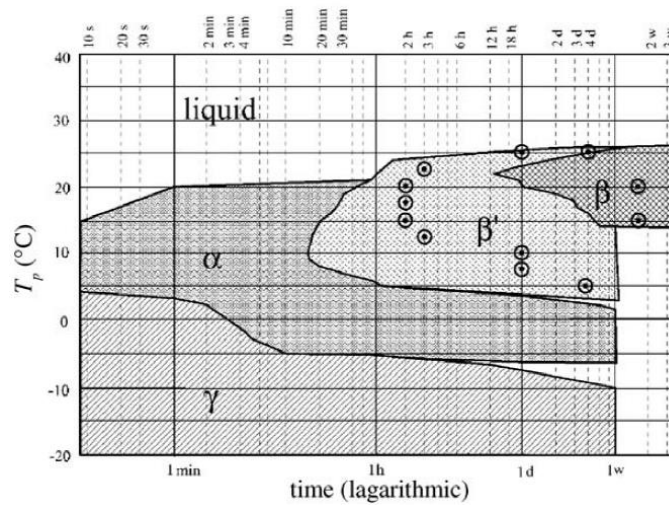
Figure 5.2 Complete isothermal phase transition scheme of cocoa butter under mechanically static conditions [21].

As stated before, the oily phase of margarine should be crystallised in the β' polymorphic form. Nevertheless, Garti et al. [12] showed that α crystals can be obtained through quenching of hydrogenated fats and the final structured W/O emulsions can be stabilised by a mixture of α and β'submicron crystals.

Hindle et al. [26] prepared West African cocoa butter emulsions as model systems for studying droplet collision processes. They also observed that emulsified cocoa butter crystallised in the α form, whereas Campbell et al. [27] observed β crystals in palm oil and lard emulsions. Lopez et al. [28] compared the behaviour of pure milk-fat and emulsified milk-fat. They observed that, in the emulsion, fat nucleated in the α form and later partly converted into the β' form, whereas bulk milk-fat first crystallised as β' and the α form formed later [29].

Norton et al. [19] prepared a W/O cocoa butter emulsion (Figure 5.3) as potential alternative to commercial chocolate, in order to reduce the number of calories in chocolate. For this purpose, cocoa butter within the samples should be in polymorphic form V (β2), which consumers find the most attractive, as it melts between 32 and 34°C. Using a high shear mixer, the authors obtained a stable emulsion with a water content of up to 20%w/w.
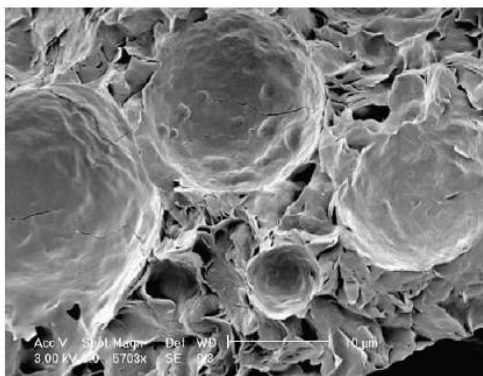
Figure 5.3 Cyro-SEM of a cocoa butter emulsion indicating a continuous fat phase with water droplets dispersed [19].

The aim of the present Chapter is the rheological characterisation of olive oil-based, structured W/O emulsions, as potential margarine substitutes. The structuration of the oily phase was achieved through organogelation, following the results reported in Chapter 3. In particular, the role of cocoa butter as thickening agent was investigated.

Furthermore, polymorphic transitions during ageing and their effect on rheological properties were investigated.

5.2 Materials and methods

5.2.1 Samples ingredients and preparation

W/O emulsions were produced using distilled water 0.1 M NaCl (Carlo Erba Reagents, Italy) as the aqueous phase, whereas the oil phase contained extra virgin olive oil (kindly supplied by Gabro S.r.l., Italy), cocoa butter (Icam S.p.A., Italy) and Myverol 18-04K (Kerry Group, Ireland, referred to as "Myverol" throughout the chapter). The detailed composition of raw materials is reported in Chapter 2.

With the aim of studying the effect of cocoa butter/olive oil (B/O) ratio on the final rheological properties of structured emulsions, samples were prepared at different B/O without changing Myverol and water mass fraction. According to the results shown in Chapter 3, the Myverol fraction was chosen in order to ensure that $T_{co} \approx T_g$ with T_{co} well above room temperature [30]. The analysed samples are listed in Table 5.1.

Sample ID	Oil phase [%$_{w/w}$]	Water [%$_{w/w}$]	B/O [-]
E0B	88	12	0
E10B	88	12	0.13
E20B	88	12	0.31

Table 5.1 Samples ID and composition. The oil phase includes olive oil, cocoa butter and organogelator (Myverol). Myverol mass fraction is maintained constant for all samples, whereas the ratio between cocoa butter and olive oil is varied according to the indicated values.

Emulsions were prepared according to a procedure elsewhere described in the literature [17]. Aqueous and oil phases were obtained separately. Sodium chloride was dissolved in distilled water at room temperature using a magnetic agitator (VELP Scientifica, Italy). The oily phase was prepared adding contemporary cocoa butter and Myverol to the oil, previously warmed up to 70°C in a water bath thermostatically controlled by a plate heater (VELP Scientifica, Italy). The system was mixed continuously using a laboratory stirrer (RW 20, IKA, Germany). After the mixture reached the preparation temperature (70°C), the mixing was prolonged for a further 5 minutes. Then, the oily phase was subjected to a quenching step: the system was poured into a thermostatic cold bath (0°C) and gently stirred until reaching 11°C. Finally, the two phases were emulsified at room temperature adding the water phase to the oily one and using a rotor stator system (Ultra-Turrax T50, IKA, Germany) equipped with a G 45 F dispersing element. All samples were stored at 4°C until tests were performed.

The influence of storage temperature on the stability and rheological properties of sample E20B was investigated. Samples were prepared according to the procedure described above and stored at different conditions. Immediately after preparation, samples were stored at -18°C. Then, after different rest times (see Table 5.2), storage was prolonged at 4°C. Rheological measurements were repeated almost every 24 h during ageing.

Sample ID	Composition	Days of storage at -18°C [d]
E1	E20B	1
E2	E20B	2
E3	E20B	3
E4	E20B	4

Table 5.2 Samples ID and storage period at -18°C.

5.2.2 Rheological characterisation

A controlled strain rheometer ARES-RFS (TA Instruments, USA), equipped with a parallel plate geometry (ϕ=25mm, gap=2±0.1mm) was used for emulsion characterisation. The temperature control (±0.1°C) was guaranteed by a Peltier system acting under the lower plate.

For all samples a rheological characterisation based on Small Amplitude Oscillation Tests (SAOTs) was performed. Time Cure Tests on samples E0B, E10B and E20B were carried out in linear viscoelastic conditions at a constant frequency of 1Hz. Both melting and crystallisation curves were recorded, applying a constant heating/cooling rate of 1°C/min: samples were loaded on the lower plate of the rheometer (previously cooled at the temperature of sample storage, 4°C) and the rheological properties were measured heating the material from 4°C to 50°C and then cooling it from 50°C to 4°C. Preliminary Strain Sweep Tests were carried out at different temperatures during both heating and cooling steps in order to follow potential changes in linear conditions as a function of temperature. For each Strain Sweep Test, the material was heated (heating step) or heated and then cooled (cooling step) to the desired temperature using a thermal ramp of 1°C/min and applying the minimum strain within the instrument limits. Then, Strain Sweep Tests were performed at the desired temperature. Finally, Time Cure Tests were carried out applying different constant strain values in different temperature ranges, in order to guarantee the linear viscoelastic conditions in the investigated temperature range.

The rheological properties of sample E20B upon ageing were further investigated at 25°C performing Frequency Sweep Tests in linear viscoelastic conditions, in the frequency range 0.1-10Hz. The results obtained were analysed applying the "weak gel" model. According to this model [31], many foods can be schematically described as 3-D networks where weak interactions ensure the stability of the structure; hence, from a macroscopic

point of view, they behave as a solid under small deformations while they flow under large stresses owing to weak bonds breakage. From a rheological point of view, in a limited range of frequency (usually 0.1-100Hz), the complex modulus *G** can be expressed as a function of frequency ω as follows:

$$G^*(T, \omega) = \sqrt{G'^2 + G''^2} = A(T) \cdot \omega^{1/z(T)} \tag{5.2.1}$$

where *A* represents the strength of the interactions among interconnected unities, whereas *z* represents the number of interacting rheological unities within the network; hence, it is related to network connectivity.

  Data fitting was performed through Table Curve 2D Software (Jandel Scientific, USA).

5.2.3 Microscopy study

The microstructure of the emulsions was qualitatively investigated through microscopy. A MX500 (MEIJI, Japan) microscope equipped with contrast phase objective 40X was employed for microscopy tests. Using the same instrument, microphotographs in optical microscopy were also recorded. Samples were placed on a glass slide inside a cover imaging chamber (Sigma-Aldrich, USA). Then, the chamber was covered with a cover slide, in order to avoid the direct contact between the sample and the lens.

5.3 Results and discussion

5.3.1 Rheological characterisation of water in olive oil emulsions containing cocoa butter

All the investigated emulsions exhibited similar rheological behaviour during Time Cure Tests. As an example, Figure 5.4 shows dynamic moduli, *G'* and *G''*, and the loss tangent during Time Cure Test for sample E20B. At low temperature, the material was characterised by very high values of both moduli, even though at very low temperature *G''* seemed to increase with increasing temperature, owing to instrument limits when the measurement of highly structured systems is required. The elastic modulus curve initially decreased with increasing temperature with a constant slope, because of kinetic effects, until a critical temperature is reached: at around 21°C the beginning of a "softening" region can be observed, with a sudden decrease of both moduli. The observed decrease can be attributed to the partial melting of the cocoa butter, as will be discussed later in more

detail. At higher temperatures, dynamic moduli remained almost constant and a further decrease was observed at around 43°C. This temperature corresponds to the temperature of crystallisation onset of an olive oil based organogel containing the same amount of Myverol as the oily phase of the emulsion contains. At even higher temperatures, the organogel structure was melted and the emulsion partially destabilised, therefore data (especially for the loss tangent) appeared scattered. Nevertheless, it is worth noticing that the loss tangent values were lower than unity during the whole test (with the exception of a few points at high temperatures); therefore, in the temperature range investigated the structure was not completely destroyed. In fact, the loss tangent being defined as the ratio between G''/G', the moduli crossover (verified at loss tangent equal to unity) is often considered as an indication of the structural change in complex materials [32, 33]. In this case, it can be attributed to a de-structuration temperature of the fat crystals network.

During the cooling step, dynamic moduli initially increased (in the temperature range between 50°C and about 40°C), owing to organogel re-crystallisation, and then remained almost constant in the temperature range investigated. In cold conditions, at a temperature value of about 6°C, a small change in the slope of dynamic moduli curves can be observed, probably due to olive oil crystallisation. Furthermore, from Figure 5.4 it can be noticed that, at the end of the heating and cooling cycle, the material was not able to recover the initial rheological properties, in fact, both moduli curves showed a broad hysteresis.
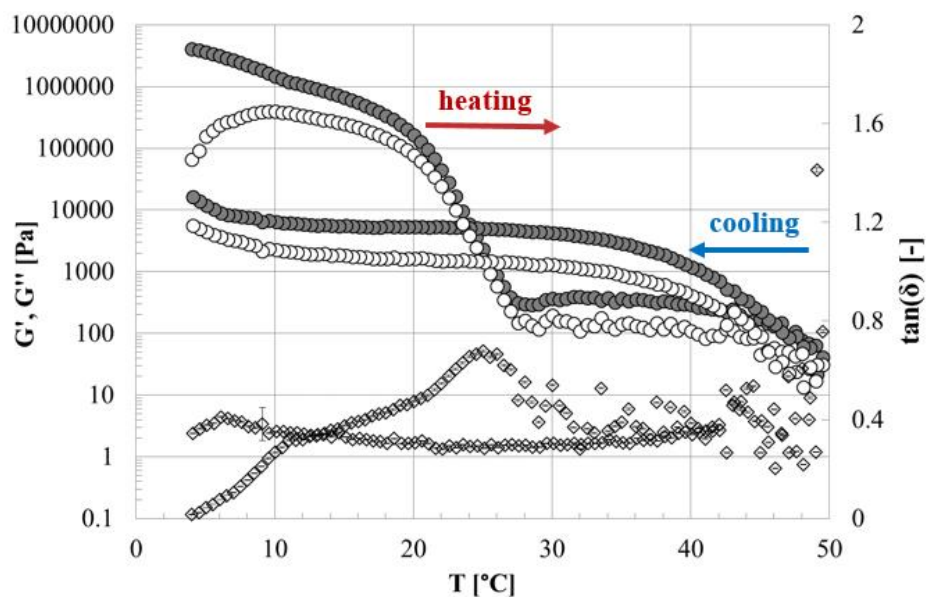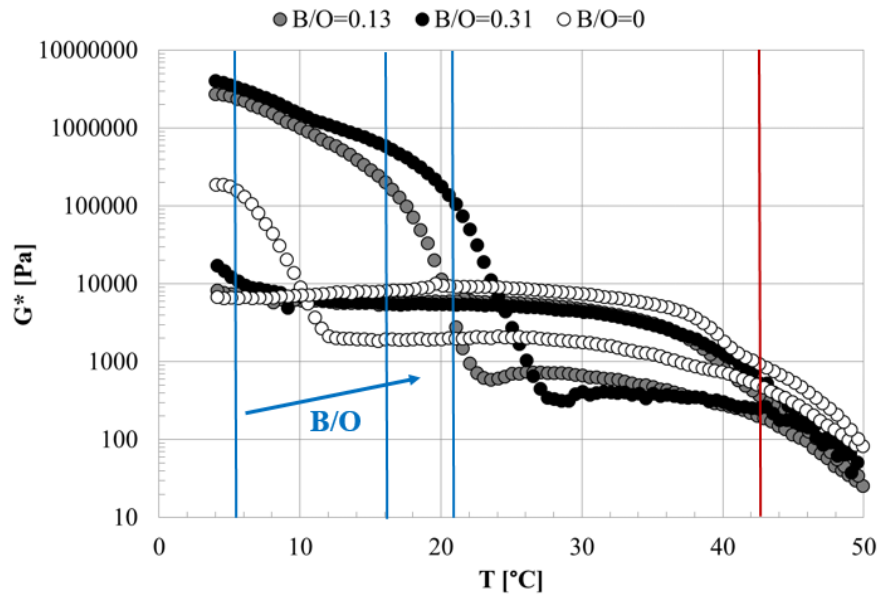

Figure 5.4 Time Cure Test (heating and cooling cycle) on sample E20B.

Figure 5.5 shows the results obtained from Time Cure Tests in terms of complex modulus G^* for samples E0B, E10B and E20B. As stated above, the rheological behaviour of samples produced with different B/O (cocoa butter/olive oil) ratio during the heating and cooling cycle was found to be qualitatively similar. At low temperature, complex modulus values of sample E0B (B/O=0) were dramatically lower than the values exhibited by samples E10B and E20B, indicating that cocoa butter plays an important role as a thickening agent for the oily phase of structured emulsions. The main difference among all the emulsions investigated was the "softening" temperature: the temperature at which the first sudden and sharp decrease in the complex modulus was observed during the heating step. In Figure 5.5 it appears that the softening temperature is shifted towards higher values with increasing the B/O ratio of the emulsion. Therefore, it can be concluded that cocoa butter greatly affected the thermal stability of structured W/O emulsions, which is an important parameter in order to detect the potential uses of the materials investigated as shortening substitutes. On the contrary, the de-structuration temperature (corresponding to the second sharp decrease of the complex modulus) was found to be equal for all emulsions investigated (about 43°C); hence, it was determined only by the organogelator fraction within the oily phase.

The rheological properties of all emulsions during the cooling step did not show any relevant differences.

Figure 5.5 Complex modulus G* during Time Cure Tests (heating and cooling) at different B/O (0, 0.13 and 0.31 corresponding to samples E0B, E10B and E20B, respectively). Blue lines indicate the "softening" temperature, whereas red line indicates the melting temperature of emulsions during the heating step.

The characteristic stability and rheological properties of structured W/O emulsions, such as butter and margarine, are determined by the presence of a fat crystal network in the continuous phase [34, 35, 36]. The fat crystal network is responsible for preventing the water droplets from sedimenting, as well as determining the spreadability of the product [34]. If there are too many fat crystals, the product is firm and not easily spreadable, but if there are too few crystals, the product is soft and collapses under its own weight. Selection of a fat with the appropriate melting characteristics is therefore one of the most important aspects of margarine and spread production [34, 37]. Sample E20B seemed to be the most suitable emulsion investigated as potential shortening substitute, because of its thermal stability and its elastic modulus values (see Figure 5.4) very close to those of commercial margarines (*G'* of margarine at 1Hz and 20°C between $2.5 \cdot 10^4$ and $5 \cdot 10^6$ Pa [38, 17]).

5.3.2 Microscopic analysis

A microscopic analysis was performed with the aim of investigating the microstructure of structured emulsions produced with different B/O ratios. As shown in Figure 5.6, the microphotographs of samples E10B and E20B evidenced the formation of a close packed network, whereas sample E0B exhibited a less densely packed structure. Moreover, the

presence of a more structured network led to the formation of smaller droplets aggregates. In fact, comparing sample E0B to samples E10B and E20B a decrease of droplets average dimension and polydispersity was encountered.
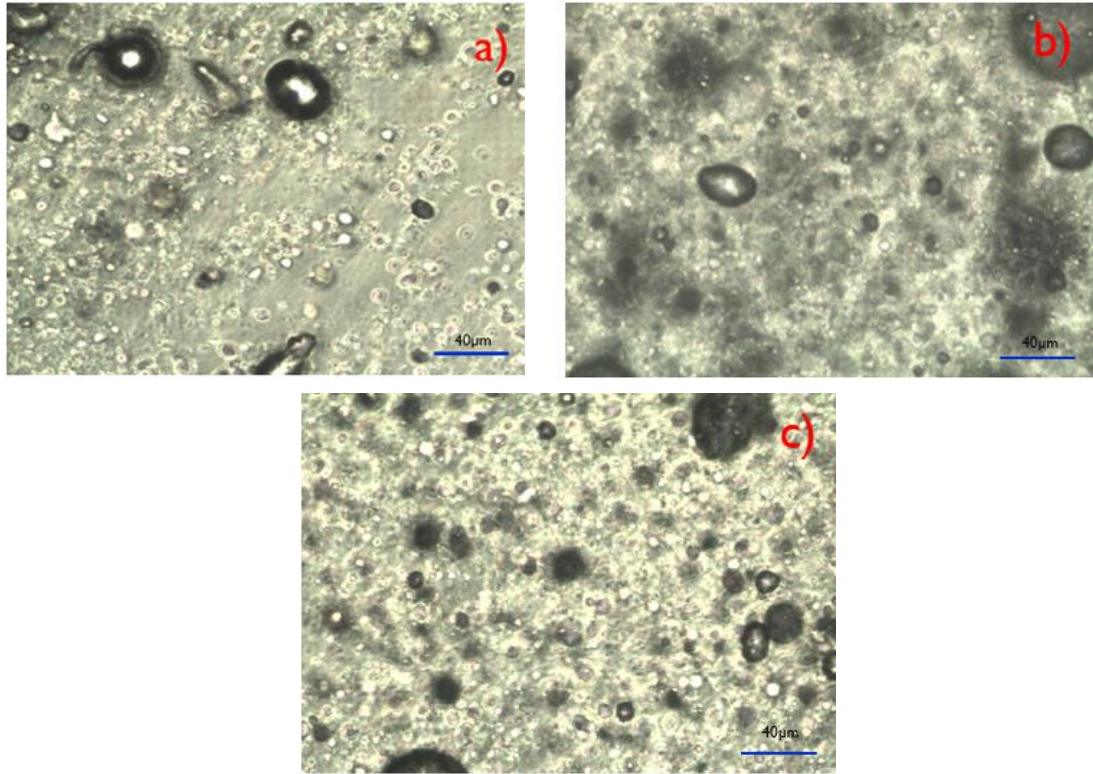
Figure 5.6 Microphotographs of sample E0B (a), E10B (b) and E20B (c) with contrast phase microscopy (control bar is 40μm).

Micro-photographs taken with optical microscopy (Figure 5.7) confirmed the presence of a well-interconnected network structure in samples E10B and E20B, whereas the emulsion produced without cocoa butter (E0B) was characterised by the presence of crystals arranged in a less close-packed network structure. Furthermore, from Figure 5.12 it can be deduced that a larger number of large air bubbles were incorporated during emulsification of sample E0B.
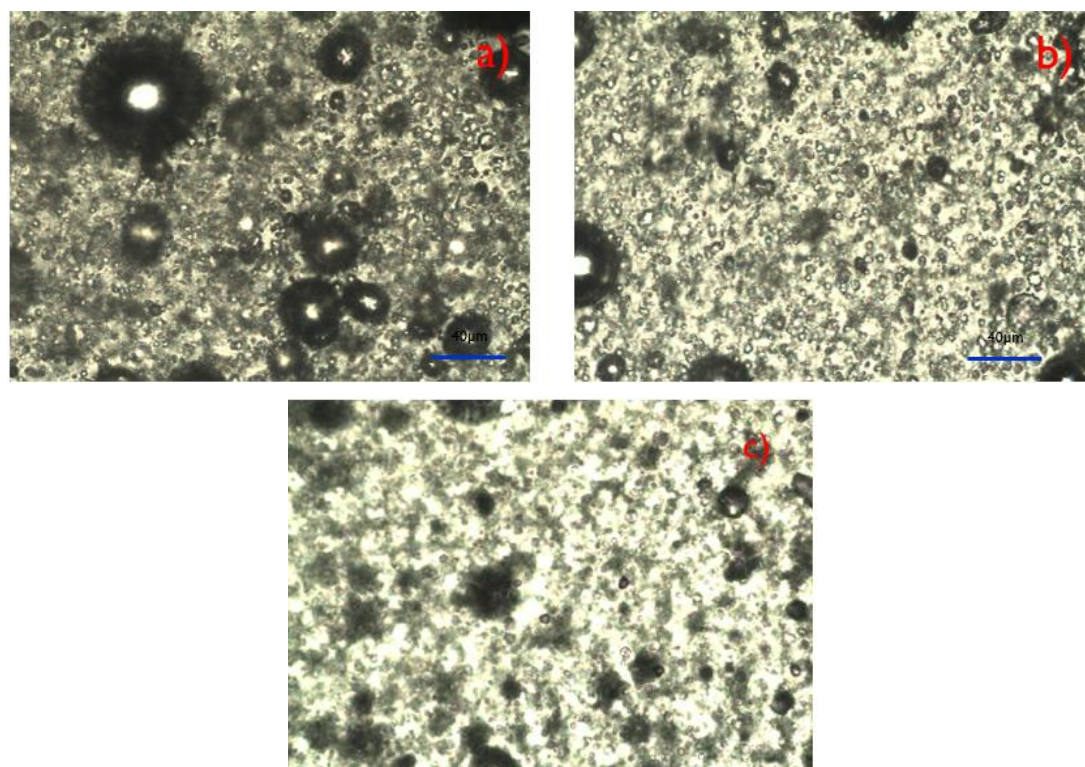
Figure 5.7 Microphotographs of sample E0B (a), E10B (b) and E20B (c) with optical microscopy (control bar is 40μm).

5.3.3 Effect of storage temperature on the rheological properties

The effect of different storage conditions on samples with the same composition of E20B was investigated. Samples E1-E4 were stored at the controlled temperature of -18°C immediately after preparation. Then, after different rest times at -18°C (as reported in Table 5.2), storage was prolonged at 4°C. Frequency Sweep Tests at 25°C were performed on sample E1 (1d of storage at -18°C) every 24h. The results are shown in Figure 5.8. As expected, during storage the sample was always characterised by a solid-like behaviour, the loss tangent being always lower than unity and, therefore, the phase angle smaller than 45°. From Figure 5.8, it can be seen that the complex modulus G^* increased during storage, although after 4d of storage at 4°C a small decrease was observed. On the other hand, the phase angle initially decreased and then remained almost constant upon ageing. This behaviour was confirmed by the application of the Weak Gel model (see Table 5.3 and Figure 5.9). In fact, the parameter A, related to the network strength, increased until 4d of storage at 4°C and then decreased, whereas the coordination number z initially increased and then remained almost constant.
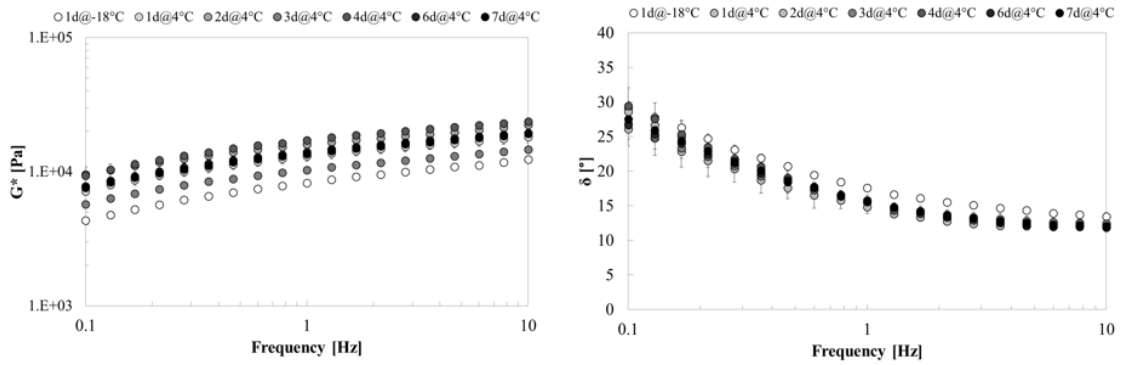
Figure 5.8 Frequency Sweep Tests in terms of G* and phase angle on sample E1 during storage.

Days of storage	A [Pa·s$^{1/z}$]	z [-]
1d@-18°C	7961±78	4.96±0.16
1d@4°C	12535±132	5.79±0.24
2d@4°C	15455±111	6.01±0.18
3d@4°C	15923±87	5.64±0.19
4d@4°C	16436±177	5.76±0.24
6d@4°C	13464±137	5.69±0.22
7d@4°C	13098±121	5.60±0.12

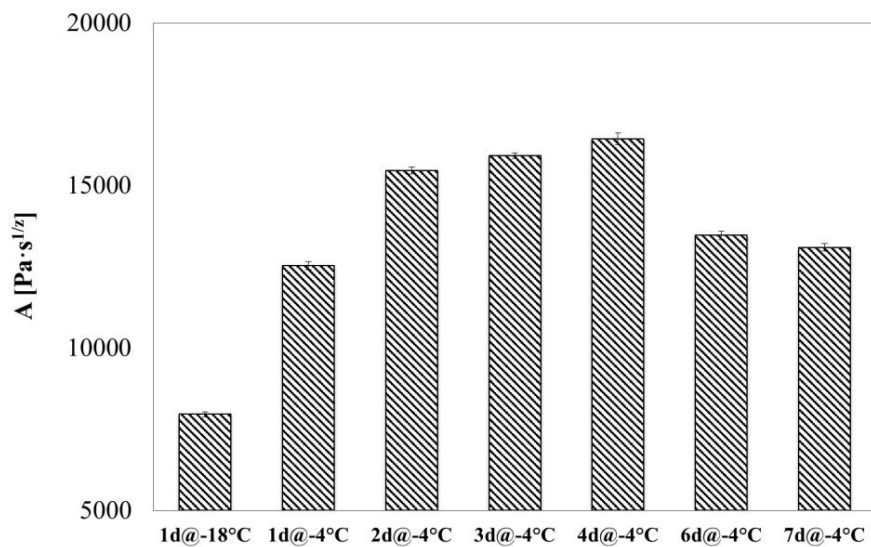**Table 5.3 Weak Gel parameters for sample E1 during storage.**

Figure 5.9 A for sample E1 during storage.

The initial increase of complex modulus and the correspondent decrease of phase angle indicated the progress of network development upon ageing. In particular, interactions among interconnected unities became stronger, as confirmed by the initial increase of the parameter *A* (see Figure 5.9). The differences observed in the rheological properties after 4d of storage at 4°C could be attributed to polymorphic transitions of fat crystals. Polymorphic transitions of fat crystals into β' form are crucial also in the industrial production of margarine. In fact, as mentioned above, the chilling process of margarine is divided into two steps: a first quenching step (to obtain a large number of α crystals) and a second slower step (to transform α crystals into the desired polymorphic form β'). Applying a slow cooling rate, β' crystals could be formed directly from the melt; however, a slow cooling rate leads to the formation of a more disordered network and, therefore, characterised by a smaller elastic modulus [39]. For the system investigated, α crystals can be formed during sample preparation because of the fast cooling rate applied; they are partially destroyed during the emulsification step and formed again because of the following quenching at -18°C. Hence, changes in the rheological properties upon ageing at 4°C could be related to the network re-organisation because of crystal transition into the more stable β' form.

Sample E2 (2d of storage at -18°C) evidenced more fluctuations in the values of the complex modulus during storage, as can be seen in Figure 5.10, whereas the phase angle remained nearly constant. Weak Gel parameters are listed in Table 5.4. The coordination number *z* decreased after 1d of storage at 4°C then increased again, even if small differences were detected. Variations in the network strength *A* were more relevant (see Figure 5.11): as can be appreciated in Figure 5.12, even though sample E2 after 2d of storage at -18°C ($t=t_0$) showed a very high value of *A*, the final value after 7d of storage at 4°C was lower than the value calculated for sample E1.
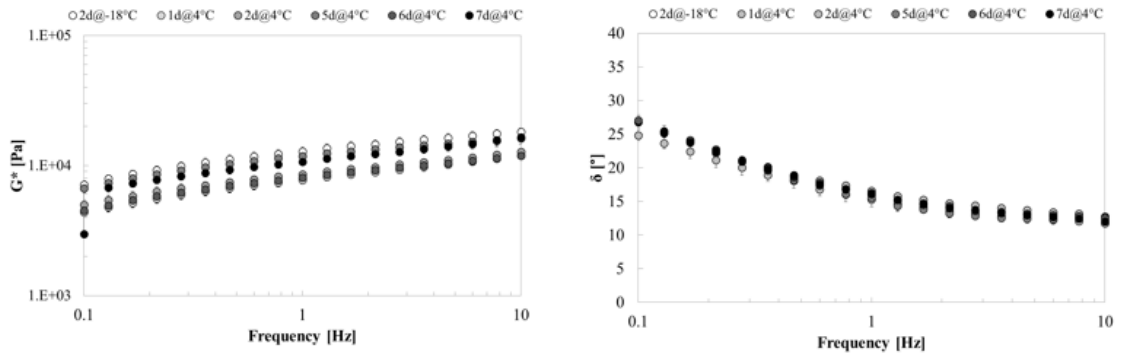
Figure 5.10 Frequency Sweep Tests in terms of G* and phase angle on sample E2 during storage.

Days of storage	A [Pa·s$^{1/z}$]	z [-]
2d@-18°C	12424±113	5.60±0.19
1d@4°C	7576±43	4.98±0.09
2d@4°C	8421±50	5.54±0.13
5d@4°C	11351±114	5.94±0.24
6d@4°C	7879±57	5.36±0.14
7d@4°C	10554±45	5.30±0.08

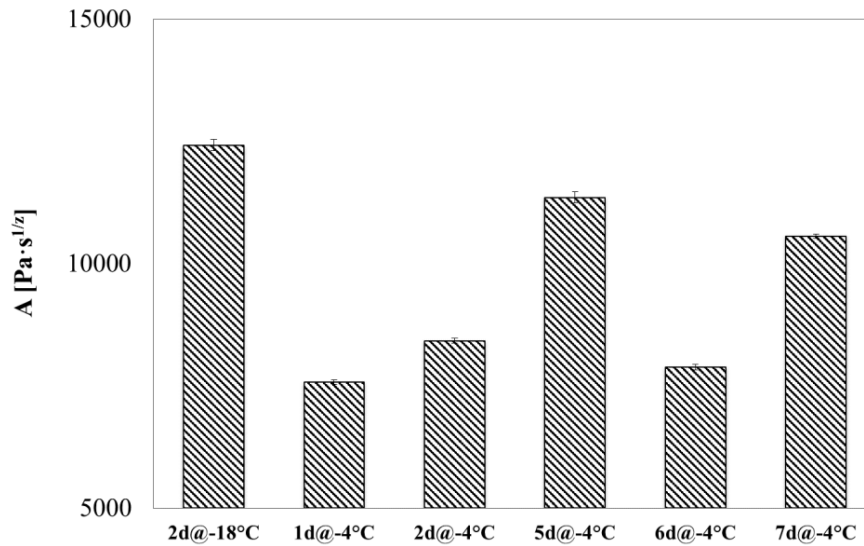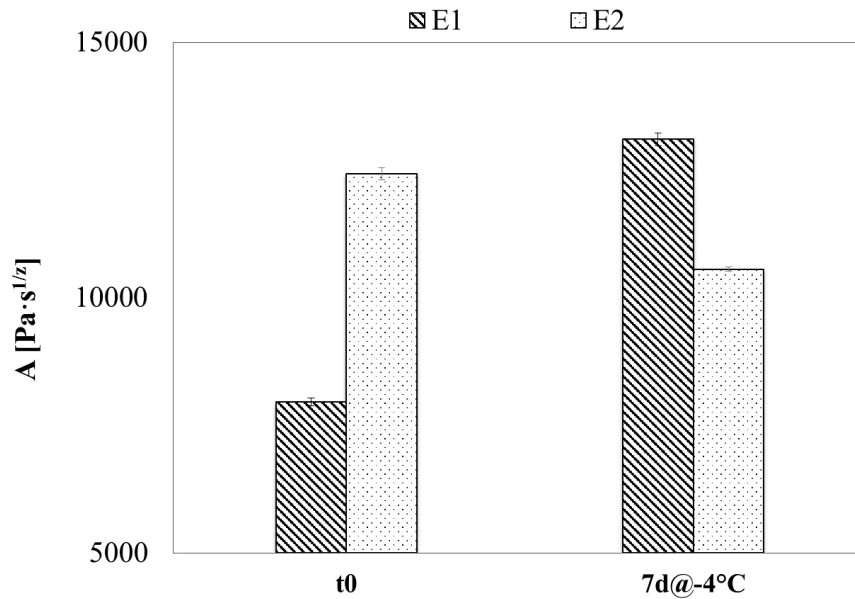**Table 5.4 Weak Gel parameters for sample E2 during storage.**

Figure 5.11 A for sample E2 during storage.

Figure 5.12 A for samples E1 and E2 at *t=t0* (1d@-18°C for E1 and 2d@-18°C for E2) and at *t=7d@-18°C*.

A similar behaviour was observed also for samples E3 (3d at -18°C) and E4 (4d at -18°C), as shown in Figures 5.13 and 5.14. Increasing the time of storage at -18°C, the following polymorphic transitions of fat crystals and the network re-organisation were slower and the final values of the complex modulus were found to be lower than the values measured for samples E1 and E2. Although small differences were detected in the network extension *z* among all investigated samples (see Tables 5.5 and 5.6), differences in the network strength *A* were more significant (lower values for sample E3 and E4 in comparison to samples E1 and E2). Probably, prolonging the time of storage at 4°C, *A* values of samples E3 and E4 would have increased and become similar to those of samples E1 and E2; however, a long period of storage is not suitable for practical and industrial uses.
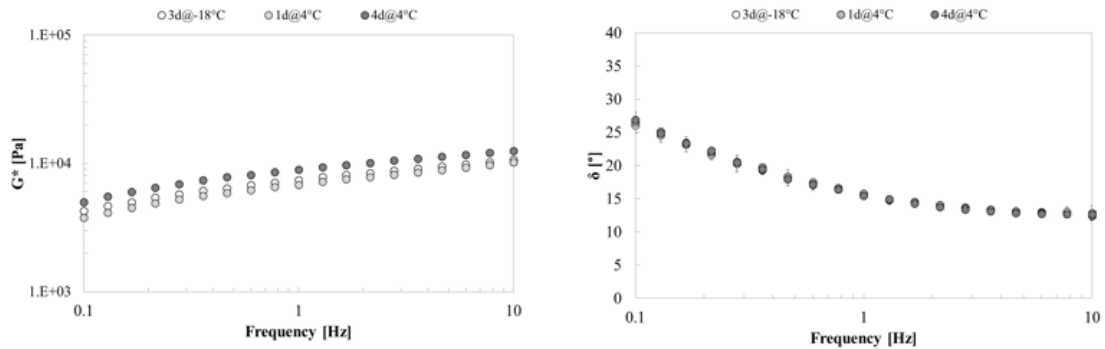
Figure 5.13 Frequency Sweep Tests in terms of G* and phase angle on sample E3 during storage.

Days of storage	A [Pa·s$^{1/z}$]	z [-]
3d@-18°C	7146±56	5.52±0.16
1d@4°C	6678±50	5.31±0.15
4d@4°C	8631±97	5.77±0.21

Table 5.5 Weak Gel parameters for sample E3 during storage.
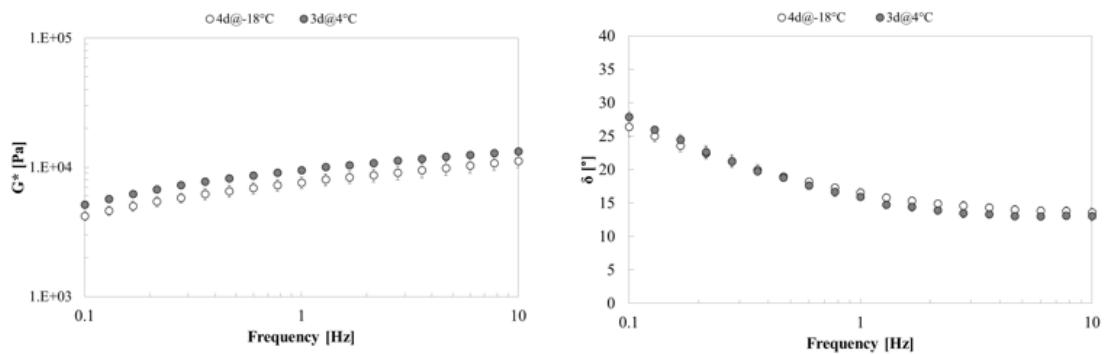
Figure 5.14 Frequency Sweep Tests in terms of G* and phase angle on sample E4 during storage.

Days of storage	A [Pa·s$^{1/z}$]	z [-]
4d@-18°C	7400±59	5.27±0.15
3d@4°C	9163±99	5.56±0.23

Table 5.6 Weak Gel parameters for sample E4 during storage.

Conclusions

Olive oil-based structured emulsions were characterised from a rheological and microstructural point of view in order to investigate their potential use as healthy

shortening substitutes. The effect of cocoa butter on the rheological properties was studied first, showing that it played an important role as thickening agent (the complex modulus of the emulsion increased with increasing cocoa butter fraction). In addition, it was found that cocoa butter increased the thermal stability of W/O emulsions, shifting the "softening" temperature to higher values, whereas the melting temperature was only dependent on the organogelator fraction. Emulsion containing a B/O ratio of 0.31 seemed to be the most suitable for industrial use.

Microphotographs with contrast phase and optical microscopy revealed that structured emulsions containing cocoa butter were characterised by a more densely packed structure in comparison to the sample produced without this natural saturated fat.

Moreover, the optimal storage conditions (for the emulsion with B/O=0.31) were studied. Samples were initially stored at -18°C for different rest times and then storage was prolonged at 4°C. The initial storage at very low temperature for short periods of time (1 or 2d) and the following storage at 4°C for 7-8d yielded the best results in terms of network strength and extension, whereas storage at -18°C for long periods (more than 2d) slowed the desired polymorphic transition into β' crystals and led to the formation of a weaker network.

References

[1] Van Dalen, G., *Determination of the water droplet size distribution of fat spreads using confocal scanning laser microscopy*, Journal of Microscopy, 2002. 208: p. 116–133.

[2] Juriaanse, A.C., and Heertje, I., *Microstructure of shortenings, margarine and butter – a review*, Food Microstructure, 1988. 7: p. 181–188.

[3] Ghotra, B.S., Dyal, S.D., and S.S., Narine, *Lipid shortenings: a review*, Food Research International, 2002. 35: p. 1015–1048.

[4] Patel, A.R., Rajarethinem, P.S., Gredowska, A., Turhan, O., Lesaffer, A., De Vos, W.H., Van de Walle, D., and K., Dewettincka, *Edible applications of shellac oleogels: spreads, chocolate paste and cakes*, Food & Function, 2014. 5: p. 645-652.

[5] Marangoni, A.G., and N., Garti, *Edible Oleogels: Structure and Health Implications*, AOCS Press, Urbana, 2011.

[6] Stanley, J.C., *Stearic acid or palmitic acid as a substitute for trans fatty acids?*, Lipid Technology, 2009. 21: p. 195-198.

[7] Blanco Muñoz, M.A., *Olive oil in food spreads*, Grasas y Aceites, 2004. 55: p. 92-94.

[8] Caggiula, A.W., and V.A., Mustad, *Effects of dietary fat and fatty acids on coronary artery disease risk and total and lipoprotein cholesterol concentrations: epidemiologic studies*, The American Journal of Clinical Nutrition, 1997. 65: p. 1597S-1610S.

[9] Kromhout, D., and C.C., de Lezenne, *Diet, prevalence and 10-year mortality from coronary heart disease in 871 middle-aged men. The Zutphen Study*, American Journal of Epidemiology, 1984. 119: p. 733-741.

[10] Mensink, R.P., and M.B., Katan, M.B., *Effect of dietary trans fatty acids on high-density and low-density lipoprotein cholesterol levels in healthy subjects*, The New English Journal of Medicine, 1990. 323: p. 439-445.

[11] Flöter, E., *Structuring oils without highly saturated fats – how far are we?*, European Journal of Lipid Science and Technology, 2012. 114: p. 983–984.

[12] Garti, N., Binyamin, H., and A., Aserin, *Stabilization of Water-in-Oil Emulsions by Submicrocrystalline α-Form Fat Particles*, Journal of the American Oil Chemists' Society, 1998. 75: p. 1825-1831.

[13] Ghosh, S., and D., Rousseau, *Fat crystals and water-in-oil emulsion stability*, Current Opinion in Colloid & Interface Science, 2011. 16: p. 421–431.

[14] Hoerr, C.W., *Morphology of fats oils and shortening*, Journal of American Oil Chemists' Society, 1960. 37: p. 539–546.

[15] Narine, S.S., and A.G., Marangoni, *Relating structure of fat crystal networks to mechanical properties: a review*, Food Research International, 1999. 32: p. 227–248.

[16] Narine, S.S., and Marangoni, A.G., *Fractal nature of fat crystal networks*, Physical Review, 1999. 59: p. 1908–1920.

[17] Lupi, F.R., Gabriele, D., de Cindio, B., Sánchez, M.C., and C., Gallegos, *A rheological analysis of structured water-in-olive oil emulsions*, Journal of Food Engineering, 2011. 107: p. 296–303.

[18] Wiederman, L.H., *Margarine and Margarine Oil, Formulation and Control*, Journal of the American Oil Chemists' Society, 1978. 55: p. 823-829.

[19] Norton, J.E., Fryer, P.J., Parkinson, J., and P.W., Cox, *Development and characterisation of tempered cocoa butter emulsions containing up to 60% water*, Journal of Food Engineering, 2009. 95: p. 172–178.

[20] Borwankar, R.P., Frye, L.A., Blaurock, A.E., and F.J., Sasevich, *Rheological characterization of melting of margarines and tablespreads*, Journal of Food Engineering, 1992. 16: p. 55–74.

[21] Schenk, H., and R., Peschar, R., *Understanding the structure of chocolate*, Radiation Physics and Chemistry, 2004. 71: p. 829–835.

[22] Rousseau, D., *Fat crystals and emulsion stability - a review*, Food Research International, 2000. 33: p. 3-14.

[23] Brooker, B.E., *The stabilization of air in foods containing air - a review*, Food Structure, 1993. 12: p. 115-122.

[24] Jahanavial, F., *Process for preparing high liquid oil, no trans, very low saturated, regular margarine with phospholipids*, patent US 2005/0233056 A1, international classification A23D007/00.

[25] Salas, J.J., Bootello, M.A., Martínez-Force, E., and R., Garcés, *Production of stearate-rich butters by solvent fractionation of high stearic–high oleic sunflower oil*, Food Chemistry, 2011. 124: p. 450–458.

[26] Hindle, S., Povey, M.J.W., and K., Smith, *Kinetics of Crystallization in n-Hexadecane and Cocoa Butter Oil-in-Water Emulsions Accounting for Droplet Collision-Mediated Nucleation*, Journal of Colloid and Interface Science, 2000. 232: p. 370–380.

[27] Campbell, S.D., Goff, H.D., and D., Rousseau, "Relating bulk-fat properties to emulsified systems: Characterization of emulsion destabilization by crystallizing fats", in: *Crystallization and solidification properties of lipids*, AOCS Press, Urbana, 2001.

[28] Lopez, C., Lesieur, P., Bourgaux, C., Keller, G., and M., Ollivon, *Thermal and structural behavior of milk fat 2. Crystalline forms obtained by slow cooling of cream*, Journal of Colloid and Interface Science, 2001. 240: p. 150-161.

[29] Coupland, J.N., *Crystallization in emulsions*, Current Opinion in Colloid and Interface Science, 2002. 7: p. 445–450.

[30] de Cindio B., Lupi F.R., Gabriele D., Baldino N., and M., Petramale, *Rheologically-controlled vegetable spread oils*, EP2827719A1/WO 2013111058 A1 European Patent, 2013.

[31] Gabriele, D., de Cindio, B., D'Antona, P., *A weak gel model for foods*, Rheological Acta, 2001. 40: p. 120-127.

[32] Núñez-Santiago, M. C., Tecante, A., Garnier, C., and J.L., Doublier, *Rheology and microstructure of κ-carrageenan under different conformations induced by several concentrations of potassium ion*, Food Hydrocolloids, 2011. 25: p. 32–41.

[33] Lupi F. R., Gabriele D., Greco V., Baldino N., Seta L., de Cindio B., *A rheological characterisation of an olive oil/fatty alcohols organogel*, Food Research International, 2013. 51: p. 510-517.

[34] McClements, D.J., "Emulsion ingredients", in: *Food Emulsions: Principles, Practices, and Techniques*, CRC Press, Boca Raton, 2004.

[35] Moran, D.P.J., "Fats in spreadable products", in: *Fats in Food Products*, Blackie Academic and Professional, London, 1994.

[36] Chrysam, M.M., "Margarine and spreads", in: *Bailey's Industrial Oil and Fat Products*, *5th ed*., Hui, Y.H., Ed., John Wiley, New York, 1996.

[37] Gunstone, F.D. and Norris, F.A., *Lipids in Foods: Chemistry, Biochemistry and Technology*, Pergamon Press, Oxford, 1983.

[38] Vithanage, C.R., Grimson, M.J., and B.G., Smith, *The effect of temperature on the rheology of butter, a spreadable blend and spreads*, Journal of Texture Studies, 2009. 40: p. 346–369.

[39] Fessas, D., Signorelli, M., and A., Schiraldi, *Polymorphous transitions in cocoa butter – a quantitative DSC study*, Journal of Thermal Analylis and Calorimetry, 2005. 82: p. 691-702.

Conclusions

In the present PhD thesis, the rheological and microstructural analysis of vegetable oil-based organogels and of their emulsions with water, has been reported. Organogelation is one of the most promising and innovative techniques for structuring liquid oils. The structuration is achieved through the gelation of either low molecular weight compounds or polymers able to self-assemble into aggregates that build a three-dimensional network. The most interesting potential food application of organogelation is the formulation of new soft matters, with the functionality and texture of commercial fats but, at the same time, with the nutritional profile of liquid edible oils. For this purpose, the rheological and structural study of organogels produced with vegetable oils and two different low molecular weight organogelators has been carried out.

After a complete characterisation of raw materials (reported in Chapter 2), MAG/olive oil organogels were studied performing a rheological, thermal and spectroscopic analysis (Chapter 3). Rheological analysis allowed the temperature of crystallisation onset and the gelation point to be determined, whereas through thermal analysis polymorphic transitions were detected. Spectroscopy revealed that the presence of intermolecular hydrogen bonding was essential for MAG organogel formation. Moreover, the fractal model has been applied and different empirical equations were proposed in order to relate the crystallisation onset and the rate of structure formation to the organogelator concentration. Furthermore, it has been shown that the source of vegetable oil used as the solvent affects the microstructure of the material and hard fats added to the system, like cocoa butter, can act as a thickening agent for the investigated systems.

Policosanol/olive oil organogels were studied using the same techniques already described for MAG organogels, as reported in Chapter 4. Obtained results were similar to those shown in Chapter 3, even if van der Waals interactions instead of hydrogen bonds were the main driving force for policosanol organogel formation. It was found that policosanol is not only a nutraceutical compound, as already reported in the literature, but it is also a strong organogelator for vegetable oils.

Successively, the organogelation properties of mixtures of monoglycerides and policosanol were investigated, as structured materials for potential cosmetic and food uses.

It has been concluded that thermo-rheological properties of organogels produced with mixture of organogelators are determined by the strongest organogelator of the mixture.

Finally, Chapter 5 dealt with the production of structured W/O emulsions for which the structuration of the oil phase was obtained through organogelation. For these potential commercial fats replacers, the optimal storage conditions after preparation were determined. The rheological and structural study was essential for designing healthy and highly-innovative food products.

List of publications

International Journals

Lupi, F.R., Gabriele, D., **Greco, V.**, Baldino, N., Seta, L., and B., de Cindio, *A rheological characterisation of an olive oil/fatty alcohols organogel*, Food Research International, 2013. 51: p. 510–517.

Proceedings of Conferences

Lupi, F.R., Gabriele, D., **Greco, V.**, Baldino, N., Mijovic, P., Puoci, F., and O.I., Parisi, *An olive oil/policosanol organogel for Ferulic Acid controlled delivery*, 1st International Conference on Rheology and Modeling of Materials, Miskolc-Lillafüred (Hungary), 7-11 October 2013.

Lupi, F.R., Gabriele, D., **Greco, V.**, Baldino, N., Seta, L., and B., de Cindio, *Rheological modeling of olive oil/policosanol organogels*, 1st International Conference on Rheology and Modeling of Materials, Miskolc-Lillafüred (Hungary), 7-11 October 2013.

Greco, V., Lupi, F.R., Gabriele, D., Baldino, N., de Cindio, B., and P., Fischer, *Analisi reologico-strutturale di organogel olio d'oliva/monogliceridi*, XIII Convegno Nazionale di Reologia, Brescia (Italy), 7-10 September 2014.

Lupi, F.R., Gabriele, D., **Greco, V.**, Seta, L., Baldino, N., and B., de Cindio, *Stabilizzazione innovativa di salse a base di carne ed oli vegetali mediante organogelazione*, XIII Convegno Nazionale di Reologia, Brescia (Italy), 7-10 September 2014.

Greco, V., Lupi, F.R., Gabriele, D., Baldino, N., de Cindio, B., and P., Fischer, *A rheological and microstructural characterisation of monoglycerides/olive oil organogels*, 7th International Symposium on Food and Rheology Structure, Zürich (Switzerland), 8-11 June 2015.